BEILSTEIN JOURNAL OF ORGANIC CHEMISTRY

Chemical ecology

Edited by Christine Beemelmanns

Imprint

Beilstein Journal of Organic Chemistry
www.bjoc.org
ISSN 1860-5397
Email: journals-support@beilstein-institut.de

The *Beilstein Journal of Organic Chemistry* is published by the Beilstein-Institut zur Förderung der Chemischen Wissenschaften.

Beilstein-Institut zur Förderung der Chemischen Wissenschaften
Trakehner Straße 7–9
60487 Frankfurt am Main
Germany
www.beilstein-institut.de

BEILSTEIN JOURNAL OF ORGANIC CHEMISTRY

On the mass spectrometric fragmentations of the bacterial sesterterpenes sestermobaraenes A–C

Anwei Hou and Jeroen S. Dickschat*

Letter

Open Access

Address:
Kekulé-Institute for Organic Chemistry and Biochemistry, University of Bonn, Gerhard-Domagk-Strasse 1, 53127 Bonn, Germany

Email:
Jeroen S. Dickschat* - dickschat@uni-bonn.de

* Corresponding author

Keywords:
isotopes; mass spectrometry; reaction mechanisms; sesterterpenes; *Streptomyces mobaraensis*

Beilstein J. Org. Chem. **2020,** *16,* 2807–2819.
https://doi.org/10.3762/bjoc.16.231

Received: 07 October 2020
Accepted: 12 November 2020
Published: 19 November 2020

This article is part of the thematic issue "Chemical ecology".

Guest Editor: C. Beemelmanns

Abstract

A ^{13}C-labelling was introduced into each individual carbon of the recently discovered sestermobaraenes by the enzymatic conversion of the correspondingly ^{13}C-labelled isoprenyl diphosphate precursors with the sestermobaraene synthase from *Streptomyces mobaraensis*. The main compounds sestermobaraenes A, B, and C were analysed by gas chromatography–mass spectrometry (GC–MS), allowing for a deep mechanistic investigation of the electron impact mass spectrometry (EIMS) fragmentation reactions of these sesterterpene hydrocarbons.

Introduction

The sestermobaraenes A–F (**1**–**6**) and sestermobaraol (**7**) are a series of bacterial sesterterpenes that were recently discovered by us from the actinomycete *Streptomyces mobaraensis* through a genome mining approach (Figure 1) [1]. All seven compounds are produced by a canonical terpene synthase, representing the first reported sesterterpene synthase of the classical type I from bacteria, that is characterised by an aspartate-rich motif (DDXXD) and an NSE triad (NDLXSXXXE) for binding of a trinuclear Mg^{2+} cluster [2,3]. The Mg^{2+} cations in turn bind to the diphosphate moiety of an isoprenoid diphosphate precursor and cause substrate ionisation by a diphosphate abstraction to initiate a cationic cyclisation cascade, leading to structurally highly complex and usually polycyclic terpenes in just one enzymatic transformation. The initially formed products are non-functionalised terpene hydrocarbons or, if the terminal cationic intermediate of the cyclisation cascade is trapped by water, simple alcohols. These volatile compounds can efficiently be trapped by specialised methods including the closed-loop stripping apparatus (CLSA) [4] technique or solid-phase microextraction (SPME) [5,6], and then analysed by gas chromatography–mass spectrometry (GC–MS) [7]. Through these and related techniques the volatiles from many bacteria, fungi, and plants have been investigated [8-10], which provides rapid information about the production of volatile terpenes. This

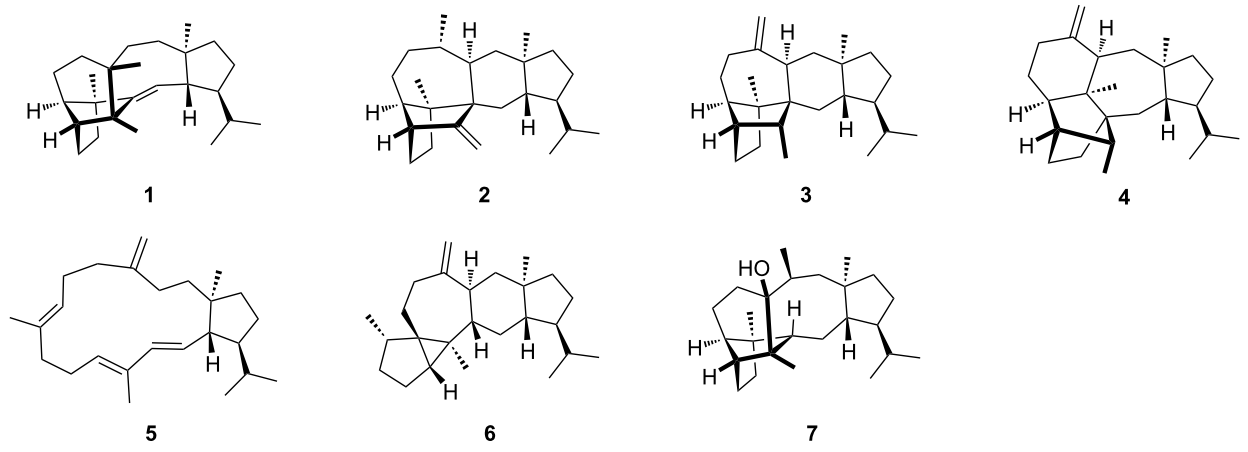

Figure 1: The structures of the bacterial sesterterpenes sestermobaraenes A–F (**1**–**6**) and sestermobaraol (**7**) from *Streptomyces mobaraensis*.

information is particularly useful in the combination with the genome sequences of the producing organism, because it allows to identify interesting candidate genes coding for terpene synthases for further studies by genome mining. A major difficulty in the GC–MS-based identification of terpenes is associated with the high similarity of the mass spectra of structurally related terpenes. For this reason, the unambiguous identification of terpenes requires either the direct comparison to an authentic standard, or, since such a standard is not always available, a very good match of the measured mass spectrum to a library spectrum and of the measured retention index to literature data. Mass spectrometric fragmentations proceed through reactions that are classified as σ-bond cleavages, α-fragmentations, inductive cleavages, McLafferty rearrangements [11], retro-Diels–Alder fragmentations [12,13], and the recently observed unusual radical-induced retro-Cope rearrangement (herein, "retro" indicates that the mass spectrometric reaction proceeds in reverse order of a thermal reaction promoted by the thermal conditions of the gaschromatographic analysis) [14]. The fragmentation reactions of structurally simple compounds such as fatty acid methyl esters have been well investigated by isotopic labelling experiments [15,16] and the knowledge allows for structural predictions based on GC–MS data [17]. The deuterium labelling technique was also applied to other compound classes such as alkylbenzenes and ketones [18-21]. For terpenes, structural proposals can only be made based on the mass spectra for structurally less complicated cases, as was exemplified for the side products of bacterial 2-methylisoborneol synthases [22], but in general the structural complexity of terpenes does not allow for such approaches. Nevertheless, more knowledge about the MS fragmentation reactions of terpenes is desirable, but represents a challenging objective as it is difficult to get access to the isotopically labelled terpenes needed for deep and conclusive insights. The early investigations by Djerassi and co-workers have made use of semisynthetic deuterated terpenes [23-25]. While deuterium can reveal specific hydrogen migrations in the fragmentation reactions, is comparably cheap, and can often easily be introduced, e.g., into C,H-acidic positions, a drawback of deuterium usage lies in possible kinetic isotope effects [21]. Also MS/MS-based techniques have been used to study the fragmentations of terpenes [26-28], but isotopic labelling experiments can give more detailed and conclusive insights. We have recently investigated the MS fragmentation mechanisms of several sesqui- and diterpenes in a series of studies that made use of ^{13}C-labelled terpene precursors to systematically introduce single labellings into each individual carbon position by enzymatic synthesis [14,29-32]. Here we report on the MS fragmentation mechanisms for the bacterial compounds sestermobaraenes A, B, and C, representing the first mechanistic study of this kind for sesterterpenes.

Results and Discussion

Experimental basis

The 25 isotopomers of (^{13}C)geranylfarnesyl diphosphate (GFPP) were enzymatically prepared from the correspondingly labelled geranyl diphosphate (GPP), farnesyl diphosphate (FPP), geranylgeranyl diphosphate (GGPP), and isopentenyl diphosphate (IPP) with geranylfarnesyl diphosphate synthase (GFPPS) and then converted into mixtures of the sesterterpenes **1**–**7** by the sestermobaraene synthase from *Streptomyces mobaraensis* (SmTS1). All ^{13}C-labelled terpene precursors were made available by synthesis in our laboratory in high isotopic purity with ^{13}C substitutions of nearly 100% [33-37]. The compound mixtures were subsequently analysed by GC–MS and the mass spectra of the unlabelled compounds **1**–**3** and their 25 singly ^{13}C-labelled isotopomers are summarised in Figures S1–S3 in Supporting Information File 1. Investigations

on the mass spectrometric fragmentation mechanisms for the minor products **4**–**7** of SmTS1 are not included in this study, because in some cases no high quality mass spectra could be obtained. The mass spectra of the unlabelled compounds show several pronounced signals for fragment ions (*m*/*z*, mass-to-charge ratio). If a signal in a mass spectrum for a particular ^{13}C-labelled isotopomer of a compound under investigation is in comparison to the non-labelled compound clearly increased by 1 Da, this means that the labelled carbon fully contributes to the fragment ion. Accordingly, if the signal is clearly not shifted, this means the labelled carbon is not part of the fragment ion. Also cases in between these clear situations exist, namely if a signal in the mass spectrum is a result of two or more fragment ions formed from different parts of the molecule, a labelled carbon may or may not contribute to its formation. A quick overview can be given in a position-specific mass shift analysis for a fragment ion *m*/*z* ($PMA_{m/z}$), in which fully contributing carbons are marked by red dots, partially contributing carbons by green dots, and carbons that do not contribute remain without a mark (Figures 2–4, vide infra). Because usually multiple fragmentation reactions lead to the formation of the ions observed in the low molecular weight region, their formation will not be discussed (an exception is the base peak at *m*/*z* = 120 for all three compounds). The method also finds its limitations for fragment ions buried within a group of peaks. Such fragment ions will not be discussed in this work.

Fragmentation mechanisms for sestermobaraene A (**1**)

The position-specific mass shift analyses (Figure 2) for several prominent fragment ions observed in the mass spectrum of sestermobaraene A (**1**) are based on a comparison of the mass spectrum of the unlabelled compound **1** to the mass spectra of the 25 isotopomers of (^{13}C)-**1** (Figure S1, Supporting Information File 1). As can be concluded from these analyses, the fragment ions observed at *m*/*z* = 312, *m*/*z* = 206, and the base peak at *m*/*z* = 120 are formed by a loss of a clearly defined portion of **1**, while the fragment ions at *m*/*z* = 325 and *m*/*z* = 297 arise through various reactions with losses of different portions of the molecule that can, however, still be rationalised. For the other fragment ions in the mass spectrum of **1** the situation is less clear and their formation will not be discussed here.

The formation of the fragment ion at *m*/*z* = 325 requires the loss of one methyl group for which only C22, C23, C24, and C25, but not C20 and C21 show a significant participation. The most prominent loss is observed for C23 in an allylic position of the double bond in **1**. After electron impact ionisation preferentially at the π-system of the olefinic double bond the radical cation $\mathbf{1}^{\bullet+}$ is obtained from which the methyl group C23 can directly be lost by an α-cleavage leading to fragment $\mathbf{a1}^{+}$ (Scheme 1A).

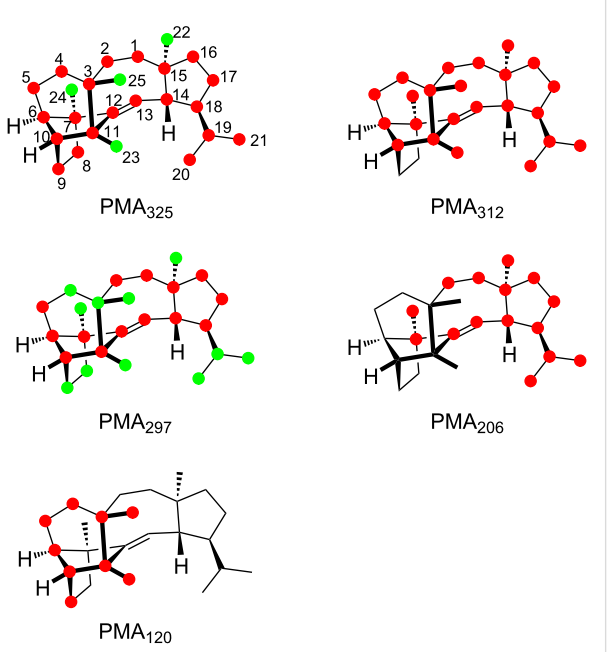

Figure 2: Position-specific mass shift analyses for **1**. Carbons that contribute fully to the formation of a fragment ion are indicated by red dots, partially contributing carbons are marked by green dots, and unlabelled carbons do not contribute and are thus cleaved off by the fragmentation reaction.

However, the radical centred at the bridgehead carbon C11 is orthogonal to, or in other words, not in conjugation with the radical cation at C12–13. Therefore, an energetically more feasible process may be represented by an inductive cleavage leading to $\mathbf{b1}^{\bullet+}$, a hydrogen rearrangement to $\mathbf{c1}^{\bullet+}$, and an α-cleavage to $\mathbf{d1}^{+}$ (Scheme 1B). The formation of the fragment ion at *m*/*z* = 312 proceeds through a highly specific loss of the C8–9 portion of **1**. This is explainable from $\mathbf{b1}^{\bullet+}$ by a sequence of two α-cleavages first to $\mathbf{e1}^{\bullet+}$ and then to $\mathbf{f1}^{\bullet+}$ with a neutral loss of ethylene (Scheme 1C). The fragment ion at *m*/*z* = 297 requires the loss of C_3H_7 which can be achieved by various reactions, as indicated by the PMA_{297}. This may be realised by the cleavage of an intact C_3H_7 unit originating from the isopropyl group C20–19–21 or, by involving multiple C–C bond cleavages and hydrogen rearrangements, from the C25–3–4 portion. Alternatively, a combined loss of the C8–9 moiety and one methyl group (C22, C23, C24, or C25) is possible which basically combines the fragmentations of Scheme 1A and Scheme 1B. The loss of the isopropyl group C20–19–21 can be achieved by an inductive cleavage of $\mathbf{1}^{\bullet+}$ to $\mathbf{g1}^{\bullet+}$ followed by an α-cleavage to $\mathbf{h1}^{+}$ (Scheme 1D). Starting from $\mathbf{c1}^{\bullet+}$, two α-cleavages with the extrusion of ethylene can lead to $\mathbf{i1}^{\bullet+}$ that upon a third α-fragmentation with loss of the methyl group C23 results in $\mathbf{j1}^{+}$ (Scheme 1E). The fragmentation of the C25–3–4 portion can be explained starting from $\mathbf{1}^{\bullet+}$ by a hydrogen rearrangement to $\mathbf{k1}^{\bullet+}$ and α-cleavage to $\mathbf{l1}^{\bullet+}$ (Scheme 1F). Another

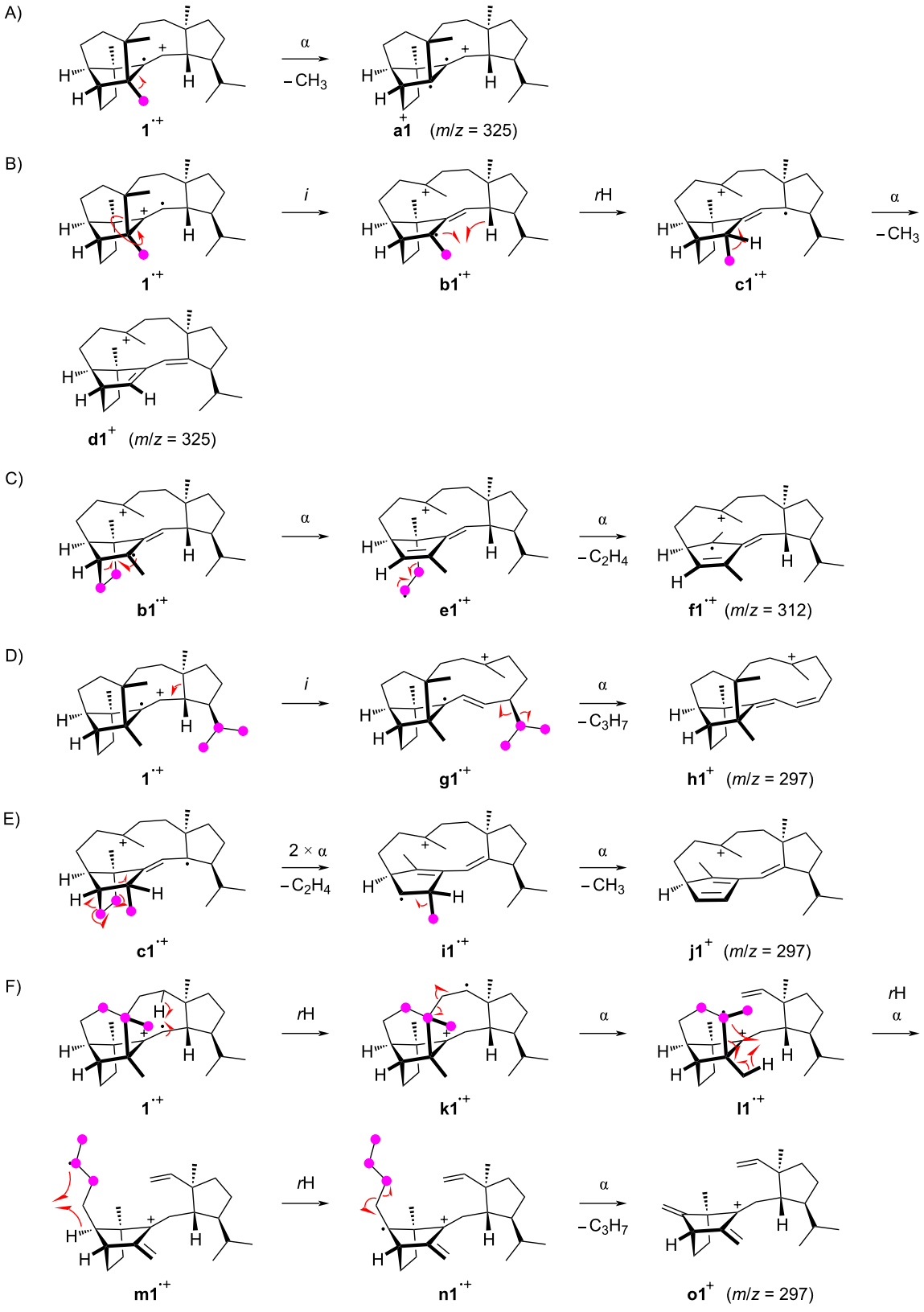

Scheme 1: The EIMS fragmentation mechanisms for **1** explaining the formation of the fragment ions at *m*/*z* = 325, 312, and 297. Lost carbons are marked by purple dots.

hydrogen rearrangement combined with an α-fragmentation then leads to the allyl cation **m1**$^{\bullet+}$ which may undergo a third hydrogen rearrangement to **n1**$^{\bullet+}$ and final cleavage of a propyl group to **o1**$^{+}$.

The formation of the fragment ion at *m*/*z* = 206 proceeds with the loss of the portion represented by carbons C25–3–4–5–6–10(–9–8)–11–23 and can be proposed as shown in Scheme 2A. After the ionisation to **1**$^{\bullet+}$ a hydrogen rearrangement leads to **p1**$^{\bullet+}$ that further reacts by an inductive ring opening and α-cleavage to **q1**$^{\bullet+}$. Another α-fragmentation to **r1**$^{\bullet+}$ may be followed by a hydrogen rearrangement to **s1**$^{\bullet+}$ and two α-cleavages to **t1**$^{\bullet+}$, giving an alternative mechanistic explanation for the fragment ion at *m*/*z* = 312 by loss of C8–9. Another the hydrogen rearrangement to **u1**$^{\bullet+}$ sets the stage for a final α-fragmentation with the neutral loss of *o*-xylene to **v1**$^{\bullet+}$. The base peak in the mass spectrum of **1** is formed from carbons C25–3–4–5–6–10(–9)–11–23, which can also be explained starting from **p1**$^{\bullet+}$ by three sequential α-cleavages through **w1**$^{\bullet+}$ to **x1**$^{\bullet+}$ (Scheme 2B). The inductive cleavage with hydride migration leads to **y1**$^{\bullet+}$ representing the minor fragment ion at *m*/*z* = 122 that may efficiently lose two hydrogens to give the conjugated system in **z1**$^{\bullet+}$.

Fragmentation mechanisms for sestermobaraene B (**2**)

The position-specific mass shift analyses for sestermobaraene B (**2**) are based on the mass spectrum of the unlabelled compound

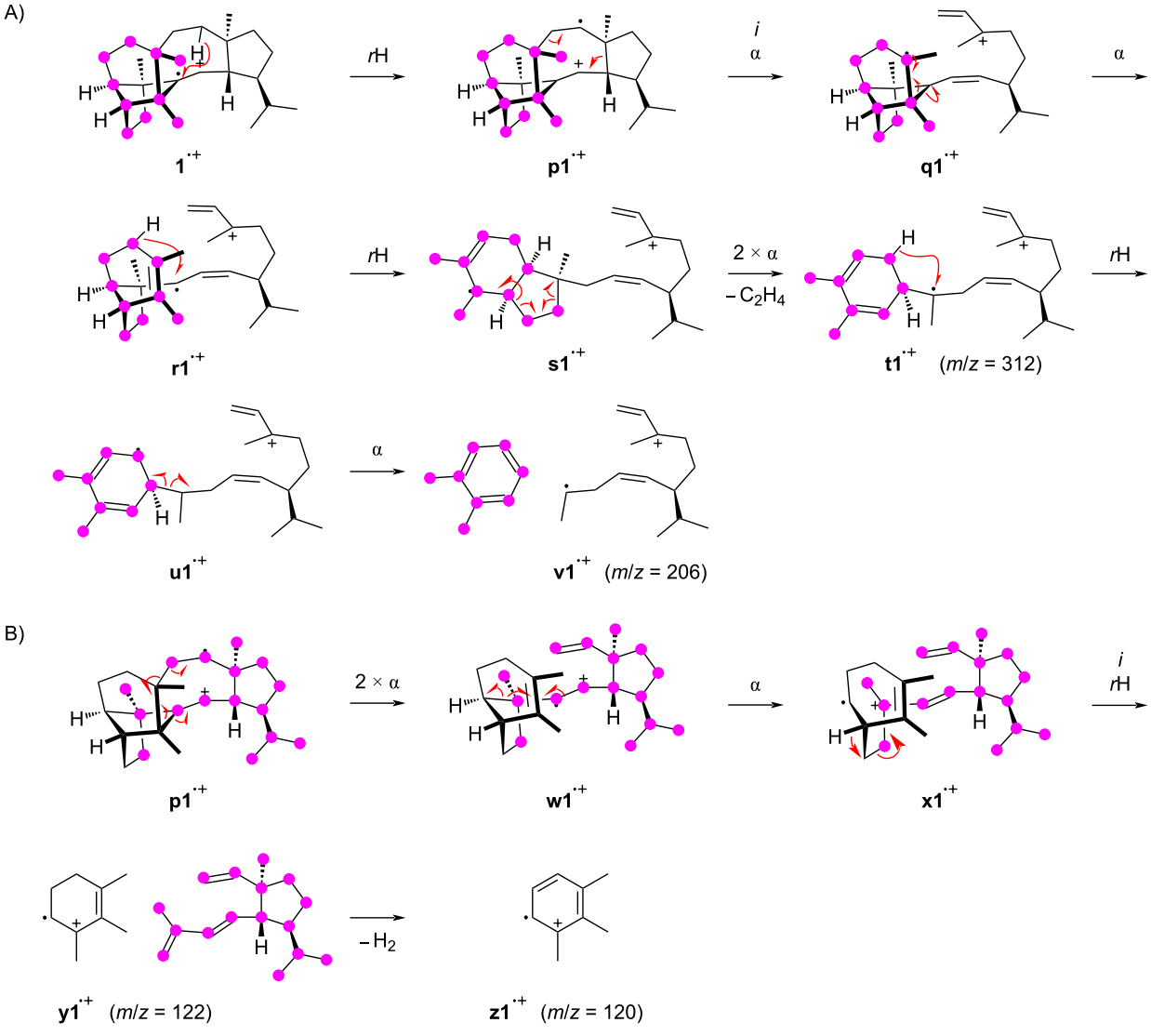

Scheme 2: The EIMS fragmentation mechanisms for **1** explaining the formation of fragment ions at *m*/*z* = 206 and 120. Lost carbons are marked by purple dots.

in comparison to those of its 25 ^{13}C-labelled isotopomers (Figure S2 in Supporting Information File 1). Clear results could be obtained for the fragment ions in the high mass region at *m*/*z* = 325, 312, and 297, for the base peak at *m*/*z* = 120, and the prominent fragment ion at *m*/*z* = 203. The results of the analyses are summarised in Figure 3.

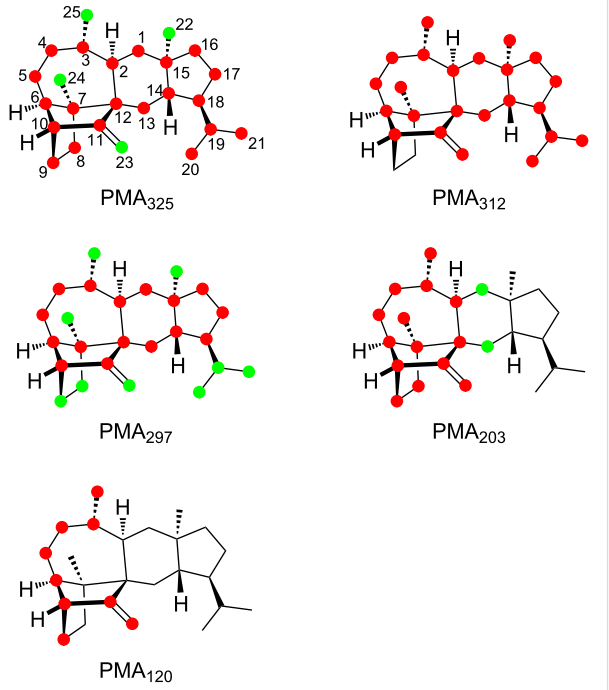

Figure 3: Position-specific mass shift analyses for **2**. The carbons that contribute fully to the formation of a fragment ion are indicated by red dots, partially contributing carbons are marked by green dots, and unlabelled carbons do not contribute and are thus cleaved off by the fragmentation reaction.

Similarly to the observations made for **1**, also for **2** the formation of the fragment ion at *m*/*z* = 325 by loss of one methyl group proceeds by the cleavage of C22, C23, C24, or C25, while the fragmentation of C20 or C21 does not make a significant contribution. Notably, even from the olefinic methylene group C23 a methyl group can be cleaved off, which requires hydrogen rearrangements prior to the fragmentation. A possible mechanism starts from **2**$^{\bullet+}$ by the hydrogen rearrangement to **a2**$^{\bullet+}$ and a hydride shift to **b2**$^{\bullet+}$ (Scheme 3A). This hydride migration is in reverse order compared to a similar step along the cationic cyclisation cascade during the biosynthesis of **2** (Scheme S1 in Supporting Information File 1). The subsequent inductive ring opening to **c2**$^{\bullet+}$ and α-cleavage of C23 result in **d2**$^{+}$. The losses of the other methyl groups can be understood more easily, e.g., two α-fragmentations from **2**$^{\bullet+}$ explain the formation of **e2**$^{+}$ with the loss of C25 (Scheme 3B). The fragment ion at *m*/*z* = 312 arises by the loss of the C8–9 portion through a double α-cleavage from **2**$^{\bullet+}$, yielding to **f2**$^{\bullet+}$ (Scheme 3C). Also for compound **2** different mechanisms for the formation of the fragment ion at *m*/*z* = 297 are observed, including the loss of the isopropyl group C20–19–21 or the loss of C8–9 and one methyl group. The cleavage of the isopropyl group is possible from **c2**$^{\bullet+}$ by an inductive ring opening to **g2**$^{\bullet+}$ and α-fragmentation to **h2**$^{+}$ (Scheme 3D). Alternatively, **c2**$^{\bullet+}$ can react by two α-cleavages leading to **i2**$^{\bullet+}$ with a neutral loss of ethylene, followed by another α-cleavage of C23 to **j2**$^{+}$ (Scheme 3E). The fragment ion at *m*/*z* = 297 can also be rationalised from **f2**$^{\bullet+}$ by two α-fragmentations with the loss of C25 to result in **k2**$^{+}$ (Scheme 3F).

The position-specific mass shift analysis for *m*/*z* = 203 indicates the formation of this fragment ion by two overlaid mechanisms that both involve the loss of C14–15(–22)–16–17–18–19(–21)–20 plus either C13 or C1. A mechanistic model for the first case with loss of C13 starts from **2**$^{\bullet+}$ by a hydrogen rearrangement to **l2**$^{\bullet+}$ and an α-fragmentation to **m2**$^{\bullet+}$, followed by another hydrogen transfer to **n2**$^{\bullet+}$ and α-cleavage to **o2**$^{+}$ (Scheme 4A). The second possibility with the loss of C1 is explainable from **l2**$^{\bullet+}$ by a hydrogen migration to **p2**$^{\bullet+}$ and an α-fragmentation to **q2**$^{\bullet+}$, followed by two more α-fragmentations to **r2**$^{\bullet+}$ (Scheme 4B). A final α-cleavage then yields the target ion **s2**$^{+}$. The generation of the base peak ion at *m*/*z* = 120 from the C25–3–4–5–6–10(–9)–11–23 moiety of **2** is more difficult to understand, as it must proceed with four C–C bond cleavages. Interestingly, for **2** the base peak is made up from the same portion of the molecule as for **1**, but while **1** has a bond between C3 and C11, this bond is missing in **2** that has a bond between C2 and C12 instead. For **1** the base peak was nicely explainable by the formation of an ionised aromatic ring system. In the first instance, it seems difficult to parallel this for **2**, but if for the first steps after ionisation to **2**$^{\bullet+}$ a skeletal rearrangement to **t2**$^{\bullet+}$ and a hydrogen transfer to **u2**$^{\bullet+}$ are assumed, the parallelism of the fragmentation mechanisms becomes more obvious (Scheme 4C). Subsequent steps may include an inductive ring opening to **v2**$^{\bullet+}$, another hydrogen rearrangement to **w2**$^{\bullet+}$, and two α-cleavages to **x2**$^{\bullet+}$. Another hydrogen rearrangement and elimination of two hydrogen atoms lead to **y2**$^{\bullet+}$ which is identical to **z1**$^{\bullet+}$ in the fragmentation mechanism for the base peak ion of **1**.

Fragmentation mechanisms for sestermobaraene C (**3**)

For sestermobaraene C (**3**) the position-specific mass shift analyses based on the mass spectra of the unlabelled versus all 25 isotopomers of the singly ^{13}C-labelled material (Figure S3 in Supporting Information File 1) also gave unambiguous results for the fragment ions at *m*/*z* = 325, 312, 297, 206, and the base peak at *m*/*z* = 120 (Figure 4), which is similar to the correspond-

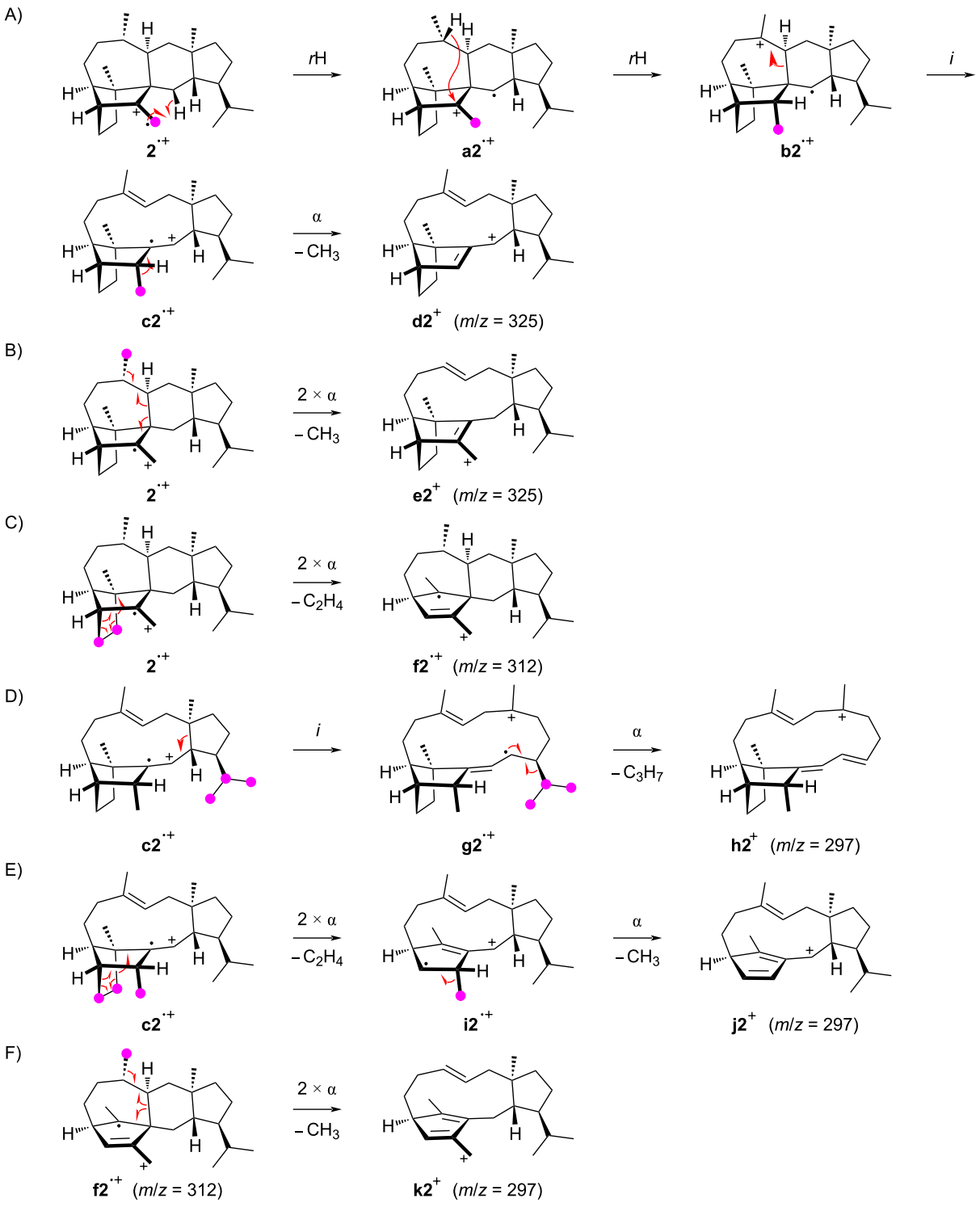

Scheme 3: The EIMS fragmentation mechanisms for **2** explaining the formation of the fragment ions at *m*/*z* = 325, 312, and 297. Lost carbons are marked by purple dots.

ing analyses for **1** and **2** not only in the nominal masses of the fragment ions, but also in terms of the portions of the carbon skeletons these fragments arise from. Thus, it can be expected that similar fragmentation reactions as discussed for **1** and **2** above can lead to their formation. One notable difference is observed for the fragment ions at *m*/*z* = 312 and 297 that are formed with a partial loss of C11–23, which was not observed for compounds **1** and **2**.

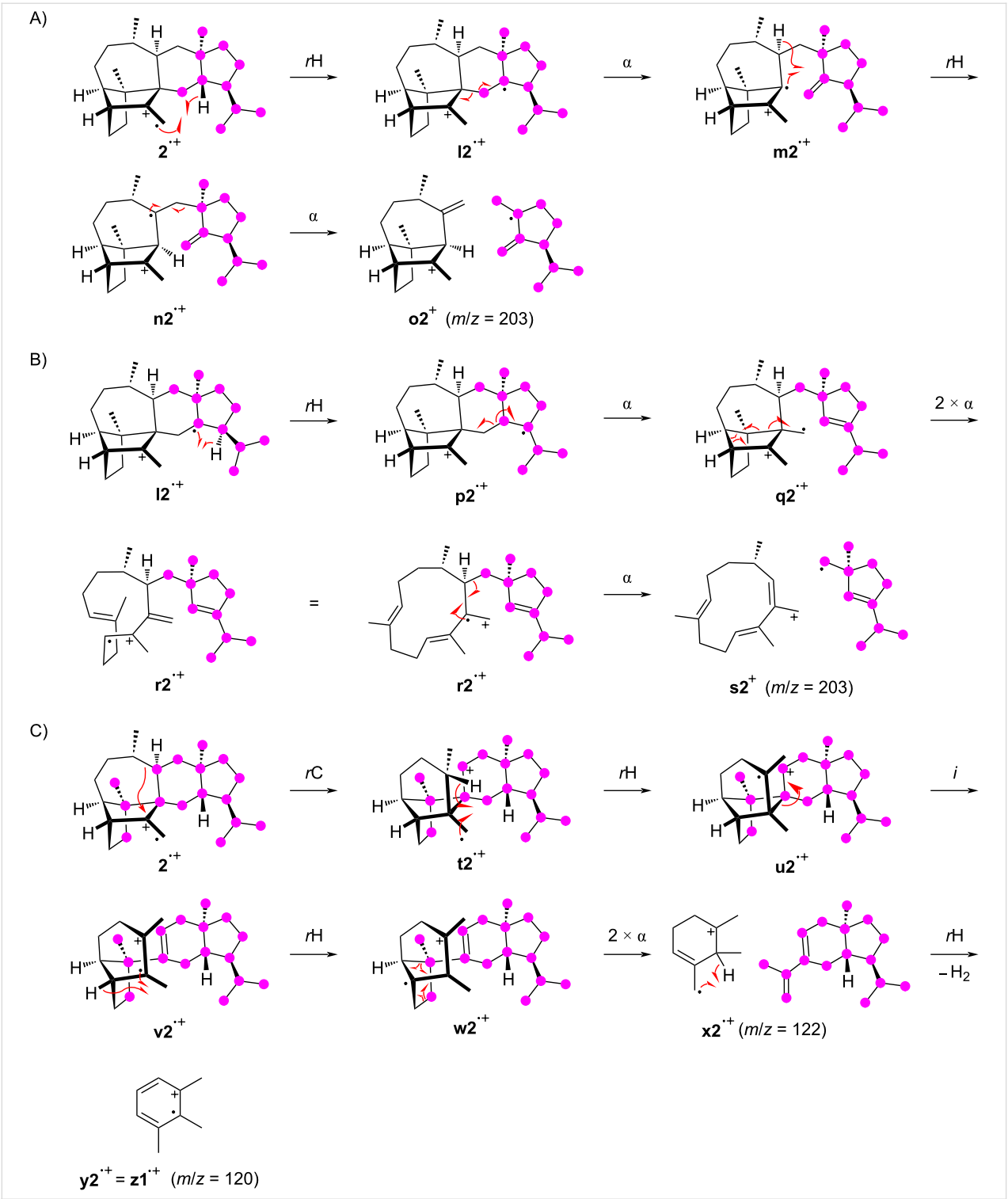

Scheme 4: The EIMS fragmentation mechanisms for **2** explaining the formation of the fragment ions at *m*/*z* = 203 and 120. Lost carbons are marked by purple dots.

The formation of the fragment ion at *m*/*z* = 325 proceeds with cleavage of C22, C23, C24, or C25, as observed before for compounds **1** and **2**. Especially noteworthy is the cleavage of the methylene carbon C25, which is explainable from $\mathbf{3}^{\bullet+}$ by a hydrogen rearrangement to $\mathbf{a3}^{\bullet+}$, followed by a hydride shift to $\mathbf{b3}^{\bullet+}$ and an α-fragmentation to $\mathbf{c3}^{+}$ (Scheme 5A). The alternative loss of C22 is possible from $\mathbf{3}^{\bullet+}$ by two sequential α-cleavages via $\mathbf{d3}^{\bullet+}$ to $\mathbf{e3}^{+}$ (Scheme 5B). The fragment ion at

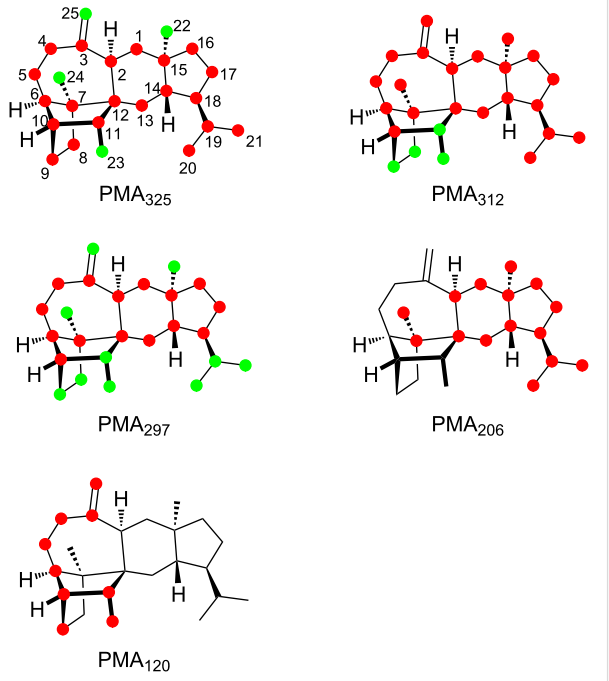

Figure 4: The position-specific mass shift analyses for **3**. Carbons that contribute fully to the formation of a fragment ion are indicated by red dots, partially contributing carbons are marked by green dot, and unlabelled carbons do not contribute and are thus cleaved off by the fragmentation reaction.

m/*z* = 312 involves the loss of either the C8–9 or the C11–23 portion. The first case can be understood starting from **b3**$^{\bullet+}$ by two inductive cleavages with the neutral loss of ethylene to **f3**$^{\bullet+}$ and then **g3**$^{\bullet+}$ (Scheme 5C), while the second case may start from **a3**$^{\bullet+}$ by an α-cleavage with hydrogen rearrangement to **h3**$^{\bullet+}$ and another subsequent α-fragmentation to **i3**$^{\bullet+}$ (Scheme 5D). Similar to the observations for compounds **1** and **2**, the fragment ion at *m*/*z* = 297 of **3** is generated by the loss of C8–9 and one methyl group or of the isopropyl group C20–19–21. In addition, the combined loss of C11–23 and one methyl group also contributes to its formation. The possible mechanistic models include a simple α-fragmentation with the loss of C25 from **g3**$^{\bullet+}$ to **j3**$^{+}$ (Scheme 5E), a sequence of three α-cleavages from **3**$^{\bullet+}$ through **k3**$^{\bullet+}$ leading to **l3**$^{+}$ (Scheme 5F), and a double α-fragmentation in **i3**$^{\bullet+}$ that explains the formation of **m3**$^{+}$ (Scheme 5G).

The fragment ion at *m*/*z* = 206 arises from the C25–3–4–5–6–10(–9–8)–11–23 moiety of **3**. Its formation requires multiple bond cleavages and hydrogen transfers and is thus a multistep process (Scheme 6A). Starting from **3**$^{\bullet+}$, a hydride shift to **n3**$^{\bullet+}$ and skeletal rearrangement lead to **o3**$^{\bullet+}$. A subsequent hydrogen rearrangement of this primary radical yields the tertiary radical **p3**$^{\bullet+}$ that can undergo an α-fragmentation to **q3**$^{\bullet+}$, followed by hydrogen rearrangement to **r3**$^{\bullet+}$, setting the stage for the next α-cleavage to **s3**$^{\bullet+}$. The same principle can explain the last bond cleavage: A hydride shift to **t3**$^{\bullet+}$ adjusts the reactivity for the α-fragmentation to **u3**$^{\bullet+}$. Notably, the intermediate **q3**$^{\bullet+}$ is also a good starting point to explain the formation of the base peak ion at *m*/*z* = 120 (Scheme 6B). The inductive ring opening produces **v3**$^{\bullet+}$ that, upon α-cleavage with hydrogen rearrangement, leads to **w3**$^{\bullet+}$ (*m*/*z* = 122). The base peak ion **x3**$^{\bullet+}$ then results by the loss of two hydrogens.

Conclusion

In this work we demonstrated that ^{13}C-labellings can efficiently be introduced by terpene synthase catalysed reactions into each single position of a terpene, which is useful for the deep investigations on mass spectrometric fragmentation reactions. The present study provides the first example for such investigations on sesterterpene fragmentations. The applied method, once the synthetic ^{13}C-labelled oligoprenyl diphosphates are at hand, is superior to any other approach for the introduction of labellings, also because the labelled terpene precursors can be used for studies on many different terpenes for which terpene synthases are available. In the present case it is intriguing to learn that, although the structures of the three investigated sesterterpenes are different, not only similar fragment ions are observed, but also similar reactions lead to their formation, which is most prominently observed for the common base peak ion at *m*/*z* = 120 for all three compounds. This means that the sesterterpenes have a common intrinsic reactivity that is in the first instance reflected by their joint biosynthesis, but also by their similar behaviour in the comparably high-energy chemistry of mass spectrometric fragmentation reactions. Further support for the similar reactivity of the investigated compounds during biosynthesis and mass spectrometric fragmentations is given by the notable observation of hydride shifts that occur in both of these processes. However, the three compounds show also some differences in their mass spectrometric fragmentation, e.g., for compound **2** a strong fragment ion is observed at *m*/*z* = 203, which is much less relevant for the other two compounds. It should be emphasised that the mechanistic hypotheses presented in this work are solely based on the ^{13}C-labellings, while specific hydrogen migrations would need to be followed by deuterium labellings, but in these cases data interpretation may be hampered by kinetic isotope effects. Nevertheless, at the current stage it cannot be excluded that such experiments could demonstrate the need for a refinement of the fragmentation mechanisms for certain fragment ions presented here. We will continue our investigations on terpene fragmentations in EIMS in the future by the strategy applied in this work to learn more about the underlying reaction mechanisms.

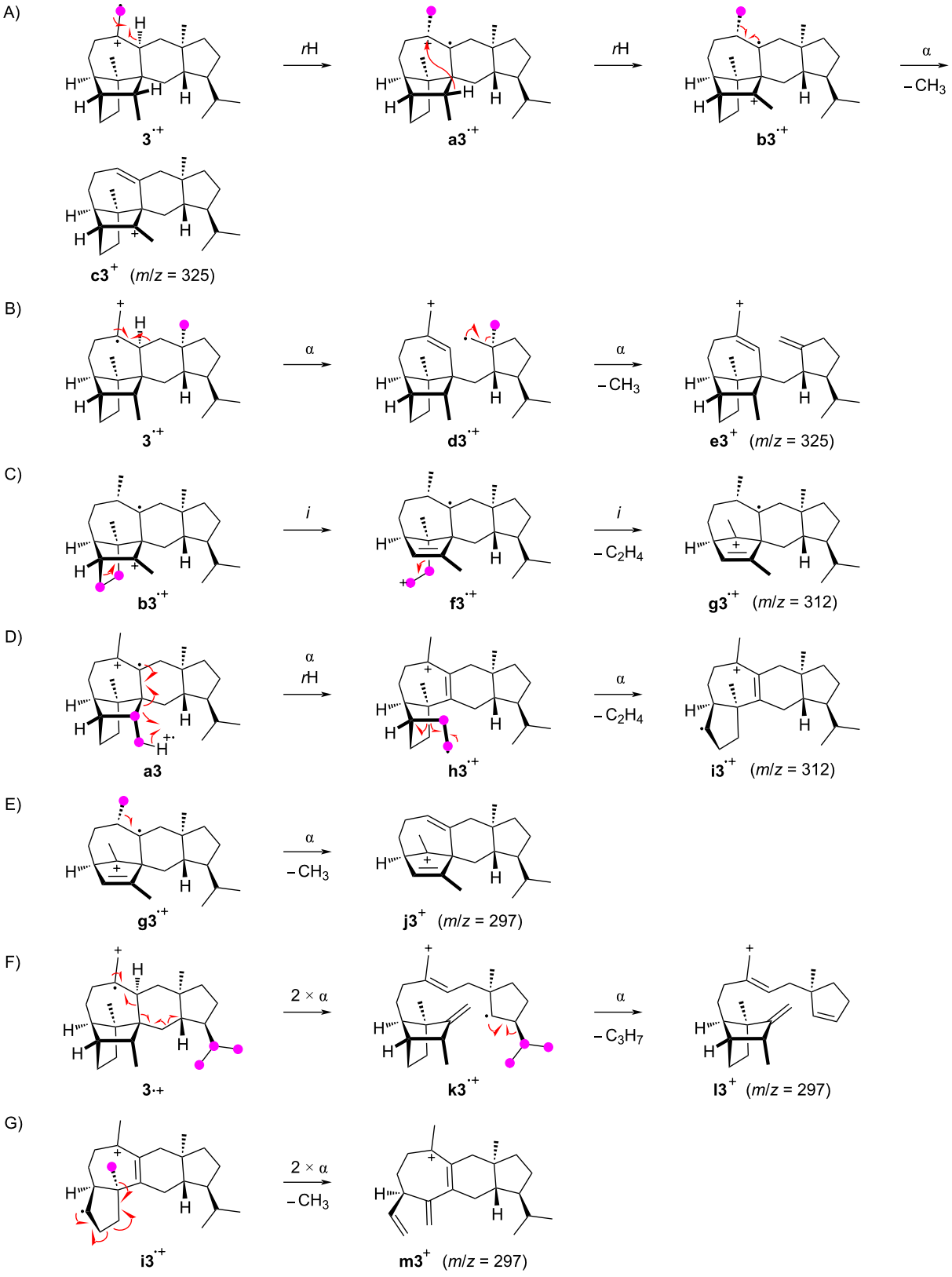

Scheme 5: The EIMS fragmentation mechanisms for **3** explaining the formation of the fragment ions at *m/z* = 325, 312, and 297. Lost carbons are marked by purple dots.

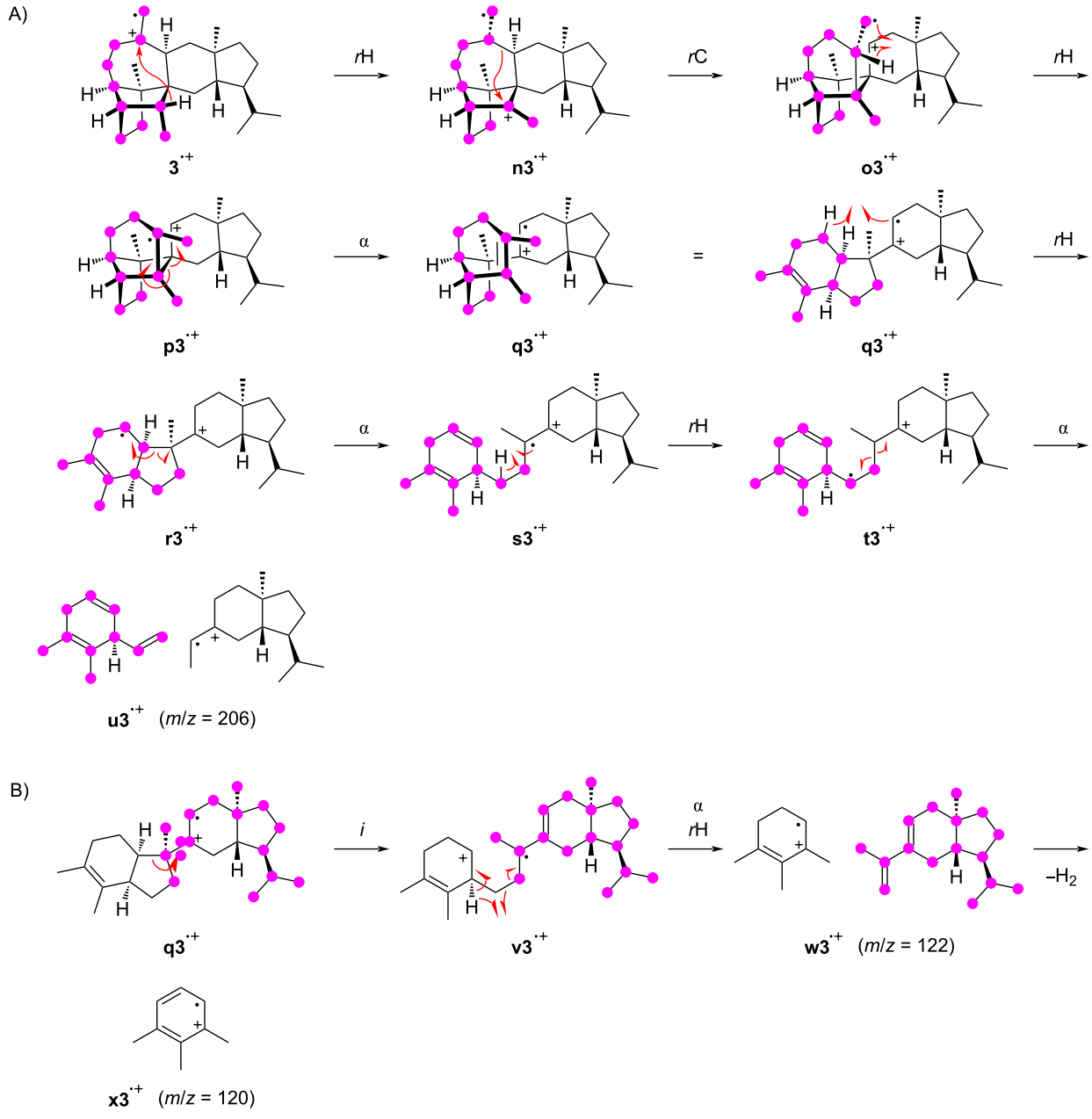

Scheme 6: The EIMS fragmentation mechanisms for **3** explaining the formation of the fragment ion at *m*/*z* = 206 and the base peak ion at *m*/*z* = 120. Lost carbons are marked by purple dots.

Experimental

Preparation of ^{13}C-labelled compounds **1**–**3** and GC–MS analysis

The 25 isotopomers of (^{13}C)-**1**, (^{13}C)-**2**, and (^{13}C)-**3** were prepared enzymatically with SmTS1 from the correspondingly labelled oligoprenyl diphosphates as reported previously [1]. The compounds were obtained as mixtures that were directly analysed by GC–MS. The GC–MS analyses were performed using a 7890A GC connected to a 5977A mass selective detector (Agilent, Hewlett-Packard Company, Wilmington, USA). The gas chromatographic separation was done using a HP5-MS fused silica capillary column (30 m, 0.25 mm i.d., 0.25 µm film, Agilent). The GC settings were 1) inlet pressure: 77.1 kPa, He 23.3 mL min^{-1}; 2) injector temperature: 250 °C; 3) injection volume: 2 µL; 4) injector operation mode: splitless (60 s valve time); 5) carrier gas: He at 1.2 mL min^{-1}; 6) temperature program: 5 min at 50 °C, then increasing with a ramp of 5 °C min^{-1} to 320 °C. The MS settings were 1) transfer line: 300 °C; 2) electron energy: 70 eV.

Supporting Information

Supporting Information File 1

Mass spectra of the unlabelled and ^{13}C-labelled compounds **1**–**3**, and the cyclisation mechanism from GFPP to **1**–**3** by SmTS1.
[https://www.beilstein-journals.org/bjoc/content/supplementary/1860-5397-16-231-S1.pdf]

Funding

This work was funded by the DFG (DI1536/7-2).

ORCID® iDs

Jeroen S. Dickschat - https://orcid.org/0000-0002-0102-0631

References

1. Hou, A.; Dickschat, J. S. *Angew. Chem., Int. Ed.* **2020,** *59,* 19961–19965. doi:10.1002/anie.202010084
2. Starks, C. M.; Back, K.; Chappell, J.; Noel, J. P. *Science* **1997,** *277,* 1815–1820. doi:10.1126/science.277.5333.1815
3. Christianson, D. W. *Chem. Rev.* **2017,** *117,* 11570–11648. doi:10.1021/acs.chemrev.7b00287
4. Grob, K.; Zürcher, F. *J. Chromatogr.* **1976,** *117,* 285–294. doi:10.1016/0021-9673(76)80005-2
5. Arthur, C. L.; Pawliszyn, J. *Anal. Chem. (Washington, DC, U. S.)* **1990,** *62,* 2145–2148. doi:10.1021/ac00218a019
6. Zhang, Z.; Pawliszyn, J. *Anal. Chem. (Washington, DC, U. S.)* **1993,** *65,* 1843–1852. doi:10.1021/ac00062a008
7. Dickschat, J. S. *Nat. Prod. Rep.* **2014,** *31,* 838–861. doi:10.1039/c3np70080a
8. Schulz, S.; Dickschat, J. S. *Nat. Prod. Rep.* **2007,** *24,* 814–842. doi:10.1039/b507392h
9. Dickschat, J. S. *Nat. Prod. Rep.* **2017,** *34,* 310–328. doi:10.1039/c7np00003k
10. Hammerbacher, A.; Coutinho, T. A.; Gershenzon, J. *Plant, Cell Environ.* **2019,** *42,* 2827–2843. doi:10.1111/pce.13602
11. McLafferty, F. W. *Anal. Chem. (Washington, DC, U. S.)* **1959,** *31,* 82–87. doi:10.1021/ac60145a015
12. Biemann, K. *Angew. Chem., Int. Ed. Engl.* **1962,** *1,* 98–111. doi:10.1002/anie.196200981
13. Budzikiewicz, H.; Brauman, J. I.; Djerassi, C. *Tetrahedron* **1965,** *21,* 1855–1879. doi:10.1016/s0040-4020(01)98656-9
14. Rinkel, J.; Dickschat, J. S. *Org. Lett.* **2019,** *21,* 2426–2429. doi:10.1021/acs.orglett.9b00725
15. Rohwedder, W. K. *Prog. Lipid Res.* **1985,** *24,* 1–18. doi:10.1016/0163-7827(85)90006-2
16. Ryhage, R.; Stenhagen, E. *Ark. Kemi* **1960,** *15,* 291–315.
17. Dickschat, J. S.; Bruns, H.; Riclea, R. *Beilstein J. Org. Chem.* **2011,** *7,* 1697–1712. doi:10.3762/bjoc.7.200
18. Kuck, D.; Grützmacher, H.-F. *Z. Naturforsch., B: Anorg. Chem., Org. Chem.* **1979,** *34,* 1750–1764. doi:10.1515/znb-1979-1224
19. Kuck, D.; Grützmacher, H.-F. *Org. Mass Spectrom.* **1978,** *13,* 81–89. doi:10.1002/oms.1210130205
20. Kuck, D.; Grützmacher, H.-F. *Org. Mass Spectrom.* **1978,** *13,* 90–102. doi:10.1002/oms.1210130206
21. MacLeod, J. K.; Djerassi, C. *Tetrahedron Lett.* **1966,** *7,* 2183–2187. doi:10.1016/s0040-4039(00)72818-8
22. Brock, N. L.; Ravella, S. R.; Schulz, S.; Dickschat, J. S. *Angew. Chem., Int. Ed.* **2013,** *52,* 2100–2104. doi:10.1002/anie.201209173
23. Weinberg, D. S.; Djerassi, C. *J. Org. Chem.* **1966,** *31,* 115–119. doi:10.1021/jo01339a024
24. Karliner, J.; Djerassi, C. *J. Org. Chem.* **1966,** *31,* 1945–1956. doi:10.1021/jo01344a063
25. Muccino, R. R.; Djerassi, C. *J. Am. Chem. Soc.* **1973,** *95,* 8726–8733. doi:10.1021/ja00807a037
26. Danuello, A.; Cardoso de Castro, R.; Pilon, A. C.; Pires Bueno, P. C.; Pivatto, M.; Magela Vieira Júnior, G.; Carvalho, F. A.; Bombarda Oda, F.; Javiera Perez, C.; Peporine Lopez, N.; Gonzaga Dos Santos, A.; Rocha Ifa, D.; Cavalheiro, A. J. *Rapid Commun. Mass Spectrom.* **2020,** *34,* e8781. doi:10.1002/rcm.8781
27. da Cunha Pinto, A.; Vessecchi, R.; Gomes da Silva, C.; Lourenco Amorim, A. C.; dos Santos Júnior, H. M.; Cunha Rezende, M. J.; Gates, P. J.; Moraes Rezende, C.; Peporine Lopez, N. *Rapid Commun. Mass Spectrom.* **2016,** *30,* 61–68. doi:10.1002/rcm.7411
28. Aguiar, G. P.; Crevelin, E. J.; Dias, H. J.; Ambrósio, S. R.; Bastos, J. K.; Heleno, V. C. G.; Vessecchi, R.; Crotti, A. E. M. *J. Mass Spectrom.* **2018,** *53,* 1086–1096. doi:10.1002/jms.4284
29. Rabe, P.; Barra, L.; Rinkel, J.; Riclea, R.; Citron, C. A.; Klapschinski, T. A.; Janusko, A.; Dickschat, J. S. *Angew. Chem., Int. Ed.* **2015,** *54,* 13448–13451. doi:10.1002/anie.201507615
30. Rabe, P.; Klapschinski, T. A.; Dickschat, J. S. *ChemBioChem* **2016,** *17,* 1333–1337. doi:10.1002/cbic.201600237
31. Rabe, P.; Dickschat, J. S. *Beilstein J. Org. Chem.* **2016,** *12,* 1380–1394. doi:10.3762/bjoc.12.132
32. Rinkel, J.; Rabe, P.; Dickschat, J. S. *Eur. J. Org. Chem.* **2019,** 351–359. doi:10.1002/ejoc.201800217
33. Rabe, P.; Rinkel, J.; Dolja, E.; Schmitz, T.; Nubbemeyer, B.; Luu, T. H.; Dickschat, J. S. *Angew. Chem., Int. Ed.* **2017,** *56,* 2776–2779. doi:10.1002/anie.201612439
34. Rinkel, J.; Lauterbach, L.; Dickschat, J. S. *Angew. Chem., Int. Ed.* **2019,** *58,* 452–455. doi:10.1002/anie.201812216
35. Mitsuhashi, T.; Rinkel, J.; Okada, M.; Abe, I.; Dickschat, J. S. *Chem. – Eur. J.* **2017,** *23,* 10053–10057. doi:10.1002/chem.201702766
36. Bian, G.; Rinkel, J.; Wang, Z.; Lauterbach, L.; Hou, A.; Yuan, Y.; Deng, Z.; Liu, T.; Dickschat, J. S. *Angew. Chem., Int. Ed.* **2018,** *57,* 15887–15890. doi:10.1002/anie.201809954
37. Quan, Z.; Dickschat, J. S. *Org. Biomol. Chem.* **2020,** *18,* 6072–6076. doi:10.1039/d0ob01470b

BEILSTEIN JOURNAL OF ORGANIC CHEMISTRY

Secondary metabolites of *Bacillus subtilis* impact the assembly of soil-derived semisynthetic bacterial communities

Heiko T. Kiesewalter[1], Carlos N. Lozano-Andrade[1], Mikael L. Strube[2] and Ákos T. Kovács[*1]

Full Research Paper

Open Access

Address:
[1]Bacterial Interactions and Evolution Group, DTU Bioengineering, Technical University of Denmark, Kgs. Lyngby, Denmark and [2]Bacterial Ecophysiology and Biotechnology Group, DTU Bioengineering, Technical University of Denmark, Kgs. Lyngby, Denmark

Email:
Ákos T. Kovács[*] - atkovacs@dtu.dk

* Corresponding author

Keywords:
Bacillus subtilis; bacterial community; chemical ecology; *Lysinibacillus fusiformis*; nonribosomal peptides; surfactin

Beilstein J. Org. Chem. **2020,** *16,* 2983–2998.
https://doi.org/10.3762/bjoc.16.248

Received: 20 August 2020
Accepted: 18 November 2020
Published: 04 December 2020

This article is part of the thematic issue "Chemical ecology".

Guest Editor: C. Beemelmanns

Abstract

Secondary metabolites provide *Bacillus subtilis* with increased competitiveness towards other microorganisms. In particular, nonribosomal peptides (NRPs) have an enormous antimicrobial potential by causing cell lysis, perforation of fungal membranes, enzyme inhibition, or disruption of bacterial protein synthesis. This knowledge was primarily acquired in vitro when *B. subtilis* was competing with other microbial monocultures. However, our understanding of the true ecological role of these small molecules is limited. In this study, we have established soil-derived semisynthetic mock communities containing 13 main genera and supplemented them with *B. subtilis* P5_B1 WT, the NRP-deficient strain *sfp*, or single-NRP mutants incapable of producing surfactin, plipastatin, or bacillaene. Through 16S amplicon sequencing, it was revealed that the invasion of NRP-producing *B. subtilis* strains had no major impact on the bacterial communities. Still, the abundance of the two genera *Lysinibacillus* and *Viridibacillus* was reduced. Interestingly, this effect was diminished in communities supplemented with the NRP-deficient strain. Growth profiling of *Lysinibacillus fusiformis* M5 exposed to either spent media of the *B. subtilis* strains or pure surfactin indicated the sensitivity of this strain towards the biosurfactant surfactin. Our study provides a more in-depth insight into the influence of *B. subtilis* NRPs on semisynthetic bacterial communities and helps to understand their ecological role.

Introduction

In nature, bacteria live in complex communities where they interact with various other microorganisms. Most microbial communities are influencing biochemical cycles and impact agriculture, from which the latter is primarily mediated due to plant-growth promotion [1-4]. Extensive research has been conducted in the last decade to scrutinise the occurring natural pro-

cesses and their impact on the environment, to investigate the functions and interactions of community members, such as metabolite cross-feeding interactions, and to eventually engineer them [5-7]. The soil is one of the five main habitats of bacteria and archaea [8]. Soil is very heterogeneous since it exhibits spatial variability in terms of nutrient availability and geochemical features [9]. Therefore, soil consists of microbial hotspots, indicating faster process rates than the average soil [10]. One such microbial hotspot is the rhizosphere, harbouring microbial communities where various interactions between bacteria, fungi, and plants take place [11]. The composition of microbial communities depends on multiple factors. Studies have revealed that the composition of bacterial soil communities varies at the same sampling site during different seasons [12,13]. Moreover, it has been recently demonstrated that precipitation rates have a significant impact on bacterial communities since bacterial soil communities have a higher diversity in dry than in rainy seasons [14]. Besides the seasonal factors, even different plant species with varying root exudates as well as various soil types impact the microbial community composition in the rhizosphere [15-20]. Microbial communities can consist of hundreds and thousands of diverse species, which makes investigations very challenging and hard to reproduce. One alternative approach is to establish a host-associated synthetic community, usually with members of the same kingdom, with a defined composition but fewer members [19,21]. Lebeis et al. used an artificial community of 38 bacterial strains to demonstrate that plant phytohormones sculpt the root microbiome [19]. In comparison, Niu et al. established a seven-species bacterial community based on host selection to mimic the principle root microbiome of maize [22].

Secondary metabolites (SMs) are believed to be important mediators of the interactions between microorganisms [23]. Many of them are well-studied in vitro, but the true ecological role of SMs is still the subject of investigations. Different opinions about their primary role in nature exist in the literature; some share the view that SMs are mainly microbial weapons but others instead designate them as signalling molecules [24-27]. Additionally, Pettit [28] and Wakefield et al. [29] have demonstrated in 2009 and 2017, respectively, that some bacterial or fungal biosynthetic gene clusters are silent when strains are grown in monocultures under standard laboratory conditions but are expressed in intra- or interkingdom co- or multicultures. Furthermore, they could show that some SMs had a higher production rate in multicultures, highlighting that neighbouring organisms induce and increase the SM production in the tested strains.

Bacillus subtilis is a well-studied soil bacterium and is used as a model organism for biofilm formation and sporulation [30]. It has been shown that several members of the *B. subtilis* species complex have exceptional plant growth promoting and plant health improving properties by suppressing plant pathogenic bacteria and fungi [31]. However, it is not completely understood how soil-administered *Bacillus* spp. affect the indigenous microbial communities. Gadhave et al. have shown that the supplementation of *B. subtilis*, *Bacillus amyloliquefaciens* (now identified as *Bacillus velezensis*), and *Bacillus cereus* to the roots of broccoli plants led to species-dependent changes in the diversity, evenness, and relative abundances of endophytic bacterial communities [32]. Like many other soil bacteria, *B. subtilis* and other *Bacillus* spp. produce various SMs [33,34]. The most prominent and bioactive SMs are nonribosomal peptides (NRPs), of which isoforms belong to the families of surfactins, fengycins, or iturins [35,36] (Figure 1). They are biosynthesised by large enzyme complexes, nonribosomal peptide synthetases (NRPSs). For the biosynthesis of *B. subtilis* NRPs, the phosphopantetheinyl transferase *Sfp* is needed since it has been shown to activate the peptidyl carrier protein domains, converting it from the inactive apo-form to the active holo-form [37]. *B. subtilis* has four *sfp*-dependent SMs, of which three are synthesised by NRPS gene clusters (surfactin, plipastatin, and bacillibactin) and one by a hybrid NRPS–PKS gene cluster (bacillaene, Figure 1). The well-studied biosurfactant surfactin, encoded by the *srfAA-AD* gene cluster, reduces the surface tension needed for swarming and sliding motility [38,39]. The surfactin bioactivity is specifically evoked by the surfactant activity triggering cell lysis due to penetration of the bacterial lipid bilayer membranes and the formation of ion-conducting channels [40-42]. The bioactivity of surfactin was shown against *Listeria* spp. and *Legionella monocytogenes* [43,44]. It is presumed that the antifungal plipastatin, expressed from the *ppsA-E* gene cluster, acts as an inhibitor of phospholipase A2, forming pores in the fungal membrane and causing morphological changes in the fungal membrane and cell wall [45,46]. This antifungal potential was demonstrated primarily against various filamentous fungi [47-51]. The broad-spectrum antibiotic bacillaene, synthesised by the *pksB-S* gene cluster, is mainly targeting bacterial protein synthesis [52]. Still, it was also shown that it could protect cells and spores from predation [53]. We recently demonstrated that the production of these NRPs varies among coisolated *B. subtilis* environmental strains due to missing core genes or potentially altered gene regulation, highlighting the existing natural diversity of SM production in this species [51].

In this study, we focus on soil-derived semisynthetic bacterial mock communities and describe how these are affected by a *B. subtilis* strain that was previously isolated from the same sampling site from which the bacterial mock communities originated. With an NRP-mutant-based approach, we investigated

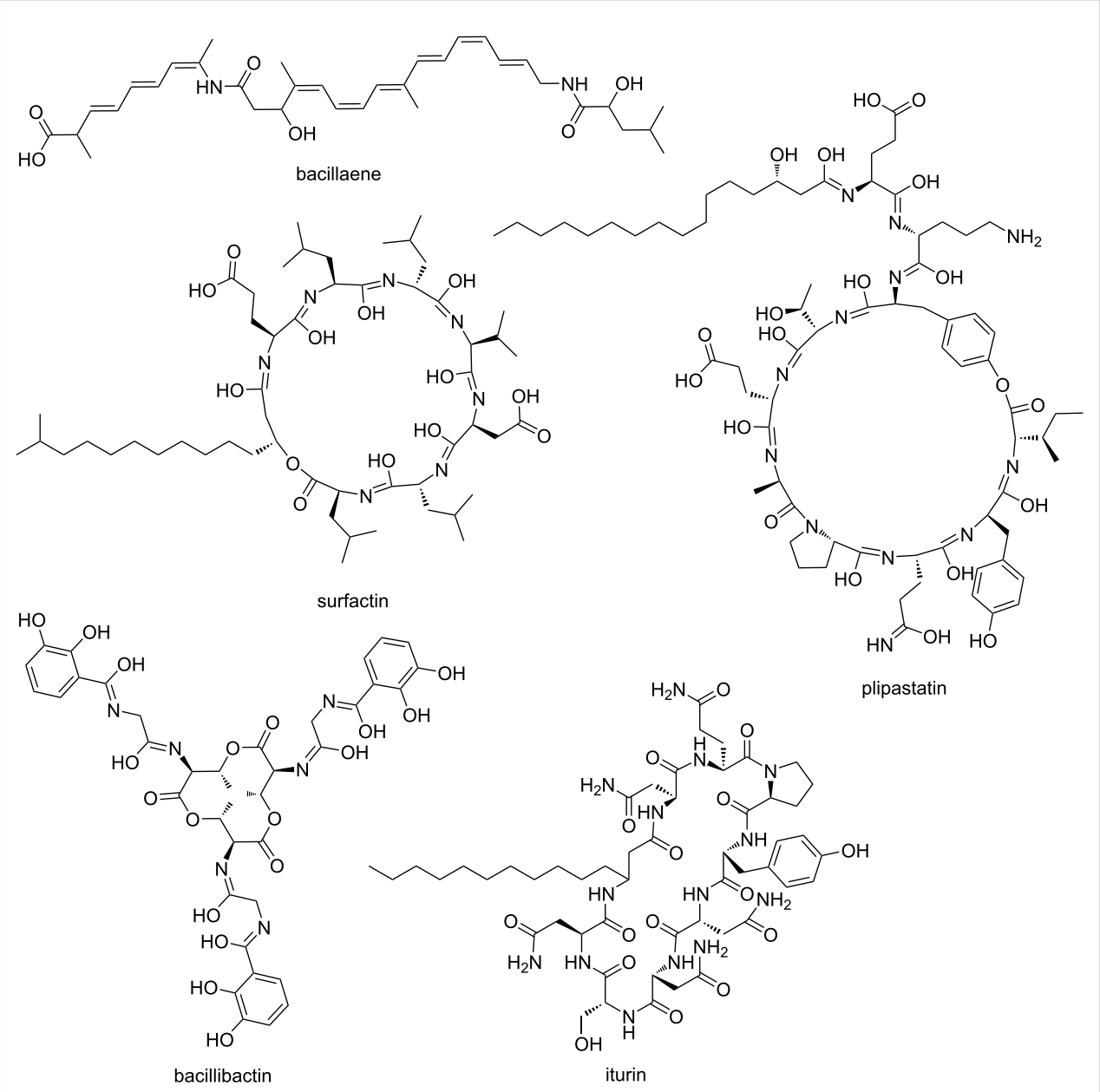

Figure 1: Overview of the NRPs surfactin, plipastatin, bacillibactin, and iturin as well as the hybrid NRP-PK bacillaene produced by *Bacilli*.

the impact of NRPs on the establishment and composition of the bacterial communities. We previously demonstrated that the strain P5_B1 produces the NRPs surfactin and plipastatin and has further BGC predictions for the NRPs bacillaene and bacillibactin [51]. It was revealed by 16S rRNA amplicon sequencing that the established semisynthetic mock communities contained 13 genera with a relative abundance of >0.19% in at least one mock community. Furthermore, it was demonstrated that the addition of *B. subtilis* suppressed the genera *Lysinibacillus* and *Viridibacillus*. Additional optical density (OD)-based growth monitoring of the selected strain *Lysinibacillus fusiformis* M5 confirmed the impact of *B. subtilis*-produced surfactin on the growth.

Results

Impact of *B. subtilis* secondary metabolites on taxonomic groups in semisynthetic mock communities

We established soil-derived semisynthetic mock communities and supplemented them with *B. subtilis* WT P5_B1, the corresponding NRP-deficient strain *sfp*, or the single-NRP mutants

srfAC, Δ*ppsC*, and Δ*pksL*, respectively, incapable of producing either surfactin, plipastatin, or bacillaene, and kept the untreated culture as a control (Figure 2). To investigate the impact of *B. subtilis* NRPs on the bacterial community composition, we sequenced and analysed amplicons of the V3-V4 region of the 16S rRNA gene. The taxonomic summaries give an overview on the relative abundance of the most frequent genera present in each assay and replicate (Figure 3). We investigated the taxonomic level genus since we could not observe any differences among the treated and untreated communities at the class level

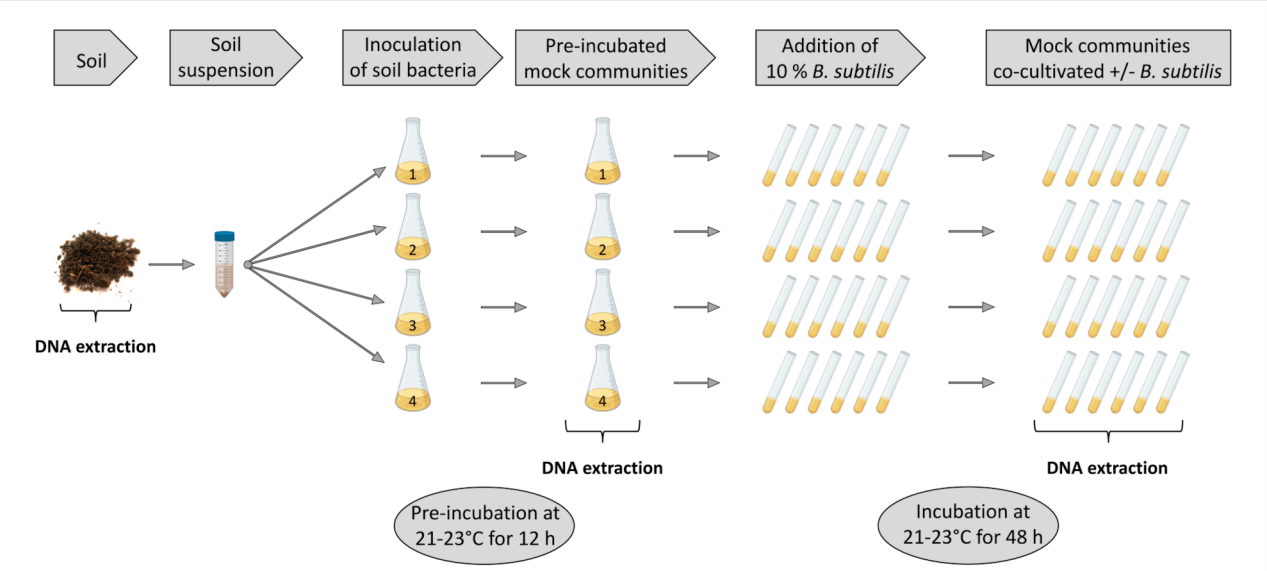

Figure 2: Overview of the experimental setup. A soil suspension, obtained from a soil sample, was used as an inoculum for four independent replicates and preincubated for 12 h. Enriched precultures were aliquoted and supplemented with 10% *B. subtilis* strains or left untreated and incubated for 48 h. DNA was extracted from the soil sample, preincubated soil suspensions, and mock communities. Parts of this figure were created using BioRender.com.

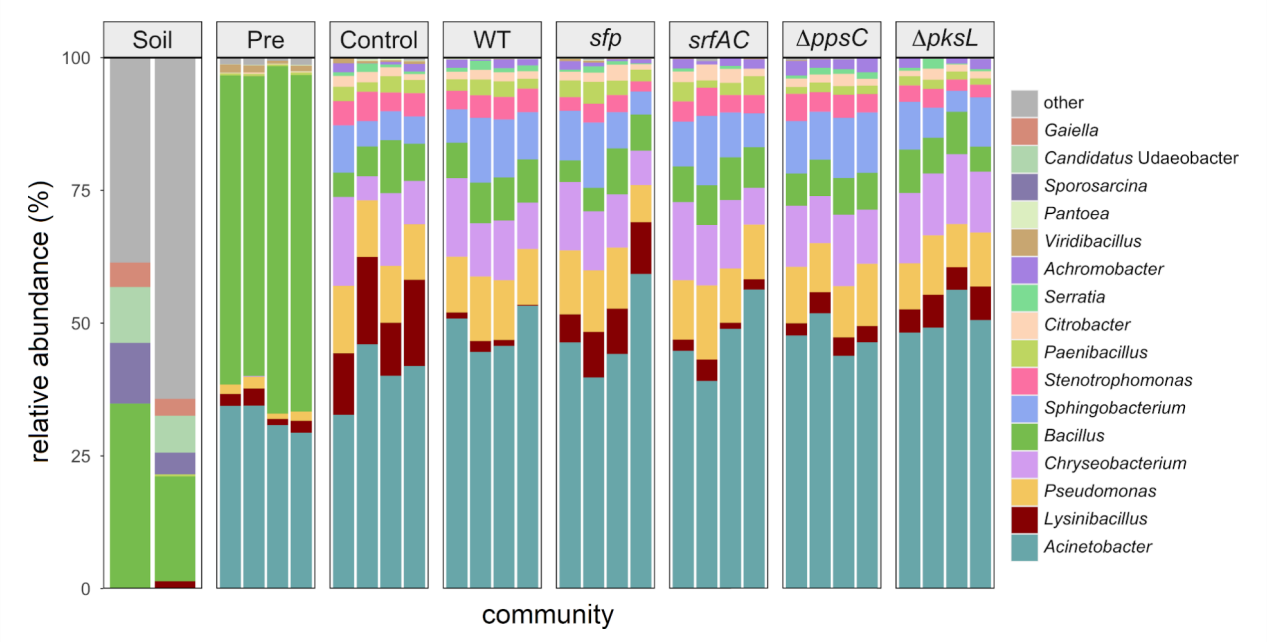

Figure 3: The taxonomic summaries are showing the relative abundance of the most abundant genera for each replicate of the soil sample ("soil"), 12 h preincubated soil suspensions ("Pre"), and untreated ("Control") or treated mock communities with either *B. subtilis* wild type ("WT"), the NRP-deficient strain *sfp*, the surfactin mutant *srfAC*, the plipastatin mutant Δ*ppsC*, or the bacillaene mutant Δ*pksL*, cocultivated for 48 h. Genera are classified as "other" when the relative abundance is <2% ("Soil"), <1% ("Pre"), or <0.19% (in all differently treated mock communities).

and similar observations between the family and the genus levels. Moreover, the targeted V3-V4 region of the 16S rRNA gene does not allow sufficient distinction below this rank. Unsurprisingly, the two soil samples differed tremendously from the in vitro samples and indicated a higher genus richness. We determined that *Bacillus* was the most abundant genus in the two soil samples, with a relative proportion between 19% and 35%. Other genera with an abundance higher than 2% were *Sporosarcina* (4–11%), *Candidatus* Udaeobacter (7–10%), and *Gaiella* (3–4%). The communities of the 12 h precultivated soil suspension consisted primarily of the two genera *Bacillus* (56–65%) and *Acinetobacter* (29–34%). Additional genera with an abundance higher than 1% were *Lysinibacillus* (1.2–3.2%), *Pseudomonas* (1.0–2.2%), and *Viridibacillus* (0.6–1.5%). The genus richness of the four precultured soil suspensions was between 12 and 18 of the total 21 genera.

Diversity analyses were performed to determine the overall impact of the NRPs on the diversity of the bacterial mock communities. The read numbers varied among the different samples (Table S3, Supporting Information File 1), but we had to exclude the sample "Soil 1" from the analysis since it had the lowest read number, and the rarefaction curve was not reaching a clear asymptote (Figure S1, Supporting Information File 1). The alpha diversity revealed that the mock communities cocultivated for 48 h had Shannon indexes between 2.7 and 3.3, and thus a similar genus richness and evenness (Figure 4A). However, it also highlighted that the precultivated communities had the lowest Shannon indexes between 1.8 and 2.1. Consequently, these communities have a lower species evenness and are therefore dominated by fewer species. The soil sample had the highest Shannon index (6.3), which highlights that the richness and evenness are expectedly larger than in the in vitro communities. The alpha diversity of the soil sample and preincubated soil suspensions differed from the mock communities, but we could not see differences between the mock communities.

Therefore, we determined the beta diversity only for the treated and untreated mock communities cocultivated for 48 h. The analysis underlined a high similarity in the composition of the mock communities treated with *B subtilis* strains (Figure 4B). However, the control mock communities separated from the majority of the treated communities along the nonmetric multidimensional scaling 1 (nMDS1) axis. Interestingly, two replicates of the *sfp*-treated communities had a low Bray–Curtis dissimilarity to the control communities, emphasising a high similarity to the untreated control communities. In contrast, the communities supplemented with NRP-producing *B. subtilis* strains clustered together and indicated a lower dissimilarity to each other than to the control communities. Notably, the communities treated with the *srfAC* mutant had a higher dispersion, likely owing to a low number of reads in two of the replicates. We fitted the most correlating ($R^2 > 0.6$) amplicon sequence variants (ASVs) to the nMDS ordination and plotted them as vectors to investigate the differences between the mock communities. The analysis indicated that three ASVs, taxonom-

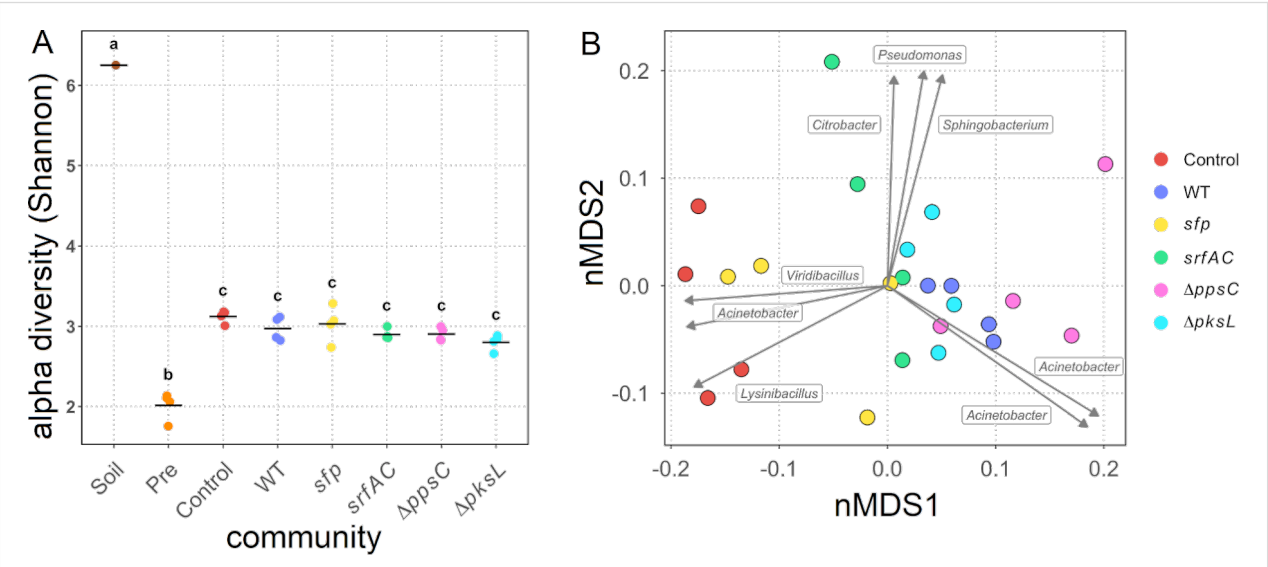

Figure 4: Diversity analyses of the soil sample ("Soil"), 12 h preincubated soil suspensions ("Pre"), and untreated ("Control") or treated mock communities with either *B. subtilis* wild type ("WT"), the NRP-deficient strain *sfp*, the surfactin mutant *srfAC*, the plipastatin mutant Δ*ppsC*, or the bacillaene mutant Δ*pksL*, cocultivated for 48 h. A) Alpha diversity (in Shannon) of the different samples. Each point represents a replicate, while the line indicates the mean of the Shannon diversity indexes. B) Beta diversity of the mock communities calculated with the Bray–Curtis dissimilarity and visualised as circles in a nMDS. The vectors, each labelled with the corresponding genus, represent the ASVs, with the highest correlating with the nMDS ordination. The vector lengths are proportional to the level of correlation.

ically assigned to the genera *Lysinibacillus*, *Acinetobacter*, and *Viridibacillus*, correlated with the control and two *sfp*-treated communities. This observation suggests that the absence of NRP-producing *B. subtilis* resulted in an increased abundance of these. Furthermore, two ASVs of the genus *Acinetobacter* correlated best with the communities supplemented with the NRP-producing *B. subtilis* strains, hinting a higher frequency of these in NRP-treated communities. Additionally, three ASVs, identified as *Pseudomonas*, *Citrobacter*, and *Sphingobacterium*, correlated with two communities treated with the surfactin mutant. A similar but smaller correlation with two bacillaene mutant-treated communities was detectable as well. These results imply a negative impact of either surfactin or bacillaene on the four ASVs. Interestingly, the vector-based analysis suggests that, depending on the ASVs, the genus *Acinetobacter* is both positively and negatively affected by the NRPs.

In conclusion, the alpha diversity analyses revealed that species richness and evenness were reduced in the in vitro communities compared to the soil community. Furthermore, 12 h preincubated soil suspensions showed a reduced diversity compared to the mock communities incubated for 48 h. Nevertheless, we could not detect an effect of the supplemented *B. subtilis* strains on the diversity. However, the beta diversity results suggested that the addition of NRP-producing *B. subtilis* strains influenced the composition of the mock communities. Mainly ASVs belonging to the genera *Lysinibacillus*, *Viridibacillus*, and *Acinetobacter* were affected by the presence or absence of *B. subtilis* NRPs in the bacterial mock communities.

The diversity, in particular the species evenness, increased independently of the treatment in all established mock communities, compared to the precultivated soil suspensions and contained 11–18 genera (Figure 3). The most abundant genera, having a proportion greater than 0.19% in at least one *B. subtilis*-treated or untreated mock community were *Acinetobacter*, *Lysinibacillus*, *Pseudomonas*, *Chryseobacterium*, *Bacillus*, *Sphingobacterium*, *Stenotrophomonas*, *Paenibacillus*, *Citrobacter*, *Serratia*, *Achromobacter*, *Viridibacillus*, and *Pantoea*. Noteworthy, the prevalence of the *Bacillus* genus was comparable in the *B. subtilis*-treated communities (4–9%) and the control (5–10%). In the latter, the present *Bacillus* ssp. originated only from the soil suspension, highlighting that the additional supplementation of *B. subtilis* did not affect the relative abundance of the genus *Bacillus* after 48 h cocultivation. Interestingly, the only genera detected in both the in vitro mock communities and the soil samples were *Bacillus*, *Lysinibacillus*, and *Paenibacillus*. The remaining most abundant genera in the mock communities were below the detection limit.

The comparison of the abundance ratios between the control communities and *B. subtilis* WT-treated communities revealed that *Lysinibacillus* and *Viridibacillus* were significantly decreased 9.4-fold ($P \leq 0.001$) and 8.3-fold ($P \leq 0.01$), respectively, in the communities supplemented with *B. subtilis* WT (Figure 5A). None of the other genera was affected by the addition of this strain. In comparison, we could only detect a 1.8-fold significant reduction ($P \leq 0.05$) of *Lysinibacillus* in the *sfp*-treated communities compared to the untreated communities, and thus a greatly diminished effect compared to the

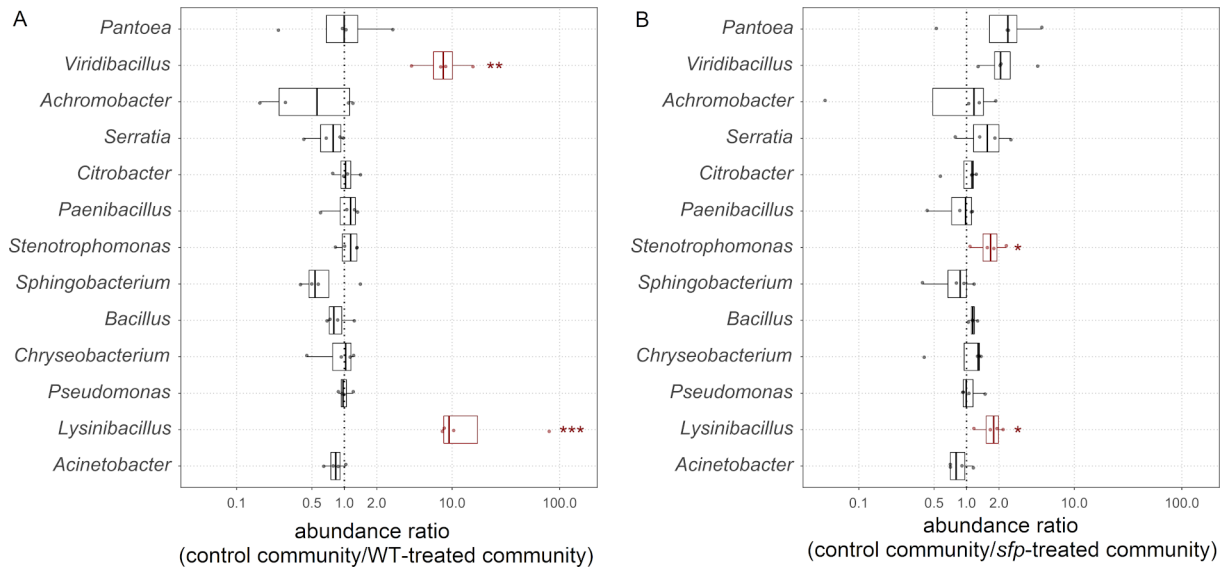

Figure 5: Abundance ratios for each genus and replicate (points) in the control community compared to the WT-treated (A) and to the *sfp*-treated community (B). Red-box plots highlight the statistical significance, which is defined as $P \leq 0.05$ (*), $P \leq 0.01$ (**), and $P \leq 0.001$ (***).

WT-treated samples was evident (Figure 5B). Also, we could not observe a significant reduction of *Viridibacillus*, but besides *Lysinibacillus*, also *Stenotrophomonas* was 1.7-fold ($P \leq 0.05$) significantly reduced in these communities. The direct comparison of WT- and *sfp*-treated communities confirmed the NRP-dependent suppression of both *Lysinibacillus* and *Viridibacillus* in the WT-treated communities and the suppression of *Stenotrophomonas* in the *sfp*-treated communities (Figure S2, Supporting Information File 1).

Concentrating on *Lysinibacillus*, the highest abundance of this genus was discernible in the control assays (13.9%), which was significantly different compared to all other *B. subtilis*-treated assays (Figure 6). However, when *B. subtilis* P5_B1 WT was added to the mock communities, a significant decrease ($P \leq 0.001$) of *Lysinibacillus* (1.2%) compared to the control communities was discovered. Furthermore, when we added the NRP-deficient strain *sfp*, we could notice a significantly higher abundance of *Lysinibacillus* (8.6%) compared to the WT-treated communities ($P \leq 0.001$) but still a significantly lower prevalence compared to the control communities ($P \leq 0.05$). Compared to the WT-treated communities, the frequency of *Lysinibacillus* was slightly but not significantly higher in the communities treated with the single-NRP mutants *srfAC* (2.0%) and Δ*ppsC* (3.3%). The abundance of *Lysinibacillus* in the assays containing the Δ*pksL* strain (5.3%) was significantly higher ($P \leq 0.01$) than in the WT-treated assays. However, the *Lysinibacillus* abundance in Δ*pksL*-treated communities was not significantly different from the Δ*ppsC*- or *sfp*-treated communities. In summary, *Lysinibacillus* was affected by the addition of *B. subtilis* independent of the NRPs, but when *B. subtilis* strains capable of producing them were present, the impact on *Lysinibacillus* was enhanced. Furthermore, the results indicate that bacillaene had the strongest and surfactin the weakest effect on *Lysinibacillus* in the mock communities.

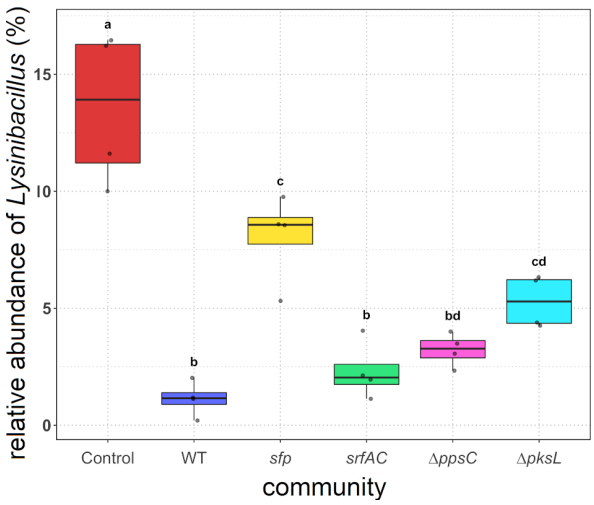

Figure 6: The relative abundance of *Lysinibacillus* in the untreated ("Control") and treated mock communities with either *B. subtilis* wild type ("WT"), the NRP-deficient strain *sfp*, the surfactin mutant *srfAC*, the plipastatin mutant Δ*ppsC*, or the bacillaene mutant Δ*pksL*, cocultivated for 48 h. The points represent the abundance in each replicate. Treatments with different letters are significantly different ($P \leq 0.05$).

The second genus affected by the addition of *B. subtilis* was *Viridibacillus*, which had a very low abundance in the control mock communities (0.49%) compared to *Lysinibacillus* (Figure S3, Supporting Information File 1). However, when *B. subtilis* WT was added to the community, *Viridibacillus* indicated a significantly lower ($P \leq 0.01$) abundance (0.03%) compared to the control communities. Notably, in two of the WT-treated community replicates, *Viridibacillus* was below the detection level. Nevertheless, the abundance of this genus in the *sfp*-treated communities (0.26%) was statistically not significant in comparison to the WT and the control communities. Furthermore, the addition of the single-NRP mutants *srfAC*, Δ*ppsC*, and Δ*pksL* resulted in communities with *Viridibacillus* frequencies similar to the WT-treated communities (0.08%, 0.05%, and 0.00%, respectively). *Viridibacillus* as well as *Lysinibacillus* was affected by the addition of *B. subtilis* to the communities. However, no particular NRP could be assigned to the reduced frequency of *Viridibacillus*.

Growth properties of *L. fusiformis* M5 supplemented with *B. subtilis* spent media

The main finding from the semisynthetic mock community experiment indicated that the genus *Lysinibacillus* was negatively affected by the addition of *B. subtilis* P5_B1 WT and that NRPs enhance the suppression. To dissect the direct impact of a particular NRP in this inhibition, we monitored the growth of *L. fusiformis* M5, a previously isolated *Lysinibacillus* species [54], over 24 h when treated with different proportions of spent media from *B. subtilis* WT and the corresponding NRP mutants (Figure 7). When we added 52.80% of spent medium to *L. fusiformis,* we observed the fastest entry into the exponential growth phase in the untreated assay. Interestingly, the addition of spent medium of either WT, Δ*ppsC*, or Δ*pksL* caused a delay of entering into this growth phase of approximately 11–13 h in *L. fusiformis* compared to the control. Such a strong effect was not observed when the spent medium of the *sfp* or *srfAC* mutant was added. The addition of these two spent media caused only a slight delay of the exponential growth phase of *L. fusiformis*, although spent *sfp* medium had a lower effect on *L. fusiformis* compared to spent *srfAC* medium. When 23.00% of spent medium was added, no growth differences could be detected anymore between the control and the *sfp*-treated assays in the exponential growth phase. Furthermore, the effect of spent WT

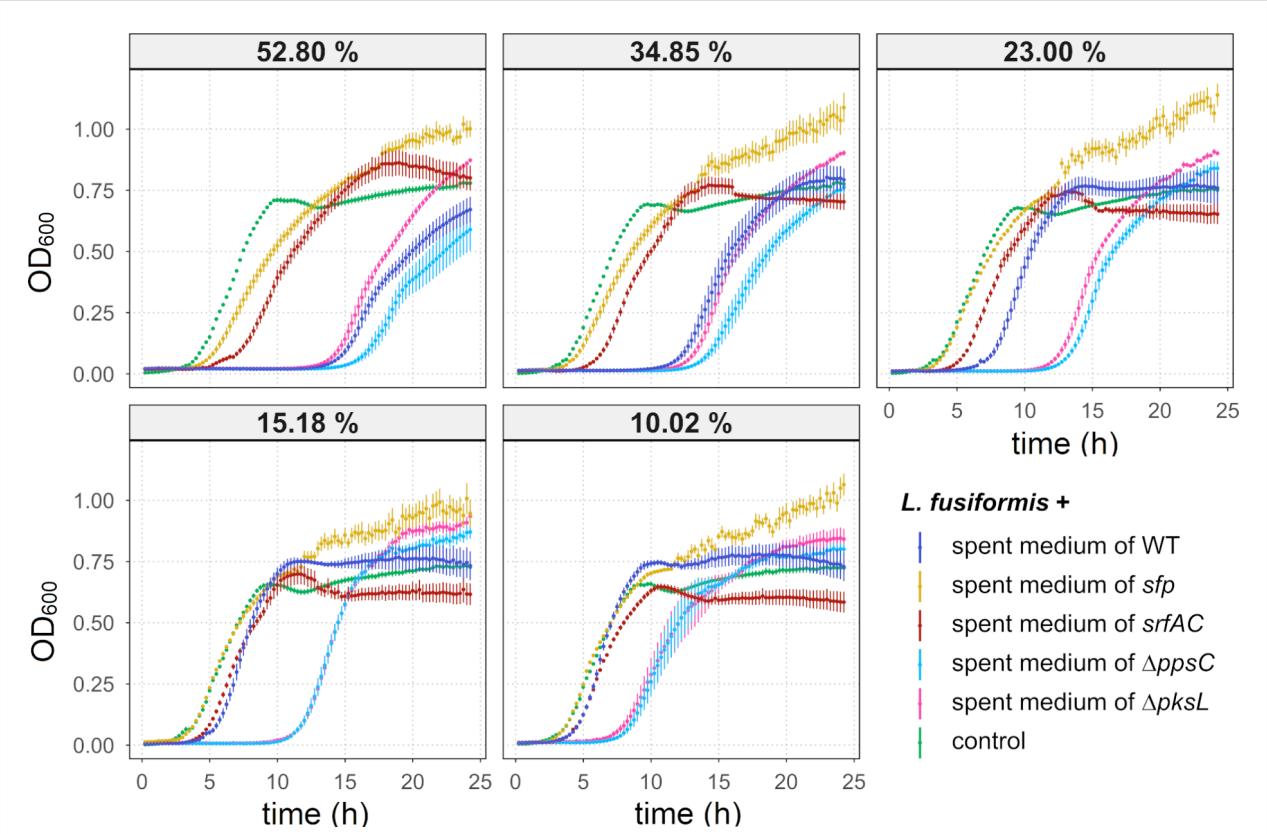

Figure 7: Growth curves of *L. fusiformis* M5 exposed to spent media from 48 h *B. subtilis* cultures and without treatment ("control"). The spent medium concentration of 10.02% to 52.80%, acquired with a serial dilution, indicates the proportion of spent medium from the total volume. The error bars represent the standard error. $N \geq 6$. OD_{600} = optical density at 600 nm.

medium seems to be reduced at this concentration, but the spent media of Δ*ppsC* and Δ*pksL* maintained their growth inhibition potential. The lowest concentration of a spent medium having an inhibitory effect was 10.02%. At this concentration, only the spent media of Δ*ppsC* and Δ*pksL* affected the growth of *L. fusiformis*, even though it was weakened compared to using higher concentrations. Intriguingly, a higher level of aggregation was observed in the *L. fusiformis* assays supplemented with the spent medium of *sfp* compared to the other assays, which caused higher and variable OD measurements in the stationary phase of the growth curves (Figure S4, Supporting Information File 1). Finally, it was noted that the final cell density was slightly higher in the assays supplemented with the spent medium compared to the control assays.

These results revealed that *B. subtilis*-mediated inhibition of *L. fusiformis* is NRP-dependent since the spent medium of the NRP-deficient strain *sfp* had an only minor impact. Moreover, we hypothesise that surfactin is responsible for the direct inhibitory effect on *L. fusiformis*, as this was the only spent medium of an NRP mutant strain with lowered inhibition compared to spent media of other single NRP mutants.

Impact of surfactin on the growth of *L. fusiformis*

To confirm the inhibitory effect of surfactin on *L. fusiformis*, we exposed this strain to different concentrations of pure surfactin dissolved in methanol and monitored its growth over 24 h. The growth of *L. fusiformis* was delayed in the exponential growth phase when surfactin was supplemented in concentrations between 31.25 µg/mL and 500 µg/mL (Figure 8). At a surfactin concentration of 500 µg/mL, the cell density in the stationary phase was lower than the control. At a concentration of 250 µg/mL, the cell density reached a level similar to the untreated control. However, when surfactin was added in concentrations between 125 and 31.25 µg/mL, after an initial growth delay into the exponential phase, the cell densities in all treatments exceeded the ones of the control. The highest concentration of the solvent methanol of 5% had only a minor inhibiting effect on *L. fusiformis,* whereas lower concentrations of methanol showed no inhibition (Figure S5, Supporting Information File 1). These results suggest that surfactin has growth inhibitory effects on *L. fusiformis,* and we hypothesise that it might act as the key inhibitory *B. subtilis* NRP under the tested conditions.

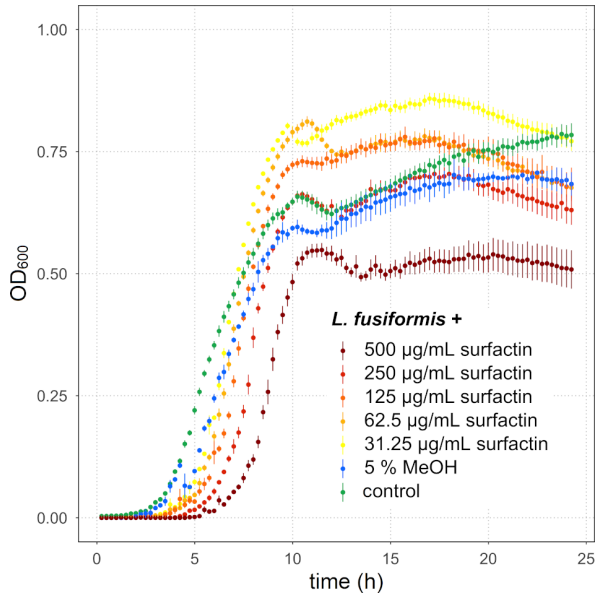

Figure 8: Growth curves of *L. fusiformis* M5 exposed to different concentrations of surfactin, the highest concentration of the solvent MeOH, and without treatment ("control"). The error bars represent the standard error. $N \geq 5$ (control and surfactin-treated assays), $N = 2$ (MeOH-treated assays).

Discussion

B. subtilis is known to produce a wide range of different SMs that target a large number of various micro- and macroorganisms [35]. Our study demonstrates that the NRPs produced by the recently isolated environmental strain of *B. subtilis* P5_B1 did not strongly impact the overall soil-derived semisynthetic mock community but reduced the abundance of the genera *Lysinibacillus* and *Viridibacillus* (Figure 9). Moreover, it reveals that the strain *L. fusiformis* M5 was directly affected by the *B. subtilis* lipopeptide surfactin in a monitored growth experiment.

We studied the bacterial community compositions by sequencing the two variable regions V3 and V4 of the 16S rRNA gene. Noteworthy, some limitations of this technique are well known. In 2014, Poretsky et al. revealed that amplicon sequencing of the 16S rRNA gene indicates a lower sequence diversity and substantial differences in the relative abundances of specific genus-assigned taxa compared to metagenomics [55]. Moreover, 16S amplicon sequencing of single variable regions rarely allows sufficient discrimination below the family or genus level, and therefore intragenus differentiation and heterogeneity cannot be addressed [55]. Furthermore, the fundamental problem is that bacteria harbour various copy numbers of the 16S rRNA gene in the genomes, which biases quantification studies [56]. Alpha diversity analyses based on the Shannon estimation revealed that diversity was strongly reduced in in vitro cultivations. Furthermore, it was disclosed that the precultured soil suspension had the lowest diversity index because mainly the genera *Bacillus* and *Acinetobacter* were enriched, which can probably be traced back to different growth rates among the present species. A substantial shift in the community compositions was observed between in vivo and in vitro communities since the majority of the genera present in the in vitro communities was below the detection limit in the soil sample. However, during the 12 h precultivation of the soil suspension, bacteria were exposed to different nutrient availabilities, changed physical conditions, such as the temperature, a liquid environment, and the loss of the spatial soil structure. These conditions were most likely selecting for generalist bacteria capable of proliferating under the given conditions and independently from other bacteria. During the following 48 h cocultivation, depletion of the primary nutrient sources and metabolic cross-feeding further shaped the community assembly. In 2018, Goldford et al. revealed that the main sources of metabolic cross-feeding are secreted metabolic byproducts from the community members [57]. They further highlighted that bacterial communities stabilised after approximately eight to nine 48 h cocultivations. In our study, bacterial communities were only cocultivated once for 48 h, suggesting that the assembly of the bacterial communities has not yet reached a stable phase, which explains the differences between the precultures and cocultivated mock communities.

The Shannon index showed no differences among the established and differently treated mock communities, which primarily consisted of 13 genera. Even though *Bacillus* was the most abundant genus in the precultures, further incubation for 48 h resulted in a decreased relative abundance independently if the respective *B. subtilis* strains were seeded or the precultures were untreated. It shows that the initial dominance of *Bacillus* could not be maintained at prolonged incubation. The *B. subtilis* strains were added at a community assembly phase when *Bacillus* was the dominating genus, so that the general genera distribution was not expected to be influenced extensively. Nevertheless, after 48 h cocultivation, the final relative abundance of the *Bacillus* genus was not increased in the communities treated with *B. subtilis* when compared to the control. This observation highlights that the presence or absence of NRPs did not affect the competitiveness of *B. subtilis*. However, the 16S amplicon sequencing did not allow the detection of interactions and competitions within the *Bacillus* genus. The composition of this genus could vary among the differently treated communities. Nonetheless, the beta diversity analysis indicated a dissimilarity between the untreated and treated mock communities. Besides, two of the communities treated with the *sfp* mutant showed the highest similarity to the untreated communities,

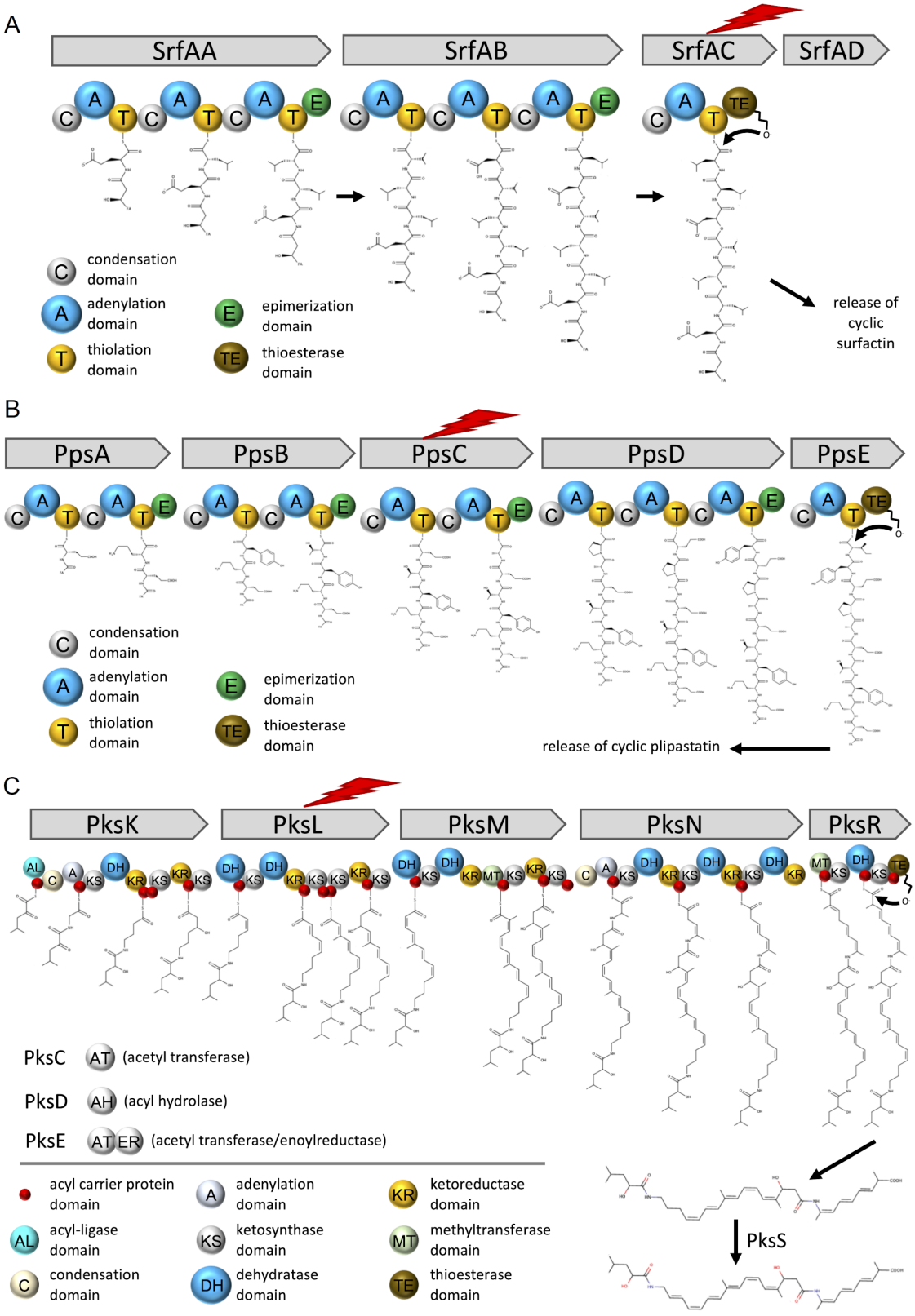

Figure 9: Overview on the biosynthetic pathways of surfactin (A), plipastatin (B), and bacillaene (C) produced by *B. subtilis*. The lightning bolt indicates the proteins for which the corresponding coding genes were deleted in the mutant strains.

suggesting that the supplementation of the NRP-producing *B. subtilis* strains affected the communities. The vectors of *Acinetobacter* ASVs had a direction either to NRP-treated or NRP-untreated communities, indicating that the NRPs influenced species within the same genus differently.

In microbial communities, the amount of interactions and relations increases with the number of community members. The established semisynthetic mock communities in this study contained at least 13 genera with a relative abundance >0.19%. Therefore, it can be assumed that various interactions between them occurred. Nevertheless, we could observe statistically significant reductions of the two genera, *Lysinibacillus* and *Viridibacillus*, in communities supplemented with the NRP-producing *B. subtilis* wild type strain. In contrast, in communities supplemented with the NRP-deficient mutant *sfp*, *Lysinibacillus* was more frequent than in the wild type-treated communities. This observation indicates that NRPs have a great impact on suppressing *Lysinibacillus*. However, further factors are involved in the suppression since the *sfp* mutant maintained a reduction of *Lysinibacillus*, even though to a weaker extent. Moreover, no particular NRP could be allocated to the inhibition of the *Lysinibacillus* genus in these semisynthetic communities, but bacillaene displayed the highest impact on the suppression. An inhibition of *Viridibacillus* mediated by NRPs was also observable, but for this genus, bacillaene had the lowest impact. However, these results must be interpreted with caution and need further investigations since *Viridibacillus* was one of the lowest abundant genera in the mock communities, and abundance calculations are sensitive to the depth of sequencing. Besides the suppression of *Lysinibacillus* and *Viridibacillus*, *Stenotrophomonas* was uniquely suppressed in the communities supplemented with the *sfp* mutant but not when the WT strain was added. This observation might be evoked by inhibiting other species, which in turn facilitates a lower inhibition of *Stenotrophomonas*.

Previous studies revealed that the introduction of SM-producing bacteria to a bacterial community had no major impact on the entire composition. The tropodithietic acid-producing marine bacterium *Phaeobacter inhibens* did not strongly influence the microbiome diversity of the oyster *Ostrea edulis* but reduced the relative abundance of the orders Vibrionales and Mycoplasmatales [58]. Similar results were achieved when *B. velezensis* FZB42 was successfully applied as a biocontrol agent to lettuce in soil [59]. The authors could not see a substantial impact on the rhizosphere bacterial community by the supplemented biocontrol strain, whereas the sampling time and additional inoculation of the fungal plant pathogen influenced the community to a greater extent. Apart from soluble SM, volatile organic compounds (VOCs) are as well capable of impacting a microbial community. In 2020, Cosetta et al. demonstrated that VOCs of cheese rind-associated fungi have both growth-stimulating and -inhibiting properties on members of the rind microbiome [60]. The authors could reveal that the VOC-mediated shift of the bacterial community was caused due to growth promotion of *Vibrio* spp. These studies and the results from the semisynthetic mock community experiment of this study highlight that the overall impact of SMs on the targeted microbial communities is low, which suggests that they are no mass destruction compounds. However, in all communities, distinct genera or species were suppressed or promoted, emphasising the potential of SMs to shape microbial communities.

To investigate if *Lysinibacillus* is sensitive to any particular NRP of *B. subtilis*, we exposed the isolate *L. fusiformis* M5 to the spent media of the respective *B. subtilis* strains and monitored the growth. *L. fusiformis* M5 has been isolated from soil and demonstrated to impact the biofilm colony development of *B. subtilis* [54]. Interestingly, the modulation of the biofilm development was mediated by the primary metabolite hypoxanthine secreted by *L. fusiformis*. Of note, the impact of *B. subtilis* was not noticed on *L. fusiformis* in the mixed colony biofilm communities, possibly due to the use of the NRP-negative *B. subtilis* strain 168, which harbours a spontaneous frameshift mutation in the *sfp* gene [54]. Testing the impact of the natural isolate *B. subtilis* P5_B1 and the corresponding NRP mutant derivatives revealed that the spent media from both the NRP-deficient strain *sfp* and the surfactin-deficient strain *srfAC* had the lowest impact on the growth of *L. fusiformis*. In addition, the spent media of Δ*ppsC* and Δ*pksL* maintained the bioactivity at low concentrations, whereas the effect of WT was already strongly reduced at this level of the spent medium. This difference could occur, on the one hand, due to higher levels of surfactin in the two mutants compared to the wild type. On the other hand, the spent medium originated from cultures with an OD_{600} value of 3.0. Cultures with higher ODs were diluted before the harvesting, and WT cultures exhibited overall the highest ODs among the strains. Since the NRPs concentration is not proportional to the final OD due to, e.g., the occurrence of cell lysis, the spent media might be slightly differently diluted among the strains. Therefore, minor differences might be observable in the assays supplemented with highly diluted spent media. The observation that *L. fusiformis* displays a slightly higher cell density when the bacterial spent medium is supplemented might be due to the availability of additional nutrients. Nevertheless, the supernatant and pure compound supplementation demonstrated that surfactin is a direct suppressor of *L. fusiformis*. However, as the spent media of the *sfp* and *srfAC* strains still had a growth inhibition effect, it is plausible that next to surfactin, further NRPs and even other compounds might provoke a slight growth suppression of *Lysinibacillus*.

When *L. fusiformis* was exposed to surfactin concentrations between 31.25 and 125 µg/mL, higher final cell densities were detectable compared to assays treated with higher levels of surfactin or in the control. Interestingly, in 2020, Arjes et al. demonstrated that surfactin enhances the availability of oxygen to *B. subtilis* by increasing the oxygen diffusivity [61], which might also positively affect the growth of *L. fusiformis*.

Experiments with differently treated semisynthetic mock communities have demonstrated that *Lysinibacillus* and *Viridibacillus* were affected by the addition of an NRPs-producing *B. subtilis* strain. *Lysinibacillus* was least affected in the mock communities supplemented with the *B. subtilis* Δ*pksL* strain incapable of producing bacillaene, suggesting that bacillaene is the most active compound against this genus. In contrast, the growth curve experiments showed that *L. fusiformis* M5 is most sensitive to surfactin. Importantly, our analysis does not reveal which *Lysinibacillus* species were present in the mock communities, and therefore their sensitivity might be different from the test species *L. fusiformis* used. Moreover, the spent medium was harvested from pure cultures of *B. subtilis* grown in an undiluted complex medium, which might have changed the production of NRPs due to the lacking impact of the community members and the level of nutrients. Thus, lower concentrations of the NRPs in the mock communities might affect *Lysinibacillus* differently compared to the monoculture growth experiments supplemented with spent media. Finally, *Lysinibacillus* can also be affected indirectly by *B. subtilis* NRPs in the mock communities. Bacillaene is described as a wide-spectrum antibiotic disrupting the protein synthesis in bacteria [34,52]. The observations suggest that it has the most substantial impact on specific members of the mock community, and consequently an indirect effect on *Lysinibacillus*. Nevertheless, the exact mechanisms at play remain to be deciphered.

Interestingly, the two genera *Lysinibacillus* and *Viridibacillus* of the mock communities are, besides *Paenibacillus*, the closest relatives of *B. subtilis*. The fact that suppression effects are only observable for these genera could presumably be caused by the higher overlap in the ecological niches, triggering competition for the same nutrients. Indeed, a higher phylogenetic and metabolic similarity between bacteria increases the probability of antagonism [62].

We could not quantify the concentrations of *B. subtilis* NRPs in the mock communities since the detection of low concentrations is still under development. However, a better understanding of their impact on the mock communities could be realised by further experiments investigating the effect of supplemented pure NRP compounds, e.g., surfactin and bacillaene. The impact of antibiotics on algae-associated bacterial communities was investigated by Geng et al. in 2016, who revealed a dose-depended influence of pure tropodithietic acid on the microbiome structure of *Nannochloropsis salina* [63]. Such pure NRP supplementations in various concentrations would allow exploring their effects on bacterial community assembly. Furthermore, in vivo experiments could reveal the impact of NRPs on microbial communities in complex natural systems, similar to the study from Chowdhury et al. from 2013 [59]. Noteworthy, our study focused only on NRPs, but additional SMs, such as bacteriocins, are predicted for *B. subtilis* P5_B1 as well [51]. Future investigations should investigate the impact of both bacteriocins and NRPs on microbial communities.

Conclusion

In summary, this study demonstrates that nonribosomal peptides of *B. subtilis* P5_B1 have only a minor impact on the overall structure of soil-derived semisynthetic bacterial mock communities but suppress the genera *Lysinibacillus* and *Viridibacillus* significantly. Furthermore, it highlights the bioactivity of surfactin against *L. fusiformis* M5.

Experimental

Strains, media, and chemicals

All strains used in this study are listed in Table S1, Supporting Information File 1. For routine growth, bacterial cells were cultured in tryptic soy broth (TSB, CASO Broth, Sigma-Aldrich) containing 17 $g \cdot L^{-1}$ casein peptone, 3 $g \cdot L^{-1}$ soy peptone, 5 $g \cdot L^{-1}$ sodium chloride, 2.5 $g \cdot L^{-1}$ dipotassium hydrogen phosphate, and 2.5 $g \cdot L^{-1}$ glucose.

Semisynthetic mock community assay

Semisynthetic soil communities were obtained from the soil of sampling site P5 (55.788800, 12.558300) [51,64]. 1 g soil was mixed in a 1:9 ratio with a 0.9% saline solution, vortexed on a rotary shaker for 15 min, and allowed to sediment for 2 min. Four independent communities were established by inoculating 10-times diluted TSB (0.1 × TSB) with 1% soil suspension taken from the middle part of the liquid phase, followed by incubation at 21–23 °C and 250 rpm for 12 h. Simultaneously, pregrown *B. subtilis* P5_B1 WT and the corresponding NRP mutant derivatives were inoculated in 0.1 × TSB and incubated in parallel using the same conditions. After 12 h precultivation, 3 mL aliquots of the soil suspension were transferred into six glass tubes. One tube was left untreated and functioned as control, whereas the remaining five were supplemented with respective *B. subtilis* strains by adding 10% of the final volume. The cultures were incubated at 21–23 °C and 250 rpm for 48 h. DNA was extracted from two replicates of the initial soil sample, the 12 h precultivated soil suspensions and the

B. subtilis-treated or untreated mock communities cocultivated for 48 h.

DNA extraction

Environmental- and semisynthetic-community genomic DNA was extracted from either 250 mg soil or 250 µL bacterial culture, respectively, by using the DNeasy PowerSoil Pro Kit (QIAGEN) and following the manufacturer's instructions.

Amplification of 16S rRNA hypervariable regions V3-V4

The V3-V4 region of the 16S rRNA gene was PCR-amplified from the extracted DNA samples using Fw_V3V4 (5'-CCTACGGGNGGCWGCAG-3') and Rv_V3V4 (5'-GACTACHVGGGTATCTAATCC-3') primers that were tagged with short barcodes with a length of eight nucleotides, listed in Table S2, Supporting Information File 1. The PCR reactions contained 10.6 µL DNase-free water, 12.5 µL TEMPase Hot Start 2x Master Mix, 0.8 µL of each primer (10 µM), and 0.3 µL of 50 ng/µL DNA template. The PCR was performed using the conditions of 95 °C for 15 min, followed by 30 cycles of 95 °C for 30 s, 62 °C for 30 s, 72 °C for 30 s, and finally, 72 °C for 5 min. All V3-V4 amplicons were purified using the NucleoSpin gel and PCR cleanup kit (Macherey-Nagel) and pooled in equimolar ratios. The amplicon pool was submitted to Novogene Europe Company Limited (United Kingdom) for high-throughput sequencing on an Illumina NovaSeq 6000 platform with 2 million reads (2 × 250 bp paired-end reads). Raw sequence data is available at NCBI: PRJNA658074.

Sequencing data preprocessing

The multiplexed sequencing data was imported into the QIIME 2 pipeline (version 2020.6) [65,66]. The paired-end sequences were demultiplexed with the QIIME 2 plugin cutadapt [67]. The minimum overlap of partial matches between the read and the barcode sequence was set to 5 nucleotides to reduce random matches. The QIIME 2 implementation DADA2 was used to denoise and merge paired-end reads [68]. In total, 362,475 reads were assigned to the respective samples with an average of 12,083 reads per sample (range: 751 to 34,802; Table S3, Supporting Information File 1). The 16S rRNA reference sequences with a 99% identity criterion obtained from the SILVA database release 132 were trimmed to the V3-V4 region, bound by the primer pair used for amplification, and the product length was limited to 200–500 nucleotides [69]. The taxonomy was assigned to the sequences in the feature table generated by DADA2 by using the VSEARCH-based consensus taxonomy classifier [70]. A tree for phylogenetic diversity analyses was generated with FastTree 2 from the representative sequences [71-73].

Relative species abundance and phylogenetic diversity analyses

QIIME 2 artefacts were imported into the R software (4.0.2) with the R package qiime2R, and further analyses were conducted in the R package phyloseq [74-76]. The taxonomy summaries were achieved by merging ASVs of the same genera and calculating their relative abundance in each sample. Differences in the presence of the most abundant genera in the control communities, in the communities supplemented with *B. subtilis* WT as well as in the communities supplemented with *B. subtilis sfp*, were investigated by calculating the abundance ratios of the different treated communities for each replicate. If species were not detected in some of the replicates, 0 values were replaced with the lowest detected value of the genus to avoid infinite values or 0 values in the ratio calculations. Rarefaction curves of the samples were calculated and visualised with the R package ranacapa [77]. Diversity analyses of the *B. subtilis*-treated and untreated samples were performed with ASV counts multiplied by factor 100,000 and transformed into integer proportions. The alpha diversity was estimated with the Shannon diversity index in the R package phyloseq [76]. The beta diversity was determined by dissimilarities among the samples with the Bray–Curtis distance and visualised in a nMDS with the R package vegan [78]. The correlation of individual ASVs on the overall bacterial community composition was calculated with the envfit function with 999 permutations from the R package vegan. The most correlating ($R^2 > 0.6$) ASVs were added to the nMDS ordination plot. All graphical visualisations were realised with ggplot2 [79].

Statistical analysis

The statistical significance was determined with the square roots of the tested values. The normality and equality of the variances were tested with the Shapiro–Wilk normality test and the Levene test, respectively. If one of the tests was rejected, the nonparametric Kruskal–Wallis rank sum test was performed instead. The statistical significance of pairs was determined with the Welch two-sample t-test, and the differences among groups >2 was determined with the one-way analysis of variance (ANOVA) test and the Tukey HSD test. The statistical significance was determined with an alpha level <0.05.

Growth monitoring of *L. fusiformis* supplemented with *B. subtilis* spent media and pure surfactin

Spent media of *B. subtilis* strains were harvested from cultures grown in TSB medium at 37 °C and 250 rpm for 48 h immediately before the growth experiments. The cultures were adjusted to OD_{600} 3.0 and centrifuged for 4 min at 5,000*g*. Subsequently,

the supernatants were passed through 0.22 µm filters and stored at 4 °C. The growth experiments were performed in 96-well microplates. The wells of the first column were filled with 30 µL 10 × TSB, 30 µL *L. fusiformis* culture adjusted to OD_{600} 0.1 in 1 × TSB, and 240 µL of the appropriate spent *B. subtilis* medium or water (untreated control). 100 µL *L. fusiformis* culture adjusted to OD_{600} 0.01 in 1 × TSB was added to the wells of the remaining columns. A 1.5-fold serial dilution of the spent media was performed column-by-column. A surfactin stock solution was prepared by dissolving 10 mg of surfactin (Sigma-Aldrich) in 1 mL methanol (MeOH). The wells of the first column were filled with 170 µL 1 × TSB, 20 µL *L. fusiformis* culture adjusted to OD_{600} 0.1 in 1 × TSB, and 10 µL surfactin, 10 µL MeOH (solvent control), or 10 µL 1 × TSB (untreated control). To the wells of the remaining columns, 100 µL *L. fusiformis* culture was added adjusted to OD_{600} 0.01 in 1 × TSB. A 2-fold serial dilution of surfactin or MeOH was performed column-by-column. In both assays, the growth of *L. fusiformis* was monitored in a microplate reader (BioTek Synergy HTX Multi-Mode Microplate Reader). The microplates were incubated at 30 °C with continuous shaking (548 cpm, 2 mm), and the OD_{600} was measured in 15 min intervals over 24 h. All graphical visualisations were prepared using ggplot2 [79].

Supporting Information

Supporting Information File 1

Bacterial strains used in this study, 16S rRNA V3-V4 primer list, number of sequencing reads per sample, and supporting figures.
[https://www.beilstein-journals.org/bjoc/content/supplementary/1860-5397-16-248-S1.pdf]

Acknowledgements

The authors thank the suggestions of Lone Gram and the CeMiSt centre members on the project. A part of the graphical abstract was created using BioRender.com.

Funding

This project was supported by the Danish National Research Foundation (DNRF137) for the Center for Microbial Secondary Metabolites (CeMiSt).

ORCID® iDs

Heiko T. Kiesewalter - https://orcid.org/0000-0001-9966-5894
Carlos N. Lozano-Andrade - https://orcid.org/0000-0003-2805-4505
Mikael L. Strube - https://orcid.org/0000-0003-0905-5705
Ákos T. Kovács - https://orcid.org/0000-0002-4465-1636

Preprint

A non-peer-reviewed version of this article has been previously published as a preprint: https://doi.org/10.1101/2020.08.20.259788

References

1. Falkowski, P. G.; Fenchel, T.; Delong, E. F. *Science* **2008,** *320,* 1034–1039. doi:10.1126/science.1153213
2. Sunagawa, S.; Coelho, L. P.; Chaffron, S.; Kultima, J. R.; Labadie, K.; Salazar, G.; Djahanschiri, B.; Zeller, G.; Mende, D. R.; Alberti, A.; Cornejo-Castillo, F. M.; Costea, P. I.; Cruaud, C.; d'Ovidio, F.; Engelen, S.; Ferrera, I.; Gasol, J. M.; Guidi, L.; Hildebrand, F.; Kokoszka, F.; Lepoivre, C.; Lima-Mendez, G.; Poulain, J.; Poulos, B. T.; Royo-Llonch, M.; Sarmento, H.; Vieira-Silva, S.; Dimier, C.; Picheral, M.; Searson, S.; Kandels-Lewis, S.; Bowler, C.; de Vargas, C.; Gorsky, G.; Grimsley, N.; Hingamp, P.; Iudicone, D.; Jaillon, O.; Not, F.; Ogata, H.; Pesant, S.; Speich, S.; Stemmann, L.; Sullivan, M. B.; Weissenbach, J.; Wincker, P.; Karsenti, E.; Raes, J.; Acinas, S. G.; Bork, P. *Science* **2015,** *348,* 1261359. doi:10.1126/science.1261359
3. Martiny, J. B. H.; Bohannan, B. J. M.; Brown, J. H.; Colwell, R. K.; Fuhrman, J. A.; Green, J. L.; Horner-Devine, M. C.; Kane, M.; Krumins, J. A.; Kuske, C. R.; Morin, P. J.; Naeem, S.; Øvreås, L.; Reysenbach, A.-L.; Smith, V. H.; Staley, J. T. *Nat. Rev. Microbiol.* **2006,** *4,* 102–112. doi:10.1038/nrmicro1341
4. Berendsen, R. L.; Pieterse, C. M. J.; Bakker, P. A. H. M. *Trends Plant Sci.* **2012,** *17,* 478–486. doi:10.1016/j.tplants.2012.04.001
5. Fuhrman, J. A. *Nature* **2009,** *459,* 193–199. doi:10.1038/nature08058
6. Friedman, J.; Higgins, L. M.; Gore, J. *Nat. Ecol. Evol.* **2017,** *1,* No. 109. doi:10.1038/s41559-017-0109
7. Antoniewicz, M. R. *Curr. Opin. Biotechnol.* **2020,** *64,* 230–237. doi:10.1016/j.copbio.2020.07.001
8. Flemming, H.-C.; Wuertz, S. *Nat. Rev. Microbiol.* **2019,** *17,* 247–260. doi:10.1038/s41579-019-0158-9
9. Phillips, J. D. *Soil Sci.* **2017,** *182,* 117–127. doi:10.1097/ss.0000000000000204
10. Kuzyakov, Y.; Blagodatskaya, E. *Soil Biol. Biochem.* **2015,** *83,* 184–199. doi:10.1016/j.soilbio.2015.01.025
11. Whipps, J. M. *J. Exp. Bot.* **2001,** *52* (Suppl. 1), 487–511. doi:10.1093/jxb/52.suppl_1.487
12. Smit, E.; Leeflang, P.; Gommans, S.; van den Broek, J.; van Mil, S.; Wernars, K. *Appl. Environ. Microbiol.* **2001,** *67,* 2284–2291. doi:10.1128/aem.67.5.2284-2291.2001
13. Dunfield, K. E.; Germida, J. J. *Appl. Environ. Microbiol.* **2003,** *69,* 7310–7318. doi:10.1128/aem.69.12.7310-7318.2003
14. Lan, G.; Li, Y.; Lesueur, D.; Wu, Z.; Xie, G. *Sci. Total Environ.* **2018,** *626,* 826–834. doi:10.1016/j.scitotenv.2018.01.147
15. Garbeva, P.; van Elsas, J. D.; van Veen, J. A. *Plant Soil* **2008,** *302,* 19–32. doi:10.1007/s11104-007-9432-0
16. Singh, B. K.; Munro, S.; Potts, J. M.; Millard, P. *Appl. Soil Ecol.* **2007,** *36,* 147–155. doi:10.1016/j.apsoil.2007.01.004
17. Berg, G.; Smalla, K. *FEMS Microbiol. Ecol.* **2009,** *68,* 1–13. doi:10.1111/j.1574-6941.2009.00654.x
18. Lundberg, D. S.; Lebeis, S. L.; Paredes, S. H.; Yourstone, S.; Gehring, J.; Malfatti, S.; Tremblay, J.; Engelbrektson, A.; Kunin, V.; Del Rio, T. G.; Edgar, R. C.; Eickhorst, T.; Ley, R. E.; Hugenholtz, P.; Tringe, S. G.; Dangl, J. L. *Nature* **2012,** *488,* 86–90. doi:10.1038/nature11237

19. Lebeis, S. L.; Paredes, S. H.; Lundberg, D. S.; Breakfield, N.; Gehring, J.; McDonald, M.; Malfatti, S.; Del Rio, T. G.; Jones, C. D.; Tringe, S. G.; Dangl, J. L. *Science* **2015,** *349,* 860–864. doi:10.1126/science.aaa8764
20. Bulgarelli, D.; Rott, M.; Schlaeppi, K.; Ver Loren van Themaat, E.; Ahmadinejad, N.; Assenza, F.; Rauf, P.; Huettel, B.; Reinhardt, R.; Schmelzer, E.; Peplies, J.; Gloeckner, F. O.; Amann, R.; Eickhorst, T.; Schulze-Lefert, P. *Nature* **2012,** *488,* 91–95. doi:10.1038/nature11336
21. Bai, Y.; Müller, D. B.; Srinivas, G.; Garrido-Oter, R.; Potthoff, E.; Rott, M.; Dombrowski, N.; Münch, P. C.; Spaepen, S.; Remus-Emsermann, M.; Hüttel, B.; McHardy, A. C.; Vorholt, J. A.; Schulze-Lefert, P. *Nature* **2015,** *528,* 364–369. doi:10.1038/nature16192
22. Niu, B.; Paulson, J. N.; Zheng, X.; Kolter, R. *Proc. Natl. Acad. Sci. U. S. A.* **2017,** *114,* E2450–E2459. doi:10.1073/pnas.1616148114
23. Patin, N. V.; Schorn, M.; Aguinaldo, K.; Lincecum, T.; Moore, B. S.; Jensen, P. R. *Appl. Environ. Microbiol.* **2017,** *83,* e02676-16. doi:10.1128/aem.02676-16
24. Foster, K. R.; Bell, T. *Curr. Biol.* **2012,** *22,* 1845–1850. doi:10.1016/j.cub.2012.08.005
25. Romero, D.; Traxler, M. F.; Lopez, D.; Kolter, R. *Chem. Rev.* **2011,** *111,* 5492–5505. doi:10.1021/cr2000509
26. Linares, J. F.; Gustafsson, I.; Baquero, F.; Martinez, J. L. *Proc. Natl. Acad. Sci. U. S. A.* **2006,** *103,* 19484–19489. doi:10.1073/pnas.0608949103
27. Straight, P. D.; Willey, J. M.; Kolter, R. *J. Bacteriol.* **2006,** *188,* 4918–4925. doi:10.1128/jb.00162-06
28. Pettit, R. K. *Appl. Microbiol. Biotechnol.* **2009,** *83,* 19–25. doi:10.1007/s00253-009-1916-9
29. Wakefield, J.; Hassan, H. M.; Jaspars, M.; Ebel, R.; Rateb, M. E. *Front. Microbiol.* **2017,** *8,* 1284. doi:10.3389/fmicb.2017.01284
30. Kovács, Á. T. *Trends Microbiol.* **2019,** *27,* 724–725. doi:10.1016/j.tim.2019.03.008
31. Hashem, A.; Tabassum, B.; Fathi Abd_Allah, E. *Saudi J. Biol. Sci.* **2019,** *26,* 1291–1297. doi:10.1016/j.sjbs.2019.05.004
32. Gadhave, K. R.; Devlin, P. F.; Ebertz, A.; Ross, A.; Gange, A. C. *Microb. Ecol.* **2018,** *76,* 741–750. doi:10.1007/s00248-018-1160-x
33. Stein, T. *Mol. Microbiol.* **2005,** *56,* 845–857. doi:10.1111/j.1365-2958.2005.04587.x
34. Kaspar, F.; Neubauer, P.; Gimpel, M. *J. Nat. Prod.* **2019,** *82,* 2038–2053. doi:10.1021/acs.jnatprod.9b00110
35. Harwood, C. R.; Mouillon, J.-M.; Pohl, S.; Arnau, J. *FEMS Microbiol. Rev.* **2018,** *42,* 721–738. doi:10.1093/femsre/fuy028
36. Ongena, M.; Jacques, P. *Trends Microbiol.* **2008,** *16,* 115–125. doi:10.1016/j.tim.2007.12.009
37. Quadri, L. E. N.; Weinreb, P. H.; Lei, M.; Nakano, M. M.; Zuber, P.; Walsh, C. T. *Biochemistry* **1998,** *37,* 1585–1595. doi:10.1021/bi9719861
38. Kearns, D. B.; Losick, R. *Mol. Microbiol.* **2003,** *49,* 581–590. doi:10.1046/j.1365-2958.2003.03584.x
39. Grau, R. R.; de Oña, P.; Kunert, M.; Leñini, C.; Gallegos-Monterrosa, R.; Mhatre, E.; Vileta, D.; Donato, V.; Hölscher, T.; Boland, W.; Kuipers, O. P.; Kovács, Á. T. *mBio* **2015,** *6,* e00581–15. doi:10.1128/mbio.00581-15
40. Sheppard, J. D.; Jumarie, C.; Cooper, D. G.; Laprade, R. *Biochim. Biophys. Acta, Biomembr.* **1991,** *1064,* 13–23. doi:10.1016/0005-2736(91)90406-x
41. Heerklotz, H.; Wieprecht, T.; Seelig, J. *J. Phys. Chem. B* **2004,** *108,* 4909–4915. doi:10.1021/jp0371938
42. Heerklotz, H.; Seelig, J. *Eur. Biophys. J.* **2007,** *36,* 305–314. doi:10.1007/s00249-006-0091-5
43. Loiseau, C.; Schlusselhuber, M.; Bigot, R.; Bertaux, J.; Berjeaud, J.-M.; Verdon, J. *Appl. Microbiol. Biotechnol.* **2015,** *99,* 5083–5093. doi:10.1007/s00253-014-6317-z
44. Sabaté, D. C.; Audisio, M. C. *Microbiol. Res.* **2013,** *168,* 125–129. doi:10.1016/j.micres.2012.11.004
45. Umezawa, H.; Aoyagi, T.; Nishikiori, T.; Okuyama, A.; Yamagishi, Y.; Hamada, M.; Takeuchi, T. *J. Antibiot.* **1986,** *39,* 737–744. doi:10.7164/antibiotics.39.737
46. Deleu, M.; Paquot, M.; Nylander, T. *J. Colloid Interface Sci.* **2005,** *283,* 358–365. doi:10.1016/j.jcis.2004.09.036
47. Romero, D.; de Vicente, A.; Rakotoaly, R. H.; Dufour, S. E.; Veening, J.-W.; Arrebola, E.; Cazorla, F. M.; Kuipers, O. P.; Paquot, M.; Pérez-García, A. *Mol. Plant-Microbe Interact.* **2007,** *20,* 430–440. doi:10.1094/mpmi-20-4-0430
48. Alvarez, F.; Castro, M.; Príncipe, A.; Borioli, G.; Fischer, S.; Mori, G.; Jofré, E. *J. Appl. Microbiol.* **2012,** *112,* 159–174. doi:10.1111/j.1365-2672.2011.05182.x
49. Falardeau, J.; Wise, C.; Novitsky, L.; Avis, T. J. *J. Chem. Ecol.* **2013,** *39,* 869–878. doi:10.1007/s10886-013-0319-7
50. Zhang, L.; Sun, C. *Appl. Environ. Microbiol.* **2018,** *84,* e00445-18. doi:10.1128/aem.00445-18
51. Kiesewalter, H. T.; Lozano-Andrade, C. N.; Wibowo, M.; Strube, M. L.; Maróti, G.; Snyder, D.; Jørgensen, T. S.; Larsen, T. O.; Cooper, V. S.; Weber, T.; Kovács, Á. T. *bioRxiv* **2020**. doi:10.1101/2020.08.05.238063
52. Patel, P.; Huang, S.; Fisher, S.; Pirnik, D.; Aklonis, C.; Dean, L.; Meyers, E.; Fernandes, P.; Mayerl, F. *J. Antibiot.* **1995,** *48,* 997–1003. doi:10.7164/antibiotics.48.997
53. Müller, S.; Strack, S. N.; Hoefler, B. C.; Straight, P. D.; Kearns, D. B.; Kirby, J. R. *Appl. Environ. Microbiol.* **2014,** *80,* 5603–5610. doi:10.1128/aem.01621-14
54. Gallegos-Monterrosa, R.; Kankel, S.; Götze, S.; Barnett, R.; Stallforth, P.; Kovács, Á. T. *J. Bacteriol.* **2017,** *199,* e00204–17. doi:10.1128/jb.00204-17
55. Poretsky, R.; Rodriguez-R, L. M.; Luo, C.; Tsementzi, D.; Konstantinidis, K. T. *PLoS One* **2014,** *9,* e93827. doi:10.1371/journal.pone.0093827
56. Louca, S.; Doebeli, M.; Parfrey, L. W. *Microbiome* **2018,** *6,* 41. doi:10.1186/s40168-018-0420-9
57. Goldford, J. E.; Lu, N.; Bajić, D.; Estrela, S.; Tikhonov, M.; Sanchez-Gorostiaga, A.; Segrè, D.; Mehta, P.; Sanchez, A. *Science* **2018,** *361,* 469–474. doi:10.1126/science.aat1168
58. Dittmann, K. K.; Sonnenschein, E. C.; Egan, S.; Gram, L.; Bentzon-Tilia, M. *Environ. Microbiol. Rep.* **2019,** *11,* 401–413. doi:10.1111/1758-2229.12698
59. Chowdhury, S. P.; Dietel, K.; Rändler, M.; Schmid, M.; Junge, H.; Borriss, R.; Hartmann, A.; Grosch, R. *PLoS One* **2013,** *8,* e68818. doi:10.1371/journal.pone.0068818
60. Cosetta, C. M.; Kfoury, N.; Robbat, A.; Wolfe, B. E. *Environ. Microbiol.* **2020,** *22,* 4745–4760. doi:10.1111/1462-2920.15223
61. Arjes, H. A.; Vo, L.; Dunn, C. M.; Willis, L.; DeRosa, C. A.; Fraser, C. L.; Kearns, D. B.; Huang, K. C. *Curr. Biol.* **2020,** *30,* 1011–1022.e6. doi:10.1016/j.cub.2020.01.073
62. Russel, J.; Røder, H. L.; Madsen, J. S.; Burmølle, M.; Sørensen, S. J. *Proc. Natl. Acad. Sci. U. S. A.* **2017,** *114,* 10684–10688. doi:10.1073/pnas.1706016114
63. Geng, H.; Tran-Gyamfi, M. B.; Lane, T. W.; Sale, K. L.; Yu, E. T. *Front. Microbiol.* **2016,** *7,* 1155. doi:10.3389/fmicb.2016.01155

64. Kiesewalter, H. T.; Lozano-Andrade, C. N.; Maróti, G.; Snyder, D.; Cooper, V. S.; Jørgensen, T. S.; Weber, T.; Kovács, Á. T. *Microbiol. Resour. Announce.* **2020,** *9,* e01406–19. doi:10.1128/mra.01406-19
65. Bolyen, E.; Rideout, J. R.; Dillon, M. R.; Bokulich, N. A.; Abnet, C. C.; Al-Ghalith, G. A.; Alexander, H.; Alm, E. J.; Arumugam, M.; Asnicar, F.; Bai, Y.; Bisanz, J. E.; Bittinger, K.; Brejnrod, A.; Brislawn, C. J.; Brown, C. T.; Callahan, B. J.; Caraballo-Rodríguez, A. M.; Chase, J.; Cope, E. K.; Da Silva, R.; Diener, C.; Dorrestein, P. C.; Douglas, G. M.; Durall, D. M.; Duvallet, C.; Edwardson, C. F.; Ernst, M.; Estaki, M.; Fouquier, J.; Gauglitz, J. M.; Gibbons, S. M.; Gibson, D. L.; Gonzalez, A.; Gorlick, K.; Guo, J.; Hillmann, B.; Holmes, S.; Holste, H.; Huttenhower, C.; Huttley, G. A.; Janssen, S.; Jarmusch, A. K.; Jiang, L.; Kaehler, B. D.; Kang, K. B.; Keefe, C. R.; Keim, P.; Kelley, S. T.; Knights, D.; Koester, I.; Kosciolek, T.; Kreps, J.; Langille, M. G. I.; Lee, J.; Ley, R.; Liu, Y.-X.; Loftfield, E.; Lozupone, C.; Maher, M.; Marotz, C.; Martin, B. D.; McDonald, D.; McIver, L. J.; Melnik, A. V.; Metcalf, J. L.; Morgan, S. C.; Morton, J. T.; Naimey, A. T.; Navas-Molina, J. A.; Nothias, L. F.; Orchanian, S. B.; Pearson, T.; Peoples, S. L.; Petras, D.; Preuss, M. L.; Pruesse, E.; Rasmussen, L. B.; Rivers, A.; Robeson, M. S., II; Rosenthal, P.; Segata, N.; Shaffer, M.; Shiffer, A.; Sinha, R.; Song, S. J.; Spear, J. R.; Swafford, A. D.; Thompson, L. R.; Torres, P. J.; Trinh, P.; Tripathi, A.; Turnbaugh, P. J.; Ul-Hasan, S.; van der Hooft, J. J. J.; Vargas, F.; Vázquez-Baeza, Y.; Vogtmann, E.; von Hippel, M.; Walters, W.; Wan, Y.; Wang, M.; Warren, J.; Weber, K. C.; Williamson, C. H. D.; Willis, A. D.; Xu, Z. Z.; Zaneveld, J. R.; Zhang, Y.; Zhu, Q.; Knight, R.; Caporaso, J. G. *Nat. Biotechnol.* **2019,** *37,* 852–857. doi:10.1038/s41587-019-0209-9
66. McDonald, D.; Clemente, J. C.; Kuczynski, J.; Rideout, J. R.; Stombaugh, J.; Wendel, D.; Wilke, A.; Huse, S.; Hufnagle, J.; Meyer, F.; Knight, R.; Caporaso, J. G. *GigaScience* **2012,** *1,* No. 7. doi:10.1186/2047-217x-1-7
67. Martin, M. *EMBnet j.* **2011,** *17,* 10. doi:10.14806/ej.17.1.200
68. Callahan, B. J.; McMurdie, P. J.; Rosen, M. J.; Han, A. W.; Johnson, A. J. A.; Holmes, S. P. *Nat. Methods* **2016,** *13,* 581–583. doi:10.1038/nmeth.3869
69. Quast, C.; Pruesse, E.; Yilmaz, P.; Gerken, J.; Schweer, T.; Yarza, P.; Peplies, J.; Glöckner, F. O. *Nucleic Acids Res.* **2013,** *41,* D590–D596. doi:10.1093/nar/gks1219
70. Rognes, T.; Flouri, T.; Nichols, B.; Quince, C.; Mahé, F. *PeerJ* **2016,** *4,* e2584. doi:10.7717/peerj.2584
71. Price, M. N.; Dehal, P. S.; Arkin, A. P. *PLoS One* **2010,** *5,* e9490. doi:10.1371/journal.pone.0009490
72. Katoh, K.; Standley, D. M. *Mol. Biol. Evol.* **2013,** *30,* 772–780. doi:10.1093/molbev/mst010
73. Lane, D. J. In *Nucleic Acid Techniques in Bacterial Systematics;* Stackebrandt, E.; Goodfellow, M., Eds.; John Wiley & Sons: New York, NY, USA, 1991; pp 115–175.
74. R Core Team. R: A Language and Environment for Statistical Computing. Vienna, Austria 2020.
75. Bisanz, J. E. Qiime2R: Importing QIIME2 Artifacts and Associated Data into R Sessions, 2018.
76. McMurdie, P. J.; Holmes, S. *PLoS One* **2013,** *8,* e61217. doi:10.1371/journal.pone.0061217
77. Kandlikar, G. S.; Gold, Z. J.; Cowen, M. C.; Meyer, R. S.; Freise, A. C.; Kraft, N. J. B.; Moberg-Parker, J.; Sprague, J.; Kushner, D. J.; Curd, E. E. *F1000Research* **2018,** *7,* 1734. doi:10.12688/f1000research.16680.1
78. Oksanen, J.; Blanchet, F. G.; Friendly, M.; Kindt, R.; Legendre, P.; McGlinn, D.; Minchin, P. R.; O'Hara, R. B.; Simpson, G. L.; Solymos, P.; Stevens, M. H. H.; Szoecs, E.; Wagner, H. Vegan: Community Ecology Package, 2019.
79. Wickham, H. *WIREs Comp. Stat.* **2011,** *3,* 180–185. doi:10.1002/wics.147

License and Terms

BEILSTEIN JOURNAL OF ORGANIC CHEMISTRY

Identification of volatiles from six marine *Celeribacter* strains

Anuj Kumar Chhalodia[1], Jan Rinkel[1], Dorota Konvalinkova[1], Jörn Petersen[2] and Jeroen S. Dickschat[*1]

Full Research Paper

Open Access

Address:
[1]Kekulé Institute of Organic Chemistry and Biochemistry, University of Bonn, Gerhard-Domagk-Straße 1, 53121 Bonn, Germany and [2]Leibniz-Institut DSMZ - Deutsche Sammlung von Mikroorganismen und Zellkulturen GmbH, Inhoffenstraße 7b, 38124 Braunschweig, Germany

Email:
Jeroen S. Dickschat* - dickschat@uni-bonn.de

* Corresponding author

Keywords:
GC–MS; isotopes; *Roseobacter*; sulfur metabolism; volatiles

Beilstein J. Org. Chem. **2021,** *17,* 420–430.
https://doi.org/10.3762/bjoc.17.38

Received: 07 December 2020
Accepted: 02 February 2021
Published: 11 February 2021

This article is part of the thematic issue "Chemical ecology".

Guest Editor: C. Beemelmanns

Abstract

The volatiles emitted from six marine *Rhodobacteraceae* species of the genus *Celeribacter* were investigated by GC–MS. Besides several known compounds including dimethyl trisulfide and *S*-methyl methanethiosulfonate, the sulfur-containing compounds ethyl (*E*)-3-(methylsulfanyl)acrylate and 2-(methyldisulfanyl)benzothiazole were identified and their structures were verified by synthesis. Feeding experiments with [*methyl*-$^{2}H_3$]methionine, [*methyl*-^{13}C]methionine and [^{34}S]-3-(dimethylsulfonio)propanoate (DMSP) resulted in the high incorporation into dimethyl trisulfide and *S*-methyl methanethiosulfonate, and revealed the origin of the methylsulfanyl group of 2-(methyldisulfanyl)benzothiazole from methionine or DMSP, while the biosynthetic origin of the benzothiazol-2-ylsulfanyl portion could not be traced. The heterocyclic moiety of this compound is likely of anthropogenic origin, because 2-mercaptobenzothiazole is used in the sulfur vulcanization of rubber. Also in none of the feeding experiments incorporation into ethyl (*E*)-3-(methylsulfanyl)acrylate could be observed, questioning its bacterial origin. Our results demonstrate that the *Celeribacter* strains are capable of methionine and DMSP degradation to widespread sulfur volatiles, but the analysis of trace compounds in natural samples must be taken with care.

Introduction

Bacteria from the roseobacter group belong to the most abundant microbial species in marine ecosystems [1,2]. They are present from polar to tropical regions, in marine sediments, in estuarine and open ocean environments in different pelagic zones ranging from surface waters to depths of >2,000 m [3,4]. Some species are associated with other marine organisms, e.g., *Thalassococcus halodurans* DSM 26915^{T} has been isolated from the marine sponge *Halichondria panicea* [5], and *Phaeobacter gallaeciensis* DSM 26640^{T} is an isolate from the scallop *Pecten maximus* [6]. Important interactions are also observed between bacteria from the roseobacter group and various types of marine algae, e.g., the first described organisms

Roseobacter litoralis DSM 6996^T and *R. denitrificans* DSM 7001^T were obtained from seaweed [7], while *Dinoroseobacter shibae* DSM 16493^T and *Marinovum algicola* DSM 10251^T are both isolates from the dinoflagellate *Prorocentrum lima* [8,9]. Especially in algal blooms bacteria of the roseobacter group are highly abundant [10], and here they belong to the main players involved in the enzymatic degradation of the algal sulfur metabolite 3-(dimethylsulfonio)propanoate (DMSP, Scheme 1) [11]. Its catabolism leads either through the demethylation pathway by action of the enzymes DmdABCD to methanethiol (MeSH, Scheme 1A) [12] or through lysis by DddD [13] or hydrolytic cleavage by one of the known DMSP lyases (DddW [14], DddP [15], DddQ [16], DddL [17], DddY [18] or DddK [19]) to dimethyl sulfide (DMS, Scheme 1B).

It has already been pointed out in the 1970s and 1980s that atmospheric DMS is important for the global sulfur cycle [20] and influences the climate on Earth, known as CLAW hypothesis according to the authors' initials (Carlson, Lovelock, Andreae, Warren) [21], which underpins the relevance of this algal–bacterial interaction. Isotopic labeling experiments demonstrated that also in laboratory cultures roseobacter group bacteria efficiently degrade DMSP into sulfur volatiles [22,23], but also from other sulfur sources including 2,3-dihydroxypropane-1-sulfonic acid (DHPS, Scheme 1C) labeling was efficiently incorporated into sulfur volatiles [24,25]. Notably, DHPS is produced in large quantities by the marine diatom *Thalassiosira pseudonana* [26], and diatoms from this genus live in symbiotic relationship with bacteria of the roseobacter group [27]. Another interesting aspect of sulfur metabolism in marine bacteria from the roseobacter group is the production of the sulfur-containing antibiotic tropodithietic acid (TDA) in *Phaeobacter piscinae* DSM 103509^T [28], a compound that is in equilibrium with its tautomer thiotropocin [29] that was first described from *Pseudomonas* sp. CB-104 [30]. Its biosynthesis depends on the clustered *tda* genes [31] and has been studied by

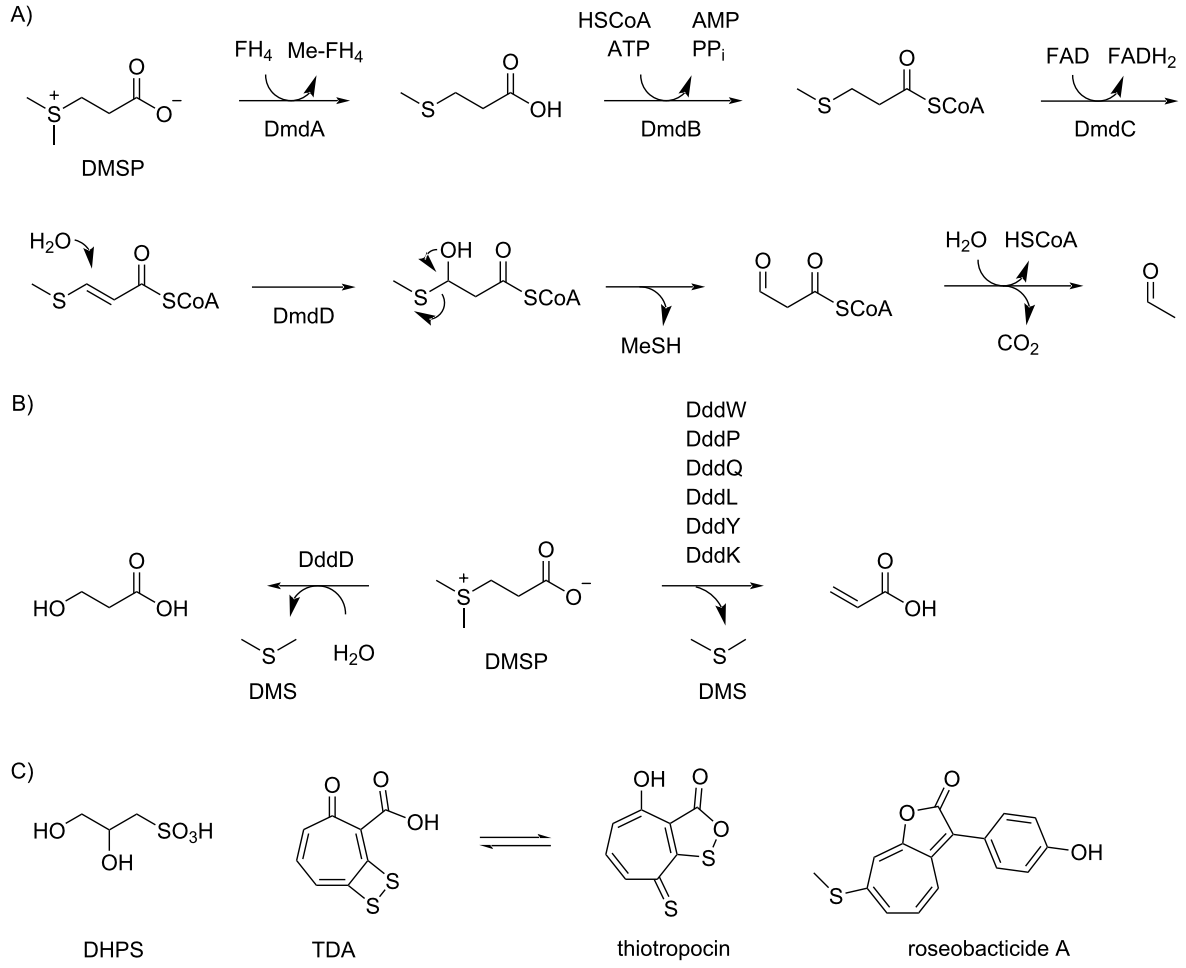

Scheme 1: Sulfur metabolism in bacteria from the roseobacter group. A) DMSP demethylation by DmdABCD, B) DMSP hydrolysis by DddP and lysis by DddW, DddP, DddQ, DddL, DddY or DddK, and C) structures of DHPS and sulfur-containing secondary metabolites.

feeding experiments with labeled precursors to the wildtype and gene knockout strains of *P. inhibens* DSM 17395^T, demonstrating the formation of TDA from phenylalanine through phenylacetyl-CoA and the phenylacetyl-CoA catabolon [32,33]. These experiments also led to a suggestion for the mechanism for sulfur incorporation, but further research is required for a deep understanding of TDA biosynthesis. Besides its function as an antibiotic, TDA acts as a signaling molecule, similar to *N*-acylhomoserine lactones, at concentrations 100 times lower than required for a significant antibiotic activity [34]. The biosynthesis of tropone [35] and of the algicidal sulfur-containing roseobacticides [36] are most likely connected to the TDA pathway. Interestingly, in the interaction with marine algae *P. inhibens* can change its lifestyle from a symbiotic relationship during which the antibiotic TDA and growth stimulants are produced to a pathogenic interaction promoted by lignin degradation products in fading algal blooms that induce roseobacticide biosynthesis [36]. All these examples demonstrate the importance of sulfur metabolism for marine bacteria from the roseobacter group. Here we report on the volatiles emitted by six *Celeribacter* species with a special focus on sulfur volatiles. The results from feeding studies with labeled precursors demonstrate that the *Celeribacter* strains can form sulfur volatiles from methionine and DMSP, but also showed that some of the detected sulfur compounds are not or only partly of bacterial origin.

Results and Discussion

Headspace analysis

The volatiles released by six marine *Celeribacter* type strains, including *C. marinus* DSM 100036^T, *C. neptunius* DSM 26471^T, *C. manganoxidans* DSM 27541^T, *C. baekdonensis* DSM 27375^T, *C. halophilus* DSM 26270^T and *C. indicus* DSM 27257^T, were collected through a closed-loop stripping apparatus (CLSA) on charcoal [37]. After extraction with dichloromethane the obtained extracts were analyzed by GC–MS (Figure 1). The compounds were identified by the comparison of the recorded EI mass spectra to library spectra and of retention indices [38] to tabulated literature data (Table 1), or by a direct comparison to authentic standards. The structures of the identified compounds are shown in Figure 2.

While the headspace extracts from *C. marinus*, *C. neptunius* and *C. manganoxidans* were particularly rich, the extracts from *C. baekdonensis*, *C. halophilus* and *C. indicus* contained fewer compounds. Most of the observed volatiles are well known [56,57] and were thus readily identified from their mass spectra and retention indices. Pyrazines including methylpyrazine (**1**), 2,5-dimethylpyrazine (**2**) and trimethylpyrazine (**3**) were present in the extracts from all six strains. Notably, also several α-hydroxyketones that have been described as biosynthetic precursors to pyrazines [40], represented by 3-hydroxypentan-2-one (**4**), 2-hydroxypentan-3-one (**5**) and 2-hydroxyhexan-3-one (**6**), were observed in some of the investigated strains. A series of aldehydes ranging from hexanal (**7**) to tetradecanal (**13**) was found in strain specific patterns, with all identified compounds present in the bouquet from *C. manganoxidans*. A similar series of γ-lactones spanning from pentan-4-olide (**14**) to dodecan-4-olide (**20**), in addition to 3-methylbutan-4-olide (**21**) and 4-methylhex-5-en-4-olide (**22**), was detected in strain-specific patterns, with almost all of these compounds present in *C. marinus*; only *C. halophilus* did not emit lactones. Furans included furan-2-ylmethanol (**23**), furfural (**24**), and 2-acetylfuran (**25**). Cyclohexanol (**26**) was observed only once in *C. marinus*, and aromatic compounds included benzyl alcohol (**27**), benzaldehyde (**28**) and salicylaldehyde (**29**), acetophenone (**30**) and *o*-aminoacetophenone (**31**), 2-phenylethanol (**32**), and phenylacetone (**33**). 6-Methylhept-5-en-2-one (**34**) was detected in all strains, while its saturated analog 6-methylheptan-2-one (**35**) was only emitted by *C. baekdonensis* and geranylacetone (**36**) only by the three productive species *C. marinus*, *C. neptunius*, and *C. manganoxidans*. Compounds **34** and **36** have been described as non-enzymatic degradation products arising from the side chain in menaquinones [58]. Sulfur-containing compounds included dimethyl trisulfide (**37**), released by all six species, *S*-methyl methanethiosulfonate (**38**), 2-acetylthiazole (**39**), and benzothiazole (**40**), the latter also in the extracts from all six strains. In addition, the extracts from the three species *C. marinus*, *C. neptunius* and *C. baekdonensis* contained an additional volatile (**41**) whose mass spectrum (Figure 3A) was not included in our libraries. Furthermore, ethyl 3-(methylsulfanyl)acrylate (**42**) was found in *C. marinus* and *C. manganoxidans*, but the measured retention index (I = 1177) did not allow to distinguish between the *E* and the *Z* isomer for which retention indices of I = 1144 (*E*) and I = 1158 (*Z*) were reported [53]. Therefore, for an unambiguous structural assignment for compounds **41** and **42** the synthesis of reference compounds was required.

Synthesis of reference compounds

The mass spectrum of the component **41** showed strong similarities to the library mass spectrum of 2-mercaptobenzothiazole that has a molecular weight of 167 Da. The isotope pattern of the molecular ion at m/z = 213 indicated the presence of three sulfur atoms. The strong base peak at m/z = 167 in the mass spectrum of **41** suggested a benzothiazol-2-ylsulfanyl moiety, while the mass difference to the molecular ion pointed to the connection to a methylsulfanyl group. Taken together, this analysis resulted in the structural proposal of 2-(methyldisulfanyl)benzothiazole for **41**. For the structural verification a synthesis was performed by a $BF_3{\cdot}OEt_2$-catalyzed reaction of bis(benzothiazol-2-yl)disulfane with dimethyl disulfide, giving

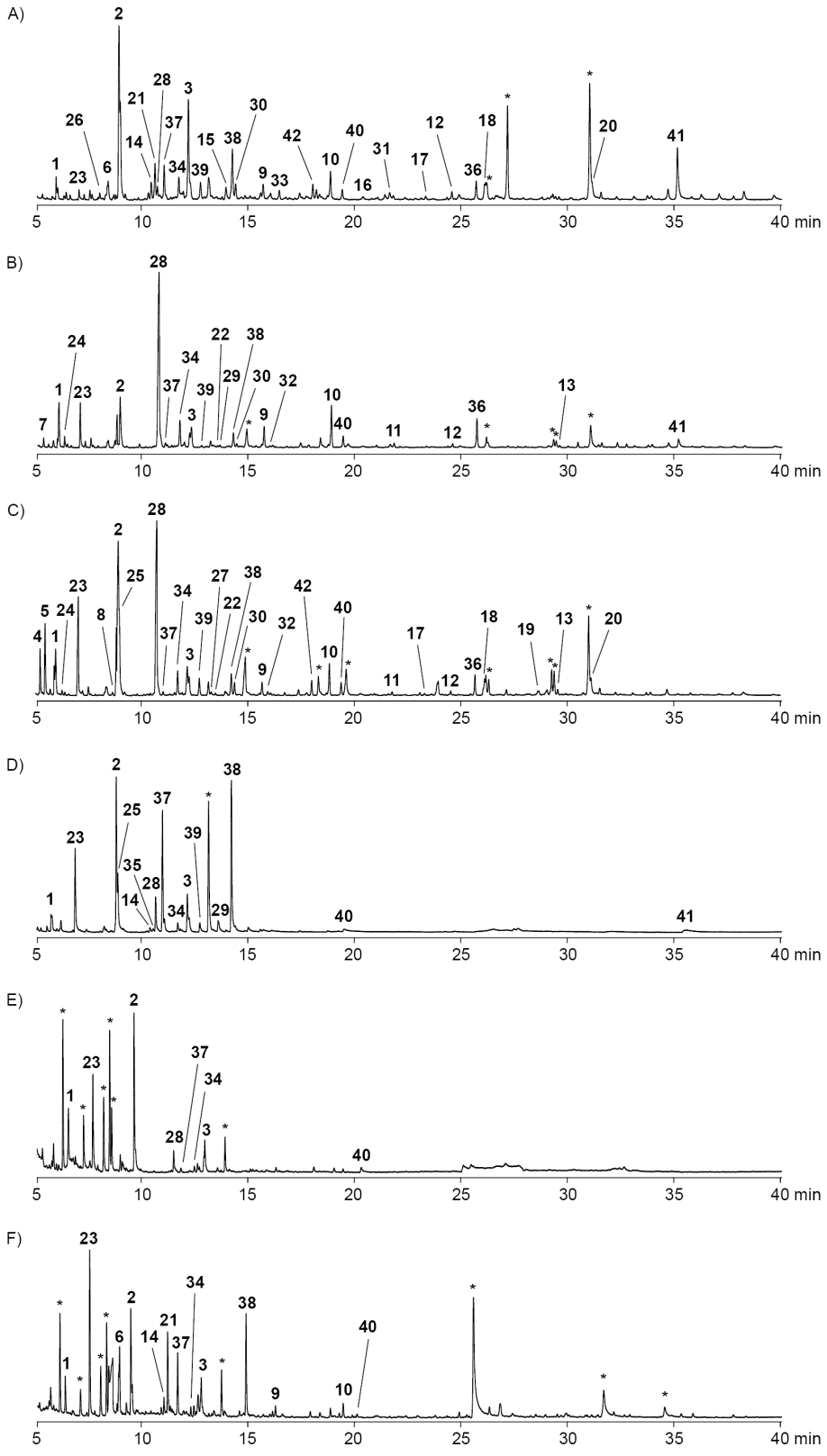

Figure 1: Total ion chromatograms of headspace extracts from A) *C. marinus* DSM 100036^T, B) *C. neptunius* DSM 26471^T, C) *C. manganoxidans* DSM 27541^T, D) *C. baekdonensis* DSM 27375^T, E) *C. halophilus* DSM 26270^T, and F) *C. indicus* DSM 27257^T. Peaks arising from known contaminants are indicated by asterisks.

Table 1: Volatiles from *Celeribacter* spp.

Compound[a]	*I*[b]	*I*(lit.)[b]	Id.[c]	Occurrence[d]					
3-hydroxypentan-2-one (**4**)	812	815 [39]	ri, ms			C			
hexanal (**7**)	813	806 [39]	ri, ms		B				
2-hydroxypentan-3-one (**5**)	818	818 [40]	ri, ms			C			
methylpyrazine (**1**)	831	826 [41]	ri, ms	A	B	C	D	E	F
furfural (**24**)	841	841 [42]	ri, ms		B	C			
furan-2-ylmethanol (**23**)	861	863 [43]	ri, ms	A	B	C	D	E	F
cyclohexanol (**26**)	888	886 [44]	ri, ms	A					
2-hydroxyhexan-3-one (**6**)	899	900 [40]	ri, ms	A					F
heptanal (**8**)	906	901 [45]	ri, ms			C			
2,5-dimethylpyrazine (**2**)	912	908 [45]	ri, ms	A	B	C	D	E	F
2-acetylfuran (**25**)	913	909 [45]	ri, ms			C	D		
pentan-4-olide (**14**)	953	956 [46]	ri, ms	A			D		F
3-methylbutan-4-olide (**21**)	957	958 [47]	ri, ms	A					F
6-methylheptan-2-one (**35**)	959	962 [48]	ri, ms				D		
benzaldehyde (**28**)	961	952 [45]	ri, ms	A	B	C	D	E	
dimethyl trisulfide (**37**)	970	968 [49]	ri, ms	A	B	C	D	E	F
6-methylhept-5-en-2-one (**34**)	988	981 [45]	ri, ms	A	B	C	D	E	F
trimethylpyrazine (**3**)	1000	1000 [45]	ri, ms	A	B	C	D	E	F
2-acetylthiazole (**39**)	1017	1014 [45]	ri, ms	A	B	C	D		
benzyl alcohol (**27**)	1033	1026 [45]	ri, ms			C			
4-methylhex-5-en-4-olide (**22**)	1039	1034 [45]	ri, ms		B	C			
salicylaldehyde (**29**)	1042	1039 [45]	ri, ms		B		D		
hexan-4-olide (**15**)	1052	1056 [50]	ri, ms	A					
S-methyl methanethiosulfonate (**38**)	1061	1068 [51]	ri, ms	A	B	C	D		F
acetophenone (**30**)	1065	1059 [45]	ri, ms	A	B	C			
nonanal (**9**)	1103	1100 [45]	ri, ms	A	B	C			F
2-phenylethanol (**32**)	1111	1106 [45]	ri, ms		B	C			
phenylacetone (**33**)	1127	1124 [52]	ri, ms	A					
ethyl (*E*)-3-(methylsulfanyl)acrylate (**42**)	1177	*1144* [53]	ms	A		C			
decanal (**10**)	1203	1201 [45]	ri, ms	A	B	C			F
benzothiazole (**40**)	1221	1222 [54]	ri, ms	A	B	C	D	E	F
octan-4-olide (**16**)	1252	1250 [45]	ri, ms	A					
o-aminoacetophenone (**31**)	1292	1296 [55]	ri, ms	A					
undecanal (**11**)	1298	1305 [45]	ri, ms		B	C			
nonan-4-olide (**17**)	1354	1358 [45]	ri, ms	A		C			
dodecanal (**12**)	1400	1408 [45]	ri, ms	A	B	C			
geranylacetone (**36**)	1445	1453 [45]	ri, ms	A	B	C			
decan-4-olide (**18**)	1461	1465 [45]	ri, ms	A		C			
undecan-4-olide (**19**)	1568	1569 [45]	ri, ms			C			
tetradecanal (**13**)	1605	1611 [45]	ri, ms		B	C			
dodecan-4-olide (**20**)	1673	1676 [45]	ri, ms	A		C			
2-(methyldisulfanyl)benzothiazole (**41**)	1860		std	A	B		D		

[a]Identified by GC–MS, known typical contaminants such as plasticizers are not included and all listed compounds were not detected in blank runs with medium plates (except traces of benzaldehyde); [b]retention index on a HP5-MS GC column and comparison to literature data from the same or a similar type of GC column; [c]identification based on ri: matching retention index (difference between measured retention index and literature data ≤10 points), ms: mass spectrum matching to a database spectrum, std: direct comparison to an authentic standard; [d]occurrence in A: *C. marinus* DSM 100036^T, B: *C. neptunius* DSM 26471^T, C: *C. manganoxidans* DSM 27541^T, D: *C. baekdonensis* DSM 27375^T, E: *C. halophilus* DSM 26270^T, and F: *C. indicus* DSM 27257^T.

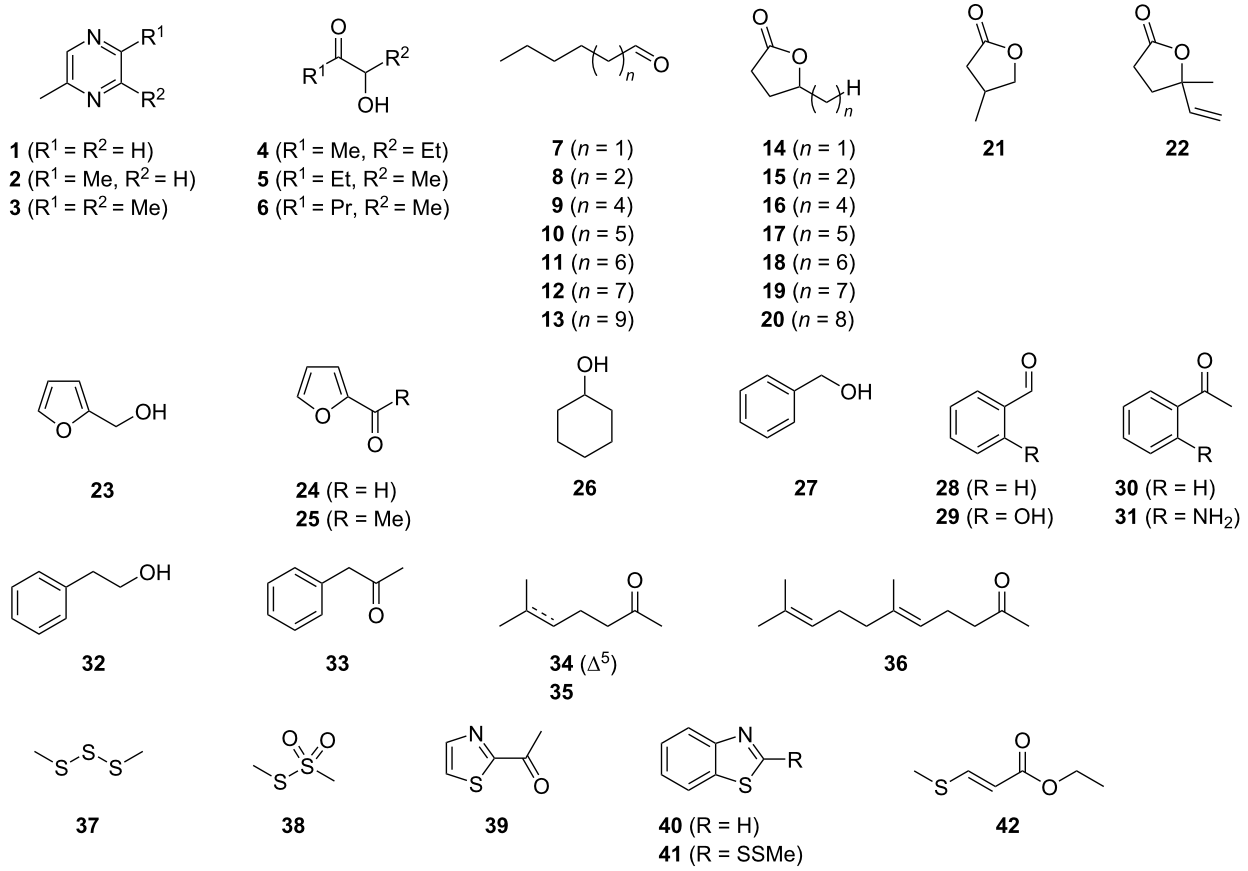

Figure 2: Structures of the identified volatile compounds in the headspace extracts from six *Celeribacter* type strains.

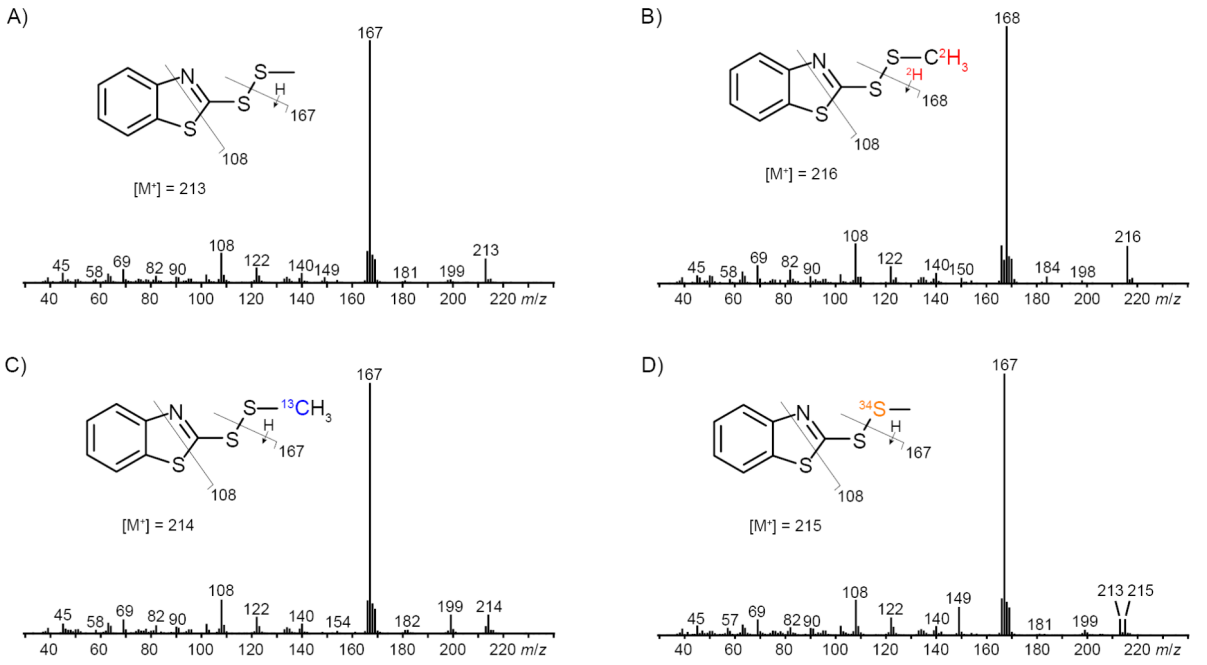

Figure 3: EI mass spectra of A) unlabeled 2-(methyldisulfanyl)benzothiazole (**41**) and of labeled **41** after feeding of B) (*methyl*-$^{2}H_3$)methionine, C) (*methyl*-^{13}C)methionine and D) (^{34}S)DMSP.

access to **41** with a yield of 64% (Scheme 2). The synthetic compound **41** showed an identical mass spectrum and retention index compared to the volatile in the *Celeribacter* extracts. The *Z* and *E* stereoisomers of **42** were obtained by the Michael addition of NaSMe to ethyl propiolate (**45**), yielding a mixture of stereoisomers inseparable by silica gel column chromatography (92%). The major stereoisomer was found to be (*Z*)-**42** (dr 94:6), whose preferred formation may be a result of a chalcogen–chalcogen interaction between the sulfur and an ester oxygen. This phenomenon was first described in supramolecular structures by Gleiter [59] and later also used to explain the outcome of organocatalytic reactions [60]. The pure stereoisomers of **42** were isolated by preparative HPLC, for which the best separation was achieved using a YMC ChiralART Cellulose-SC column. This yielded 70% of (*Z*)-**42** and 6% of (*E*)-**42**, and their analysis by GC–MS showed retention indices of I = 1177 for (*E*)-**42** and I = 1200 for (*Z*)-**42**, revealing that the compound in the headspace extracts of *C. marinus* DSM 100036^T and *C. manganoxidans* DSM 27541^T was identical to (*E*)-**42**.

Feeding experiments with isotopically labeled precursors

The biosynthesis of sulfur volatiles in *C. marinus* was investigated in a series of feeding experiments with isotopically labeled precursors. Feeding of (*methyl*-$^2H_3$)methionine resulted in the efficient incorporation of labeling into **37** (79% incorporation rate, Figure S1B in Supporting Information File 1), **38** (78%, Figure S1F in Supporting Information File 1) and the *S*-methyl group of **41** (84%), as indicated by a shift of the molecular ion from m/z = 213 to 216 (Figure 3B, deuterated compounds can be separated from their non-deuterated analogs by gas chromatography [61]). The base peak appears at m/z = 168, demonstrating its formation with participation of one deuterium from the *S*-methyl group. Analogous results were obtained by feeding of (*methyl*-^{13}C)methionine, showing incorporation into **37** (74%, Figure S1C in Supporting Information File 1), **38** (71%, Figure S1G in Supporting Information), and the MeS group of **41** (71%, Figure 3C; the signal at m/z = 213 represents unlabeled **41** that, in contrast to a deuterated compound, cannot be separated from ^{13}C-labeled **41** by gas chromatography). Furthermore, feeding of [^{34}S]DMSP gave an incorporation into the MeS groups of **37** (50%, Figure S1D), into both sulfur atoms of **38** (47%, Figure S1H in Supporting Information File 1), but only into one sulfur atom of **41** (46%), as indicated by the molecular ion at m/z = 215, while no signals at m/z = 217 and 219 were visible that would account for the incorporation of labeling into two or three of the sulfur atoms in **41** (Figure 3D; also here the signal at m/z = 213 represents inseparable unlabeled **41**). In this experiment, the base peak did not change which allowed the localization of labeling specifically in the MeS group of **41**.

The fact that no incorporation was observed for the other two sulfur atoms of **41** prompted us to further investigate the biosynthetic origin of the benzothiazol-2-ylsulfanyl portion of **41** to establish its natural origin. Several feeding experiments with central primary metabolites including ($^{13}C_6$)glucose, ($^{13}C_5$)ribose and (*indole*-$^2H_5$)tryptophan were performed, but none of these experiments resulted in a detectable incorporation of labeling. Conclusively, a non-biological origin of this part of the molecule seems likely, which may also explain why the detection of **41** in *Celeribacter* was not always reproducible. Notably, 2-mercaptobenzothiazole is used in the sulfur vulcanization of rubber and could react spontaneously with MeSH of bacterial origin in the presence of oxygen to form **41**, giving a reasonable explanation for its formation.

Also none of the feeding experiments with the various labeled precursors resulted in an incorporation of labeling into the

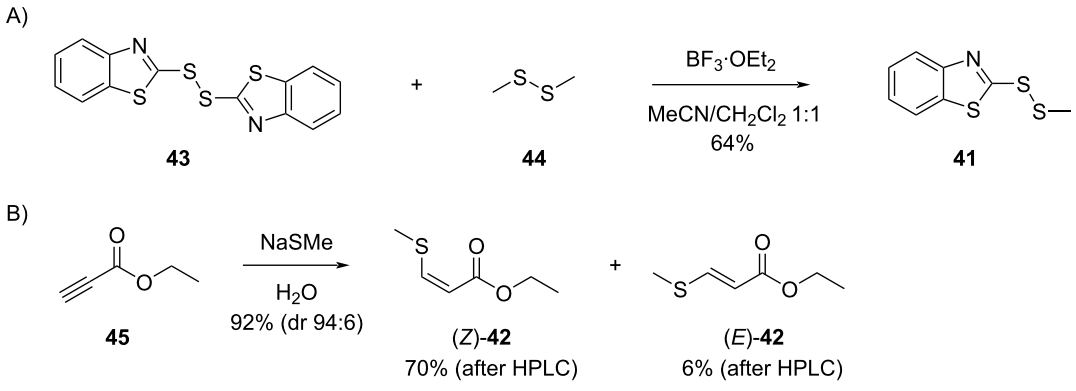

Scheme 2: Synthesis of sulfur-containing compounds detected in the *Celeribacter* headspace extracts. A) Synthesis of 2-(methyldisulfanyl)benzothiazole (**41**) and B) synthesis of ethyl (*Z*)- and (*E*)-3-(methylsulfanyl)acrylate (**42**).

sulfur volatiles **39**, **40**, and **42**, which also questioned their natural origin. This finding is rather surprising for **42**, especially regarding the feeding experiment with (^{34}S)DMSP, because its formation would be explainable by a DMSP degradation through the demethylation pathway, for which all relevant enzymes are encoded in the six *Celeribacter* strains (only a DmdA homolog is missing in *C. indicus*, Table S1 in Supporting Information File 1), and e.g., transesterification of the DmdC product with EtOH (Scheme 1A). Compound **42** is not a widespread sulfur volatile, but has been reported before from pineapples [53], pears [62], passion fruits [63], and apples [64].

Conclusion

Six marine *Celeribacter* strains were investigated for their volatiles, leading to the identification of 42 compounds from different classes, including several sulfur volatiles. However, feeding experiments with isotopically labeled precursors suggested that only the widespread compounds dimethyl trisulfide (**37**) and *S*-methyl methanethiosulfonate (**38**) are of natural origin, while no labeling from any of the fed precursors was incorporated into 2-acetylthiazole (**39**), benzothiazole (**40**), and ethyl (*E*)-3-(methylsulfanyl)acrylate (**42**), thus questioning their natural source from *Celeribacter*. These results demonstrate that the six *Celeribacter* strains are able to degrade methionine and DMSP with formation of MeSH as a source for the likely non-enzymatic oxidation in the presence of air to **37** and **38**, opening possibilities for future studies on methionine and DMSP degrading enzymes and pathways in *Celeribacter*. Our study also shows that the results from trace compound analyses must be taken with care and contaminations from other sources must always be taken into consideration. For the unusual compound 2-(methyldisulfanyl)benzothiazole (**41**) the incorporation of labeling was observed only into the MeS group, while the benzothiazol-2-ylsulfanyl portion is likely of anthropogenic origin from the rubber vulcanization agent 2-mercaptobenzothiazole that reacts with MeSH from the bacterial metabolism.

Experimental

Strains, culture conditions, and feeding experiments

All six *Celeribacter* type strains were cultivated at 28 °C on marine broth agar plates. In case of feeding experiments, the isotopically labeled compound (1 mM) was added to the agar medium before inoculation.

Collection of volatiles

The volatiles emitted by *Celeribacter* spp. agar plate cultures were collected on charcoal filters (Chromtech, Idstein, Germany, precision charcoal filters charged with 5 mg of charcoal) by use of a closed-loop stripping apparatus as developed by Grob and Zürcher [37]. After a collection time of 24 h the charcoal was extracted with CH_2Cl_2 (50 µL) and the extract was analyzed by GC–MS.

GC–MS

GC–MS analyses were carried out through a 7890B GC – 5977A MD system (Agilent, Santa Clara, CA, USA). The GC was equipped with a HP5-MS fused silica capillary column (30 m, 0.25 mm i.d., 0.50 µm film) and operated with the settings 1) inlet pressure: 77.1 kPa, He flow: 23.3 mL min^{-1}, 2) injection volume: 2 µL, 3) splitless injection, 4) temperature program: 5 min isothermic at 50 °C, then increasing with 5 °C min^{-1} to 320 °C, and 5) He carrier gas flow: 1.2 mL min^{-1}. The parameters of the MS were 1) transfer line temperature: 250 °C, 2) ion source temperature: 230 °C, 3) quadrupole temperature: 150 °C, and 4) electron energy: 70 eV. Retention indices were calculated from retention times in comparison to those of a homologous series of *n*-alkanes (C_7–C_{40}).

General synthetic and analytical methods

Reactions were carried out in oven-dried flasks under Ar atmosphere and using distilled and dried solvents. Chemicals were obtained from Sigma-Aldrich (St. Louis, USA). Column chromatography was performed on silica gel (0.04–0.06 nm) purchased from Acros Organics (Geel, Belgium) with distilled solvents. NMR spectroscopy was performed on a Bruker (Billerica, USA) Avance III HD Ascend (500 MHz) spectrometer. Solvent peaks were used for referencing (^{1}H NMR: $CDCl_3$ residual proton signal δ = 7.26 ppm, ^{13}C NMR: $CDCl_3$ δ = 77.16 ppm) [65]. Multiplicities are indicated by s (singlet) and d (doublet), coupling constants *J* are given in Hz. IR spectra were recorded on a Bruker α spectrometer equipped with a diamond-ATR probe, and qualitative signal intensities are reported by w (weak), m (medium), and s (strong). HPLC purification of compound **42** was performed on an Azura HPLC system (Knauer, Berlin, Germany) equipped with a UV–vis detector MWL 2.1L (deuterium lamp, 190–700 nm) and a YMC ChiralART Cellulose-SC column (5 µm; 250 × 20 mm) with a guard column of the same type (30 × 20 mm). The elution was performed with hexane/propanol 60:40 (isocratic) at a flow rate of 10 mL min^{-1} (36 bar). The UV–vis absorption was monitored at 275 nm.

Synthesis of 2-(methyldisulfanyl)benzothiazole (**41**)

1,2-Bis(benzothiazol-2-yl)disulfane (**43**, 1.00 g, 3.00 mmol, 1 equiv) and dimethyl sulfide (**44**, 0.28 g, 3.00 mmol, 1 equiv) were dissolved in dry CH_3NO_2 (10 mL) and dry CH_2Cl_2 (10 mL). The solution was cooled to 0 °C and then treated with $BF_3{\cdot}Et_2O$ (43 mg, 0.3 mmol, 0.1 equiv). After stirring at 0 °C for 3 hours and at room temperature overnight, the reaction was

quenched by the addition of water (10 mL) and extracted with ethyl acetate (3 × 50 mL). The combined extracts were dried with $MgSO_4$ and concentrated. The residue was purified by column chromatography (cyclohexane/ethyl acetate 1:1) to give **41** as a colorless solid (0.82 g, 3.85 mmol, 64%). R_f 0.60 (cyclohexane/ethyl acetate 5:1; TLC visualized with UV illumination at 366 nm); GC (HP-5MS): I = 1854; IR (diamond-ATR) ṽ: 3060 (s), 2916 (s), 1425 (w), 1310 (s), 1236 (s), 1005 (w), 756 (w), 431 (s) cm^{-1}; ^1H NMR (500 MHz, $CDCl_3$, 298 K) δ 7.88 (ddd, J = 8.1, 1.2, 0.7 Hz, 1H, CH), 7.87 (ddd, J = 7.9, 1.2, 0.6 Hz, 1H, CH), 7.43 (ddd, J = 8.3, 7.3, 1.2 Hz, 1H, CH), 7.33 (ddd, J = 8.2, 7.2, 1.2 Hz, 1H, CH), 2.67 (s, 3H, CH_3) ppm; ^{13}C NMR (125 MHz, $CDCl_3$, 298 K) δ 172.50 (C), 155.17 (C), 135.90 (C), 126.37 (CH), 124.70 (CH), 122.24 (CH), 121.27 (CH), 23.62 (CH_3) ppm.

Synthesis of ethyl (*Z*)-3-(methylsulfanyl)acrylate ((*Z*)-**42**) and ethyl (*E*)-3-(methylsulfanyl)acrylate ((*E*)-**42**)

Ethyl propiolate (**45**, 70 mg, 0.71 mmol, 1 equiv) was dissolved in distilled water (5 mL) followed by the addition of sodium methanethiolate (50 mg, 0.71 mmol, 1 equiv). The solution was stirred for 30 minutes at room temperature. Water (5 mL) was added and the product was extracted with ethyl acetate (3 × 10 mL). The combined extracts were dried over $MgSO_4$ and concentrated to afford the crude product. Purification by column chromatography (cyclohexane/ethyl acetate 99:1) gave a mixture of stereoisomers (*Z*)-**42** and (*E*)-**42** as pale yellow oil (96 mg, 0.65 mmol, 92%, dr 94:6 by ^1H NMR). The product mixture was separated by preparative HPLC to give pure (*Z*)-**42** (73 mg, 0.50 mmol, 70%) and (*E*)-**42** (6 mg, 0.04 mmol, 6%).

(*Z*)-42. R_f 0.74 (cyclohexane/ethyl acetate 1:1); GC (HP-5MS): I = 1200; IR (diamond-ATR) ṽ: 2982 (w), 2927 (w),1695 (m), 1569 (m), 1434 (w), 1374 (w), 1300 (w), 1266 (w), 1213 (m), 1166 (s), 1095 (w), 1033 (w), 986 (w), 961 (w), 800 (w), 727 (w), 687 (w) cm^{-1}; ^1H NMR (700 MHz, $CDCl_3$, 298 K) δ 7.04 (d, J = 10.14 Hz, 1H, CH), 5.83 (d, J = 10.14 Hz, 1H, CH), 4.20 (q, J = 7.15 Hz, 2H, CH_2), 2.39 (s, 3H, CH_3), 1.29 (t, J = 7.17 Hz, 3H, CH_3) ppm; ^{13}C NMR (175 MHz, $CDCl_3$, 298 K) δ 166.75 (C), 151.84 (CH), 113.18 (CH), 60.17 (CH_2), 19.28 (CH_3), 14.44 (CH_3) ppm.

(*E*)-42. R_f 0.76 (cyclohexane/ethyl acetate 1:1); GC (HP-5MS): I = 1177; IR (diamond-ATR) ṽ: 2980 (w), 2925 (w), 1701 (s), 1578 (s), 1444 (w), 1366 (w), 1322 (w), 1297 (m), 1251 (s), 1161 (s), 1095 (w), 1037 (m), 945 (m), 886 (w), 832 (w), 799 (w), 702 (w) cm^{-1}; ^1H NMR (700 MHz, $CDCl_3$, 298 K) δ 7.76 (d, J = 14.93 Hz, 1H, CH), 5.68 (d, J = 14.90 Hz, 1H, CH), 4.21 (q, J = 7.14 Hz, 2H, CH_2), 2.35 (s, 3H, CH_3), 1.31 (t, J = 7.13 Hz, 3H, CH_3) ppm; ^{13}C NMR (175 MHz, $CDCl_3$, 297 K) δ 165.59 (C), 147.21 (CH),113.56 (CH), 60.55 (CH_2), 27.26 (CH_3), 14.67 (CH_3) ppm.

Supporting Information

Supporting Information File 1

DMSP demethylation pathway in *Celeribacter* spp. and copies of spectra.
[https://www.beilstein-journals.org/bjoc/content/supplementary/1860-5397-17-38-S1.pdf]

Acknowledgements

We thank Andreas Schneider (Bonn) for HPLC separation of (*E*)- and (*Z*)-**42**.

Funding

This work was funded by the Deutsche Forschungsgemeinschaft (DFG, German Research Foundation) – Project-ID 34509606 – TRR 51 within the frame of the Transregional Collaborative Research Center “Roseobacter”.

ORCID® iDs

Jeroen S. Dickschat - https://orcid.org/0000-0002-0102-0631

References

1. Giovannoni, S. J.; Stingl, U. *Nature* **2005,** *437,* 343–348. doi:10.1038/nature04158
2. González, J. M.; Moran, M. A. *Appl. Environ. Microbiol.* **1997,** *63,* 4237–4242. doi:10.1128/aem.63.11.4237-4242.1997
3. Selje, N.; Simon, M.; Brinkhoff, T. *Nature* **2004,** *427,* 445–448. doi:10.1038/nature02272
4. Brinkhoff, T.; Giebel, H.-A.; Simon, M. *Arch. Microbiol.* **2008,** *189,* 531–539. doi:10.1007/s00203-008-0353-y
5. Lee, O. O.; Tsoi, M. M. Y.; Li, X.; Wong, P.-K.; Qian, P.-Y. *Int. J. Syst. Evol. Microbiol.* **2007,** *57,* 1919–1924. doi:10.1099/ijs.0.64801-0
6. Ruiz-Ponte, C.; Cilia, V.; Lambert, C.; Nicolas, J. L. *Int. J. Syst. Bacteriol.* **1998,** *48,* 537–542. doi:10.1099/00207713-48-2-537
7. Shiba, T. *Syst. Appl. Microbiol.* **1991,** *14,* 140–145. doi:10.1016/s0723-2020(11)80292-4
8. Biebl, H.; Allgaier, M.; Tindall, B. J.; Koblizek, M.; Lünsdorf, H.; Pukall, R.; Wagner-Döbler, I. *Int. J. Syst. Evol. Microbiol.* **2005,** *55,* 1089–1096. doi:10.1099/ijs.0.63511-0
9. Lafay, B.; Ruimy, R.; Rausch de Traubenberg, C.; Breittmayer, V.; Gauthier, M. J.; Christen, R. *Int. J. Syst. Bacteriol.* **1995,** *45,* 290–296. doi:10.1099/00207713-45-2-290
10. Gonzalez, J. M.; Simo, R.; Massana, R.; Covert, J. S.; Casamayor, E. O.; Pedros-Alio, C.; Moran, M. A. *Appl. Environ. Microbiol.* **2000,** *66,* 4237–4246. doi:10.1128/aem.66.10.4237-4246.2000

11. Dickschat, J. S.; Rabe, P.; Citron, C. A. *Org. Biomol. Chem.* **2015,** *13,* 1954–1968. doi:10.1039/c4ob02407a
12. Reisch, C. R.; Stoudemayer, M. J.; Varaljay, V. A.; Amster, I. J.; Moran, M. A.; Whitman, W. B. *Nature* **2011,** *473,* 208–211. doi:10.1038/nature10078
13. Todd, J. D.; Rogers, R.; Li, Y. G.; Wexler, M.; Bond, P. L.; Sun, L.; Curson, A. R. J.; Malin, G.; Steinke, M.; Johnston, A. W. B. *Science* **2007,** *315,* 666–669. doi:10.1126/science.1135370
14. Todd, J. D.; Kirkwood, M.; Newton-Payne, S.; Johnston, A. W. B. *ISME J.* **2012,** *6,* 223–226. doi:10.1038/ismej.2011.79
15. Kirkwood, M.; Le Brun, N. E.; Todd, J. D.; Johnston, A. W. B. *Microbiology (London, U. K.)* **2010,** *156,* 1900–1906. doi:10.1099/mic.0.038927-0
16. Todd, J. D.; Curson, A. R. J.; Kirkwood, M.; Sullivan, M. J.; Green, R. T.; Johnston, A. W. B. *Environ. Microbiol.* **2011,** *13,* 427–438. doi:10.1111/j.1462-2920.2010.02348.x
17. Curson, A. R. J.; Rogers, R.; Todd, J. D.; Brearley, C. A.; Johnston, A. W. B. *Environ. Microbiol.* **2008,** *10,* 757–767. doi:10.1111/j.1462-2920.2007.01499.x
18. Curson, A. R. J.; Sullivan, M. J.; Todd, J. D.; Johnston, A. W. B. *ISME J.* **2011,** *5,* 1191–1200. doi:10.1038/ismej.2010.203
19. Sun, J.; Todd, J. D.; Thrash, J. C.; Qian, Y.; Qian, M. C.; Temperton, B.; Guo, J.; Fowler, E. K.; Aldrich, J. T.; Nicora, C. D.; Lipton, M. S.; Smith, R. D.; De Leenheer, P.; Payne, S. H.; Johnston, A. W. B.; Davie-Martin, C. L.; Halsey, K. H.; Giovannoni, S. J. *Nat. Microbiol.* **2016,** *1,* 16065. doi:10.1038/nmicrobiol.2016.65
20. Lovelock, J. E.; Maggs, R. J.; Rasmussen, R. A. *Nature* **1972,** *237,* 452–453. doi:10.1038/237452a0
21. Charlson, R. J.; Lovelock, J. E.; Andreae, M. O.; Warren, S. G. *Nature* **1987,** *326,* 655–661. doi:10.1038/326655a0
22. Dickschat, J. S.; Zell, C.; Brock, N. L. *ChemBioChem* **2010,** *11,* 417–425. doi:10.1002/cbic.200900668
23. Brock, N. L.; Citron, C. A.; Zell, C.; Berger, M.; Wagner-Döbler, I.; Petersen, J.; Brinkhoff, T.; Simon, M.; Dickschat, J. S. *Beilstein J. Org. Chem.* **2013,** *9,* 942–950. doi:10.3762/bjoc.9.108
24. Brock, N. L.; Menke, M.; Klapschinski, T. A.; Dickschat, J. S. *Org. Biomol. Chem.* **2014,** *12,* 4318–4323. doi:10.1039/c4ob00719k
25. Celik, E.; Maczka, M.; Bergen, N.; Brinkhoff, T.; Schulz, S.; Dickschat, J. S. *Org. Biomol. Chem.* **2017,** *15,* 2919–2922. doi:10.1039/c7ob00357a
26. Durham, B. P.; Sharma, S.; Luo, H.; Smith, C. B.; Amin, S. A.; Bender, S. J.; Dearth, S. P.; Van Mooy, B. A. S.; Campagna, S. R.; Kujawinski, E. B.; Armbrust, E. V.; Moran, M. A. *Proc. Natl. Acad. Sci. U. S. A.* **2015,** *112,* 453–457. doi:10.1073/pnas.1413137112
27. Mönnich, J.; Tebben, J.; Bergemann, J.; Case, R.; Wohlrab, S.; Harder, T. *ISME J.* **2020,** *14,* 1614–1625. doi:10.1038/s41396-020-0631-5
28. Bruhn, J. B.; Nielsen, K. F.; Hjelm, M.; Hansen, M.; Bresciani, J.; Schulz, S.; Gram, L. *Appl. Environ. Microbiol.* **2005,** *71,* 7263–7270. doi:10.1128/aem.71.11.7263-7270.2005
29. Greer, E. M.; Aebisher, D.; Greer, A.; Bentley, R. *J. Org. Chem.* **2008,** *73,* 280–283. doi:10.1021/jo7018416
30. Kintaka, K.; Ono, H.; Tsubotani, S.; Harada, S.; Okazaki, H. *J. Antibiot.* **1984,** *37,* 1294–1300. doi:10.7164/antibiotics.37.1294
31. Geng, H.; Bruhn, J. B.; Nielsen, K. F.; Gram, L.; Belas, R. *Appl. Environ. Microbiol.* **2008,** *74,* 1535–1545. doi:10.1128/aem.02339-07
32. Berger, M.; Brock, N. L.; Liesegang, H.; Dogs, M.; Preuth, I.; Simon, M.; Dickschat, J. S.; Brinkhoff, T. *Appl. Environ. Microbiol.* **2012,** *78,* 3539–3551. doi:10.1128/aem.07657-11
33. Brock, N. L.; Nikolay, A.; Dickschat, J. S. *Chem. Commun.* **2014,** *50,* 5487–5489. doi:10.1039/c4cc01924e
34. Beyersmann, P. G.; Tomasch, J.; Son, K.; Stocker, R.; Göker, M.; Wagner-Döbler, I.; Simon, M.; Brinkhoff, T. *Sci. Rep.* **2017,** *7,* 730. doi:10.1038/s41598-017-00784-7
35. Thiel, V.; Brinkhoff, T.; Dickschat, J. S.; Wickel, S.; Grunenberg, J.; Wagner-Döbler, I.; Simon, M.; Schulz, S. *Org. Biomol. Chem.* **2010,** *8,* 234–246. doi:10.1039/b909133e
36. Seyedsayamdost, M. R.; Case, R. J.; Kolter, R.; Clardy, J. *Nat. Chem.* **2011,** *3,* 331–335. doi:10.1038/nchem.1002
37. Grob, K.; Zürcher, F. *J. Chromatogr.* **1976,** *117,* 285–294. doi:10.1016/0021-9673(76)80005-2
38. Kováts, E. *Helv. Chim. Acta* **1958,** *41,* 1915–1932. doi:10.1002/hlca.19580410703
39. Elmore, J. S.; Mottram, D. S.; Enser, M.; Wood, J. D. *Meat Sci.* **2000,** *55,* 149–159. doi:10.1016/s0309-1740(99)00137-0
40. Dickschat, J. S.; Wickel, S.; Bolten, C. J.; Nawrath, T.; Schulz, S.; Wittmann, C. *Eur. J. Org. Chem.* **2010,** 2687–2695. doi:10.1002/ejoc.201000155
41. Cerny, C.; Guntz-Dubini, R. *J. Agric. Food Chem.* **2006,** *54,* 574–577. doi:10.1021/jf052222s
42. Spadone, J.-C.; Takeoka, G.; Liardon, R. *J. Agric. Food Chem.* **1990,** *38,* 226–233. doi:10.1021/jf00091a050
43. Lee, S.-R.; Macku, C.; Shibamoto, T. *J. Agric. Food Chem.* **1991,** *39,* 1972–1975. doi:10.1021/jf00011a017
44. Pino, J. A.; Mesa, J.; Muñoz, Y.; Martí, M. P.; Marbot, R. *J. Agric. Food Chem.* **2005,** *53,* 2213–2223. doi:10.1021/jf0402633
45. Adams, R. P. *Identification of Essential Oil Components by Gas Chromatography/Mass Spectrometry;* Allured Pub Corp.: Carol Stream, IL, 2009.
46. Ansorena, D.; Gimeno, O.; Astiasarán, I.; Bello, J. *Food Res. Int.* **2001,** *34,* 67–75. doi:10.1016/s0963-9969(00)00133-2
47. Citron, C. A.; Rabe, P.; Dickschat, J. S. *J. Nat. Prod.* **2012,** *75,* 1765–1776. doi:10.1021/np300468h
48. Owens, J. D.; Allagheny, N.; Kipping, G.; Ames, J. M. *J. Sci. Food Agric.* **1997,** *74,* 132–140. doi:10.1002/(sici)1097-0010(199705)74:1<132::aid-jsfa779>3.0.co;2-8
49. Cha, Y. J.; Cadwallader, K. R. *J. Agric. Food Chem.* **1998,** *46,* 1123–1128. doi:10.1021/jf970380g
50. Wickel, S. M.; Citron, C. A.; Dickschat, J. S. *Eur. J. Org. Chem.* **2013,** 2906–2913. doi:10.1002/ejoc.201300049
51. Kubec, R.; Drhová, V.; Velíšek, J. *J. Agric. Food Chem.* **1998,** *46,* 4334–4340. doi:10.1021/jf980379x
52. Ferhat, M. A.; Tigrine-Kordjani, N.; Chemat, S.; Meklati, B. Y.; Chemat, F. *Chromatographia* **2007,** *65,* 217–222. doi:10.1365/s10337-006-0130-5
53. Takeoka, G. R.; Buttery, R. G.; Teranishi, R.; Flath, R. A.; Güntert, M. *J. Agric. Food Chem.* **1991,** *39,* 1848–1851. doi:10.1021/jf00010a032
54. Nawrath, T.; Mgode, G. F.; Weetjens, B.; Kaufmann, S. H. E.; Schulz, S. *Beilstein J. Org. Chem.* **2012,** *8,* 290–299. doi:10.3762/bjoc.8.31
55. Citron, C. A.; Barra, L.; Wink, J.; Dickschat, J. S. *Org. Biomol. Chem.* **2015,** *13,* 2673–2683. doi:10.1039/c4ob02609h
56. Schulz, S.; Dickschat, J. S. *Nat. Prod. Rep.* **2007,** *24,* 814–842. doi:10.1039/b507392h
57. Dickschat, J. S. *Nat. Prod. Rep.* **2017,** *34,* 310–328. doi:10.1039/c7np00003k

58. Ueda, D.; Matsugane, S.; Okamoto, W.; Hashimoto, M.; Sato, T. *Angew. Chem., Int. Ed.* **2018,** *57,* 10347–10351. doi:10.1002/anie.201805383
59. Werz, D. B.; Staeb, T. H.; Benisch, C.; Rausch, B. J.; Rominger, F.; Gleiter, R. *Org. Lett.* **2002,** *4,* 339–342. doi:10.1021/ol016953z
60. Leverett, C. A.; Purohit, V. C.; Romo, D. *Angew. Chem., Int. Ed.* **2010,** *49,* 9479–9483. doi:10.1002/anie.201004671
61. Dickschat, J. S. *Nat. Prod. Rep.* **2014,** *31,* 838–861. doi:10.1039/c3np70080a
62. Takeoka, G. R.; Buttery, R. G.; Flath, R. A. *J. Agric. Food Chem.* **1992,** *40,* 1925–1929. doi:10.1021/jf00022a040
63. Werkhoff, P.; Güntert, M.; Krammer, G.; Sommer, H.; Kaulen, J. *J. Agric. Food Chem.* **1998,** *46,* 1076–1093. doi:10.1021/jf970655s
64. Ferreira, L.; Perestrelo, R.; Caldeira, M.; Câmara, J. S. *J. Sep. Sci.* **2009,** *32,* 1875–1888. doi:10.1002/jssc.200900024
65. Fulmer, G. R.; Miller, A. J. M.; Sherden, N. H.; Gottlieb, H. E.; Nudelman, A.; Stoltz, B. M.; Bercaw, J. E.; Goldberg, K. I. *Organometallics* **2010,** *29,* 2176–2179. doi:10.1021/om100106e

License and Terms

BEILSTEIN JOURNAL OF ORGANIC CHEMISTRY

Breakdown of 3-(allylsulfonio)propanoates in bacteria from the *Roseobacter* group yields garlic oil constituents

Anuj Kumar Chhalodia and Jeroen S. Dickschat*

Full Research Paper

Open Access

Address:
Kekulé Institute of Organic Chemistry and Biochemistry, University of Bonn, Gerhard-Domagk-Straße 1, 53121 Bonn, Germany

Email:
Jeroen S. Dickschat* - dickschat@uni-bonn.de

* Corresponding author

Keywords:
Allium sativum; allyl sulfides; 3-(dimethylsulfonio)propanoate; *Roseobacter*; volatiles

Beilstein J. Org. Chem. **2021,** *17,* 569–580.
https://doi.org/10.3762/bjoc.17.51

Received: 22 December 2020
Accepted: 19 February 2021
Published: 26 February 2021

This article is part of the thematic issue "Chemical ecology".

Guest Editor: C. Beemelmanns

Abstract

Two analogues of 3-(dimethylsulfonio)propanoate (DMSP), 3-(diallylsulfonio)propanoate (DAllSP), and 3-(allylmethylsulfonio)propanoate (AllMSP), were synthesized and fed to marine bacteria from the *Roseobacter* clade. These bacteria are able to degrade DMSP into dimethyl sulfide and methanethiol. The DMSP analogues were also degraded, resulting in the release of allylated sulfur volatiles known from garlic. For unknown compounds, structural suggestions were made based on their mass spectrometric fragmentation pattern and confirmed by the synthesis of reference compounds. The results of the feeding experiments allowed to conclude on the substrate tolerance of DMSP degrading enzymes in marine bacteria.

Introduction

The name of the allyl group has been introduced by Wertheim in 1844 when he investigated the constituents of garlic oil and derives from the botanical name of garlic (*Allium sativum*) [1]. During that time, the structures of the garlic oil constituents and also of the allyl group remained unknown, but its formula was correctly assigned as C_3H_5. Five decades later, Semmler reported on the nature of allyl propyl disulfide (**1**), diallyl disulfide (**2**), diallyl trisulfide (**3**), and diallyl tetrasulfide (**4**) from garlic oil (Scheme 1A) [2]. The antibacterial principle in garlic was identified in 1944 by Cavallito et al. as allicin (**5**) [3], a formal oxidation product of disulfide **2**. Not only **5**, but also several other sulfur compounds from garlic are today known to exhibit diverse biological activities, including inter alia antibacterial, antifungal, antioxidant, anti-inflammatory, and anticancer effects [4]. Later on, also heterocyclic compounds including 2-vinyl-4*H*-1,3-dithiine (**6**) and 3-vinyl-3,4-dihydro-1,2-dithiine (**7**) were discovered [5]. The formation of these volatile sulfur compounds starts from alliin (**9**) [6], a non-volatile precursor that is stored in garlic and related plants and only degraded into sulfur volatiles upon wounding by the pyridoxal phosphate (PLP) dependent alliinase (Scheme 1B) [7]. This initial enzyme-catalyzed reaction yields one equivalent of allyl-

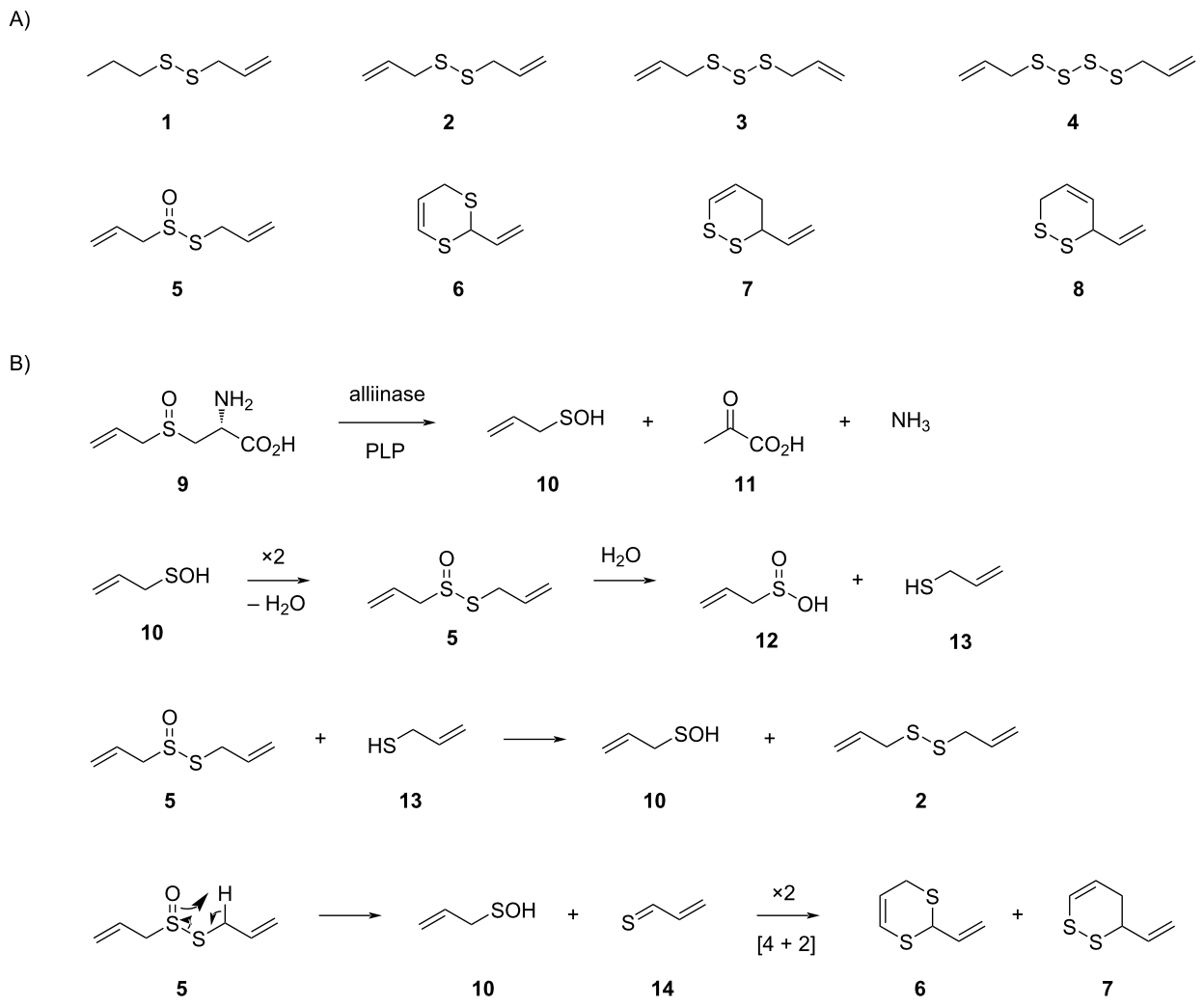

Scheme 1: Volatile allyl sulfides. A) Compounds known from garlic oil, B) mechanism of formation from alliin (**9**) by the PLP-dependent allinase (PLP: pyridoxalphosphate) and subsequent spontaneous reactions.

sulfenic acid (**10**), pyruvic acid (**11**), and ammonia from **9**, followed by a series of proposed spontaneous reactions [5,8]. Through these transformations, acid **10** can undergo a dimerization with elimination of water to allicin (**5**). The hydrolysis of **5** results in allylsulfinic acid (**12**) and allyl thiol (**13**), the latter of which can react with another molecule of **5** to yield **10** and **2**. Alternatively, **5** can decompose to **10** and thioacroleine (**14**) by a Cope elimination, which explains the formation of the heterocycles **6** and **7** by dimerization through a [4 + 2] cycloaddition [5]. Compounds **6** and **7** were also reported to be formed from **5** during gas chromatographic (GC) analysis by an unknown mechanism [9] (**7** was confused with its double bond regioisomer 3-vinyl-3,6-dihydro-1,2-dithiine (**8**) in this study [5]). Under these conditions the formation of the heterocyclic disulfides **7** and **8** may not involve a dimerization of **14**, as a [4 + 2] cycloaddition is not a preferred gas-phase reaction.

The ecology of marine bacteria in their interaction with algae is particularly interesting in which the bacteria can promote the algal growth, but can also kill their host [10,11]. For both processes, the phytohormone indole-3-acetic acid is used as a messenger molecule [10]. For the macroalga *Ulva mutabilis* the presence of bacteria from the *Roseobacter* group is even mandatory for proper algal development, and 3-(dimethylsulfonio)propanoate (DMSP) is used as a chemotactic signal by the bacteria attracting them towards the algal host [12]. Many bacteria and fungi also release sulfur volatiles [13,14] that are especially important headspace constituents from marine bacteria of the *Roseobacter* group [15-17]. In these organisms, sulfur volatiles are to a large extent generated from algal (DMSP), a metabolite that is produced in massive amounts by algae [18], thus giving another example for the complex interactions between marine bacteria and algae. Known DMSP degradation pathways include its hydrolysis to dimethyl sulfide

(DMS) and 3-hydroxypropanoic acid (**15**) by the enzyme DddD [19], or the lysis to DMS and acrylic acid (**16**) for which various enzymes including DddL [20], DddP [21], DddQ [22], DddY [23], DddW [24], and DddK [25] have been described (Scheme 2A). Furthermore, a demethylation pathway is known through which DMSP is first converted into methylmercaptopropanoic acid (**17**) by the tetrahydrofolate (FH_4)-dependent demethylase, DmdA (Scheme 2B) [26]. Compound **17** can be transformed into the coenzyme A thioester **18** by the CoA ligase DmdB, followed by FAD-dependent oxidation to the α,β-unsaturated compound **19** by DmdC. The attack of water to the Michael acceptor catalyzed by the enoyl-CoA hydratase DmdD yields the hemithioacetal **20** that spontaneously collapses to methanethiol (MeSH) and malonyl-CoA semialdehyde (**21**). This compound further degrades to acetaldehyde (**22**) through the thioester hydrolysis and decarboxylation [27].

Feeding of (*methyl*-$^2H_6$)DMSP to *Phaeobacter inhibens* DSM 17395 and *Ruegeria pomeroyi* DSM 15171 resulted in the efficient uptake of labelling into dimethyl disulfide (DMDS), the oxidative dimerization product from MeSH, showing the activity of the demethylation pathway in these bacteria. However, knockout of the *dmdA* gene in *R. pomeroyi* still gave a low incorporation of labelling into DMDS, suggesting the presence of another gene responsible for the demethylation activity [28]. Also the labelling from (^{34}S)DMSP was efficiently incorporated into DMDS and dimethyl trisulfide (DMTS) [29]. Our previous investigations have also demonstrated that synthetic, i.e., non-natural DMSP analogues such as 3-(ethylmethyl)sulfoniopropanoate (EMSP), 3-(diethylsulfonio)propanoate (DESP), 3-(dimethylselenio)propanoate (DMSeP; this compound is also formed naturally in *Spartina alterniflora* in the presence of sodium selenate [30]), and even 3-(dimethyltellurio)propanoate (DMTeP) are converted by the demethylation pathway into ethanethiol, methaneselenol, and methanetellurol, respectively, that further react to various volatiles containing EtS, MeSe, and MeTe groups [31]. The in vitro incubations of these DMSP analogues with recombinant DddQ and DddW from *R. pomeroyi* and DddP from *P. inhibens* demonstrated that all substrate analogues can be degraded through the lysis pathway into the corresponding dialkyl chalcogenides; only DMTeP was not cleaved by DddQ [32]. Here we describe the synthesis of the new DMSP analogues 3-(allylmethylsulfonio)propanoate (AllMSP) and 3-(diallylsulfonio)propanoate (DAllSP) and their

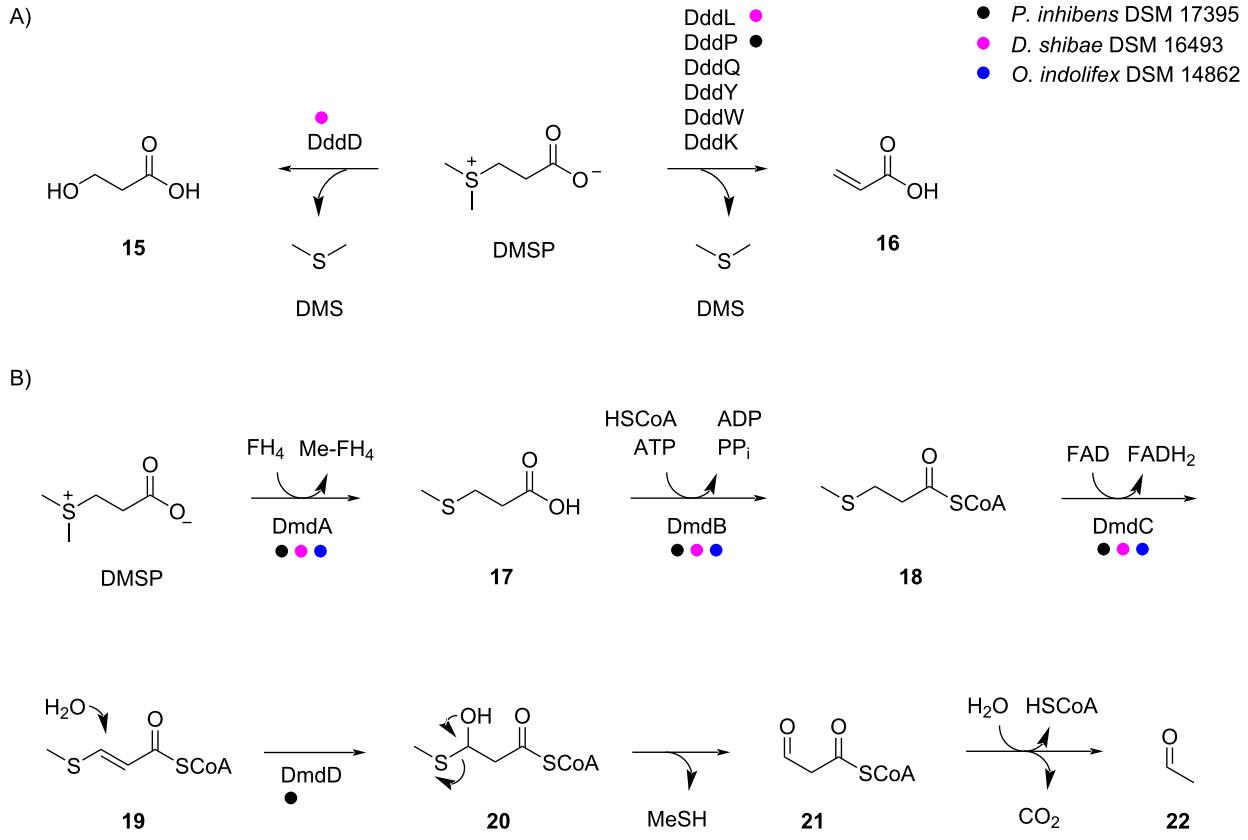

Scheme 2: Degradation of DMSP by marine bacteria. A) Hydrolysis or lysis to DMS, B) demethylation pathway leading to MeSH. The color code shows which enzymes are encoded in the genomes of the strains investigated in this study.

conversion into typical garlic odor constituents by marine bacteria from the *Roseobacter* group that do not naturally occur in these organisms.

Results and Discussion

3-(Diallylsulfonio)propanoate (DAllSP) and 3-(allylmethylsulfonio)propanoate (AllMSP) were synthesized by the acid-catalyzed addition of allyl methyl sulfide and diallyl sulfide, respectively, to acrylic acid (Scheme 3). The obtained DMSP analogues were fed to marine broth agar plate cultures of three strains from the *Roseobacter* group with fully sequenced genomes, including *P. inhibens* DSM 17395, *Dinoroseobacter shibae* DSM 16493, and *Oceanibulbus indolifex* DSM 14862. In all cases the bacterial cultures released a strong garlic-like odor, presumptively due to a degradation of the DMSP derivatives to sulfur-containing volatiles, similar to the compounds known from garlic, through one of the pathways shown in Scheme 2. The emitted volatiles were captured on charcoal filter traps using a closed-loop stripping apparatus (CLSA) [33], followed by the extraction of the filters with CH_2Cl_2 and analysis by gas chromatography–mass spectrometry (GC–MS) of the resulting extracts. Most of the compounds were readily identified by the comparison of their mass spectra and retention indices to published data. Every experiment was performed in triplicate to check for the reproducibility of the results. For comparison, the volatiles from all three strains grown on marine broth medium without the addition of DMSP or its analogues have been reported before [31].

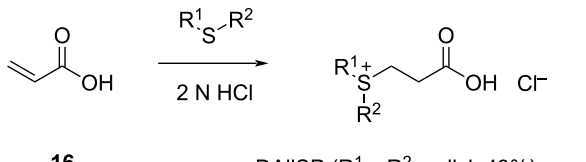

Scheme 3: Synthesis of DMSP derivatives.

Feeding of DAllSP to *P. inhibens* resulted in the production of sulfur volatiles including several allyl derivatives (Figure 1, Figure 2A, Table 1, and Figure S1 in Supporting Information File 1). Besides the methylated sulfur compounds dimethyl trisulfide (**31**), dimethyl tetrasulfide (**33**), and *S*-methyl methanethiosulfonate (**28**) that were reported previously from *P. inhibens* [31], large amounts of diallyl sulfide (**29**) were observed, pointing to an efficient degradation of DAllSP through the lysis pathway, for which the DMSP lyase DddP can account in this organism (Scheme 2). Furthermore, the compounds allyl methyl disulfide (**30**), diallyl disulfide (**2**), allyl methyl trisulfide (**32**), and traces of diallyl trisulfide (**3**) and allyl methyl tetrasulfide (**34**) were observed. The formation of these compounds is explainable by the deallylation of DAllSP to 3-(allylsulfanyl)propanoic acid (**37**) and further degradation to allyl thiol (**13**) through the enzymes of the demethylation pathway that is fully established in *P. inhibens* by genes coding for DmdA–D (Scheme 4A). In the presence of air thiol **13** can then undergo an oxidative dimerization, or react analogously with MeSH to form allyl methyl disulfide (**30**, Scheme 4B). Similar oxidations requiring one additional unit of hydrogen sulfide can lead to the trisulfides **3** and **32** (Scheme 4C), while higher polysulfides such as **34** can arise through a metathesis reaction of two trisulfides (Scheme 4D). Also traces of methyl 3-(allylsulfanyl)propanoate (**24**), methyl 3-(methyldisulfanyl)propanoate (**25**), and methyl 3-(allyldisulfanyl)propanoate (**26**) were observed. While the presence of **24** can be explained by the *O*-methylation of the DmdA product **37** with *S*-adenosylmethionine (SAM, Scheme 4E), compounds **25** and **26** require a second deallylation of **37** to 3-mercaptopropanoic acid (**38**) possibly by DmdA, the reaction with a corresponding thiol MeSH or **13**, and *O*-methylation (Scheme 4F).

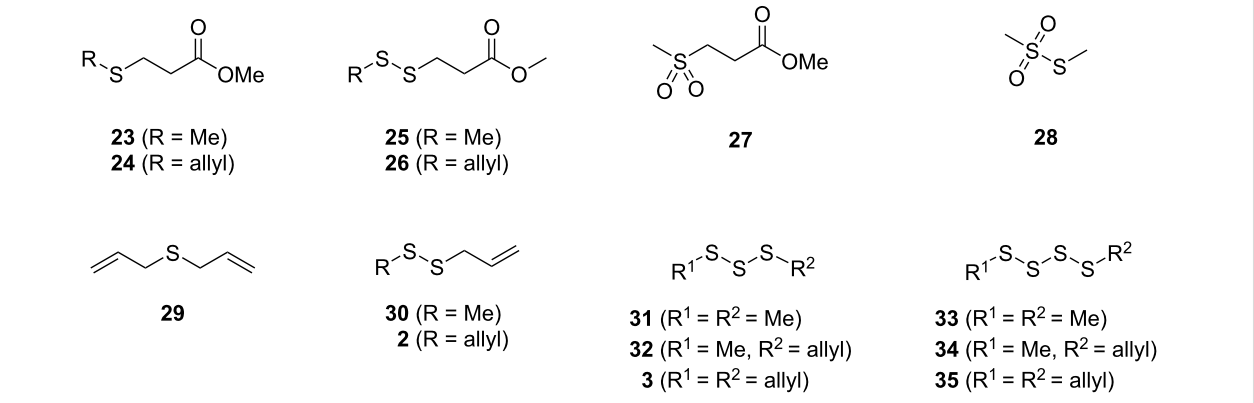

Figure 1: Sulfur volatiles released by agar plate cultures of marine bacteria fed with DAllSP or AllMSP.

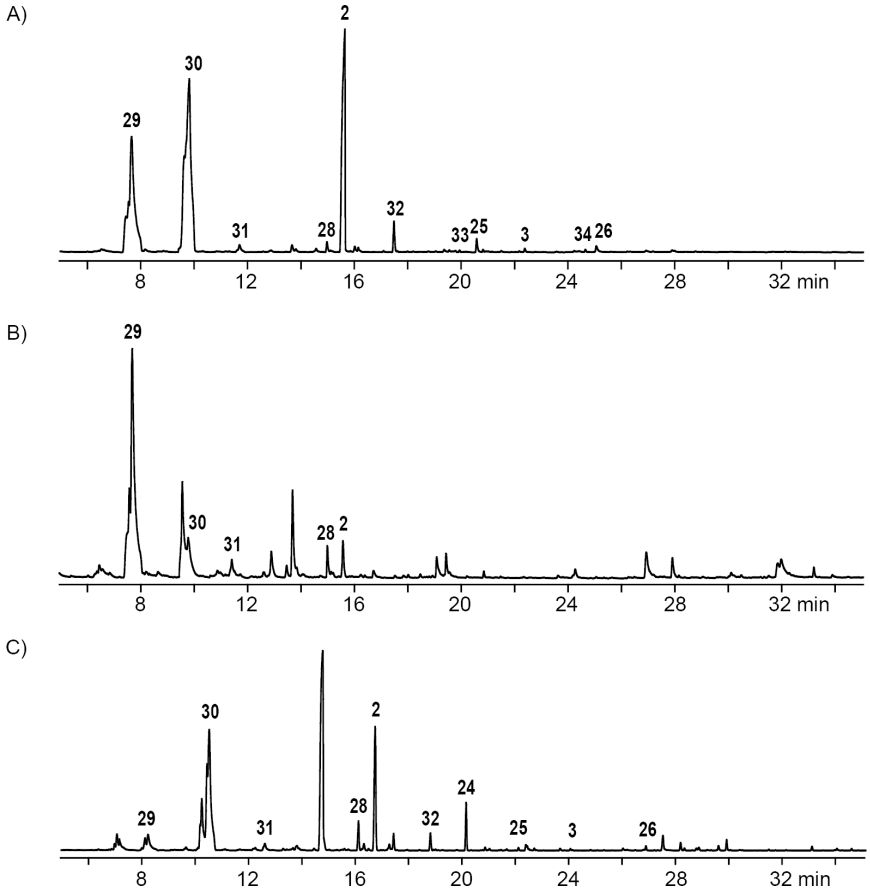

Figure 2: Total ion chromatograms of CLSA extracts obtained from feeding experiments with DAllSP fed to A) *P. inhibens*, B) *D. shibae*, and C) *O. indolifex*. Numbers at peaks refer to compounds in Figure 1. Peaks without numbers are unidentified.

Table 1: Volatiles from agar plate cultures fed with DAllSP.

Compound[a]	*I*	$I_{lit.}$[b]	*P. in.*[c]	*D. sh.*[c]	*O. in.*[c]
diallyl sulfide (**29**)*	849	848 [34]	●●●	●●●	●●●
allyl methyl disulfide (**30**)	910	912 [34]	●●●	●●●	●●●
dimethyl trisulfide (**31**)*	967	970 [35]	●●●	●○●	●●○
S-methyl methanethiosulfonate (**28**)*	1063	1068 [35]	●●●	●●●	●●○
diallyl disulfide (**2**)*	1074	1075 [34]	●●●	●●●	●●●
allyl methyl trisulfide (**32**)	1136	1133 [36]	●●●	○○●	●●●
methyl 3-(allylsulfanyl)-propanoate (**24**)	1177	–	○●○	○○○	●●●
dimethyl tetrasulfide (**33**)	1216	1215 [37]	●●●	○○○	○○○
methyl 3-(methyldisulfanyl)-propanoate (**25**)*	1236	–	●●●	○○●	●○●
diallyl trisulfide (**3**)	1300	1300 [38]	●●●	○○○	●○●
allyl methyl tetrasulfide (**34**)	1382	1371 [39]	●●○	○○○	○○●
methyl 3-(allyldisulfanyl)-propanoate (**26**)*	1397	–	●●●	○○●	●○●
diallyl tetrasulfide (**35**)	1551	1540 [38]	○○○	○○○	○○●

[a]Asterisks indicate the identity to a commercially available or synthetic reference standard. [b]Retention index literature data for a HP5-MS or a similar GC column. [c]Abbreviations are *P. in.* = *Phaeobacter inhibens*, *D. sh.* = *Dinoroseobacter shibae*, and *O. in.* = *Oceanibulbus indolifex*. Filled circles indicate the presence, non-filled circles indicate the absence of a compound in the headspace extract. The colors of the circles refer to the chromatograms in Figure 2 and Figure S1–S3 in Supporting Information File 1 with the same color.

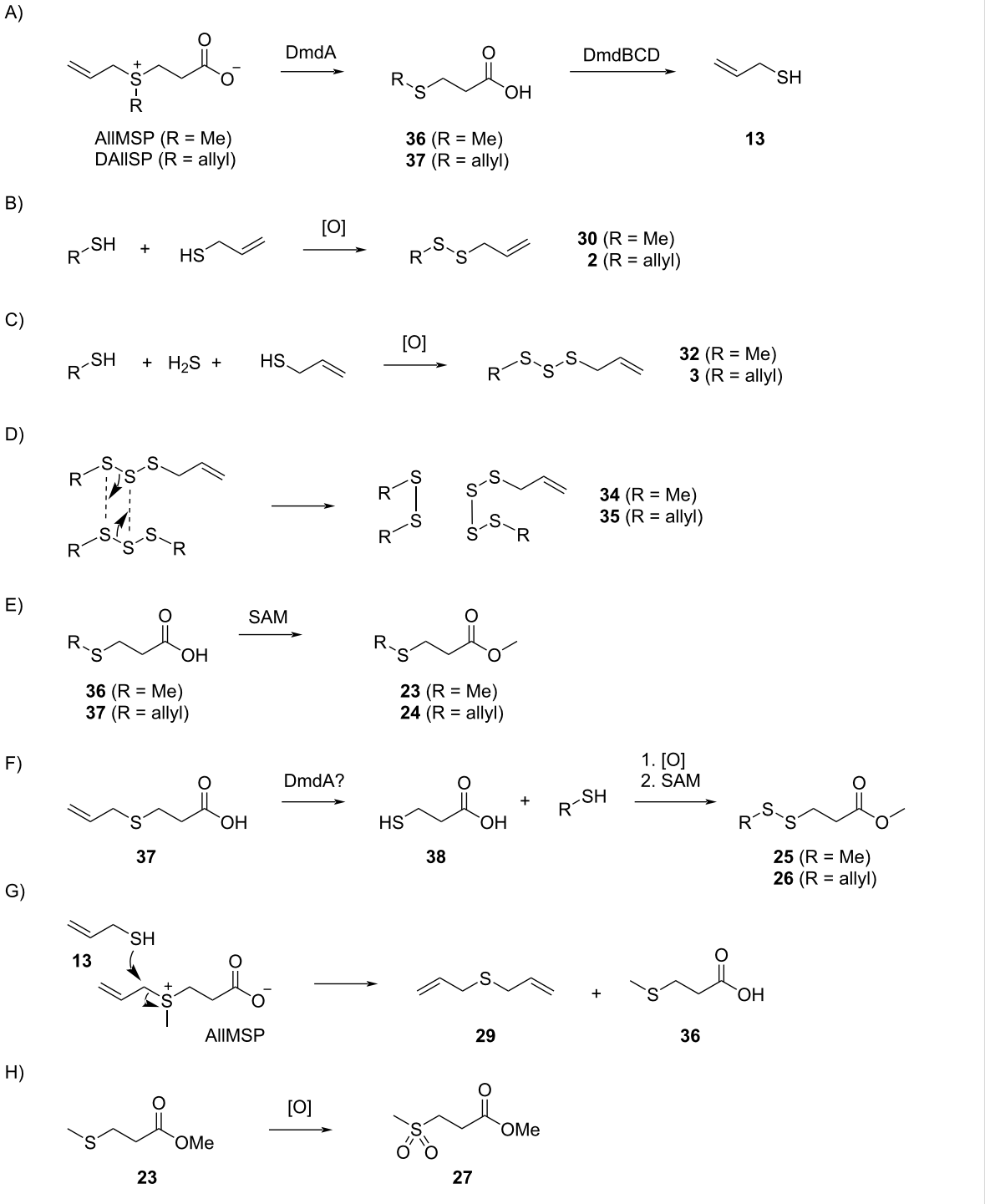

Scheme 4: Proposed mechanisms for the formation of sulfur volatiles from DAllSP and AllMSP.

Very similar patterns of volatiles were obtained in the feeding experiments of DAllSP with *D. shibae* and *O. indolifex* (Figure 2B,C, Table 1 and Figures S2 and S3 in Supporting Information File 1). An additionally observed compound in one analysis of *O. indolifex* was diallyl tetrasulfide (**35**). Both organisms also encode the DMSP demethylation pathway in their genomes, but with missing *dmdD* genes in both cases. A possible explanation is, that another enoyl-CoA hydratase, e.g., from fatty acid degradation, may functionally substitute for DmdD. *Dinoroseobacter shibae* additionally encodes genes for the DMSP hydrolase DddD and the DMSP lyase DddL, explaining the formation of **29**, while no DMSP hydrolase or

lyase is found in *O. indolifex*. Still, compound **29** is observed within this organism, but in lower quantities than in *P. inhibens* or *D. shibae*, and may point to the presence of another, yet unidentified type of DMSP lyase in this organism, because control experiments with medium plates with DAllSP added did not show a spontaneous degradation to **29** that could explain its observation.

The compound identification was based on a comparison to an authentic standard or of mass spectra to data base spectra in our MS libraries and confirmed for most cases by comparison of the retention indices to literature data, only for the mass spectrum of **26** no data base hit was returned. Therefore, a structural suggestion for this compound was based on the observed fragmentation pattern of the mass spectrum (Figure 3A). The molecular ion together with its isotope pattern pointed to two sulfur atoms, while the fragment ion at m/z = 64 ($[S_2]^+$) pointed to a disulfide. The fragment ions at m/z = 59 ($[C_2O_2H_3]^+$) and 161 ($[M - OMe]^+$) indicated a methyl ester, and the series of m/z = 105 ($[C_3H_5S_2]^+$), 73 ($[C_3H_5S]^+$), and 41 ($[C_3H_5]^+$) suggested an allyl disulfide. Taken together, the structure of methyl 3-(allyldisulfa-nyl)propanoate was delineated for compound **26** that was further supported by additional fragmentations as shown in Figure 3A. In addition, compound **26** was synthesized by a method reported previously for the related compound **25** [40], through dimerization of methyl 3-mercaptopropanoate (**39**) to dimethyl 3,3'-disulfanediyldipropanoate (**40**), followed by the $BF_3{\cdot}OEt_2$-mediated metathesis with **2** (Scheme 5A). The synthetic compound **26** was identical by mass spectrum and retention index to the unknown volatile.

The feeding of AllMSP to *P. inhibens* resulted in the formation of large amounts of methyl 3-(methylsulfanyl)propanoate (**23**) in addition to smaller quantities of methyl 3-(allylsulfanyl)propanoate (**24**, Figure 4A, Table 2 and Figure S4 in Supporting Information File 1). While compound **23** can arise from AllMSP by deallylation to 3-(methylsulfanyl)propanoic acid (**36**), potentially through DmdA, and *O*-methylation, the deriva-

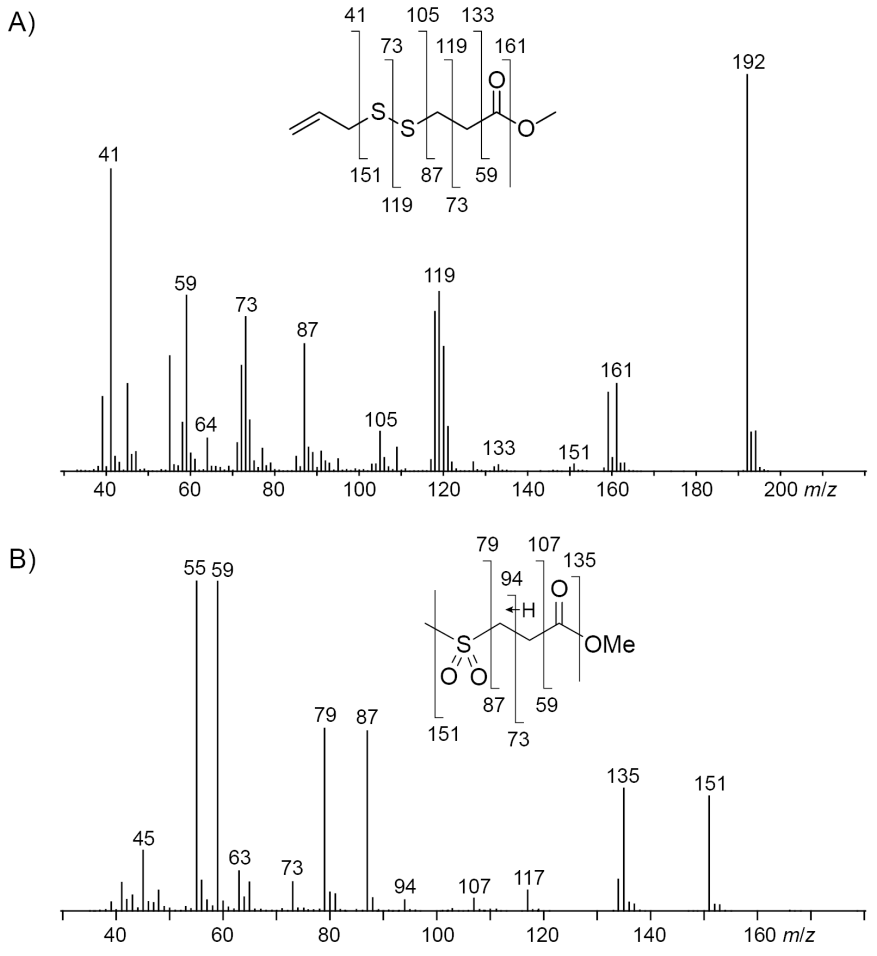

Figure 3: EI mass spectrum and fragmentation pattern of the unknown volatiles A) methyl 3-(allyldisulfanyl)propanoate (**26**) and B) methyl 3-(methylsulfonyl)propanoate (**27**).

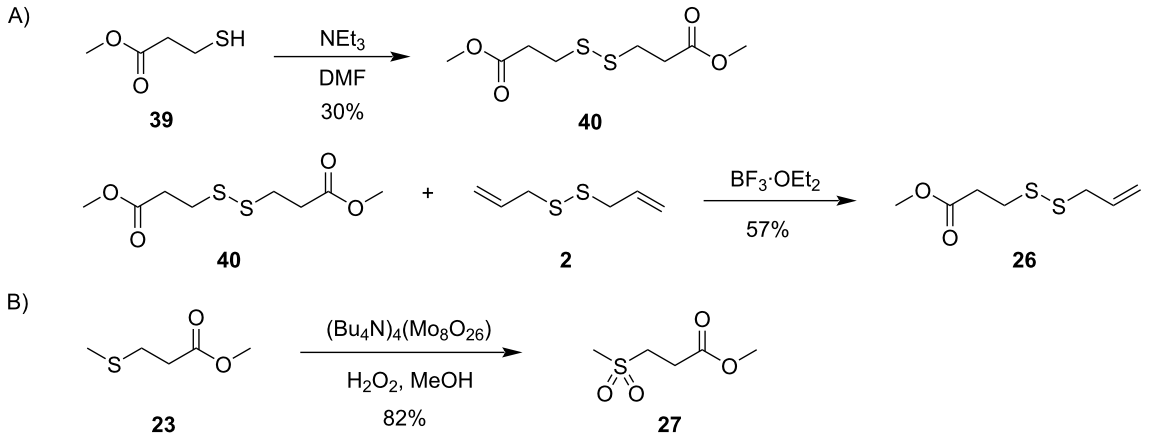

Scheme 5: Synthesis of A) methyl 3-(allyldisulfanyl)propanoate (**26**) and B) methyl 3-(methylsulfonyl)propanoate (**27**).

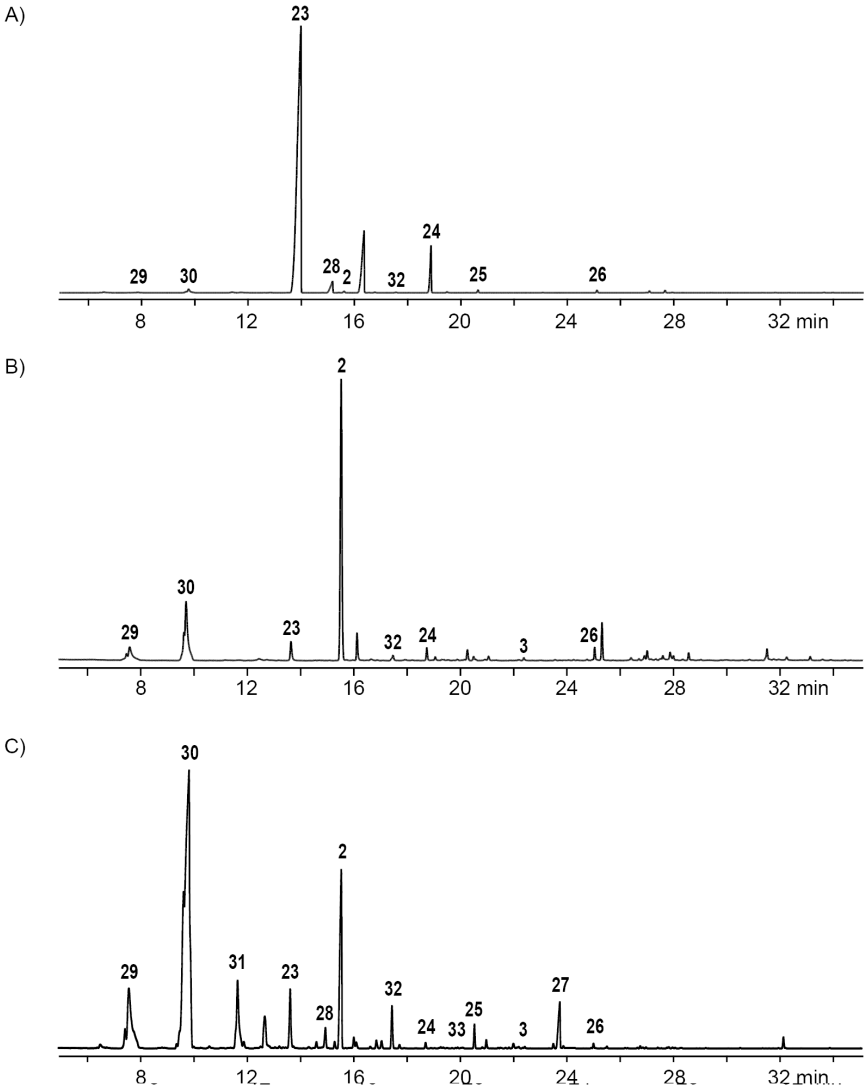

Figure 4: Total ion chromatograms of CLSA extracts obtained from the feeding experiments with AllMSP fed to A) *P. inhibens*, B) *D. shibae*, and C) *O. indolifex*. Numbers at peaks refer to compounds in Figure 1. Peaks without numbers are unidentified.

Table 2: Volatiles from agar plate cultures fed with AllMSP.

Compound[a]	I	$I_{lit.}$[b]		*P. in.*[c]	*D. sh.*[c]	*O. in.*[c]
diallyl sulfide (**29**)*	849	848 [34]	1	●○●	●●●	●●○
allyl methyl disulfide (**30**)	910	912 [34]	2	●●●	●●●	●●●
dimethyl trisulfide (**31**)*	967	970 [35]	3	○○●	○●●	●●○
methyl 3-(methylsulfanyl)-propanoate (**23**)*	1020	1023 [41]	4	●●●	●●●	●●●
S-methyl methanethiosulfonate (**28**)*	1063	1068 [35]	5	●●●	○●●	●●○
diallyl disulfide (**2**)*	1074	1075 [34]	6	●●●	●●●	●●●
allyl methyl trisulfide (**32**)	1136	1133 [36]	7	●●●	●●●	●●●
methyl 3-(allylsulfanyl)propanoate (**24**)	1177	–	8	●●●	●●●	●●●
dimethyl tetrasulfide (**33**)	1216	1215 [37]	9	○○○	○●●	●●○
methyl 3-(methyldisulfanyl)-propanoate (**25**)*	1236	–	10	●●●	○●●	●●●
diallyl trisulfide (**3**)	1300	1300 [38]	11	○○○	●●●	●●●
methyl 3-(methylsulfonyl)propanoate (**27**)*	1353	–	12	○○○	○○○	●●○
methyl 3-(allyldisulfanyl)propanoate (**26**)*	1397	–	13	●●●	●●●	●●●

[a]Asterisks indicate the identity to a commercially available or synthetic reference standard. [b]Retention index literature data for a HP5-MS or a similar GC column. [c]Abbreviations are *P. in.* = *Phaeobacter inhibens*, *D. sh.* = *Dinoroseobacter shibae*, and *O. in.* = *Oceanibulbus indolifex*. Filled circles indicate the presence, non-filled circles indicate the absence of a compound in the headspace extract. The colors of the circles refer to the chromatograms in Figure 4 and Figures S4–S6 in Supporting Information File 1 with the same color.

tive **24** may be formed analogously through intermediate **37** (Scheme 4A and E). The higher production of **23** in comparison to **24** suggests that the deallylation of AllMSP is more efficient than its demethylation, which is surprising, because naturally DmdA catalyzes a methyl-group transfer. This finding may reflect the high reactivity of the allyl group towards nucleophiles. Other compounds originating from AllMSP included the di- and trisulfides **2**, **26**, **30**, and **32** that pointed to a breakdown of AllMSP to **13** through the DMSP demethylation pathway and subsequent oxidative polysulfide formation (Scheme 4A–C), but their formation was lower than from DAllSP, likely because of the discussed efficient deallylation of AllMSP. Small amounts of diallyl sulfide (**29**) were also detected, which is the formal lysis product of DAllSP, but not of AllMSP. In first instance, its formation from AllMSP was surprising, but it is explainable by a degradation of AllMSP to **13**, followed by a nucleophilic attack at the allyl group of another AllMSP molecule (Scheme 4G). For *D. shibae* and *O. indolifex* the same pattern of compounds was found (Figure 4B,C, and Figures S5 and S6 in Supporting Information File 1), only the production of the deallylated compound **23** was lower, while in turn the production of the di- and trisulfides from **13** and of **29** was increased. This suggests that the deallylation of AllMSP by the DmdA variants in these organisms may be less efficient than was observed for *P. inhibens*. Besides these sulfur compounds, only *O. indolifex*, but not the other two strains, released another compound, **27**, whose mass spectrum was not included in our databases. The analysis of the fragmentation pattern (Figure 3B) suggested that **27** could be methyl 3-(methylsulfonyl)propanoate, an oxidation product of **23**. This hypothesis was confirmed by the chemical oxidation of **23**, yielding methyl 3-(methylsulfonyl)propanoate with an identical mass spectrum and retention index to the volatile **27** (Scheme 5B). This compound may arise from **23** by the action of an oxygenase that is restricted to *O. indolifex* and not encoded in the genomes of the other two species. Its spontaneous formation from **23** in the presence of air can be excluded, because other cultures forming **23** did not show the release of **27**.

Conclusion

Bacteria from the *Roseobacter* group can degrade DMSP analogues with *S*-allyl groups including AllMSP and DAllSP, likely with the participation of the enzymes for DMSP (hydro)lysis and from the DMSP demethylation pathway. Because MeSH can also originate from other sources, the DMSP derivatives used in this study can lead to products that can indicate which metabolic pathways are used for their conversion. Interestingly, the volatiles formed from AllMSP and DAllSP closely resemble flavoring compounds from garlic. The demethylation pathway with all four enzymes DmdABCD is fully established in *P. inhibens*, while genes for DmdD are missing in *D. shibae* and *O. indolifex*, suggesting that another enzyme with a low sequence homology may substitute for DmdD, leading to allylthiol and several sulfur volatiles derived from it in all three strains. The DMSP hydrolase DddD and the lyase DddL are present in *D. shibae*, and *P. inhibens* has a DMSP lyase DddP, which can explain the conversion of

DAllSP into diallyl sulfide, while the reason for its formation in *O. indolifex* is currently unclear and may point to an unknown type of DMSP lyase in this organism. Since the observed patterns of allylated sulfur volatiles in the three investigated strains are different, it seems possible that the DMSP (hydro)lases and the enzymes from the DMSP demethylation pathway have different activities towards AllMSP and DAllSP. In vitro studies with recombinant purified enzymes and mutational work will be needed for more detailed insights to support our hypotheses regarding the involved enzymes in AllMSP and DAllSP breakdown and will be performed in our laboratories in the future.

Experimental

Strains and culture condition

Phaeobacter inhibens DSM 14862, *Dinoroseobacter shibae* DSM 16493, *Oceanibulbus indolifex* DSM 14862 were precultured in full strength marine broth medium (MB 2216, Roth) at 28 °C with shaking at 180 rpm until the OD value reached about 1.0.

Feeding experiments and sampling of volatiles

Headspace samplings for each strain were done in triplicates. For the feeding experiments, DAllSP or AlMSP (1 mM) were added to the full strength marine broth agar medium (MB2216) after autoclavation. The medium was then transferred into glass Petri dishes. The agar plates were inoculated with the precultures (400 µL), incubated for two days at 28 °C and then subjected for headspace extraction to a CLSA [33] for 24 h. The released volatiles were collected on charcoal filters (Chromtech, Idstein, Germany), followed by the extraction of the filters with dichloromethane (50 µL), and analysis of the extracts by GC–MS. For comparison, blank experiments with MB medium alone and with MB agar plates spiked with DAllSP or AlMSP were performed in the same way. All the volatiles mentioned in Table 1 and Table 2 were not observed in the blank experiments.

GC–MS

The GC–MS analyses were carried out on a HP7890A GC system connected to a HP5975C mass selective detector fitted with a HP-5MS fused silica capillary column (30 m × 0.22 mm i.d., 0.25 µm film, Hewlett-Packard). The conditions were: inlet pressure: 67 kPa, He 23.3 mL min^{-1}; injection volume: 1 µL; injector: 250 °C; transfer line: 300 °C; electron energy: 70 eV. The GC was programmed as follows: 50 °C (5 min isothermic), increasing at 5 °C min^{-1} to 320 °C and operated in the splitless mode (60 s valve time); carrier gas (He): 1.2 mL min^{-1}. The retention indices were determined from *n*-alkane standards (C_8–C_{32}) [42].

General synthetic methods

All chemicals were purchased from TCI (Deutschland) or Sigma-Aldrich Chemie (Germany), and used without purification. Solvents were distilled and dried by standard methods. NMR spectra were recorded on a Bruker (Billerica, USA) Avance III HD Prodigy (500 MHz) or on an Avance III HD Cryo (700 MHz) NMR spectrometer. The spectra were referenced against solvent signals (^{1}H NMR, residual proton signal: D_2O δ = 4.79 ppm, $CDCl_3$ δ = 7.26 ppm, d_6-DMSO δ = 2.50 ppm; ^{13}C NMR: $CDCl_3$ δ = 77.16 ppm, d_6-DMSO δ = 39.52 ppm). The coupling constants are given in Hz. IR spectra were recorded on a Bruker α spectrometer equipped with a diamond-ATR probe. The relative intensities of signals are indicated by w (weak), m (medium), and s (strong).

Synthesis of allyl DMSP derivatives

A mixture of acrylic acid (0.72 g, 10 mmol) and diallyl sulfide or allylmethyl sulfide (10 mmol) was treated with 2 N HCl at 80 °C for 4 h. The reaction mixture was concentrated in vacuo and the residue was purified by silica gel column chromatography (CH_2Cl_2/MeOH 5:1), followed by recrystallization from methanol/diethyl ether 1:1 to yield the pure compounds.

DAllSP·HCl. Yield: 960 mg (4.32 mmol, 43%). ^{1}H NMR (D_2O, 700 MHz) δ 5.98 (ddt, *J* = 17.5, 10.2, 7.4, 2H), 5.73 (d, *J* = 10.2, 2H), 5.72 (d, *J* = 17.0, 2H), 4.08 (d, *J* = 7.4, 4H), 3.43 (t, *J* = 6.9, 2H), 2.78 (t, *J* = 6.9, 2H); ^{13}C NMR (D_2O, 175 MHz) δ 177.05 (C), 127.65 (2 × CH), 123.54 (2 × CH_2), 41.53 (2 × CH_2), 35.08 (CH_2), 31.68 (CH_2); HRMS–EI (*m*/*z*): calcd for $[C_9H_{15}O_2S]^+$, 187.0787; found, 187.0790.

AllMSP·HCl. Yield: 1.06 g (5.41 mmol, 54%). ^{1}H NMR (D_2O, 700 MHz) δ 5.96 (ddt, *J* = 17.5, 10.2, 7.5, 1H), 5.74 (d, *J* = 10.2, 1H), 5.71 (d, *J* = 17.2, 1H), 4.13 (dd, *J* = 13.4, 7.4, 1H), 4.09 (dd, *J* = 13.4, 7.5, 1H), 3.58 (dt, *J* = 13.7, 6.9, 1H), 3.47 (dt, *J* = 13.5, 6.7, 1H), 3.04 (t, *J* = 6.8, 2H), 2.91 (s, 3H); ^{13}C NMR (D_2O, 175 MHz) δ 173.77 (C), 128.19 (CH), 122.74 (CH_2), 43.82 (CH_2), 35.84 (CH_2), 28.75 (CH_2), 21.72 (CH_3); HRMS–EI (*m*/*z*): calcd for $[C_7H_{13}O_2S]^+$, 161.0631; found, 161.0630.

Synthesis of dimethyl 3,3'-disulfanediyldipropanoate (**40**)

A solution of methyl 3-mercaptopropanoate (6.00 g, 50.0 mmol, 1.0 equiv) and triethylamine (5.05 g, 50.0 mmol) in DMF (10 mL) was treated for 24 h at 40 °C. The reaction was quenched by the addition of water and the aqueous phase extracted with ethyl acetate. The extract was dried with $MgSO_4$ and then concentrated in vacuo. The residue was purified by silica column chromatography (cyclohexane/EtOAc 5:1) to give compound **40** (1.80 g, 7.56 mmol, 30%) as pale yellow oil. TLC

R_f 0.44 (cyclohexane/EtOAc 10:3); IR (diamond-ATR) ṽ: 2998 (w), 2952 (w), 2845 (w), 2256 (w), 1730 (m), 1436 (w), 1354 (w), 1240 (w), 1215(w), 1195 (w), 1171 (w), 1139 (w), 1046 (w), 1017 (w), 979 (w), 907 (w), 822 (w), 726 (m), 648 (w), 435 (w) cm^{-1}; ^1H NMR ($CDCl_3$, 500 MHz) δ 3.64 (s, 6H), 2.87 (t, J = 7.2, 4H), 2.68 (t, J = 7.2, 4H) ppm; ^{13}C NMR ($CDCl_3$, 125 MHz) δ 172.11 (2 × C), 51.90 (2 × CH_3), 33.93 (2 × CH_2), 33.16 (2 × CH_2) ppm.

Synthesis of methyl 3-(allyldisulfanyl)propanoate (**26**)

To a solution of dimethyl 3,3'-disulfanediyldipropanoate (**40**, 0.50 g, 2.10 mmol, 1.0 equiv) and diallyl disulfide (**2**, 0.31 g, 2.10 mmol, 1.0 equiv) in dry DCM (10 mL) and CH_3NO_2 (10 mL) at 0 °C $BF_3{\cdot}OEt_2$ (30 mg, 0.21 mmol, 0.1 equiv) was added. The reaction mixture was stirred at 0 °C for 3 h and at room temperature overnight. The reaction was quenched by the addition of water and extracted with ethyl acetate. The extracts were dried with $MgSO_4$ and concentrated in vacuo. The obtained residue was purified by silica gel column chromatography (cyclohexane/EtOAc 5:1) to give compound **26** (0.23 g, 1.20 mmol, 57%). TLC R_f = 0.72 (cyclohexane/EtOAc = 1:1); IR (diamond-ATR) ṽ: 3082 (w), 2950 (w), 2845 (w), 1736 (s), 1634 (w), 1435 (w), 1354 (w), 1277 (w), 1240 (w), 1216 (w), 1172 (w), 1144 (w), 1017 (w), 985 (w), 922 (w), 859 (w), 820 (w), 756 (w), 722 (w), 669 (w), 582 (w), 478 (w), 435 (w) cm^{-1}; ^1H NMR ($CDCl_3$, 500 MHz) δ 5.83 (ddt, J = 17.1, 9.9, 7.3, 1H), 5.19 (ddt, J = 16.9, 1.3, 1.3, 1H), 5.14 (dm, J = 10.0, 1H), 3.69 (s, 3H), 3.32 (dm, J = 7.3, 2H), 2.91 (t, J = 7.2, 2H), 2.72 (t, J = 7.2, 2H) ppm; ^{13}C NMR ($CDCl_3$, 125 MHz) δ 172.14 (C), 132.71 (CH), 119.40 (CH_2), 52.04 (CH_3), 41.60 (CH_2), 33.87 (CH_2), 33.40 (CH_2) ppm; HRMS–EI (*m/z*): calcd for $[C_7H_{12}O_2S_2]^+$, 192.0273; found, 192.0289.

Synthesis of methyl 3-(methylsulfonyl)propanoate (**27**)

To a stirred solution of $[(n\text{-}C_4H_9)_4N]_4(Mo_8O_{26})$ (5 mg, 2.5 µmol, 0.001 equiv) [43] in methanol (4 mL), methyl 3-methylthiopropanoate (335 mg, 2.50 mmol, 1.0 equiv) was added at 40 °C. After the reaction mixture was stirred for 5 minutes, 30% hydrogen peroxide solution (0.52 mL, 0.57 g, 5.0 mmol, 2.0 equiv) was added dropwise. The color of the reaction mixture changed from colorless to yellow. The reaction mixture was stirred for 30 minutes at room temperature. After completion of the reaction, EtOAc (10 mL) was added, causing precipitation of the catalyst. The catalyst was filtered off, the filtrate was dried with $MgSO_4$ and concentrated in vacuo to give pure **27** (0.34 g, 2.05 mmol, 82%) as colorless solid. TLC R_f 0.17 (cyclohexane/EtOAc 1:1); IR (diamond-ATR) ṽ: 3014 (w), 2948 (w), 2932 (w), 1762 (m), 1687 (w), 1442 (w), 1433 (w), 1418 (w), 1375 (w), 1331 (w), 1306 (m), 1373 (m), 1259 (m), 1203 (w), 1180 (w), 1131 (m), 1056 (w), 1004 (w), 988 (w), 971 (w), 956 (w), 898 (w), 786 (w), 774 (w), 749 (w), 601 (w), 514 (w), 505 (w), 441 (w) cm^{-1}; ^1H NMR (d_6-DMSO, 500 MHz) δ 3.63 (s, 3H), 3.37 (t, J = 7.5, 2H), 3.01 (s, 3H), 2.78 (t, J = 7.5, 2H) ppm; ^{13}C NMR (d_6-DMSO, 125 MHz) δ 170.79 (C), 51.88 (CH_3), 49.14 (CH_2), 40.21 (CH_3), 26.89 (CH_2) ppm.

Supporting Information

Supporting Information File 1

Additional total ion chromatograms and copies of NMR spectra.
[https://www.beilstein-journals.org/bjoc/content/supplementary/1860-5397-17-51-S1.pdf]

Funding

This work was funded by the DFG (SFB TR 51 "*Roseobacter*").

ORCID® iDs

Jeroen S. Dickschat - https://orcid.org/0000-0002-0102-0631

References

1. Wertheim, T. *Ann. Chem. Pharm.* **1844,** *51,* 289–315. doi:10.1002/jlac.18440510302
2. Semmler, F. W. *Arch. Pharm. (Weinheim, Ger.)* **1892,** *230,* 434–443. doi:10.1002/ardp.18922300603
3. Cavallito, C. J.; Buck, J. S.; Suter, C. M. *J. Am. Chem. Soc.* **1944,** *66,* 1952–1954. doi:10.1021/ja01239a049
4. Shang, A.; Cao, S.-Y.; Xu, X.-Y.; Gan, R.-Y.; Tang, G.-Y.; Corke, H.; Mavumengwana, V.; Li, H.-B. *Foods* **2019,** *8,* 246. doi:10.3390/foods8070246
5. Block, E.; Ahmad, S.; Jain, M. K.; Crecely, R. W.; Apitz-Castro, R.; Cruz, M. R. *J. Am. Chem. Soc.* **1984,** *106,* 8295–8296. doi:10.1021/ja00338a049
6. Stoll, A.; Seebeck, E. *Helv. Chim. Acta* **1948,** *31,* 189–210. doi:10.1002/hlca.19480310140
7. Stoll, A.; Seebeck, E. *Helv. Chim. Acta* **1949,** *32,* 197–205. doi:10.1002/hlca.19490320129
8. Block, E. *Angew. Chem., Int. Ed. Engl.* **1992,** *31,* 1135–1178. doi:10.1002/anie.199211351
9. Brodnitz, M. H.; Pascale, J. V.; Van Derslice, L. *J. Agric. Food Chem.* **1971,** *19,* 273–275. doi:10.1021/jf60174a007
10. Segev, E.; Wyche, T. P.; Kim, K. H.; Petersen, J.; Ellebrandt, C.; Vlamakis, H.; Barteneva, N.; Paulson, J. N.; Chai, L.; Clardy, J.; Kolter, R. *eLife* **2016,** *5,* e17473. doi:10.7554/elife.17473
11. Barak-Gavish, N.; Frada, M. J.; Ku, C.; Lee, P. A.; DiTullio, G. R.; Malitsky, S.; Aharoni, A.; Green, S. J.; Rotkopf, R.; Kartvelishvily, E.; Sheyn, U.; Schatz, D.; Vardi, A. *Sci. Adv.* **2018,** *4,* eaau5716. doi:10.1126/sciadv.aau5716
12. Kessler, R. W.; Weiss, A.; Kuegler, S.; Hermes, C.; Wichard, T. *Mol. Ecol.* **2018,** *27,* 1808–1819. doi:10.1111/mec.14472

13. Schulz, S.; Dickschat, J. S. *Nat. Prod. Rep.* **2007,** *24,* 814–842. doi:10.1039/b507392h
14. Dickschat, J. S. *Nat. Prod. Rep.* **2017,** *34,* 310–328. doi:10.1039/c7np00003k
15. Dickschat, J. S.; Wagner-Döbler, I.; Schulz, S. *J. Chem. Ecol.* **2005,** *31,* 925–947. doi:10.1007/s10886-005-3553-9
16. Dickschat, J. S.; Reichenbach, H.; Wagner-Döbler, I.; Schulz, S. *Eur. J. Org. Chem.* **2005,** 4141–4153. doi:10.1002/ejoc.200500280
17. Thiel, V.; Brinkhoff, T.; Dickschat, J. S.; Wickel, S.; Grunenberg, J.; Wagner-Döbler, I.; Simon, M.; Schulz, S. *Org. Biomol. Chem.* **2010,** *8,* 234–246. doi:10.1039/b909133e
18. Dickschat, J. S.; Rabe, P.; Citron, C. A. *Org. Biomol. Chem.* **2015,** *13,* 1954–1968. doi:10.1039/c4ob02407a
19. Todd, J. D.; Rogers, R.; Li, Y. G.; Wexler, M.; Bond, P. L.; Sun, L.; Curson, A. R. J.; Malin, G.; Steinke, M.; Johnston, A. W. B. *Science* **2007,** *315,* 666–669. doi:10.1126/science.1135370
20. Curson, A. R. J.; Rogers, R.; Todd, J. D.; Brearley, C. A.; Johnston, A. W. B. *Environ. Microbiol.* **2008,** *10,* 757–767. doi:10.1111/j.1462-2920.2007.01499.x
21. Todd, J. D.; Curson, A. R. J.; Dupont, C. L.; Nicholson, P.; Johnston, A. W. B. *Environ. Microbiol.* **2009,** *11,* 1376–1385. doi:10.1111/j.1462-2920.2009.01864.x
22. Todd, J. D.; Curson, A. R. J.; Kirkwood, M.; Sullivan, M. J.; Green, R. T.; Johnston, A. W. B. *Environ. Microbiol.* **2011,** *13,* 427–438. doi:10.1111/j.1462-2920.2010.02348.x
23. Curson, A. R. J.; Sullivan, M. J.; Todd, J. D.; Johnston, A. W. B. *ISME J.* **2011,** *5,* 1191–1200. doi:10.1038/ismej.2010.203
24. Todd, J. D.; Kirkwood, M.; Newton-Payne, S.; Johnston, A. W. B. *ISME J.* **2012,** *6,* 223–226. doi:10.1038/ismej.2011.79
25. Sun, J.; Todd, J. D.; Thrash, J. C.; Qian, Y.; Qian, M. C.; Temperton, B.; Guo, J.; Fowler, E. K.; Aldrich, J. T.; Nicora, C. D.; Lipton, M. S.; Smith, R. D.; de Leenheer, P.; Payne, S. H.; Johnston, A. W. B.; Davie-Martin, C. L.; Halsey, K. H.; Giovannoni, S. J. *Nat. Microbiol.* **2016,** *1,* 16065. doi:10.1038/nmicrobiol.2016.65
26. Howard, E. C.; Henriksen, J. R.; Buchan, A.; Reisch, C. R.; Bürgmann, H.; Welsh, R.; Ye, W.; González, J. M.; Mace, K.; Joye, S. B.; Kiene, R. P.; Whitman, W. B.; Moran, M. A. *Science* **2006,** *314,* 649–652. doi:10.1126/science.1130657
27. Reisch, C. R.; Stoudemayer, M. J.; Varaljay, V. A.; Amster, I. J.; Moran, M. A.; Whitman, W. B. *Nature* **2011,** *473,* 208–211. doi:10.1038/nature10078
28. Brock, N. L.; Citron, C. A.; Zell, C.; Berger, M.; Wagner-Döbler, I.; Petersen, J.; Brinkhoff, T.; Simon, M.; Dickschat, J. S. *Beilstein J. Org. Chem.* **2013,** *9,* 942–950. doi:10.3762/bjoc.9.108
29. Brock, N. L.; Menke, M.; Klapschinski, T. A.; Dickschat, J. S. *Org. Biomol. Chem.* **2014,** *12,* 4318–4323. doi:10.1039/c4ob00719k
30. Ansede, J. H.; Pellechia, P. J.; Yoch, D. C. *Environ. Sci. Technol.* **1999,** *33,* 2064–2069. doi:10.1021/es9812296
31. Dickschat, J. S.; Zell, C.; Brock, N. L. *ChemBioChem* **2010,** *11,* 417–425. doi:10.1002/cbic.200900668
32. Burkhardt, I.; Lauterbach, L.; Brock, N. L.; Dickschat, J. S. *Org. Biomol. Chem.* **2017,** *15,* 4432–4439. doi:10.1039/c7ob00913e
33. Grob, K.; Zürcher, F. *J. Chromatogr.* **1976,** *117,* 285–294. doi:10.1016/0021-9673(76)80005-2
34. Ansorena, D.; Astiasarán, I.; Bello, J. *J. Agric. Food Chem.* **2000,** *48,* 2395–2400. doi:10.1021/jf990931y
35. Kubec, R.; Drhová, V.; Velíšek, J. *J. Agric. Food Chem.* **1998,** *46,* 4334–4340. doi:10.1021/jf980379x
36. Ansorena, D.; Gimeno, O.; Astiasarán, I.; Bello, J. *Food Res. Int.* **2001,** *34,* 67–75. doi:10.1016/s0963-9969(00)00133-2
37. Bonaïti, C.; Irlinger, F.; Spinnler, H. E.; Engel, E. *J. Dairy Sci.* **2005,** *88,* 1671–1684. doi:10.3168/jds.s0022-0302(05)72839-3
38. Zoghbi, M. d. G. B.; Andrade, E. H. A.; Maia, J. G. S. *Flavour Fragrance J.* **2002,** *17,* 133–135. doi:10.1002/ffj.1051
39. Mnayer, D.; Fabiano-Tixier, A.-S.; Petitcolas, E.; Hamieh, T.; Nehme, N.; Ferrant, C.; Fernandez, X.; Chemat, F. *Molecules* **2014,** *19,* 20034–20053. doi:10.3390/molecules191220034
40. Hahnke, S.; Brock, N. L.; Zell, C.; Simon, M.; Dickschat, J. S.; Brinkhoff, T. *Syst. Appl. Microbiol.* **2013,** *36,* 39–48. doi:10.1016/j.syapm.2012.09.004
41. Beaulieu, J. C.; Grimm, C. C. *J. Agric. Food Chem.* **2001,** *49,* 1345–1352. doi:10.1021/jf0005768
42. van Den Dool, H.; Dec. Kratz, P. *J. Chromatogr.* **1963,** *11,* 463–471. doi:10.1016/s0021-9673(01)80947-x
43. Yang, C.; Jin, Q.; Zhang, H.; Liao, J.; Zhu, J.; Yu, B.; Deng, J. *Green Chem.* **2009,** *11,* 1401–1405. doi:10.1039/b912521n

License and Terms

BEILSTEIN JOURNAL OF ORGANIC CHEMISTRY

A new glance at the chemosphere of macroalgal–bacterial interactions: In situ profiling of metabolites in symbiosis by mass spectrometry

Marine Vallet*[1], Filip Kaftan[2], Veit Grabe[3], Fatemeh Ghaderiardakani[4], Simona Fenizia[4,5], Aleš Svatoš[2], Georg Pohnert[1,4,6] and Thomas Wichard*[4]

Full Research Paper

Open Access

Address:
[1]Research Group Phytoplankton Community Interactions, Max Planck Institute for Chemical Ecology, Jena, Germany, [2]Research Group Mass Spectrometry/Proteomics, Max Planck Institute for Chemical Ecology, Jena, Germany, [3]Research Group Olfactory Coding, Department of Evolutionary Neuroethology, Max Planck Institute for Chemical Ecology, Jena, Germany, [4]Institute for Inorganic and Analytical Chemistry, Friedrich Schiller University Jena, Germany, [5]Max Planck Institute for Chemical Ecology, Jena, Germany and [6]Microverse Cluster, Friedrich Schiller University Jena, Germany

Email:
Marine Vallet* - mvallet@ice.mpg.de; Thomas Wichard* - Thomas.Wichard@uni-jena.de

* Corresponding author

Keywords:
algae; AP-SMALDI; ectoine; holobiont; high-resolution mass spectrometry; mass spectrometry imaging; marine bacteria; Ulva

Beilstein J. Org. Chem. **2021,** *17,* 1313–1322.
https://doi.org/10.3762/bjoc.17.91

Received: 31 December 2020
Accepted: 28 April 2021
Published: 19 May 2021

This article is part of the thematic issue "Chemical ecology".

Guest Editor: C. Beemelmanns

Abstract

Symbiosis is a dominant form of life that has been observed numerous times in marine ecosystems. For example, macroalgae coexist with bacteria that produce factors that promote algal growth and morphogenesis. The green macroalga *Ulva mutabilis* (Chlorophyta) develops into a callus-like phenotype in the absence of its essential bacterial symbionts *Roseovarius* sp. MS2 and *Maribacter* sp. MS6. Spatially resolved studies are required to understand symbiont interactions at the microscale level. Therefore, we used mass spectrometry profiling and imaging techniques with high spatial resolution and sensitivity to gain a new perspective on the mutualistic interactions between bacteria and macroalgae. Using atmospheric pressure scanning microprobe matrix-assisted laser desorption/ionisation high-resolution mass spectrometry (AP-SMALDI-HRMS), low-molecular-weight polar compounds were identified by comparative metabolomics in the chemosphere of *Ulva*. Choline (2-hydroxy-*N*,*N*,*N*-trimethylethan-1-aminium) was only determined in the alga grown under axenic conditions, whereas ectoine (1,4,5,6-tetrahydro-2-methyl-4-pyrimidinecarboxylic acid) was found in bacterial presence. Ectoine was used as a metabolic marker for localisation studies of *Roseovarius* sp. within the tripartite community because it was produced exclusively by these bacteria. By combining confocal laser scanning microscopy (cLSM) and AP-SMALDI-HRMS, we proved that *Roseovarius* sp. MS2 settled mainly in the rhizoidal zone (holdfast) of *U. mutabilis*. Our findings provide the fundament to decipher bacterial symbioses with multicellular hosts in aquatic ecosystems

in an ecologically relevant context. As a versatile tool for microbiome research, the combined AP-SMALDI and cLSM imaging analysis with a resolution to level of a single bacterial cell can be easily applied to other microbial consortia and their hosts. The novelty of this contribution is the use of an in situ setup designed to avoid all types of external contamination and interferences while resolving spatial distributions of metabolites and identifying specific symbiotic bacteria.

Introduction

In intertidal zones with high temporal and spatial ecosystem variations, bacteria and macroalgae establish close mutualistic relationships, in which both gain reciprocal benefits forming an ecological unit (holobiont) [1-3]. Chemical exchange and physical proximity are the basis of this algae–bacterial mutualism [4], but little is known about the spatial distribution of the bacteria on the algal host and the locally released and exchanged compounds within the algal chemosphere [3]. Bacterial biofilms on macroalgae can be crucial for developing algae and their interactions with other marine organisms. The exchange of resources in this spatially limited region is of high interest for understanding the macroalgal–bacterial interactions. The chemosphere was proposed as a region that supports chemical mediator-based cross-kingdom interactions [3]. High-throughput sequencing analysis provides the abundance and composition of the bacterial community on macroalgal surfaces [5,6]. It does not reveal any information on the metabolically active bacteria and the spatial distribution of substances exchanged. While the study of bacterial symbiosis is often limited to either chemistry or microscopy work, recent functional and metabolomics methods are available to enable chemical imaging of specialised metabolites involved in host–bacteria interactions.

In our study, comparative metabolomics using atmospheric pressure scanning microprobe matrix-assisted laser desorption/ionisation high-resolution mass spectrometry (AP-SMALDI-HRMS) enables the identification of specialised metabolites of the marine macroalga *Ulva mutabilis* (Chlorophyta) and its associated essential bacteria, a model system for cross-kingdom interactions [7]. The method provides a tool to formulate hypotheses about metabolic processes in the phycosphere while preserving spatial structure. This novel depth of insight into a multicellular host and bacteria interactions can characterise natural products in symbiotic interactions.

Algal growth and morphogenesis-promoting factors (AGMPFs) are required for the development of the model organism *U. mutabilis* [7]. They are provided by a combination of two essential bacteria, *Maribacter* sp. MS6 and *Roseovarius* sp. MS2 forming a tripartite community [3,7,8] (see also Figure 1a and the Graphical Abstract). In turn, *Roseovarius* sp. benefits from the released photosynthate glycerol as a carbon source [9]. Axenic *Ulva* germ cells (i.e. gametes) develop into a callus-like phenotype composed of undifferentiated cells with malformed cell walls [8,10]. Up to now, the bacterial sesquiterpenoid thallusin, released by *Maribacter* spp. [11,12], is the only known AGMPF that induces morphogenesis such as rhizoid and cell-wall formation in *Ulva* spp. [11,12] or thallus development in *Monostroma* spp. [13]. The *Roseovarius*-factor that promotes cell division is still unknown [3,8]. Algal substances are released into the surrounding environment to attract epiphytic bacteria and initiate the cross-kingdom interaction [14,15]. *Ulva* attracts *Roseovarius* sp. MS2 through the sulphur-containing zwitterion dimethylsulphoniopropionate (DMSP), resulting in biofilm formation on the algal surrounding [9]. The bacterium subsequently uses the provided glycerol for growth and transforms DMSP into methanethiol and dimethyl sulphide [9].

The metabolic activities of marine bacteria and algae can be surveyed using mass spectrometry-based methods. For example, stable sulphur isotope (^{34}S) labelled DMSP was used to track DMSP uptake and degradation by marine bacteria, and secondary ion mass spectrometry was applied to visualise it at the single-cell level [16]. The interaction between epibiotic bacteria on algal surfaces and their metabolic activities can be monitored in situ or using an imprinting method by desorption electrospray ionisation mass spectrometry [17,18]. In *U. mutabilis* gametophytes, matrix-assisted laser desorption ionisation mass spectrometry imaging (MALDI-MSI) was used to identify cell differentiation markers [19]. However, there has yet to be a thorough investigation of associated-mutualistic bacteria. MALDI-MSI has been shown to have high sensitivity and spatial resolution at the microscale in plant tissues, plankton, and other microbes [20,21].

The application of a MALDI matrix to a sample is an important part of the MALDI-MSI experiment. MALDI-MS can be used to identify proteins and metabolic signatures [22-24] from bacteria and microalgae, as well as biofilms [25]. The primary function of the applied matrix is to improve the quality of the MS spectra, particularly the signal intensities of the compounds of interest. In some cases, the matrix might also work in opposition to this premise, suppressing desired ions. Then, matrix-free approaches such as LDI-HRMS can overcome this limiting phenomenon and have been applied for species-level microalgal identification based on metabolic profile fingerprint matching [26-28].

Our research combines cutting-edge laser scanning microscopy and high-resolution mass spectrometry to uncover *Ulva*/bacteria interactions and specialised metabolites at the microscale level. In this study, we demonstrate that the chemosphere of *U. mutabilis* changes depending on the presence or absence of the bacterial symbionts (*Roseovarius* sp. MS2 and *Maribacter* sp. MS6). As a result, specific metabolic markers can be used to identify bacteria in the vicinity of *U. mutabilis*. We used an untargeted comparative metabolomics approach that also provides micrometre-resolved MS imaging data through AP-SMALDI-HRMS. Two sample preparations, matrix-free LDI and MALDI, were performed to increase the range of metabolites recovered with this type of ionisation. We identified significant metabolites that define the host–bacteria interactions based on spectral similarity with standards. Using combined imaging mass spectrometry and confocal laser scanning microscopy, we then linked the chemical and microscopic observations that characterise the symbiotic association (cLSM).

Results and Discussion

Comparative metabolomics using AP-SMALDI-HRMS identifies metabolites in axenic algae and those present during macroalgal–bacterial symbiosis

Axenic gametes of *U. mutabilis* (phenotype slender) were allowed to settle onto glass plates in Petri dishes filled with growth medium. In the absence of the symbionts, the axenic gametes developed into undifferentiated cells known as the callus-like form [8,29]. In the second set of samples, algae were inoculated with the two marine bacteria, *Roseovarius* sp. MS2 and *Maribacter* sp. MS6, developing into a phenotype composed of bilayer cells and organised tissues, as previously reported [8]. The algal germlings incubated with the marine bacteria showed a rhizoidal zone that serves for substrate attachment and a thallus zone. From apex to rhizoid, *Ulva* germlings had an average length of 50 to 150 µm after three weeks of growth. The samples were recovered, dried on tissue, and for MALDI, immediately covered with 2,5-dihydroxybenzoic acid (DHB) applied by spraying. We targeted either specialised tissues (rhizoidal zone versus thallus) or the whole alga germlings (axenic callus versus alga in symbiosis) using a mounted AP-SMALDI camera (Figure 1a). The metabolic profiles of tissue and whole alga were obtained from callus or alga in symbiosis using AP-SMALDI-HRMS with the two sample preparations, either with matrix deposition (MALDI-HRMS) or matrix-free analysis (LDI-HRMS) (Figure 1a and b). The data matrix was generated by processing the raw spectra, and the data tables produced were from 1534 to 4986 features (*m*/*z*) (Figure 1b and Table S1 in Supporting Information File 1). The principal component analysis (PCA) visualised differences between metabolic profiles of axenic algae, algae in symbiosis, and specialised tissues (thallus, rhizoidal zone), analysed either with LDI or MALDI-HRMS. The metabolic profiles of axenic algae and algae in symbiosis were significantly different, while tissue-specialised metabolomes were less differentiated in the PCA score plots (Figure 1b). Significant features in the loading plots were listed in a heatmap to compare their relative abundance of intensities averaged per sample class (Figure 1c). Among the statistically significant features in all datasets (Table S1, Supporting Information File 1), six metabolites were identified, which were annotated using spectral similarity with analytical standards. For example, the features *m*/*z* 104.1064 and *m*/*z* 143.0815 were selected among the significant markers of the MALDI-HRMS profiling of axenic algae and the rhizoid tissue (whole alga profiling) of *U. mutabilis* grown with the marine symbiotic bacteria, respectively (Figure 1c). The heatmap shows the complementarities of both methods, LDI or MALDI-HRMS, as the significant features *m*/*z* 104.1064 and *m*/*z* 143.0815 have only been detected by one of the two methods.

Identification of metabolites in *Ulva*–bacteria symbiosis

To identify the selected markers found by the comparative metabolomics study, we searched several mass spectra libraries, including METLIN, and determined the chemical formula based on exact mass. We also used spectral similarity matching of data acquired from analytical standards. Choline was identified from the molecular peak *m*/*z* 104.1064 for $[M]^+$ (calculated *m*/*z* as 104.1069 ± 4.8 ppm for $C_5H_{14}NO$) in the profiles of axenic *U. mutabilis* (Figure 2a). This small polar metabolite was linked to the metabolic homeostasis of *Ulva lactuca* during tidal cycles [30]. Choline is the precursor of the membrane constituent phosphatidylcholine [31]. We inferred that the accumulation of choline in axenic *U. mutabilis* germlings might correlate with the absence of the key bacterial morphogen thallusin, which induces cell wall and rhizoid formation. The accompanying formation of cell wall protrusions might disrupt the cell membrane arrangement indicated by choline accumulation. Screening the tripartite community *Ulva–Roseovarius–Maribacter* identified ectoine as a metabolic marker of the rhizoidal zone (Figure 2b). The molecular formula $C_6H_{10}N_2O_2$ was deduced from the molecular peak at *m*/*z* 143.0817 for $[M + H]^+$ (± 1.4 ppm) and *m*/*z* 165.0636 for $[M + Na]^+$ (± 1.2 ppm) detected in the AP-SMALDI-HRMS profiles of the standard and rhizoid tissue of *U. mutabilis* in symbiosis with the marine bacteria. To separate algal and bacterial metabolism, single colonies of *Roseovarius* sp. MS2 and *Maribacter* sp. MS6 were deposited onto glass slides and analysed with AP-SMALDI-HRMS/MS. Using spectral similarity matching based on the fragmentation pattern

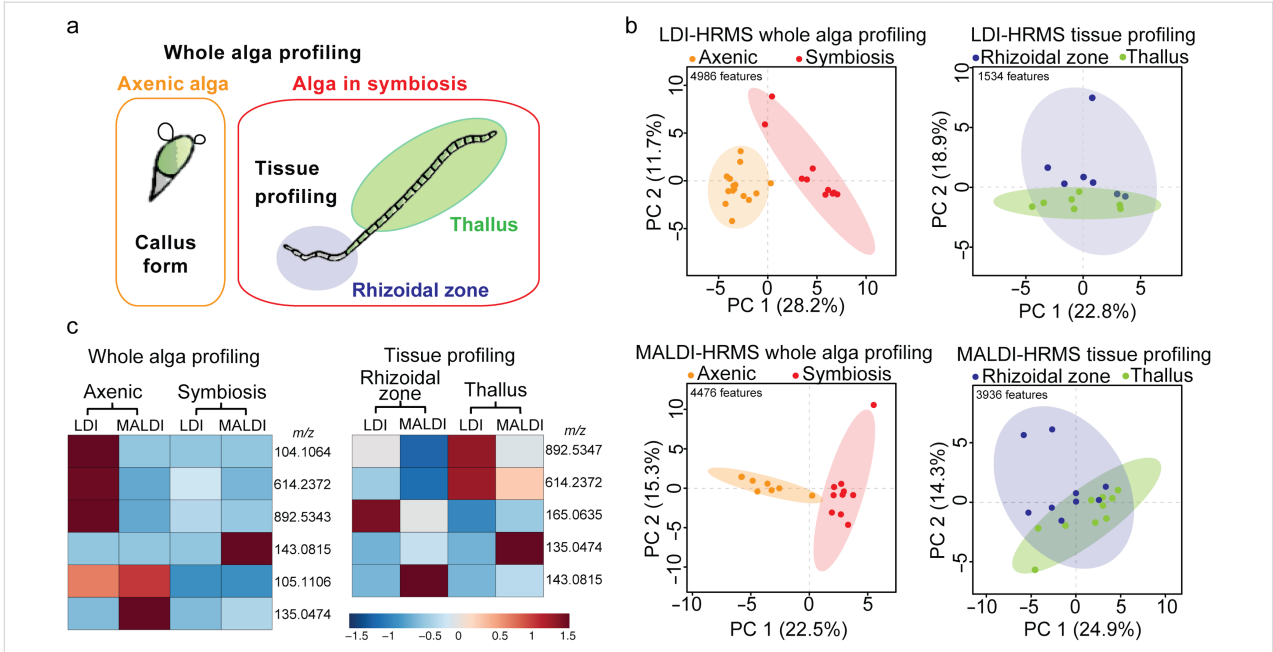

Figure 1: Untargeted comparative metabolomics using AP-SMALDI-HRMS highlighted metabolites involved in *Ulva*–bacteria symbiosis. a) The study looked at axenic algae with cell wall protrusions, the whole algae, and specific tissues with bacterial symbionts. b) The profiles of axenic alga ("axenic") were contrasted with alga with bacterial symbionts ("symbiosis") in the PCA score plots for LDI and MALDI-HRMS. The ellipses represent the 95% confidence region. c) The significant features (*m/z*) characterising axenic algae, algae in symbiosis, or differentiated tissues (blades/thalli, rhizoids) are represented in a heatmap with their relative abundance. The colour scale represents the averaged TIC normalised intensities per sample class (red colour for high intensity, blue for low intensity).

obtained from AP-SMALDI-HRMS/MS experiments, we proved that the bacterial symbiont *Roseovarius* sp. MS2 produces ectoine (Figure 2c). This observation supports earlier assumptions that the rhizoidal zone is mainly colonised by *Roseovarius* sp. MS2 [8,29].

Ectoine is a known osmoprotectant produced by marine bacteria and phytoplankton with high concentrations during saline stress conditions [32]. It has not yet been described in the *Ulva*–bacteria symbiosis. Not all essential genes for ectoine biosynthesis reported by [33] were found in the *U. mutabilis* genome [34], providing further support for the bacterial origin of ectoine. Homologs of EctA (UM017_0070.1, E value 0.34), EctB (UM084_0040.1, E value < 0.0001) that provide the central intermediate *N*-acetyl-2,4-diaminobutyrate and EctD (UM025_0127.1, E value 0.094) an ectoine hydroxylase could be identified. However, a homolog gene for EctC (ectoine synthase) is missing in the *U. mutabilis* genome. In addition, despite the low E value of EctB, the reciprocal NCBI-blast search against the anoxygenic photosynthetic halophile and ectoine-producing bacterium *Halorhodospira halochloris* [35] did not confirm the presence of the sequence in the algal genome. Therefore, it is unlikely that the alga produces ectoine. In summary, ectoine is indicative of *Roseovarius* sp. MS2 in the tripartite community and can serve for localisation studies.

Localisation of bacterial symbionts of *Ulva mutabilis* using fluorescence microscopy and imaging mass spectrometry

Based on the above results, we combined LDI-MS imaging mass spectrometry and cLSM using a non-specific fluorescence labelling probe to visualise the bacterial cells living in symbiosis with *U. mutabilis*. Following a one-month incubation in clean cuvette slides placed in Petri dishes filled with medium, axenic and bacteria-inoculated *U. mutabilis* germlings were stained with SYBR Gold, a sensitive probe forming a complex with DNA with high fluorescence quantum yield [36]. In the axenic callus-like form, the nuclei of algal cells and the bacterial cells accumulated around the rhizoidal tissue and exhibited the specific fluorescence after SYBR Gold staining (Figure 3a) as previously described [8,37]. These findings indicated that bacteria are associated with their algal host during symbiosis.

In parallel, we visualised the metabolites produced by the biofilm formed around *U. mutabilis* by imaging analysis with AP-SMALDI-HRMS. Three replicates each of the axenic algae, algae in symbiosis, germlings, and bacterial cells in monocultures were imaged after matrix deposition by AP-SMALDI-HRMS over a centimetre-scaled area (Figure 3b). The algal pigment chlorophyll was localised with the algal tissues (Figure 3b and Figure S1 in Supporting Information File 1). Even though

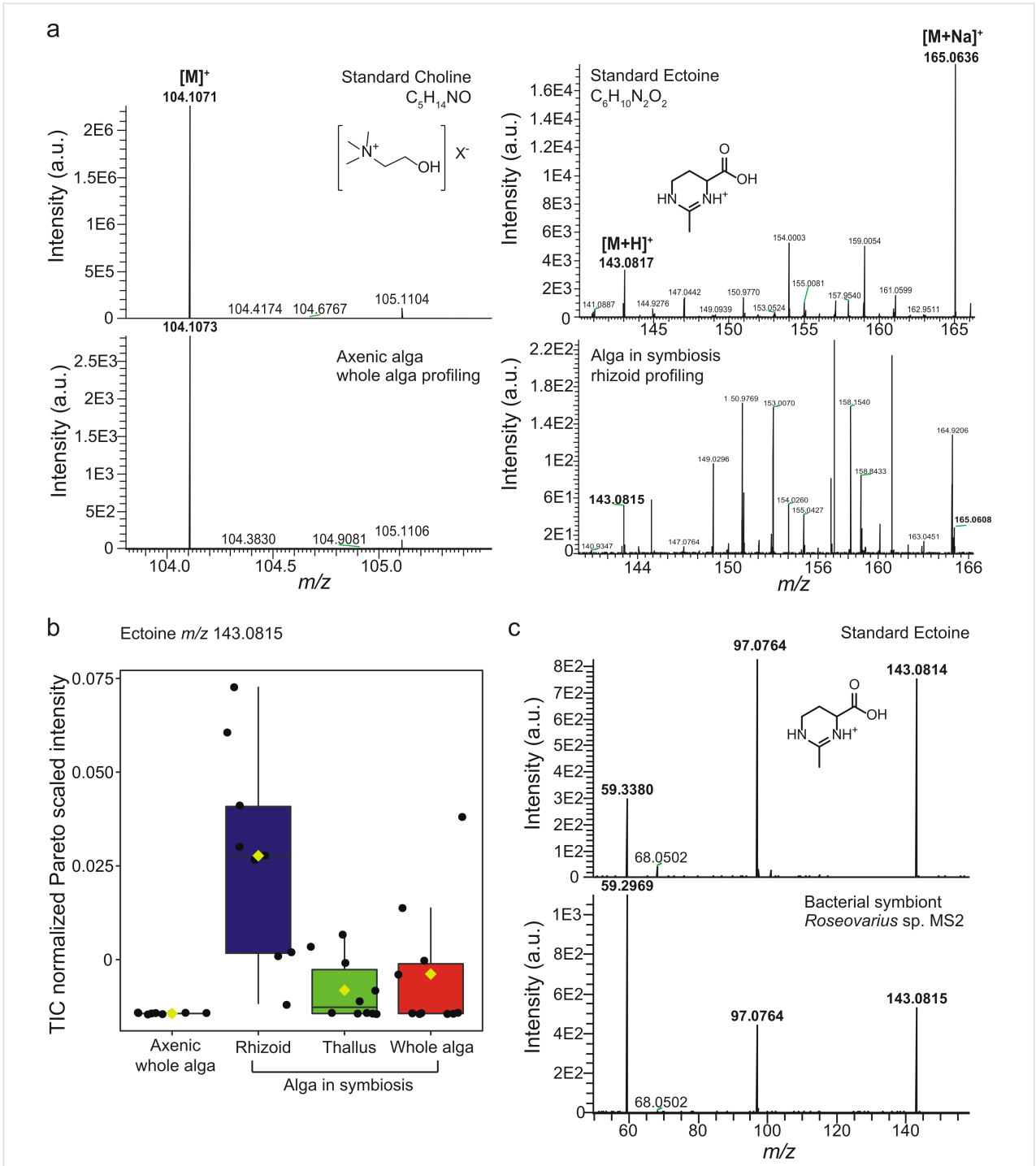

Figure 2: Identification of significant features associated with axenic or bacterial symbiont-associated alga *Ulva mutabilis* (phenotype slender). a) The structural determination was achieved by spectral matching with the analytical standards using AP-SMALDI-HRMS. b) Relative amounts of ectoine (*m/z* 143.0815 for $[M + H]^+$) were determined by AP-SMALDI-HRMS measurements to compare different tissues: axenic and algae in symbiosis. One-way ANOVA with a Fisher HSD post hoc test found choline to be significant in profiles of axenic algae ($F = 42$, P-value < 0.0001) and ectoine in profiles of rhizoidal zones of algae in symbiosis ($F = 4$, P-value < 0.005) (colour code with reference to Figure 1a). c) Ectoine (*m/z* 143.0815 for $[M + H]^+$, precursor ion) was identified in a single colony of the bacterial symbiont *Roseovarius* sp. MS2 using AP-SMALDI-HRMS/MS analysis.

most of the seawater media was removed from the *Ulva* samples during sample preparation, crystallisation of seawater salts on the sample surface occurred. The size of the crystals and their distribution within an imaged area were examined using a digital microscope and found to be homogeneous and consistent across the samples and experiments. As a result, the ion

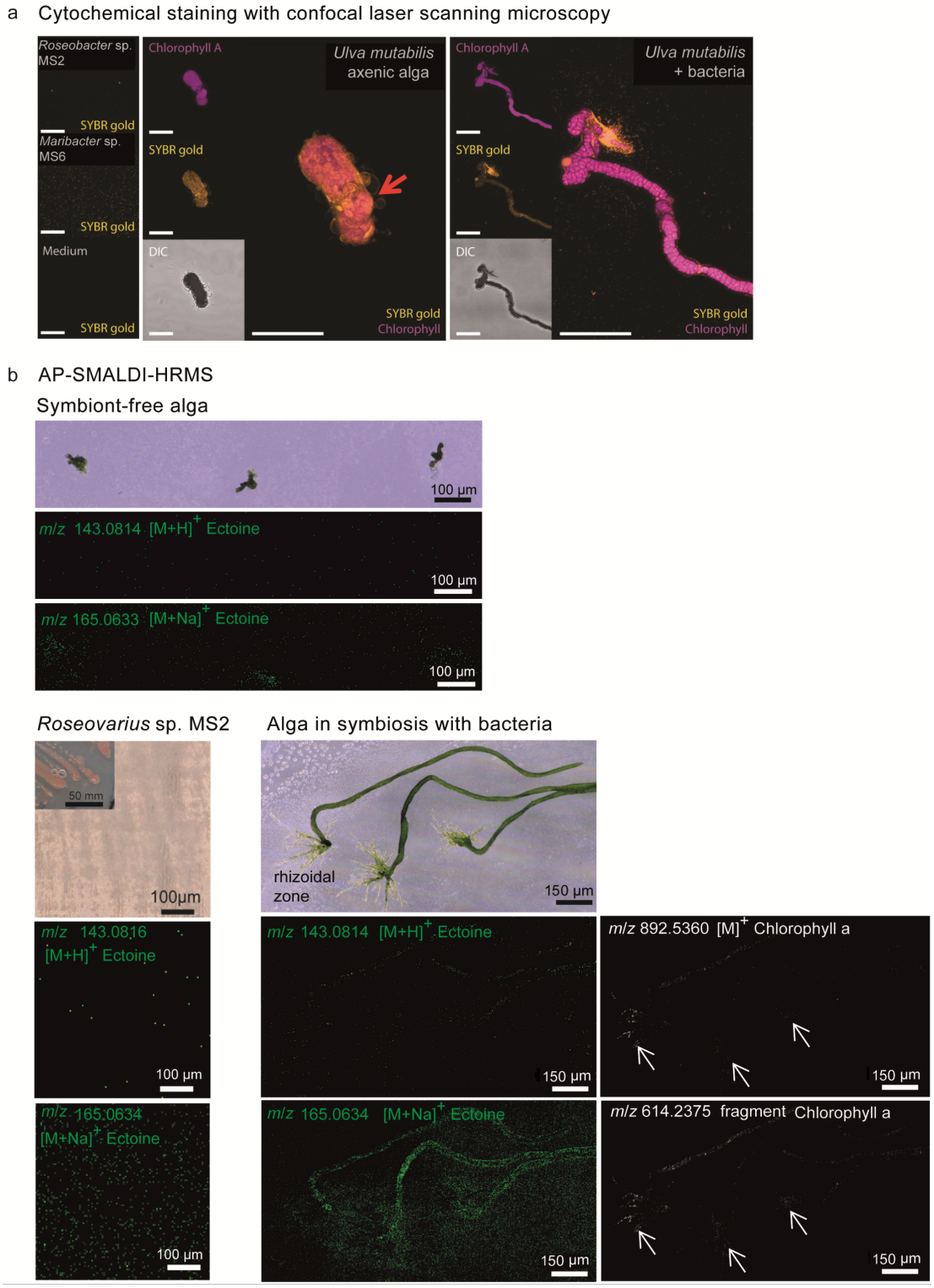

Figure 3: Visualisation of algae *Ulva mutabilis* grown under axenic conditions or with bacterial symbionts *Roseovarius* sp. MS2 and *Maribacter* sp. MS6. a) Images acquired after nucleic acid staining with SYBR gold and with confocal laser scanning microscopy. The protrusion of alga grown without bacterial symbiont is highlighted (red arrow). DIC: differential interference microscopy. b) The images show ectoine spatial localisation and thus the presence of *Roseovarius* sp. (*m*/*z* 143.0814 for $[M + H]^+$, *m*/*z* 165.0633 for $[M + Na]^+$, shown in green) as well as chlorophyll (*m*/*z* 892.5360 for $[M + H]^+$, *m*/*z* 614.2375 fragment shown in white). These metabolite traces are visible in axenic algae, symbiotic algae, and cell cultures of bacteria *Roseovarius* sp. MS2. White arrows indicate the rhizoidal zones.

suppression effect caused by the presence of seawater crystals on the *Ulva* samples and surroundings was consistent across all measurements (Supporting Information File 1, Figures S1 and S2).

Ectoine was detected in both profiling and imaging MS spectra as the $[M + Na]^+$ adduct at *m*/*z* 165.0633. Ectoine was mainly found around the rhizoid in elevated amounts. Thus, *Roseovarius* sp. MS2 became visible in the rhizoidal zone and on the thallus due to the exclusive production of ectoine within the tripartite community (Figure 3b). AP-SMALDI-HRMS studies extended to the entire clade of motile Rhodobacteraceae will reveal other characteristic metabolites of the *Ulva*–bacteria interactions. Those species attracted by *U. mutabilis* (e.g., through DMSP) that use the provided photosynthates [9], will preferentially succeed the previously described competitive colonisations of *Ulva* spp. [38,39]. Also, related species of *Roseovarius* sp. MS2 can often release unknown AGMPFs [29,40], which further foster the bacterial–algal interactions. As more species-specific metabolic markers become available, AP-SMALDI imaging will be a powerful tool to track these dynamic microbial colonisation processes using the *U. mutabilis* model system with a designed microbiome.

Conclusion

Metabolic profiling of whole alga and specialised tissues conducted with AP-SMALDI-HRMS enabled identifying specific metabolites in host–bacteria symbiosis. We report the first identification of choline and ectoine as markers of symbiont-free *U. mutabilis* and rhizoid tissue of algae in symbiosis with bacteria. We visualised the rhizoidal zone formed by the bacterial symbionts using chemical staining, confocal laser scanning microscopy, and imaging mass spectrometry. Notably, ectoine was used as a metabolic marker to identify bacteria in the biofilm associated with *U. mutabilis* and the algal surface. Visualising the spatial distribution of epiphytic bacteria in the phycosphere will contribute to the general understanding of the chemically mediated cross-kingdom interactions. The combined AP-SMALDI and cLSM imaging with resolution down to the level of a single bacterial cell introduced here can be applied to other microbial consortia and their hosts and will be instrumental for microbiome research.

Experimental

Biological experiments and imaging microscopy

The laboratory strains of *U. mutabilis* (sl-G[mt+]) are direct descendants of the original isolates collected by B. Føyn in Portugal (Ria Formosa) in 1958 [8]. This strain is used as a model organism in cross-kingdom interactions [7,34,37] and cultivated under standardised conditions [41,42]. *Ulva* strains are available from the corresponding author (Thomas Wichard, Friedrich-Schiller-Universität Jena, Germany).

Gametogenesis of *U. mutabilis* was induced by chopping harvested algal tissue, and released gametes were purified from accompanying bacteria according to the protocol of Wichard and Oertel (2010) [41]. The strains *Roseovarius* sp. MS2 (Genbank EU359909) and *Maribacter* sp. MS6 (Genbank EU359911) were originally isolated from *U. mutabilis* [8] and were cultivated in Marine Broth medium (Roth, Germany) at 20 °C. *Ulva* gametes were either grown axenically or inoculated with the bacteria (final optical density $OD_{620} = 0.001$). All algae were cultivated in *Ulva* culture medium (UCM) [43] at 18 °C with the illumination of about 60 µmol photons m^{-2} s^{-1} under a 17:7 light/dark regime. Axenic *Ulva* gametes deposited on cleaned glass slides and inoculated with bacteria MS2/MS6 were prepared following the procedure for in situ MS imaging described by Kessler et al. [19]. Briefly, algal gametes were inoculated to 10 mL medium in 9 cm diameter sterile Petri dishes with a clean and autoclaved glass slide (25 mm × 75 mm) with cavities (Paul Marienfeld, Germany) on the bottom; samples were incubated for one month at 18 °C in static conditions. An inverted microscope was used to monitor the algal growth. Transmitted light microscopy pictures were obtained using a Keyence BHX-500 digital microscope. Samples were recovered with pliers and fixed with glutaraldehyde 1% (Merck), stained with SYBR Gold (1% in DMSO, Invitrogen, Thermo Fisher); a cover slide was added, followed by incubation in the dark at 15 °C for 15 min. Cavity slides were spotted with 100 µL of SYBR Gold or unstained bacterial monoculture (*Roseovarius* sp MS2 or *Maribacter* sp. MS6) to use them as controls. Fluorescence images (1024 × 1024) were acquired using a Zeiss cLSM 880 (Carl Zeiss AG, Oberkochen, Germany) with a Plan-Apochromat 20 × 0.8 and 488 nm Argon-laser excitation (5% transmission). Emission wavelengths for SYBR Gold (490–650 nm) and chlorophyll A (653–735 nm) were separated via the spectral detection unit. Transmitted light was detected by the transmitted light-PMT. The effect of an additional quick washing step was tested by gently adding 100 µL of sterile MQ water for two seconds. The controls consisted of bacteria grown for one week in monoculture in 40 mL of marine broth medium and the axenic medium with fixative and stain. All the experiments with glass slides were performed in biological triplicates.

Genome analysis

To identify the putative biosynthetic gene cluster (*ect* gene cluster) in *U. mutabilis* [34], the algal genome was searched for the gene ectoine hydroxylase (*ectD*) and also for a specialised aspartokinase (*ask_ect*). Aspartokinase (Ask), along with

L-aspartate-β-semialdehyde-dehydrogenase (Asd), provides the precursor L-ASA for ectoine biosynthesis [33,44,45]. Homologs of the enzymes of the ectoine pathway from *Halorhodospira halochloris* were identified by BLAST searches of the *U. mutabilis* genome at ORCAE using default parameters (https://bioinformatics.psb.ugent.be/orcae/overview/Ulvmu).

AP-SMALDI-HRMS metabolic profiling and imaging

All standards and *Ulva* samples were analysed via AP-SMALDI (AP-SMALDI10, TransMit, Germany) ion source equipped with a UV (337 nm) nitrogen laser (LTB MNL-106, LTB, Germany) coupled to a high-resolution mass spectrometer Q-Exactive Plus (Thermo Fisher Scientific, Bremen, Germany). Glass slides with one month-grown algal gametophytes were gently recovered from a Petri dish filled with UCM using a sterile tweezer and dipped for one second in sterile ultrapure water to remove the excess salts before metabolic profiling. When algae were investigated directly on a glass slide before in situ MS imaging, blotting paper was used to remove sea water (see also Supporting Information File 1). The desired area of a glass slide covered with algal individuals was first marked, photographed, and finally fixed on the AP-SMALDI metal target.

AP-SMALDI profiling and imaging experiments unless otherwise stated were enhanced by a 2,5-dihydroxybenzoic acid (DHB) MALDI matrix. A methanolic solution of the DHB matrix at a concentration of 4 mg mL^{-1} was applied onto a sample via SunChrom MALDI spotter (SunChrom GmbH, Germany). The spraying method was optimised using the following parameters: line distance 2 mm, spraying speed 800 mm min^{-1} with 5 seconds drying time, and matrix solution flow rate in 4 cycles from 10 µL up to 30 µL min^{-1}. Solvents used in this study were all LCMS analytical grade. 2,5-Dihydroxybenzoic acid with a purity of above 98% and high purity MS-grade methanol were purchased from Sigma-Aldrich (Germany).

All *Ulva* samples were imaged in the positive ion mode using a step size of 5 µm and with the number of laser shots per spot set to 30 (approximately 1.2 µJ $shot^{-1}$) within the laser frequency of 60 Hz. MS spectra were acquired in a mass range from *m/z* 100 to *m/z* 1000 with a resolving power of 280000. Pseudo ion intensity maps of selected *m/z* values were generated using the Mirion V3 software package with an *m/z* width of 0.01 u.

In the profiling mode, the single *Ulva* individuals were targeted visually and ablated with a laser spot size of approximately 10 µm in positive and negative polarity in a mass range from *m/z* 100 to *m/z* 1000. The other parameters stayed like for the MSI mode. In profiling, the same area of the rhizoid and the tip of the thallus of different individuals were analysed by laser ablation over one-minute time acquisition. Axenic and alga in symbiosis germlings were profiled with a UV laser along a longitudinal axis to investigate the effect of bacteria on metabolism changes in *U. mutabilis*.

The size of the sample groups analysed by AP-SMALDI-HRMS in profiling mode was $n = 10$ for thallus tissue, $n = 9$ for rhizoid tissue, $n = 8$ for axenic callus, and $n = 10$ for alga in symbiosis. Matrix-free experiments (LDI-HRMS) were performed in profiling mode under the same experimental conditions as the AP-SMALDI-HRMS. The size of the sample groups was defined as follows: $n = 6$ for rhizoid, $n = 7$ for thallus and whole alga profiling, $n = 10$ for alga in symbiosis, and $n = 15$ for axenic alga.

The metabolic profiles of nutrient media were obtained by analysing 30 µL deposited onto cleaned glass slides and following the same protocol used for the *Ulva* samples. In the late exponential stage, bacterial monoculture was recovered from agar plates with a 10 µL loop and diluted in 100 µL of sterile water. Five microliters of the solution were spotted onto a glass slide and analysed in AP-SMALDI-HRMS mode in positive and negative polarity.

The data acquired in MSI mode were collected with Xcalibur software version 2.8 SP1 Build 2806 (Thermo Fisher Scientific, Germany) while the acquisition of spatial scans, pre-defined in the *x*- and *y*-direction as rectangular sample regions, was controlled by the MCP (Master Control Program, TransMIT GmbH, Giessen, Germany). The raw data acquired in profiling mode were visualised in Thermo Xcalibur™ version 3.0.63 (Thermo Fisher Scientific, Germany) and then converted to netCDF format using the Thermo File Converter tool. Data preprocessing was performed to extract the intensities in each profile, excluding the features of the nutrient medium using a script adapted from the MALDIquand package [46]. Spectra were de-noised with a signal-to-noise ratio of 5. Normalisation was done based on total ion current (TIC) recommended for MALDI-MS analysis [47]. All spectra, images, R data, scripts, and results from the statistical analysis were uploaded and are freely accessible in the Max Planck repository Edmond (https://dx.doi.org/10.17617/3.4v).

Significant features analysis and metabolite identification

Data analysis was conducted in MetaboAnalyst 4.0 [48] to perform univariate and multivariate statistical tests and find significant differences in intensities and the presence or absence of metabolites in the samples. Pareto scaling and cube root trans-

formation were conducted to normalise the datasets before the multivariate statistics. PCA highlighted the metabolic differences between axenic and alga in symbiosis and between thallus and rhizoid tissues. Significant features were searched in the PCA loading plots and also in the pattern hunter plots obtained from a correlation analysis based on the Pearson correlation coefficient R. A one-way ANOVA with Fisher's LSD post hoc test (P-value < 0.05) was performed, and the relative amounts of the significant features were displayed as a boxplot. The selected significant features were further searched in the raw HRMS profiles to identify those with the reliable isotopic pattern assigned to a metabolite. The m/z values were searched in the METLIN database, using a mass deviation equal to or lower than five ppm, which suggested several known natural products such as ectoine [49].

To confirm the identity of the significant features, mass spectral information was compared with analytical standards analysed with the AP-SMALDI-HRMS (DMSP, chlorophyll-a, ectoine, choline). MS/MS experiments were performed with AP-SMALDI-HRMS to match the fragmentation pattern between the standard ectoine and bacteria monoculture profile. Fragmentation spectra of ectoine were acquired from the bacterial isolate *Roseovarius* sp. MS2 and an ectoine standard. To perform a measurement, 4 µL of ectoine at concentration 50 µM was pipetted onto a clean glass slide (washed with dH_2O, acetone) and overlaid with 2 µL of a methanolic solution of the DHB matrix at a concentration of 4 mg mL^{-1}. For a bacterial isolate, the sample was prepared from one colony smeared onto a glass slide and covered with the DHB matrix, following the standard ectoine procedure. Samples were analysed in positive ion mode, with the number of laser shots per spot set to 30 (approximately 1.2 µJ $shot^{-1}$). All-ion fragmentation (AIF) mode was set as follows: molecular ion of ectoine at m/z 143.1; isolation window $m/z \pm 0.2$; 45 NCE. The peak resolution was set at 280000, and the mass range was set from m/z 50 to m/z 300.

Supporting Information

Supporting Information File 1

Details on sample preparation and additional figures.
[https://www.beilstein-journals.org/bjoc/content/supplementary/1860-5397-17-91-S1.pdf]

Funding

SF was funded by the International Max Planck Research School Exploration of Ecological Interactions with Molecular Techniques. This work was supported by an MPG Fellowship awarded to GP and by the Deutsche Forschungsgemeinschaft through Grant No. SFB 1127/2 ChemBioSys–239748522 (GP, TW) and within the framework of the priority program (SPP 1158) "Antarctic Research with comparative investigations in Arctic ice areas" under the project number #424256657 (FG, TW).

ORCID® iDs

Marine Vallet - https://orcid.org/0000-0002-6878-0459
Filip Kaftan - https://orcid.org/0000-0002-5851-945X
Veit Grabe - https://orcid.org/0000-0002-0736-2771
Fatemeh Ghaderiardakani - https://orcid.org/0000-0003-3497-8421
Simona Fenizia - https://orcid.org/0000-0002-3592-9368
Aleš Svatoš - https://orcid.org/0000-0003-1032-7288
Georg Pohnert - https://orcid.org/0000-0003-2351-6336
Thomas Wichard - https://orcid.org/0000-0003-0061-4160

References

1. Ramanan, R.; Kim, B.-H.; Cho, D.-H.; Oh, H.-M.; Kim, H.-S. *Biotechnol. Adv.* **2016,** *34,* 14–29. doi:10.1016/j.biotechadv.2015.12.003
2. Singh, R. P.; Reddy, C. R. K. *FEMS Microbiol. Ecol.* **2014,** *88,* 213–230. doi:10.1111/1574-6941.12297
3. Wichard, T.; Beemelmanns, C. *J. Chem. Ecol.* **2018,** *44,* 1008–1021. doi:10.1007/s10886-018-1004-7
4. Croft, M. T.; Lawrence, A. D.; Raux-Deery, E.; Warren, M. J.; Smith, A. G. *Nature* **2005,** *438,* 90–93. doi:10.1038/nature04056
5. Selvarajan, R.; Sibanda, T.; Venkatachalam, S.; Ogola, H. J. O.; Christopher Obieze, C.; Msagati, T. A. *Sci. Rep.* **2019,** *9,* 19835. doi:10.1038/s41598-019-56269-2
6. Burke, C.; Thomas, T.; Lewis, M.; Steinberg, P.; Kjelleberg, S. *ISME J.* **2011,** *5,* 590–600. doi:10.1038/ismej.2010.164
7. Wichard, T.; Charrier, B.; Mineur, F.; Bothwell, J. H.; Clerck, O. D.; Coates, J. C. *Front. Plant Sci.* **2015,** *6,* 72. doi:10.3389/fpls.2015.00072
8. Spoerner, M.; Wichard, T.; Bachhuber, T.; Stratmann, J.; Oertel, W. *J. Phycol.* **2012,** *48,* 1433–1447. doi:10.1111/j.1529-8817.2012.01231.x
9. Kessler, R. W.; Weiss, A.; Kuegler, S.; Hermes, C.; Wichard, T. *Mol. Ecol.* **2018,** *27,* 1808–1819. doi:10.1111/mec.14472
10. Alsufyani, T.; Weiss, A.; Wichard, T. *Mar. Drugs* **2017,** *15,* 14. doi:10.3390/md15010014
11. Alsufyani, T.; Califano, G.; Deicke, M.; Grueneberg, J.; Weiss, A.; Engelen, A. H.; Kwantes, M.; Mohr, J. F.; Ulrich, J. F.; Wichard, T. *J. Exp. Bot.* **2020,** *71,* 3340–3349. doi:10.1093/jxb/eraa066
12. Weiss, A.; Costa, R.; Wichard, T. *Bot. Mar.* **2017,** *60,* 197–206. doi:10.1515/bot-2016-0083
13. Matsuo, Y.; Imagawa, H.; Nishizawa, M.; Shizuri, Y. *Science* **2005,** *307,* 1598. doi:10.1126/science.1105486
14. Bell, W.; Mitchell, R. *Biol. Bull. (Woods Hole, MA, U. S.)* **1972,** *143,* 265–277. doi:10.2307/1540052
15. Joint, I.; Tait, K.; Callow, M. E.; Callow, J. A.; Milton, D.; Williams, P.; Cámara, M. *Science* **2002,** *298,* 1207. doi:10.1126/science.1077075
16. Raina, J.-B.; Clode, P. L.; Cheong, S.; Bougoure, J.; Kilburn, M. R.; Reeder, A.; Forêt, S.; Stat, M.; Beltran, V.; Thomas-Hall, P.; Tapiolas, D.; Motti, C. M.; Gong, B.; Pernice, M.; Marjo, C. E.; Seymour, J. R.; Willis, B. L.; Bourne, D. G. *eLife* **2017,** *6,* e23008.

17. Lane, A. L.; Nyadong, L.; Galhena, A. S.; Shearer, T. L.; Stout, E. P.; Parry, R. M.; Kwasnik, M.; Wang, M. D.; Hay, M. E.; Fernandez, F. M.; Kubanek, J. *Proc. Natl. Acad. Sci. U. S. A.* **2009,** *106,* 7314–7319. doi:10.1073/pnas.0812020106
18. Parrot, D.; Blümel, M.; Utermann, C.; Chianese, G.; Krause, S.; Kovalev, A.; Gorb, S. N.; Tasdemir, D. *Sci. Rep.* **2019,** *9,* 1061. doi:10.1038/s41598-018-37914-8
19. Kessler, R. W.; Crecelius, A. C.; Schubert, U. S.; Wichard, T. *Anal. Bioanal. Chem.* **2017,** *409,* 4893–4903. doi:10.1007/s00216-017-0430-7
20. Mandal, A.; Singha, M.; Addy, P. S.; Basak, A. *Mass Spectrom. Rev.* **2019,** *38,* 3–21. doi:10.1002/mas.21545
21. Hansen, R. L.; Lee, Y. J. *Chem. Rec.* **2018,** *18,* 65–77. doi:10.1002/tcr.201700027
22. Yang, Y.; Lin, Y.; Qiao, L. *Anal. Chem. (Washington, DC, U. S.)* **2018,** *90,* 10400–10408. doi:10.1021/acs.analchem.8b02258
23. Barbano, D.; Diaz, R.; Zhang, L.; Sandrin, T.; Gerken, H.; Dempster, T. *PLoS One* **2015,** *10,* e0135337. doi:10.1371/journal.pone.0135337
24. Sandrin, T. R.; Goldstein, J. E.; Schumaker, S. *Mass Spectrom. Rev.* **2013,** *32,* 188–217. doi:10.1002/mas.21359
25. Dunham, S. J. B.; Ellis, J. F.; Li, B.; Sweedler, J. V. *Acc. Chem. Res.* **2017,** *50,* 96–104. doi:10.1021/acs.accounts.6b00503
26. Peterson, D. S. *Mass Spectrom. Rev.* **2007,** *26,* 19–34. doi:10.1002/mas.20104
27. Baumeister, T. U. H.; Vallet, M.; Kaftan, F.; Guillou, L.; Svatoš, A.; Pohnert, G. *Metabolomics* **2020,** *16,* 28. doi:10.1007/s11306-020-1646-7
28. Baumeister, T. U. H.; Vallet, M.; Kaftan, F.; Svatoš, A.; Pohnert, G. *Front. Plant Sci.* **2019,** *10,* 172. doi:10.3389/fpls.2019.00172
29. Ghaderiardakani, F.; Coates, J. C.; Wichard, T. *FEMS Microbiol. Ecol.* **2017,** *93,* fix094. doi:10.1093/femsec/fix094
30. Gupta, V.; Kushwaha, H. R. *Sci. Rep.* **2017,** *7,* 16430. doi:10.1038/s41598-017-15994-2
31. Zeisel, S. H. Phosphatidylcholine: endogenous precursor of choline. In *Lecithin: Technological, Biological, and Therapeutic Aspects;* Hanin, I.; Ansell, G. B., Eds.; Advances in Behavioral Biology, Vol. 33; Springer US: Boston, MA, USA, 1987; pp 107–120. doi:10.1007/978-1-4757-1933-8_11
32. Fenizia, S.; Thume, K.; Wirgenings, M.; Pohnert, G. *Mar. Drugs* **2020,** *18,* 42. doi:10.3390/md18010042
33. Richter, A. A.; Mais, C.-N.; Czech, L.; Geyer, K.; Hoeppner, A.; Smits, S. H. J.; Erb, T. J.; Bange, G.; Bremer, E. *Front. Microbiol.* **2019,** *10,* 2811. doi:10.3389/fmicb.2019.02811
34. De Clerck, O.; Kao, S.-M.; Bogaert, K. A.; Blomme, J.; Foflonker, F.; Kwantes, M.; Vancaester, E.; Vanderstraeten, L.; Aydogdu, E.; Boesger, J.; Califano, G.; Charrier, B.; Clewes, R.; Del Cortona, A.; D'Hondt, S.; Fernandez-Pozo, N.; Gachon, C. M.; Hanikenne, M.; Lattermann, L.; Leliaert, F.; Liu, X.; Maggs, C. A.; Popper, Z. A.; Raven, J. A.; Van Bel, M.; Wilhelmsson, P. K. I.; Bhattacharya, D.; Coates, J. C.; Rensing, S. A.; Van Der Straeten, D.; Vardi, A.; Sterck, L.; Vandepoele, K.; Van de Peer, Y.; Wichard, T.; Bothwell, J. H. *Curr. Biol.* **2018,** *28,* 2921–2933.e5. doi:10.1016/j.cub.2018.08.015
35. Schuh, W.; Puff, H.; Galinski, E. A.; Trüper, H. G. *Z. Naturforsch., C: J. Biosci.* **1985,** *40,* 780–784. doi:10.1515/znc-1985-11-1206
36. Tuma, R. S.; Beaudet, M. P.; Jin, X.; Jones, L. J.; Cheung, C.-Y.; Yue, S.; Singer, V. L. *Anal. Biochem.* **1999,** *268,* 278–288. doi:10.1006/abio.1998.3067
37. Wichard, T. *Front. Plant Sci.* **2015,** *6,* 86. doi:10.3389/fpls.2015.00086
38. Frank, O.; Michael, V.; Päuker, O.; Boedeker, C.; Jogler, C.; Rohde, M.; Petersen, J. *Syst. Appl. Microbiol.* **2015,** *38,* 120–127. doi:10.1016/j.syapm.2014.12.001
39. Rao, D.; Webb, J. S.; Kjelleberg, S. *Appl. Environ. Microbiol.* **2006,** *72,* 5547–5555. doi:10.1128/aem.00449-06
40. Grueneberg, J.; Engelen, A. H.; Costa, R.; Wichard, T. *PLoS One* **2016,** *11,* e0146307. doi:10.1371/journal.pone.0146307
41. Wichard, T.; Oertel, W. *J. Phycol.* **2010,** *46,* 248–259. doi:10.1111/j.1529-8817.2010.00816.x
42. Nahor, O.; Morales-Reyes, C. F.; Califano, G.; Wichard, T.; Golberg, A.; Israel, Á. *Bot. Mar.* **2021,** *64,* 83–92. doi:10.1515/bot-2020-0050
43. Stratmann, J.; Paputsoglu, G.; Oertel, W. *J. Phycol.* **1996,** *32,* 1009–1021. doi:10.1111/j.0022-3646.1996.01009.x
44. Peters, P.; Galinski, E. A.; Trüper, H. G. *FEMS Microbiol. Lett.* **1990,** *71,* 157–162. doi:10.1111/j.1574-6968.1990.tb03815.x
45. Reshetnikov, A. S.; Khmelenina, V. N.; Trotsenko, Y. A. *Arch. Microbiol.* **2006,** *184,* 286–297. doi:10.1007/s00203-005-0042-z
46. Gibb, S.; Strimmer, K. Mass spectrometry analysis using MALDIquant. In *Statistical Analysis of Proteomics, Metabolomics, and Lipidomics Data Using Mass Spectrometry;* Datta, S.; Mertens, B. J. A., Eds.; Springer International Publishing: Cham, Switzerland, 2017; pp 101–124. doi:10.1007/978-3-319-45809-0_6
47. Emara, S.; Amer, S.; Ali, A.; Abouleila, Y.; Oga, A.; Masujima, T. Single-Cell Metabolomics. In *Metabolomics: From Fundamentals to Clinical Applications;* Sussulini, A., Ed.; Advances in Experimental Medicine and Biology, Vol. 965; Springer International Publishing: Cham, Switzerland, 2017; pp 323–343. doi:10.1007/978-3-319-47656-8_13
48. Chong, J.; Soufan, O.; Li, C.; Caraus, I.; Li, S.; Bourque, G.; Wishart, D. S.; Xia, J. *Nucleic Acids Res.* **2018,** *46,* W486–W494. doi:10.1093/nar/gky310
49. Guijas, C.; Montenegro-Burke, J. R.; Domingo-Almenara, X.; Palermo, A.; Warth, B.; Hermann, G.; Koellensperger, G.; Huan, T.; Uritboonthai, W.; Aisporna, A. E.; Wolan, D. W.; Spilker, M. E.; Benton, H. P.; Siuzdak, G. *Anal. Chem. (Washington, DC, U. S.)* **2018,** *90,* 3156–3164. doi:10.1021/acs.analchem.7b04424

License and Terms

BEILSTEIN JOURNAL OF ORGANIC CHEMISTRY

Volatile emission and biosynthesis in endophytic fungi colonizing black poplar leaves

Christin Walther[1], Pamela Baumann[1,2], Katrin Luck[1], Beate Rothe[1], Peter H. W. Biedermann[1,2], Jonathan Gershenzon[1], Tobias G. Köllner[1] and Sybille B. Unsicker[*1]

Full Research Paper

Open Access

Address:
[1]Department of Biochemistry, Max Planck Institute for Chemical Ecology, Hans-Knöll Str. 8, 07745 Jena, Germany and [2]Chair of Forest Entomology and Protection, Institute of Forest Sciences, University of Freiburg, Fohrenbühl 27, 79252 Stegen-Wittental, Germany

Email:
Sybille B. Unsicker[*] - sunsicker@ice.mpg.de

* Corresponding author

Keywords:
Ascomycota; *Cladosporium*; Salicaceae; terpene synthases; volatile organic compound (VOC)

Beilstein J. Org. Chem. **2021,** *17,* 1698–1711.
https://doi.org/10.3762/bjoc.17.118

Received: 24 December 2020
Accepted: 29 June 2021
Published: 22 July 2021

This article is part of the thematic issue "Chemical ecology".

Guest Editor: C. Beemelmanns

Abstract

Plant volatiles play a major role in plant–insect interactions as defense compounds or attractants for insect herbivores. Recent studies have shown that endophytic fungi are also able to produce volatiles and this raises the question of whether these fungal volatiles influence plant–insect interactions. Here, we qualitatively investigated the volatiles released from 13 endophytic fungal species isolated from leaves of mature black poplar (*Populus nigra*) trees. The volatile blends of these endophytes grown on agar medium consist of typical fungal compounds, including aliphatic alcohols, ketones and esters, the aromatic alcohol 2-phenylethanol and various sesquiterpenes. Some of the compounds were previously reported as constituents of the poplar volatile blend. For one endophyte, a species of *Cladosporium*, we isolated and characterized two sesquiterpene synthases that can produce a number of mono- and sesquiterpenes like (*E*)-β-ocimene and (*E*)-β-caryophyllene, compounds that are dominant components of the herbivore-induced volatile bouquet of black poplar trees. As several of the fungus-derived volatiles like 2-phenylethanol, 3-methyl-1-butanol and the sesquiterpene (*E*)-β-caryophyllene, are known to play a role in direct and indirect plant defense, the emission of volatiles from endophytic microbial species should be considered in future studies investigating tree-insect interactions.

Introduction

Plant volatile organic compounds (VOCs) can mediate plant–insect, plant–microbe, and plant–plant interactions [1-4]. The constitutive and herbivore-induced volatile blends of plants consist of different compound classes, including green leaf volatiles, benzenoids, terpenoids, and nitrogen-containing compounds [5-7]. Among these, terpenoids represent the largest and most diverse group of compounds. In poplar trees, large amounts of terpenoids can be emitted constitutively [8,9] and

facilitate protection against thermal and oxidative stresses [10]. In addition, terpenoids are also produced in response to biological stresses such as herbivory [9,11] and can fulfill different functions in plant–insect interactions. For instance, together with other volatiles, some terpenoids are known to attract natural enemies of insect herbivores [2,12,13] or attract insects as shown for the sesquiterpene (*E*)-β-caryophyllene (**1**) [14,15]. Another sesquiterpene, (*E*)-β-farnesene (**2**), an aphid alarm pheromone, is also produced by plant species like *Arabidopsis thaliana* [16]. Besides terpenoids, other plant VOCs are also known to mediate plant–insect interactions. For instance, 2-phenylethanol (**3**) is a typical attractant for pollinators, but is also involved in direct and indirect plant defense [17-19].

Endophytic microorganisms are fungi or bacteria that live asymptomatically within healthy plant tissue (e.g., leaves, flowers and roots) for at least a part of their life cycle [20]. Endophyte colonization is widespread in the plant kingdom, but their role in plant–insect interactions is under debate [21]. Currently, most of our knowledge on the role of endophytes in plant defense responses comes from studies with fungal grass endophytes (clavicipitaceous endophytes) that are often mutualistic for the plant. The ecological significance of nonclavicipitaceous endophytes, which occur also in trees, is more ambiguous and only poorly understood [22-24].

Endophytic fungi themselves can produce VOCs. Currently, around 300 fungal VOCs have been characterized, including aliphatic alcohols, ketones, aldehydes, acids and esters, terpenoids, benzenoids, naphthalene derivatives, and cycloalkanes [25-27]. Endophytic fungal VOCs are frequently described to exhibit antimicrobial activity; however, they are also known to induce the growth and vigor of the host plant and to shape plant community structure [27-31]. Furthermore, volatiles released from endophytic fungi can also affect insect behavior. Daisy et al. isolated the endophytic fungus *Muscodor vitigenus* and characterized the volatile blend in culture [32]. Naphthalene, an insect deterrent that is used, e.g., in mothballs [33], was the most dominant compound in the fungal volatile blend and showed a repellent effect on the wheat stem sawfly *Cephus cinctus* in a Y-tube olfactometer experiment. However, the literature on endophytic volatiles and how they influence insect behavior is scarce, especially for the endophytes of trees despite the omnipresence of fungal endophytes in forest ecosystems [34] and their potential impact on plant–insect interactions [35-38].

Among the known endophytic volatiles, sesquiterpenes have gained much attention in recent years as they can play an important role in plant–plant, plant–microbe, and microbe–microbe interactions [39,40]. Weikl et al., for instance, analyzed the volatile emission of *Alternaria alternata* and *Fusarium oxysporum* in culture and showed that both species are able to produce sesquiterpenes like (*E*)-β-farnesene (**2**), α- and β-chamigrene (**4**), and germacrene D [41]. In general, terpenes are derived from the five-carbon intermediates dimethylallyl diphosphate (DMAPP) and isopentenyl diphosphate (IPP), which are both produced by the mevalonate pathway in fungi [42]. The condensation of DMAPP with varying numbers of IPP residues results in products of various chain lengths: geranyl diphosphate (GPP, C10), farnesyl diphosphate (FPP, C15), and geranylgeranyl diphosphate (GGPP, C20). Terpene synthases (TPS) then convert the precursors GPP, FPP, and GGPP into the different terpene skeletons [42-44]. However, our knowledge on terpene synthases of endophytic fungi is scarce, specifically in comparison to the vast knowledge on these enzymes in plants and bacteria [44,45].

Typical monoterpenes like limonene and linalool (**5**), sesquiterpenes like α-farnesene, chamigrene (**4**), aromatic alcohols like 2-phenylethanol (**3**), and aliphatic alcohols like 3-methyl-1-butanol (**6**) are also found in the headspace of endophytic fungi grown in culture [46-52]. Those studies have shown that volatile blends produced by some endophytic fungi qualitatively overlap with the VOC bouquets produced by numerous plant species [53-56] including black poplar (*Populus nigra*) [57-59]. Thus, the question arises whether endophytes found in plants contribute significantly to the overall plant volatile blend by expression of their own *TPS* genes and how these fungal volatiles influence plant–insect interactions. Identification of fungal *TPS* genes is a useful tool to assess the impact of fungal terpene emission on plant volatile composition and on plant–insect interactions.

In this study, we isolated and identified endophytic fungi from leaves of a natural population of mature black poplar trees. From these fungi, we qualitatively investigated the volatiles emitted in culture and compared the blend with that emitted from black poplar trees. In addition, we used transcriptome analysis and heterologous expression to identify and characterize terpene synthases in one of the endophyte species isolated. These fungal TPSs may contribute to the volatile blend of black poplar foliage and the compounds emitted may play a role in poplar plant–insect interactions.

Results

Endophytic fungi isolated from old-growth black poplar trees

We identified 12 endophyte species from nine different genera by sequencing the internal transcribed spacer (ITS) region of the nuclear ribosomal RNA cistron. Two species were identi-

fied from the genus *Alternaria*, three from *Didymella*, two from *Aureobasidium*, and one each from *Arthrinium*, *Cladosporium*, *Fusarium*, *Sordaria*, and *Stemphylium* (Table 1). One unidentified species was also included in the volatile analysis. All the identified fungi belong to the Ascomycota, the largest fungal phylum.

Endophytic fungi emit typical plant VOCs

Altogether, we detected 77 volatile compounds in the headspaces of the 13 different endophytic species grown on agar medium. With 34 different compounds, the unidentified fungus was the endophyte emitting the most complex volatile blend. In contrast, in the headspace of both *Stemphylium* sp. and *Cladosporium* sp., only two volatile compounds were detected (Table 2). All endophytic fungi, except *Cladosporium* sp., produced aliphatic or aromatic alcohols like 2-methyl-1-propanol (**7**), 3-methyl-1-butanol (**6**) or 2-phenylethanol (**3**). Of 77 detected volatile compounds, 50 compounds are sesquiterpenes. Furthermore, seven out of 13 fungi produced sesquiterpenes. In general, the analyzed endophytic fungi have a species-specific volatile bouquet, and none of the endophytic species shared the same combination of volatile compounds. We had previously detected a number of these fungal volatiles in our volatile analyses of poplar leaves, including two alcohols 3-methyl-1-butanol (**6**) and 2-phenylethanol (**3**) and the two sesquiterpenes (*E*)-β-caryophyllene (**1**) and α-muurolene (**8**) (Table 2, Figure 1) [7,9,57-59].

Cladosporium sp. contains two sesquiterpene synthases that produce typical poplar volatile compounds in in vitro assays

The poplar fungal endophyte *Cladosporium* sp. emitted (*E*)-β-caryophyllene (**1**) in culture (Table 2, Figure 1). As this sesquiterpene is also a characteristic VOC in the constitutive and herbivore-induced blends of black poplar [57-59], we wanted to identify and characterize the responsible fungal terpene synthase, as this enzyme could contribute to the overall (*E*)-β-caryophyllene emission from the tree.

To identify terpene synthase genes potentially involved in volatile terpene formation in *Cladosporium,* we sequenced the transcriptome and performed a de novo assembly of the obtained reads. A TBLASTN analysis with *Aspergillus terreus* aristolochene synthase (pdb 20A6) as query and the de novo

Table 1: Fungal endophytes identified from leaves of mature black poplar (*Populus nigra*) trees.[a]

Species	Family	Best hit and accession number	Identity (%)
Alternaria infectoria	Pleosporaceae	*Alternaria infectoria* KX394561.1	100
Alternaria sp. 1	Pleosporaceae	*Alternaria* sp. KY788045.1	99
Stemphylium sp.	Pleosporaceae	*Stemphylium* sp. KX400960.1	99
Aureobasidium sp. 1	Dothioraceae	*Aureobasidium pullulans* KX869960.1	100
Aureobasidium sp. 2	Dothioraceae	*Aureobasidium pullulans* KT352844.1	97
Didymella glomerata	Didymellaceae	*Didymella glomerata* KY788126.1	99
Didymella sp. 1	Didymellaceae	*Didymella glomerata* KY788126.1	100
Didymella sp. 2	Didymellaceae	*Didymella glomerata* KY794938.1	100
Cladosporium sp.	Cladosporiaceae	*Cladosporium subcinereum* NR_148193.1	100
Fusarium sp.	Nectriaceae	*Fusarium armeniacum* KF944456.1	100
Sordaria sp.	Sordariaceae	*Sordaria fimicola* KX986578.1	100
Arthrinium sp.	Apiosporaceae	*Arthrinium sacchari* KY782634.1	100
unidentified species			

[a]Endophytes were isolated from leaves after surface sterilization (n = 10 tree genotypes). 12 out of 13 isolated endophytes were classified to the genus level via sequencing of the internal transcribed spacer (ITS) region of the nuclear ribosomal cistron (with primers ITS1F/ ITS4). The sequences obtained were compared to the NCBI sequence database (Supporting Information File 1, Table S1). Isolated fungi with multiple 99–100% identity hits on several species within the same genus were identified only to the genus level, but we still list the single best hit in the table.

Table 2: Volatiles emitted from endophytic fungi growing in culture on potato dextrose agar (PDA).[a]

			Endophyte species												
Volatiles class	Volatile organic compound	Kovats' RI	*Alternaria infectoria*	*Alternaria* sp. 1	*Stemphylium* sp.	*Aureobasidium* sp. 1	*Aureobasidium* sp. 2	*Didymella glomerata*	*Didymella* sp. 1	*Didymella* sp. 2	*Cladosporium* sp.	*Fusarium* sp.	*Sordaria* sp.	*Arthrinium* sp.	unidentified
aliphatic alcohol	ethanol (**17**)[b]			X		X	X	X	X	X		X	X	X	X
aliphatic ketone	2-butanone	598						X		X					
aliphatic ester	ethyl acetate	611				X									
aliphatic alcohol	2-methyl-1-propanol (**7**)	623	X	X	X	X	X	X	X	X				X	
–	unknown 1	658													X
aliphatic alcohol	3-hydroxy-2-butanone	710				X	X	X	X	X			X		X
aliphatic alcohol	**3-methyl-1-butanol (6)**[b]	730			X	X	X	X	X	X			X	X	X
aliphatic alcohol	2-methyl-1-butanol	732	X	X											
–	unknown 2	776													X
aliphatic ester	3-methylbutyl acetate	881				X								X	
aromatic hydrocarbon	ethenylbenzene	891									X				
–	unknown 3	907				X									
–	unknown 4	1044												X	
–	unknown 5	1054	X												
aromatic alcohol	**2-phenylethanol (3)**[b]	1115				X	X							X	
sesquiterpene	unknown 6	1335	X	X											
sesquiterpene	unknown 7	1343	X	X											X
sesquiterpene	α-cubebene	1355													X
–	unknown 8	1356						X							
–	unknown 9	1361						X							
–	unknown 10	1369						X							
sesquiterpene	unknown 11	1372													X
sesquiterpene	α-copaene	1381													X
–	unknown 12	1391													X
sesquiterpene	unknown 13	1395													X
sesquiterpene	sativene (**16**)	1401													X
sesquiterpene	α-gurjunene	1415	X	X											
sesquiterpene	unknown 14	1416										X			
sesquiterpene	unknown 15	1419													X
sesquiterpene	unknown 16	1420										X			
sesquiterpene	unknown 17	1423													X
sesquiterpene	aristolene (**15**)	1424	X	X											
sesquiterpene	**(*E*)-β-caryophyllene (1)**[b]	1425									X				
sesquiterpene	unknown 18	1426													X
sesquiterpene	unknown 19	1433	X	X											
sesquiterpene	unknown 20	1433						X							X
sesquiterpene	bicyclosesquiphellandrene	1436										X			
sesquiterpene	β-gurjunene[c]	1437	X	X											
sesquiterpene	unknown 21	1438													X
sesquiterpene	unknown 22	1440										X			
sesquiterpene	unknown 23	1442	X	X											

Table 2: Volatiles emitted from endophytic fungi growing in culture on potato dextrose agar (PDA).[a] (continued)

sesquiterpene	α-guaiene[c]	1447	X	X						
sesquiterpene	unknown 24	1448						X		
sesquiterpene	unknown 25	1453						X		
sesquiterpene	unknown 26	1454								X
sesquiterpene	(*E*)-β-farnesene (**2**)[c]	1456						X		
sesquiterpene	unknown 27	1462								X
sesquiterpene	unknown 28	1467								X
sesquiterpene	unknown 29	1469						X		
sesquiterpene	unknown 30	1472	X	X						
sesquiterpene	β-chamigrene[c]	1474						X		
sesquiterpene	unknown 31	1475	X							
–	unknown 32	1475								X
sesquiterpene	α-selinene[c]	1477	X	X						
sesquiterpene	γ-muurolene	1478								X
sesquiterpene	unknown 33	1483								X
sesquiterpene	unknown 34	1486	X	X						
sesquiterpene	β-selinene	1488	X	X						
sesquiterpene	unknown 35	1489								X
sesquiterpene	valencene[b]	1494	X	X						
sesquiterpene	unknown 36	1498	X	X						
sesquiterpene	**α-muurolene (8)**	1500								X
sesquiterpene	β-himachalene	1502						X		
sesquiterpene	β-bisabolene	1508						X		X
–	unknown 37	1525						X		
sesquiterpene	unknown 38[d]	1525								X
sesquiterpene	unknown 39	1533						X		
sesquiterpene	unknown 40	1544						X		
oxygenated ST	unknown 41	1549								X
–	unknown 42	1553							X	
sesquiterpene	unknown 43	1564								X
–	unknown 44	1584								X
oxygenated ST	unknown 45	1609	X	X						
–	unknown 46	1629								X
–	unknown 47	1650								X
–	unknown 48	1656								X
–	unknown 49	1702								X

[a]Volatiles were verified with authentic standards, or identified by comparing their mass spectra with reference spectra from databases (Wiley, NIST). Kovats' retention indices (RI) were calculated and compared to databases. Volatile organic compounds collected as background from fungal-free PDA plates were removed from the final dataset. Volatiles released from both the endophytic fungi and black poplar, as listed in previous reports [57,58], are depicted in bold. [b]Verified with authentic standards, otherwise verified with calculated Kovat's indices compared with Pubchem [60] or [c]NIST [61] library. [d]Kovat's indices and mass spectra suggest strongly resemblance to β-or γ-cadinene.

assembly as template revealed two genes with high similarity to other fungal *TPS* genes. The genes were designated *CxTPS1* and *CxTPS2*. For functional characterization, the complete open reading frames of *CxTPS1* and *CxTPS2* were amplified from cDNA, cloned, and heterologously expressed in *Escherichia coli*. To determine mono-, sesqui-, and diterpene-forming activity, the bacterial raw protein extracts were assayed with the substrates GPP, FPP, and GGPP, each in the presence of the co-substrate magnesium chloride.

Both protein extracts containing the respective enzymes accepted the substrate GPP and produced monoterpenes (Figure 2). CxTPS1 produced myrcene (**9**) and (*E*)-β-ocimene (**10**) in similar amounts. CxTPS2 produced (*E*)-β-ocimene (**10**) as the major product and minor amounts of myrcene (**9**), (*Z*)-β-ocimene (**11**), and linalool (**5**) (Figure 2). Only one sesquiterpene product was formed by each TPS: CxTPS1 produced (*E*,*E*)-α-farnesene (**12**) and CxTPS2 produced (*E*)-β-caryophyllene (**1**). With GGPP, no enzyme activity was recorded for

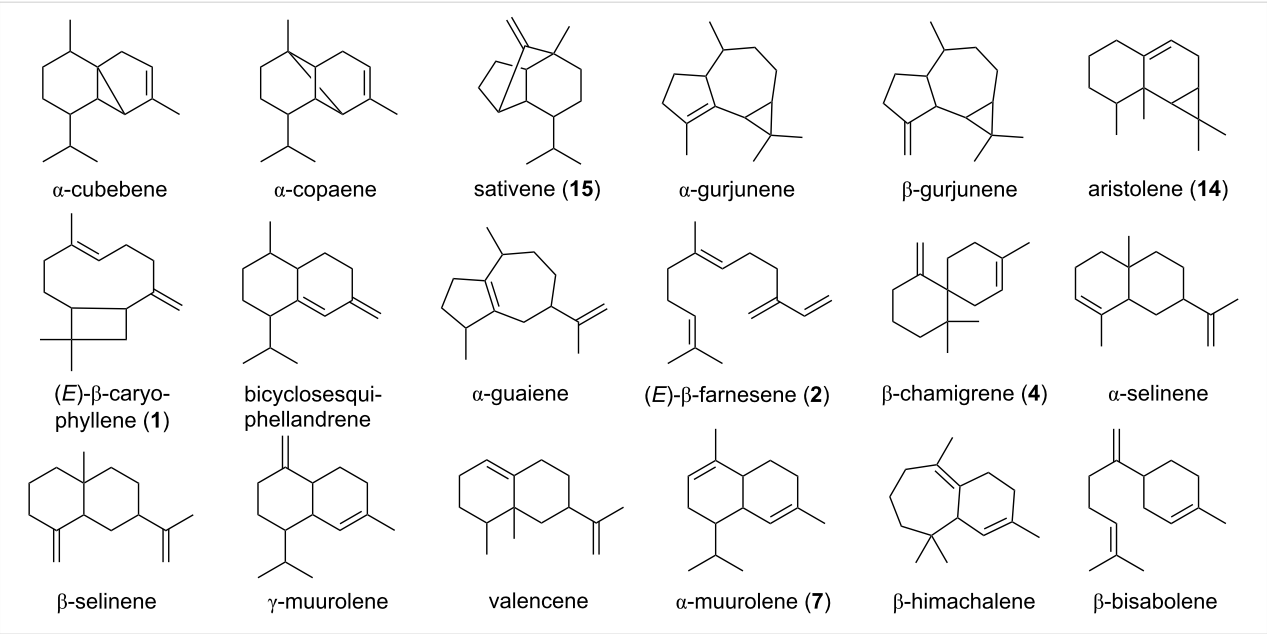

Figure 1: Chemical structures of sesquiterpenes emitted from endophytic fungi (Table 2) isolated from black poplar leaves.

CxTPS2, while CxTPS1 converted this substrate to (*E,E*)-β-springene (**13**) as the minor compound and major amounts of (*E,E,E*)-α-springene (**14**) (Figure 2).

Two terpene synthases from *Cladosporium* sp. are not closely related to each other

To investigate the phylogenetic relationships of CxTPS1 and CxTPS2 from *Cladosporium* sp. to other known terpene synthases from plant-associated Ascomycota that exhibit a pathogenic, endophytic or saprophytic lifestyle, we performed multiple sequence alignments and a subsequent dendrogram analysis.

According to the tree shown in Figure 3, CxTPS2 and CxTPS1 are not closely related to each other. While CxTPS2 forms a clade with sesquiterpene synthases of four pathogenic fungi and one endophyte, CxTPS1 is loosely related to a gene of the pathogenic fungus *Botrytis cinerea*. Further, CxTPS2, which produces (*E*)-β-caryophyllene (**1**), is more closely related to other sesquiterpene synthases from pathogens than to the caryophyllene synthases from the two endophytes *Hypoxylon* sp. CI4A and *Hypoxylon* sp. CO27.

Discussion

We were able to identify 12 different endophytic fungi from leaves of mature black poplar trees with a culture-dependent method and analyzed their volatile blends when growing on potato dextrose agar. Most of the tested fungi produced various aliphatic or aromatic alcohols, which are commonly produced by endophytic fungi and are known to act as antimicrobial agents (Table 2) [63]. Sesquiterpenes make up the largest proportion of fungus-produced terpenoids [64] and in our study we also detected several sesquiterpenes, e.g., (*E*)-β-caryophyllene (**1**), β-chamigrene (**4**), aristolene (**15**), sativene (**16**), and α-muurolene (**8**). However, monoterpenes were completely absent from the volatile bouquets of the endophytic species in our study. Weikl et al. who compared the volatiles released from *Alternaria alternata* and *Fusarium oxysporum* also did not detect any monoterpenes [41]. However, other studies on *Phomopsis* sp., *Cladosporium cladosporioides*, and *Hypoxylon anthochroum* showed that these endophytic fungi are able to produce monoterpenes like sabinene, α-pinene and 1,8-cineole, respectively [51,65,66]. In general, fungal volatile profiles are very species-specific [67], which also holds true for the species tested in our study (Table 2). However, the differences in the literature may arise from the use of different strains, volatile collection methods or variation in age, growth medium and environmental conditions, such as moisture, pH, temperature, and nutrient levels, or co-cultivation [27,41,67,68]. In our study, we measured the volatile profiles of endophytes cultivated on PDA medium at 28 °C in the dark. These profiles may differ from those released by endophytes growing under natural conditions in poplar leaves, in the possible presence of competing microbes.

While our knowledge about the volatile profiles of endophytic fungi has increased in recent years, only little is known about endophyte terpene synthases that may catalyze volatile terpene formation [44,45]. For the endophytic fungus *Cladosporium* sp., we identified and characterized two TPS, CxTPS1 and CxTPS2

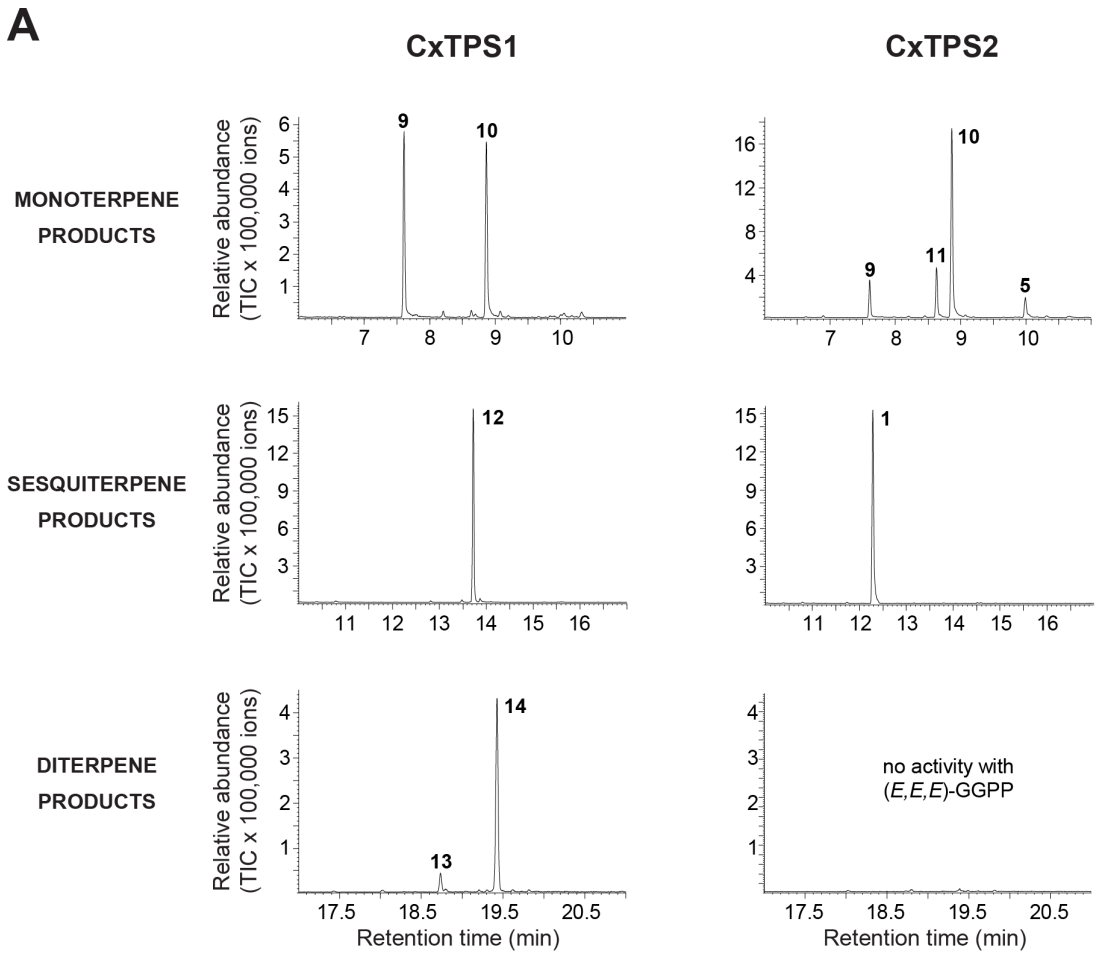

Figure 2: Terpene synthase activity of CxTPS1 and CxTPS2. A) Genes were heterologously expressed in *Escherichia coli* and partially purified proteins were assayed with GPP, (*E*,*E*)-FPP, or (*E*,*E*,*E*)-GGPP as substrates in the presence of 10 mM $MgCl_2$. Enzyme products were extracted from the assays with hexane and analyzed using gas chromatography–mass spectrometry. Myrcene (**9**); (*E*)-β-ocimene (**10**); (*Z*)-β-ocimene (**11**); linalool (**5**); (*E*,*E*)-α-farnesene (**12**); (*E*)-β-caryophyllene (**1**); (*E*,*E*)-β-springene (**13**); (*E*,*E*,*E*)-α-springene (**14**). B) Structures of the enzyme products of CxTPS1 and CxTPS2, including (*E*)-β-caryophyllene (**1**) which was the only terpene detected from *Cladosporium* sp. cultures.

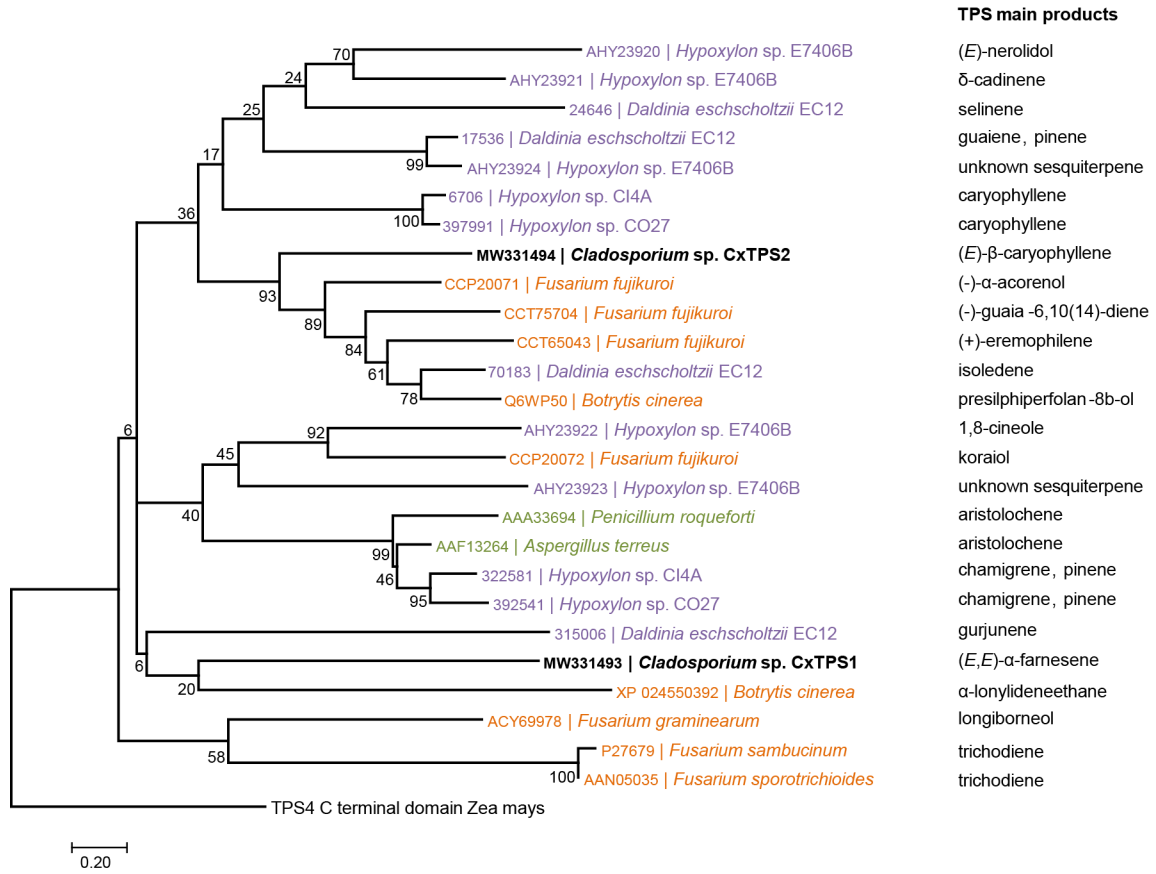

Figure 3: Dendrogram analysis (rooted tree) of CxTPS1 and CxTPS2 (bold) from *Cladosporium* sp. and characterized TPS proteins and their main products from other plant-associated Ascomycota. The tree was inferred using the Maximum Likelihood method based on the Poisson correction model and n = 1000 replicates for bootstrapping. Bootstrap values are shown next to each node. The tree is drawn to scale, with branch lengths measured in the number of amino acid substitutions per site. The alpha-domain of maize TPS4 [62] was chosen as an outgroup. TPS proteins from different Ascomycota are highlighted according to their different lifestyle: endophytic (purple), pathogenic (orange) and saprophytic (green).

(Figure 2). CxTPS1 was a multifunctional enzyme in vitro and produced the monoterpenes myrcene (**9**) and (*E*)-β-ocimene (**10**) from GPP, the sesquiterpene (*E*,*E*)-α-farnesene (**12**) from FPP, and the diterpenes (*E*,*E*)-β-springene (**13**) and (*E*,*E*,*E*)-α-springene (**14**) from GGPP. CxTPS2, in contrast, showed a narrower substrate specificity and converted GPP to myrcene (**9**), (*E*)-β-ocimene (**10**), (*Z*)-β-ocimene (**11**), and linalool (**5**) and FPP to (*E*)-β-caryophyllene (**1**). In a previous work on fungal terpene synthases, Hohn and Vanmiddlesworth found a narrow substrate specificity for the trichodiene synthase from *Fusarium sporotrichioides*, where only the sesquiterpene trichodiene was detected with FPP, while other substrates were not accepted [69]. In contrast, bi-functionality was also observed for the pinene and guaiene synthase from *Daldinia eschscholzii* EC12 and the pinene and guaiene synthase from *Hypoxylon* sp. EC28 (Figure 3) [45]. The multifunctionality of CxTPS1 and CxTPS2 was only observed when the fungal TPS was expressed heterologously in *E. coli* and assayed in vitro whereas the fungus itself only emitted (*E*)-β-caryophyllene (**1**) when growing on agar medium. Thus, we speculate that GPP, the substrate for monoterpene production, is not available in *Cladosporium* sp. In contrast, the emission of the monoterpene α-pinene has been reported for *Cladosporium cladosporioides* CL-1 [66]. Interestingly, we could not detect the emission of (*E*,*E*)-α-farnesene (**12**), a product of the in vitro assay of CxTPS1 in our fungal cultures, although the fungus must have the ability to produce the substrate FPP in sufficient quantity as it also produces the sesquiterpene (*E*)-β-caryophyllene (**1**). It might be that *CxTPS1* is not expressed in the fungus under our culture conditions or that (*E*,*E*)-α-farnesene (12) is further metabolized. To our knowledge, (*E*,*E*)-α-farnesene (**12**) has never been detected so far from any Cladosporium species.

To test whether there is a relationship between fungal lifestyle and their terpene synthases, we compared sequences of the terpene synthases CxTPS1 and CxTPS2 from *Cladosporium* sp.

with the sequences of other known terpene synthases from plant-associated Ascomycota exhibiting a pathogenic, endophytic or saprophytic lifestyle. One clade was indeed evident that contained only terpene synthases from endophytes. However, a close relationship between fungal lifestyle and their terpene synthase sequences is not observable, since different terpene synthases from the same fungal species clustered together with terpene synthases from pathogens and/or endophytes (Figure 3). CxTPS2 forms a clade with sesquiterpene synthases from four pathogenic fungi and one endophyte, while CxTPS1 is loosely related to sequences of the pathogen *Botrytis cinerea* (Figure 3). We speculate that TPS from fungi that share the same lifestyle are not clustered together because some endophytes switch from being asymptomatic leaf inhabiting fungi to becoming either latent pathogens or saprophytes [21,24,70-73]. Furthermore, it is hypothesized that endophytes may have evolved directly from pathogens, since both must defeat plant protective barriers [38,74]. Nevertheless, the bootstrap values in the dendrogram are generally too low to make a clear statement about the relationship between terpene synthases and fungal lifestyle, and more work on this question is needed [63,75].

The volatiles found to be emitted from black poplar endophytic fungi in this study could have important biological activities. For instance, ethanol (**17**) and 2-phenylethanol (**3**) are known to have antifungal and phytotoxic activity and so could help the endophyte to defend its niche within the plant against other endophytic competitors [63]. The other endophyte VOCs could promote plant growth (e.g., 2-methyl-1-propanol (**7**) [76], (*E*)-β-caryophyllene (**1**) [77], and sativene (**16**) [66]), induce plant immunity (e.g., (*E*)-β-caryophyllene (**1**) [77]), and increase photosynthetic capacity (e.g., 2-methyl-1-propanol (**7**) [78]) (Table 2) [63]. Some of the analyzed compounds are also known to play a crucial role in plant–insect interactions, where they are involved in direct and indirect plant defenses or in attracting herbivorous insects. For example, (*E*)-β-caryophyllene (**1**) emitted by *Cladosporium* sp. (Table 2) is known to act as a signal cue for the planthopper *Sogatella furcifera* [15], while this compound also attracts nematodes that feed on attacking insect herbivores [79]. Nearly all of the endophytic fungi isolated in this study were able to produce at least some volatiles known from the literature to mediate plant–insect interactions.

Of the 13 endophytes studied, 11 of them release volatiles previously reported from black poplar foliage (Table 2) [57-59]. These compounds include the alcohols 3-methyl-1-butanol (**6**) and 2-phenylethanol (**3**) and the sesquiterpenes (*E*)-β-caryophyllene (**1**), and α-muurolene (**8**) (Table 2). This raises the question of whether endophytic fungi contribute to the overall plant volatile bouquet by producing the above-mentioned volatiles. If so, this would directly affect our interpretation of certain plant-fungus and plant–insect interactions [34,37,38]. Recently, it has been shown that the pathogenic rust fungus (*Melampsora larici-populina*) alters the volatile blend of black poplar trees by contributing 1-octen-3-ol and 3-octanone, which attract caterpillars of the generalist herbivore *Lymantria dispar* [57]. Jallow et al. showed that an endophytic fungus (*Acremonium strictum*) alters the volatile composition of the tomato plant *Solanum lycopersicum* and attracts *Helicoverpa armigera* moth for oviposition [80]. The endophytic fungus *Beauveria bassiana* also increased the emission of some terpenes from tomato plants resulting in a stronger defense response against the beet armyworm (*Spodoptera exigua*) [81]. In these cases, it is not known whether the increased terpene emission results from biosynthesis by the plant or the fungus. Future work should include measurements of plant and fungal TPS expression to determine the origin of these compounds. For this, identification of TPS genes in both plants and their fungal partners is crucial.

Conclusion

We showed that endophytic fungi isolated from mature black poplar trees emitted species-specific volatile blends. Almost all the endophytes here produced short-chain aliphatic alcohols that are known to have antifungal and phytotoxic effects and may be produced to compete with other microbial species. Several also produce diverse mixtures of sesquiterpenes. Interestingly, several VOCs emitted from the endophytes were earlier reported to be emitted by black poplar. We characterized two terpene synthases from one of the endophytic fungi to lay the groundwork for comparing the biosynthesis of plant vs fungal volatiles. More knowledge about the formation of these compounds could contribute to the greater understanding of their roles in plant–insect, plant–plant and plant–microbe interactions.

Experimental

Endophyte isolation from plant material

Endophytes were isolated from leaves of mature black poplar (*Populus nigra*) trees growing in a natural population in a floodplain forest in northeastern Germany (52°34’1’’N, 14°38’3’’E). The trees were around 25 m in height and approximately 70 years old. Five branches in the lower canopy (1–7 m) from each of the 10 tree genotypes were collected and from each branch, five leaves were randomly harvested. Those leaves did not show any symptoms of pathogen infection. A culture-dependent method was used to isolate endophytic fungi growing within the leaf blades. Under a clean bench, the leaves were surface sterilized (0.5% NaOCl for 2 min, followed by 70% of EtOH for 2 min) and rinsed three times by immersion in sterile distilled water. Then, four pieces (approximately 7 × 7 mm) of

one leaf blade were placed equidistantly on potato dextrose agar (PDA; Sigma-Aldrich). Water from the last washing step was coated on PDA medium to test whether the surface of the leaves had been adequately sterilized. Petri dishes were sealed with Parafilm and incubated in the dark at 25 °C. Plates were inspected daily and morphologically distinct colonies were brought into pure culture on PDA medium using the same culturing conditions as above. Fresh mycelium was harvested from pure cultures for molecular identification of the morpho-species.

Molecular identification of endophytic fungi

DNA was extracted from fresh mycelium (approximately 5 cm in diameter) growing on PDA. The mycelium was flash frozen in liquid nitrogen and ground using plastic pestles in 1.5 mL Eppendorf tubes. After homogenization of the mycelium, 500 µL extraction buffer (100 mM Tris HCl, pH 8; 10 mM EDTA, pH 8; 2% w/v SDS) and 100 µL proteinase K (Sigma) were added and the mixture was incubated for 1 h at 60 °C. For separation of polysaccharides, 180 µL 5 M NaCl and 80 µL 10% CTAB were added and the mixture incubated further for 10 min at 65 °C.

To extract nucleic acids by phase separation, 860 µL chloroform/isoamyl alcohol (24:1) was added and incubated on ice for 30 min. The samples were centrifuged for 10 min (15,000 rpm), and the upper, aqueous phase was then transferred to a new tube and DNA was precipitated in 395 µL of 100% isopropanol (−20 °C). After centrifugation (4 °C, 20 min, 15,000 rpm) the pellet was washed with 750 µL 70% ethanol, centrifuged at 15,000 rpm (10 min), dried, and finally dissolved in 50 µL Milli-Q water (pH 6). DNA concentration and purity were determined with a NanoDrop 2000c spectrophotometer (Peqlab Biotechnology AG, Erlangen, Germany).

The primer pair ITS1F and ITS4 (Supporting Information File 1, Table S2) was used to amplify the highly conserved internal transcribed spacer region of the fungal rRNA cistron [82,83]. The reaction mix for DNA amplification (50 µL/tube) contained 2.5 µL of each primer (Sigma), 0.5 µL GoTaqX® Polymerase (Promega, Madison, WI, USA), 10 µL of GoTaqX® Reaction Buffer (Promega) and 1 µL 10 mM dNTPs (Thermo Fisher Scientific). The template volume was adjusted to a final DNA concentration of approximately 500 ng/mL. Ultrapure water (Milli-Q® Synthesis A10) was added up to a final volume of 50 µL. PCR was performed in a gradient thermal cycler (Whatman Biometra 96T) using the following program: initiation and activation of polymerase (95 °C/5 min); followed by 35 cycles of denaturation (95 °C/30 s), annealing (65 °C/30 s) and elongation (72 °C/90 s) and a single, final elongation step (72 °C/10 min).

For gel electrophoresis, 4 µL PCR product was mixed with one drop loading dye (0.3 mL 30% glycerol and 2.5 mg bromphenol blue/mL) and applied to an 1% agarose gel (1 g agarose/100 mL 0.5% TBE; 5 µL Midori Green). A 1 kb DNA ladder (Gene Ruler, Thermo Fisher Scientific) was applied to determine the fragment size of the products. Electrophoresis was performed in 0.5% TBE buffer (Thermo Fisher Scientific) for 30 min at 135 V (150 mA). The PCR products were purified with a QIAquick PCR purification kit (Qiagen, Hilden, Germany) following the manufacturer's instructions. Purified PCR products were sequenced using the Sanger method on a ABI Prism® Gen-Analysator 3130xl (Applied Biosystems, Weiterstadt, Germany). The obtained sequences were aligned using Geneious 6.0.5 [84] and compared to the NCBI sequence database [85] (Supporting Information File 1, Table S1). In case of isolates with multiple 99–100 % identity hits on several species within the same genus, we identified these only to the genus level, but still list the single best hit and its accession number (Table 1, Supporting Information File 1, Table S1).

Static headspace volatile collection from cultures and analysis

VOCs were collected from endophytes that had grown on PDA medium (25 mL) in an incubator (dark/28 °C) until the mycelium reached a diameter of 5 cm (± 0.5 cm). For each fungal species, seven replicates were used with fungus-free petri dishes with PDA medium used as blanks. Volatiles were trapped for 1 h by using four polydimethylsiloxane (PDMS) tubes. To prevent PDMS tubes from touching the mycelium, the tubes were placed with watchmaker forceps on loops of stainless steel wire that were kept at a distance of approximately 5 mm from the mycelium. PDMS tubes were prepared following the method described in Kallenbach et al. [86]. The experiment was performed under a clean bench at room temperature. After volatile collection PDMS tubes were immediately removed from the wire and stored in glass vials at −20 °C until further analysis.

Volatiles trapped on PDMS tubes were analyzed by GC–MS (GCMS-QP2010 Ultra, Shimadzu, Duisburg, Germany) coupled to a thermal desorption unit (TD-20, Shimadzu, Duisburg, Germany). A single PDMS tube from each replicate was placed in a glass tube (Supelco; Sigma-Aldrich). Desorption was achieved by a He flow (60 mL min^{-1}) at 200 °C for 8 min in the glass tube and the analytes were trapped on a Tenax® (Buchem BV, Apeldoorn, Netherlands) adsorbent trap at −17 °C. The trap was then heated to 230 °C, and the analytes injected onto the GC column (Rtx®-5MScolumn with 30 m × 0.25 mm × 0.25 µm (Restek GmbH, Bad Homburg, Germany)). The gas chromatograph was operated at a column flow rate of 1.5 mL/min (He), split injection (split ratio: 5). The oven was

set to 45 °C, held for 3 min, increased to 250 °C with a gradient of 6 °C/min and subsequently increased to 300 °C at 100 °C/ min with a 3 min hold. Electron impact (EI) mass spectra were recorded at 70 eV in scan mode from 43 to 350 *m*/*z* at a scan speed of 1111 Da/s (interface temperature, 250 °C; source temperature, 230 °C). Fungal volatiles were identified by comparing their mass spectra with those of authentic standards or reference spectra from databases (Wiley, Version 8, National Institute of Standards and Technology (NIST, Version 11)) using GCMS SOLUTION v.4.20 (Shimadzu). In addition, non-isothermal Kovats retention indices were calculated, based on chromatographic retention times of a saturated alkane mixture (C_7–$C_{40;}$ Sigma-Aldrich, Taufkirchen, Germany) [87]. The calculated Kovats retention indices were compared with indices published in Pubchem [60] or NIST [61] from the same or a similar type of GC column. Differences between calculated retention index and literature data were within ±5 points. Identified volatiles with a similarity hit above 90% and that were present in five out of seven replicates were included in this study, whereas VOCs which were also collected by blanks were removed from the final dataset. A representative total ion chromatogram for each fungus is shown in Supporting Information File 1, Figure S1. Mass spectra of unknown compounds are shown in Supporting Information File 1, Figure S2.

Fungal RNA extraction, reverse transcription, and sequencing

Total RNA was isolated from fresh mycelium (approximately 5 cm in diameter) growing on PDA using the RNeasy® Plant Mini Kit (Qiagen) according to the manufacturer's instructions. The RNA concentration was assessed using a spectrophotometer (NanoDrop 2000c, Thermo Fisher Scientific). RNA was treated with DNase I (Thermo Fisher Scientific) prior to cDNA synthesis. Single-stranded cDNA was prepared from 1 µg of DNase-treated RNA using SuperScriptTM III reverse transcriptase and oligo (dT12-18) primers (Invitrogen, Carlsbad, CA, USA).

For transcriptome sequencing, total RNA was extracted from fungal material as described above, a TruSeq RNA-compatible library was prepared, and PolyA enrichment was performed before sequencing on an IlluminaHiSeq 3000 sequencer (Max Planck Genome Centre, Cologne, Germany) with 25 Mio reads, 150 base pairs, paired end. Trimming of the obtained Illumina reads and de novo assembly were both performed with the program CLC Genomics Workbench (Qiagen Bioinformatics) using default parameters or parameters specified as follows: bubble size, 100; automatic word size; minimum contig length, 600. A BUSCO analysis (Supporting Information File 1, Figure S3) was performed to validate the completeness of the transcriptome.

Identification and heterologous expression of terpene synthase genes

To identify putative terpene synthases, a TBLASTN analysis with *Aspergillus terreus* aristolochene synthase (pdb 20A6) as query and the de novo transcriptome of *Cladosporium* sp. as a template was performed using the software BioEdit 7.0.9.0 [88]. Two terpene synthase-like sequences were found and designated as *CxTPS1* and *CxTPS2,* respectively. The complete open reading frames of *CxTPS1* and *CxTPS2* were amplified from cDNA using the primers shown in Supporting Information File 1 (Table S2) and cloned into pET100/D-TOPO vector (Thermo Fisher Scientific). The *E. coli* strain BL21 Star™ (DE3) (Thermo Fisher Scientific) was used for heterologous expression. The culture was grown at 37 °C, induced at an OD_{600} = 0.6 with 1 mM IPTG, and subsequently placed at 18 °C and grown for another 20 hours. The cells were collected by centrifugation and disrupted by a 4 × 20 s treatment with a sonicator (Bandelin UW2070, Berlin, Germany) in chilled extraction buffer (10 mM Tris-HCl, pH 7.5, 1 mM dithiothreitol, 10% (v/v) glycerol). Cell fragments were removed by centrifugation at 14,000*g* and the supernatant was further processed via an Illustra NAP-5 gravity flow desalting column (GE Healthcare, Chicago, IL, USA) and eluted in extraction buffer.

Enzyme assays were performed in a Teflon-sealed, screw-capped 1 mL GC glass vial containing 50 µL of the heterologously expressed protein and 50 µL assay buffer containing 50 µM substrate (GPP, (*E,E*)-FPP, or (*E,E,E*)-GGPP) and 20 mM $MgCl_2$. Assays were overlaid with 100 µL hexane and incubated for 60 minutes at 30 °C. One microliter of the hexane phase was injected into the GC–MS machine and the analysis was conducted using an Agilent 6890 Series gas chromatograph coupled to an Agilent 5973 quadrupole mass selective detector (interface temp, 270 °C; quadrupole temp, 150 °C; source temp, 230 °C; electron energy, 70 eV). Chromatographic separation was achieved with an initial oven temperature of 45 °C held for 2 min, which was then increased to 180 °C with a gradient of 6 °C min^{-1}, and then further increased to 300 °C with a gradient of 60 °C min^{-1} and a hold of 2 min. Compounds were identified by comparing their retention times and mass spectra to those of authentic standards, or by reference spectra in the Wiley and NIST libraries.

Sequence analysis and phylogenetic tree construction

For the estimation of a phylogenetic tree, we used the MUSCLE algorithm (gap open, −2.9; gap extend, 0; hydrophobicity multiplier, 1.2; max. iterations, 8; clustering method, upgmb) implemented in MEGA7 [89] to compute an amino acid alignment. Based on the MUSCLE alignment, the tree was constructed with MEGA7 using a Maximum Likelihood

algorithm (Poisson model). All positions with less than 80% site coverage were eliminated. A bootstrap resampling analysis with 1000 replicates was performed to evaluate the tree topology. For the phylogenetic tree, we included identified and characterized terpene synthases from plant-associated Ascomycota.

Accession numbers

Sequence data for *CxTPS1* (MW331493) and *CxTPS2* (MW331494) can be found in the NCBI GenBank [85] under the corresponding identifiers. Raw reads of the RNAseq experiment were deposited in the NCBI Sequence Read Archive under the BioProject accession PRJNA682522.

Supporting Information

Supporting Information File 1

Sequences of isolated endophytic fungi and identification according to NCBI database, primer used in this study, representative total ion chromatograms of single endophytic volatile blend, mass spectra of unknown volatile organic compounds, and BUSCO analysis of *Cladosporium* sp. de novo assembly.
[https://www.beilstein-journals.org/bjoc/content/supplementary/1860-5397-17-118-S1.pdf]

Acknowledgements

We thank Dineshkumar Kandasamy for methodological advice and Rayko Halitschke for support during TDU-GCMS analysis. A version of the symbolic tree in the graphical abstract was previously published in *Oecologia* **2018,** *187,* 377–388 by J. S. Lämke and S. B. Unsicker (© The Authors 2018, distributed under the terms of the Creative Commons Attribution 4.0 International License, https://creativecommons.org/licenses/by/4.0).

Funding

This study was funded by the Max Planck Society.

ORCID® iDs

Peter H. W. Biedermann - https://orcid.org/0000-0003-4234-5659
Jonathan Gershenzon - https://orcid.org/0000-0002-1812-1551
Tobias G. Köllner - https://orcid.org/0000-0002-7037-904X
Sybille B. Unsicker - https://orcid.org/0000-0002-9738-0075

References

1. Pare, P. W.; Tumlinson, J. H. *Plant Physiol.* **1999,** *121,* 325–332. doi:10.1104/pp.121.2.325
2. Unsicker, S. B.; Kunert, G.; Gershenzon, J. *Curr. Opin. Plant Biol.* **2009,** *12,* 479–485. doi:10.1016/j.pbi.2009.04.001
3. Baldwin, I. T. *Curr. Biol.* **2010,** *20,* R392–R397. doi:10.1016/j.cub.2010.02.052
4. McCormick, A. C.; Reinecke, A.; Gershenzon, J.; Unsicker, S. B. *J. Chem. Ecol.* **2016,** *42,* 382–393. doi:10.1007/s10886-016-0698-7
5. Arimura, G.-i.; Matsui, K.; Takabayashi, J. *Plant Cell Physiol.* **2009,** *50,* 911–923. doi:10.1093/pcp/pcp030
6. Maffei, M. E.; Gertsch, J.; Appendino, G. *Nat. Prod. Rep.* **2011,** *28,* 1359–1380. doi:10.1039/c1np00021g
7. Irmisch, S.; Jiang, Y.; Chen, F.; Gershenzon, J.; Köllner, T. G. *BMC Plant Biol.* **2014,** *14,* 270. doi:10.1186/s12870-014-0270-y
8. Schnitzler, J.-P.; Louis, S.; Behnke, K.; Loivamäki, M. *Plant Biol.* **2010,** *12,* 302–316. doi:10.1111/j.1438-8677.2009.00284.x
9. Danner, H.; Boeckler, G. A.; Irmisch, S.; Yuan, J. S.; Chen, F.; Gershenzon, J.; Unsicker, S. B.; Köllner, T. G. *Phytochemistry* **2011,** *72,* 897–908. doi:10.1016/j.phytochem.2011.03.014
10. Laothawornkitkul, J.; Taylor, J. E.; Paul, N. D.; Hewitt, C. N. *New Phytol.* **2009,** *183,* 27–51. doi:10.1111/j.1469-8137.2009.02859.x
11. Holopainen, J. K.; Gershenzon, J. *Trends Plant Sci.* **2010,** *15,* 176–184. doi:10.1016/j.tplants.2010.01.006
12. Mäntylä, E.; Alessio, G. A.; Blande, J. D.; Heijari, J.; Holopainen, J. K.; Laaksonen, T.; Piirtola, P.; Klemola, T. *PLoS One* **2008,** *3,* e2832. doi:10.1371/journal.pone.0002832
13. Kessler, A.; Baldwin, I. T. *Science* **2001,** *291,* 2141–2144. doi:10.1126/science.291.5511.2141
14. Köllner, T. G.; Held, M.; Lenk, C.; Hiltpold, I.; Turlings, T. C. J.; Gershenzon, J.; Degenhardt, J. *Plant Cell* **2008,** *20,* 482–494. doi:10.1105/tpc.107.051672
15. Wang, Q.; Xin, Z.; Li, J.; Hu, L.; Lou, Y.; Lu, J. *Physiol. Mol. Plant Pathol.* **2015,** *91,* 106–112. doi:10.1016/j.pmpp.2015.07.002
16. Beale, M. H.; Birkett, M. A.; Bruce, T. J. A.; Chamberlain, K.; Field, L. M.; Huttly, A. K.; Martin, J. L.; Parker, R.; Phillips, A. L.; Pickett, J. A.; Prosser, I. M.; Shewry, P. R.; Smart, L. E.; Wadhams, L. J.; Woodcock, C. M.; Zhang, Y. *Proc. Natl. Acad. Sci. U. S. A.* **2006,** *103,* 10509–10513. doi:10.1073/pnas.0603998103
17. Roy, B. A.; Raguso, R. A. *Oecologia* **1997,** *109,* 414–426. doi:10.1007/s004420050101
18. Galen, C.; Kaczorowski, R.; Todd, S. L.; Geib, J.; Raguso, R. A. *Am. Nat.* **2011,** *177,* 258–272. doi:10.1086/657993
19. Günther, J.; Lackus, N. D.; Schmidt, A.; Huber, M.; Stödtler, H.-J.; Reichelt, M.; Gershenzon, J.; Köllner, T. G. *Plant Physiol.* **2019,** *180,* 767–782. doi:10.1104/pp.19.00059
20. Petrini, O. Fungal Endophytes of Tree Leaves. *Microbial Ecology of Leaves;* Brock/Springer Series in Contemporary Bioscience; Springer New York: New York, NY, U.S.A., 1991; pp 179–197. doi:10.1007/978-1-4612-3168-4_9
21. Hyde, K. D.; Soytong, K. *Fungal Diversity* **2008,** *33,* 163–173.
22. Meister, B.; Krauss, J.; Härri, S. A.; Schneider, M. V.; Müller, C. B. *Basic Appl. Ecol.* **2006,** *7,* 244–252. doi:10.1016/j.baae.2005.06.002
23. Rodriguez, R. J.; White, J. F., Jr.; Arnold, A. E.; Redman, R. S. *New Phytol.* **2009,** *182,* 314–330. doi:10.1111/j.1469-8137.2009.02773.x
24. Eberl, F.; Uhe, C.; Unsicker, S. B. *Fungal Ecol.* **2019,** *38,* 104–112. doi:10.1016/j.funeco.2018.04.003
25. Effmert, U.; Kalderás, J.; Warnke, R.; Piechulla, B. *J. Chem. Ecol.* **2012,** *38,* 665–703. doi:10.1007/s10886-012-0135-5
26. Lemfack, M. C.; Nickel, J.; Dunkel, M.; Preissner, R.; Piechulla, B. *Nucleic Acids Res.* **2014,** *42,* D744–D748. doi:10.1093/nar/gkt1250

27. Roy, S.; Banerjee, D. Volatile Organic Compounds from Endophytic Fungi. In *Recent Advancement in White Biotechnology Through Fungi;* Yadav, A.; Singh, S.; Mishra, S.; Gupta, A., Eds.; Springer: Cham, Switzerland, 2019; pp 149–175. doi:10.1007/978-3-030-14846-1_5
28. Ezra, D.; Strobel, G. A. *Plant Sci.* **2003,** *165,* 1229–1238. doi:10.1016/s0168-9452(03)00330-3
29. Strobel, G.; Daisy, B.; Castillo, U.; Harper, J. *J. Nat. Prod.* **2004,** *67,* 257–268. doi:10.1021/np030397v
30. Ting, A. S. Y.; Mah, S. W.; Tee, C. S. *Am. J. Agric. Biol. Sci.* **2010,** *5,* 177–182. doi:10.3844/ajabssp.2010.177.182
31. Macías-Rubalcava, M. L.; Hernández-Bautista, B. E.; Oropeza, F.; Duarte, G.; González, M. C.; Glenn, A. E.; Hanlin, R. T.; Anaya, A. L. *J. Chem. Ecol.* **2010,** *36,* 1122–1131. doi:10.1007/s10886-010-9848-5
32. Daisy, B. H.; Strobel, G. A.; Castillo, U.; Ezra, D.; Sears, J.; Weaver, D. K.; Runyon, J. B. *Microbiology (London, U. K.)* **2002,** *148,* 3737–3741. doi:10.1099/00221287-148-11-3737
33. Sudakin, D. L.; Stone, D. L.; Power, L. *Curr. Top. Toxicol.* **2011,** *7,* 13.
34. Jia, Q.; Qu, J.; Mu, H.; Sun, H.; Wu, C. *Symbiosis* **2020,** *80,* 103–132. doi:10.1007/s13199-019-00663-x
35. Wilson, D.; Carroll, G. C. *Ecology* **1997,** *78,* 2153–2163. doi:10.1890/0012-9658(1997)078[2153:aohesb]2.0.co;2
36. Wilson, D.; Faeth, S. H. *Ecology* **2001,** *82,* 1097–1111. doi:10.1890/0012-9658(2001)082[1097:dferis]2.0.co;2
37. Albrectsen, B. R.; Björkén, L.; Varad, A.; Hagner, Å.; Wedin, M.; Karlsson, J.; Jansson, S. *Fungal Diversity* **2010,** *41,* 17–28. doi:10.1007/s13225-009-0011-y
38. Albrectsen, B. R.; Siddique, A. B.; Decker, V. H. G.; Unterseher, M.; Robinson, K. M. *Oecologia* **2018,** *187,* 535–545. doi:10.1007/s00442-018-4097-3
39. Ditengou, F. A.; Müller, A.; Rosenkranz, M.; Felten, J.; Lasok, H.; van Doorn, M. M.; Legué, V.; Palme, K.; Schnitzler, J.-P.; Polle, A. *Nat. Commun.* **2015,** *6,* 6279. doi:10.1038/ncomms7279
40. Schmidt, R.; Cordovez, V.; de Boer, W.; Raaijmakers, J.; Garbeva, P. *ISME J.* **2015,** *9,* 2329–2335. doi:10.1038/ismej.2015.42
41. Weikl, F.; Ghirardo, A.; Schnitzler, J.-P.; Pritsch, K. *Sci. Rep.* **2016,** *6,* 22152. doi:10.1038/srep22152
42. Quin, M. B.; Flynn, C. M.; Schmidt-Dannert, C. *Nat. Prod. Rep.* **2014,** *31,* 1449–1473. doi:10.1039/c4np00075g
43. Degenhardt, J.; Köllner, T. G.; Gershenzon, J. *Phytochemistry* **2009,** *70,* 1621–1637. doi:10.1016/j.phytochem.2009.07.030
44. Shaw, J. J.; Berbasova, T.; Sasaki, T.; Jefferson-George, K.; Spakowicz, D. J.; Dunican, B. F.; Portero, C. E.; Narváez-Trujillo, A.; Strobel, S. A. *J. Biol. Chem.* **2015,** *290,* 8511–8526. doi:10.1074/jbc.m114.636159
45. Wu, W.; Tran, W.; Taatjes, C. A.; Alonso-Gutierrez, J.; Lee, T. S.; Gladden, J. M. *PLoS One* **2016,** *11,* e0146983. doi:10.1371/journal.pone.0146983
46. Mitchell, A. M.; Strobel, G. A.; Moore, E.; Robison, R.; Sears, J. *Microbiology (London, U. K.)* **2010,** *156,* 270–277. doi:10.1099/mic.0.032540-0
47. Wani, M. A.; Sanjana, K.; Kumar, D. M.; Lal, D. K. *J. Basic Microbiol.* **2010,** *50,* 110–114. doi:10.1002/jobm.200900295
48. Kudalkar, P.; Strobel, G.; Riyaz-Ul-Hassan, S.; Geary, B.; Sears, J. *Mycoscience* **2012,** *53,* 319–325. doi:10.1007/s10267-011-0165-9
49. Pandey, A.; Banerjee, D. *J. Adv. Microbiol.* **2014,** *1,* 330–337.
50. Sánchez-Fernández, R. E.; Diaz, D.; Duarte, G.; Lappe-Oliveras, P.; Sánchez, S.; Macías-Rubalcava, M. L. *Microb. Ecol.* **2016,** *71,* 347–364. doi:10.1007/s00248-015-0679-3
51. Ulloa-Benítez, Á.; Medina-Romero, Y. M.; Sánchez-Fernández, R. E.; Lappe-Oliveras, P.; Roque-Flores, G.; Duarte Lisci, G.; Herrera Suárez, T.; Macías-Rubalcava, M. L. *J. Appl. Microbiol.* **2016,** *121,* 380–400. doi:10.1111/jam.13174
52. Strobel, G.; Ericksen, A.; Sears, J.; Xie, J.; Geary, B.; Blatt, B. *Microb. Ecol.* **2017,** *74,* 312–321. doi:10.1007/s00248-017-0947-5
53. Takabayashi, J.; Dicke, M.; Posthumus, M. A. *J. Chem. Ecol.* **1994,** *20,* 1329–1354. doi:10.1007/bf02059811
54. Kessler, A.; Halitschke, R.; Diezel, C.; Baldwin, I. T. *Oecologia* **2006,** *148,* 280–292. doi:10.1007/s00442-006-0365-8
55. Knudsen, J. T.; Eriksson, R.; Gershenzon, J.; Ståhl, B. *Bot. Rev.* **2006,** *72,* 1–120. doi:10.1663/0006-8101(2006)72[1:dadofs]2.0.co;2
56. Morawo, T.; Fadamiro, H. *J. Chem. Ecol.* **2014,** *40,* 1176–1185. doi:10.1007/s10886-014-0525-y
57. Eberl, F.; Hammerbacher, A.; Gershenzon, J.; Unsicker, S. B. *New Phytol.* **2018,** *220,* 760–772. doi:10.1111/nph.14565
58. McCormick, A. C.; Irmisch, S.; Boeckler, G. A.; Gershenzon, J.; Köllner, T. G.; Unsicker, S. B. *Sci. Rep.* **2019,** *9,* 7714. doi:10.1038/s41598-019-43931-y
59. Fabisch, T.; Gershenzon, J.; Unsicker, S. B. *J. Chem. Ecol.* **2019,** *45,* 162–177. doi:10.1007/s10886-019-01050-y
60. Kim, S.; Chen, J.; Cheng, T.; Gindulyte, A.; He, J.; He, S.; Li, Q.; Shoemaker, B. A.; Thiessen, P. A.; Yu, B.; Zaslavsky, L.; Zhang, J.; Bolton, E. E. *Nucleic Acids Res.* **2021,** *49,* D1388–D1395. doi:10.1093/nar/gkaa971
61. NIST Mass Spectrometry Data Center, W. E. W., director, Retention Indices. In *NIST Chemistry WebBook, NIST Standard Reference Database Number 69*, Linstrom, P. J.; Mallard, W. G., Eds. National Institute of Standards and Technology: Gaithersburg MD, 20899, retrieved May 12, 2021.
62. Köllner, T. G.; Schnee, C.; Gershenzon, J.; Degenhardt, J. *Plant Cell* **2004,** *16,* 1115–1131. doi:10.1105/tpc.019877
63. Farh, M. E.-A.; Jeon, J. *Plant Pathol. J. (Suwon, Repub. Korea)* **2020,** *36,* 193–203. doi:10.5423/ppj.rw.02.2020.0025
64. Souza, J. J. d.; Vieira, I. J. C.; Rodrigues-Filho, E.; Braz-Filho, R. *Molecules* **2011,** *16,* 10604–10618. doi:10.3390/molecules161210604
65. Singh, S. K.; Strobel, G. A.; Knighton, B.; Geary, B.; Sears, J.; Ezra, D. *Microb. Ecol.* **2011,** *61,* 729–739. doi:10.1007/s00248-011-9818-7
66. Paul, D.; Park, K. S. *Sensors* **2013,** *13,* 13969–13977. doi:10.3390/s131013969
67. Hung, R.; Lee, S.; Bennett, J. W. *Appl. Microbiol. Biotechnol.* **2015,** *99,* 3395–3405. doi:10.1007/s00253-015-6494-4
68. Polizzi, V.; Adams, A.; De Saeger, S.; Van Peteghem, C.; Moretti, A.; De Kimpe, N. *Sci. Total Environ.* **2012,** *414,* 277–286. doi:10.1016/j.scitotenv.2011.10.035
69. Hohn, T. M.; Vanmiddlesworth, F. *Arch. Biochem. Biophys.* **1986,** *251,* 756–761. doi:10.1016/0003-9861(86)90386-3
70. Sieber, T. N. *Fungal Biol. Rev.* **2007,** *21,* 75–89. doi:10.1016/j.fbr.2007.05.004
71. Promputtha, I.; Lumyong, S.; Dhanasekaran, V.; McKenzie, E. H. C.; Hyde, K. D.; Jeewon, R. *Microb. Ecol.* **2007,** *53,* 579–590. doi:10.1007/s00248-006-9117-x
72. Promputtha, I.; Hyde, K. D.; McKenzie, E. H. C.; Peberdy, J. F.; Lumyong, S. *Fungal Diversity* **2010,** *41,* 89–99. doi:10.1007/s13225-010-0024-6
73. Rashmi, M.; Kushveer, J. S.; Sarma, V. V. *Mycosphere* **2019,** *10,* 798–1079. doi:10.5943/mycosphere/10/1/19
74. Vega, F. E.; Dowd, P. F. The role of yeasts as insect endosymbionts. *Insect-Fungal Associations: Ecology and Evolution;* Oxford University Press: New York, NY, USA, 2005; pp 211–243.

75. Müller, A.; Faubert, P.; Hagen, M.; zu Castell, W.; Polle, A.; Schnitzler, J.-P.; Rosenkranz, M. *Fungal Genet. Biol.* **2013,** *54,* 25–33. doi:10.1016/j.fgb.2013.02.005
76. Naznin, H. A.; Kiyohara, D.; Kimura, M.; Miyazawa, M.; Shimizu, M.; Hyakumachi, M. *PLoS One* **2014,** *9,* e86882. doi:10.1371/journal.pone.0086882
77. Yamagiwa, Y.; Inagaki, Y.; Ichinose, Y.; Toyoda, K.; Hyakumachi, M.; Shiraishi, T. *J. Gen. Plant Pathol.* **2011,** *77,* 336–341. doi:10.1007/s10327-011-0340-z
78. Ameztoy, K.; Baslam, M.; Sánchez-López, Á. M.; Muñoz, F. J.; Bahaji, A.; Almagro, G.; García-Gómez, P.; Baroja-Fernández, E.; De Diego, N.; Humplík, J. F.; Ugena, L.; Spíchal, L.; Doležal, K.; Kaneko, K.; Mitsui, T.; Cejudo, F. J.; Pozueta-Romero, J. *Plant, Cell Environ.* **2019,** *42,* 2627–2644. doi:10.1111/pce.13601
79. Rasmann, S.; Köllner, T. G.; Degenhardt, J.; Hiltpold, I.; Toepfer, S.; Kuhlmann, U.; Gershenzon, J.; Turlings, T. C. J. *Nature* **2005,** *434,* 732–737. doi:10.1038/nature03451
80. Jallow, M. F. A.; Dugassa-Gobena, D.; Vidal, S. *Arthropod-Plant Interact.* **2008,** *2,* 53–62. doi:10.1007/s11829-008-9033-8
81. Shrivastava, G.; Ownley, B. H.; Augé, R. M.; Toler, H.; Dee, M.; Vu, A.; Köllner, T. G.; Chen, F. *Symbiosis* **2015,** *65,* 65–74. doi:10.1007/s13199-015-0319-1
82. White, T. J.; Bruns, T.; Lee, S.; Taylor, J. *PCR Protoc.: Guide Methods Appl.* **1990,** 315–322. doi:10.1016/b978-0-12-372180-8.50042-1
83. Gardes, M.; Bruns, T. D. *Mol. Ecol.* **1993,** *2,* 113–118. doi:10.1111/j.1365-294x.1993.tb00005.x
84. Kearse, M.; Moir, R.; Wilson, A.; Stones-Havas, S.; Cheung, M.; Sturrock, S.; Buxton, S.; Cooper, A.; Markowitz, S.; Duran, C.; Thierer, T.; Ashton, B.; Meintjes, P.; Drummond, A. *Bioinformatics* **2012,** *28,* 1647–1649. doi:10.1093/bioinformatics/bts199
85. NCBI Resource Coordinators. *Nucleic Acids Res.* **2018,** *46,* D8–D13. doi:10.1093/nar/gkx1095
86. Kallenbach, M.; Oh, Y.; Eilers, E. J.; Veit, D.; Baldwin, I. T.; Schuman, M. C. *Plant J.* **2014,** *78,* 1060–1072. doi:10.1111/tpj.12523
87. van Den Dool, H.; Kratz, P. D. *J. Chromatogr.* **1963,** *11,* 463–471. doi:10.1016/s0021-9673(01)80947-x
88. Hall, T. A. *BioEdit: a user-friendly biological sequence alignment editor and analysis program for Windows 95/98/NT;* Nucleic acids symposium series; Information Retrieval Ltd.: London, 1999; pp 95–98.
89. Tamura, K.; Peterson, D.; Peterson, N.; Stecher, G.; Nei, M.; Kumar, S. *Mol. Biol. Evol.* **2011,** *28,* 2731–2739. doi:10.1093/molbev/msr121

License and Terms

BEILSTEIN JOURNAL OF ORGANIC CHEMISTRY

Natural products in the predatory defence of the filamentous fungal pathogen *Aspergillus fumigatus*

Jana M. Boysen[‡1,2], Nauman Saeed[‡1,2] and Falk Hillmann[*1]

Review

Open Access

Address:
[1]Junior Research Group Evolution of Microbial Interactions, Leibniz-Institute for Natural Product Research and Infection Biology – Hans Knöll Institute (HKI), Beutenbergstr. 11a, 07745 Jena, Germany and [2]Institute of Microbiology, Friedrich Schiller University Jena, Jena, Germany

Email:
Falk Hillmann[*] - falk.hillmann@leibniz-hki.de

* Corresponding author ‡ Equal contributors

Keywords:
amoeba predation; *Aspergillus fumigatus*; fungal ecology; non-ribosomal peptides; polyketides; secondary metabolism; virulence

Beilstein J. Org. Chem. **2021,** *17,* 1814–1827.
https://doi.org/10.3762/bjoc.17.124

Received: 15 January 2021
Accepted: 14 July 2021
Published: 28 July 2021

This article is part of the thematic issue "Chemical ecology".

Guest Editor: C. Beemelmanns

Abstract

The kingdom of fungi comprises a large and highly diverse group of organisms that thrive in diverse natural environments. One factor to successfully confront challenges in their natural habitats is the capability to synthesize defensive secondary metabolites. The genetic potential for the production of secondary metabolites in fungi is high and numerous potential secondary metabolite gene clusters have been identified in sequenced fungal genomes. Their production may well be regulated by specific ecological conditions, such as the presence of microbial competitors, symbionts or predators. Here we exemplarily summarize our current knowledge on identified secondary metabolites of the pathogenic fungus *Aspergillus fumigatus* and their defensive function against (microbial) predators.

Introduction

To thrive in their natural habitats all organisms from bacteria and fungi to plants and animals need access to sufficient nutritional sources and have to defend themselves against both, competitors and predators (Figure 1). Fungi are ubiquitous, living a mostly saprophytic, parasitic or symbiotic lifestyle in various habitats including soil, water, other organisms and even salt-flats and arctic glaciers [1,2]. As fungi are not able to physically leave their habitats they must rely on mechanical barriers, physiological adaptations and chemical defence mechanisms to optimize their living conditions and resist competitors, parasites and predators [3-5]. These bioactive compounds are often considered as secondary metabolites (SM) which are involved in communication, symbiotic interactions, pathogenicity or chemical defence, e.g., by toxin production [6]. With penicillin

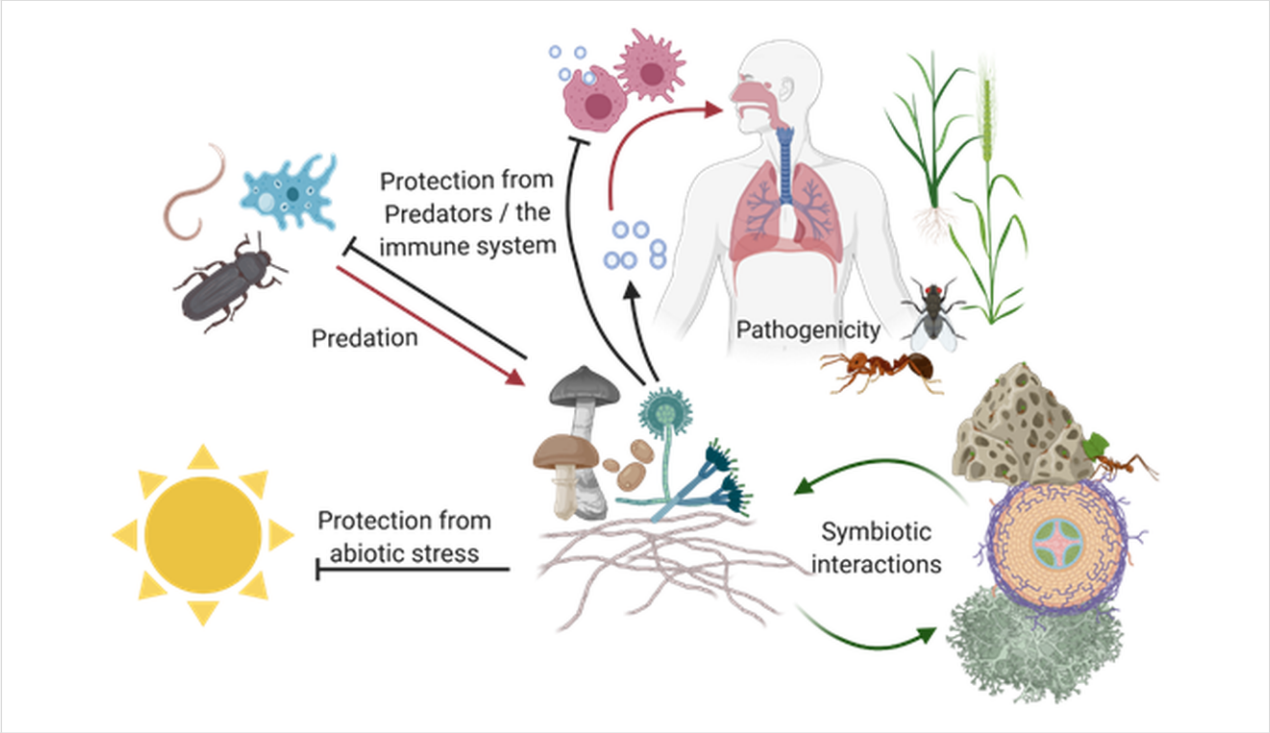

Figure 1: Schematic overview of fungal interactions in the environment. Fungi can be found in essentially all terrestrial habitats comprising saprophytic, parasitic, symbiotic or predatory lifestyles [6]. Independent of their ecological niche, they have to protect themselves against abiotic stresses, competitors and predators while also communicating with their host or partners during parasitic/pathogenic or symbiotic interactions. This figure was created with biorender.com.

as the prime example fungal secondary metabolites have raised scientific and pharmaceutical interests for nearly one century. Today's sequencing and bioinformatic analyses of fungal genomes revealed that the genetic potential far exceeds the number of known metabolites and the interest of scientists to gain access to them remains high [7-9].

Genes associated with these bioactive compounds are often organized in biosynthetic gene clusters (BGCs) which are physically linked, commonly regulated and often belong to a few distinct classes of molecules like non-ribosomal peptides (NRP), polyketides (PK), terpenes or indole alkaloids [10,11]. The vast majority of fungal BGCs is found in the genomes of members of the Basidiomycota and Ascomycota including the genus *Penicillium* in which the first BGC was identified in 1990 [12-14]. *Penicillium* species belong to the Pezizomycotina, a subdivision within the Ascomycotina including several species that are closely associated with humans at many different levels. Aside from being a source of many medically relevant compounds including antibiotics like penicillin they offer food sources in the form of naturally grown truffles (e.g., *Tuber melanosporum*) or recently cultivated meat alternatives like Quorn® (*Fusarium venenatum*) [15-17]. Species of *Aspergillus*, such as *Aspergillus fumigatus, Aspergillus flavus* and *Aspergillus niger* can affect the health of humans, plants and lifestock by acting as pathogens. It is firmly established that the ability to produce mycotoxins contributes to the virulence potential of these fungi, but as they all thrive in environmental reservoirs they must also provide an ecological advantage to their producer [18].

Indeed, many of these pathogenic fungi also produce compounds with antibacterial, antifungal and insecticidal properties to ward of both competitors and predators. The mycotoxins aflatoxin B1 (**1**) from *Aspergillus flavus* and patulin (**2**), produced by *Aspergillus* and *Penicillium* species, exhibit insecticidal activity against *Drosophila melanogaster* and might thus prevent feeding competition [19-21] (Figure 2). But not only mycotoxins protect from predation: *A. flavus* sclerotia are protected from sap beetles by asparasone and *Neurospora crassa's* neurosporin A prevents springtail grazing [22,23]. Grazing by *Folsomia candida* springtails on *Fusarium graminearum* induces several metabolites, of which especially the bisnaphthopyrone pigment aurofusarin (**3**) was shown to have antifeedant effects not only on springtails but also on mealworm *Tenebrio molitor* and woodlouse *Trichorhina tomentosa*. Not only *Fusarium* species produce bisnaphthopyrones like aurofusarin but also *Aspergillus* and *Penicilllium* species produce these metabolites which show antifeedant effects on a wide variety of arthropods [24].

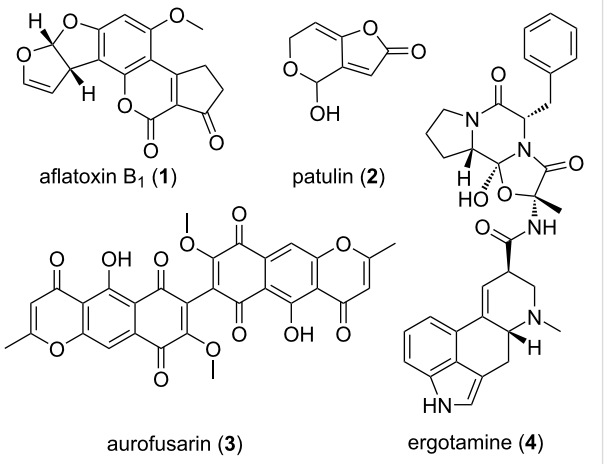

Figure 2: Fungal derived bioactive natural compounds with ecological and/or economic relevance.

Some fungal compounds can have deleterious effects on humans, livestock or crops, like the ergot alkaloids, e.g., ergotamine (**4**) present in the sclerotia of the ergot fungus *Claviceps purpurea*, which can contaminate grain products like flour. In the middle ages these contaminations caused vast epidemics of "St. Anthony's fire", a severe poisoning which could lead to death and mutilation in humans. However, midwives already knew the therapeutic potential of ergot alkaloids as early as 1582 and used it for abortion or to aid childbirth. The ecological significance of ergot alkaloids remains unclear, but they are assumed to be a feeding deterrent due to their toxicity and bad taste [25-28].

To trigger the synthesis of new SMs a number of approaches have been exploited so far, including co-cultivation with other species [9]. Amoebae offer promising possibilities to not only discover new SM but also to discover their ecological role as amoeba often cohabitate with fungi in their natural environments, especially the soil. Some, like *Protostelium aurantium*, were recently found to be exclusively fungivorous, feeding on both yeasts and filamentous fungi alike [29]. Additionally, amoeba closely resemble human phagocytic cells and the interactions of fungi and amoeba often parallels interactions of fungi and macrophages as was shown for *Aspergillus fumigatus* and its interactions with *Acanthamoeba castellanii* [30]. Thus, the adaptations that protect fungi against amoeba that were gained in the 'environmental school of virulence' might also protect fungi from the immune system [31]. Therefore, to study their interactions with human pathogenic fungi like *A. fumigatus*, one of the most common airborne fungal pathogens, might lead to new insight in virulence mechanisms and the role of SMs therein [32]. The aim of this review is to depict the fungal secondary metabolite potential and its role in an ecological context using *A. fumigatus* as an example because of its high medical importance and its diverse profile of secondary metabolites which seems to fulfil dual roles: targeting innate immune cells during virulence and protect from environmental predators in natural habitats.

Review

Natural products of Aspergillus fumigatus

The genus *Aspergillus* comprises a large number of species that are not only of scientific but also of pharmaceutical and commercial interest. While the non-pathogenic *A. niger* is used as industrial workhorse, for example in the production of citric acid, other representatives contaminate food stocks with mycotoxins (*A. flavus*) or can cause severe infections (*A. fumigatus*, *A. terreus*). Despite their different role for humans, they commonly share a high potential for the production of secondary metabolites, measured by the predicted number of secondary metabolite gene clusters identified by numerous genome sequencing projects. Due to its clinical importance as an opportunistic pathogen *A. fumigatus* is of great interest among them [33,34].

As a saprophytic decomposer of organic material in the soil, *A. fumigatus* encounters not only numerous competitors but also fungivorous predators like amoebae (e.g., *P. aurantium*), nematodes (e.g., *Aphelenchus avenae*) or arthropods like insects, mites and springtails (e.g., *F. candida*) [35-39]. However, the fungus may also act as a pathogen causing often lethal infections in immune-compromised patients, and thus its secondary metabolism was extensively studied in recent years [38,40,41]. Analysis of the *A. fumigatus* genome sequence and metabolomics revealed its potential to synthesize more than 200 compounds and the presence of over 30 secondary metabolite associated gene clusters [7,42-44]. The products of many of those gene clusters are already known and span the whole range of secondary metabolite classes. Table 1 provides an overview of the major secondary metabolites from *A. fumigatus* and lists their ecological roles as well as their impact on virulence.

Gliotoxin

Gliotoxin (GT, **5**) is the non-ribosomal peptide (NRP) derived epipolythiodioxopiperazine (ETP's) class toxin of several fungal genera including *Aspergillus*, *Penicillium*, *Trichoderma*, and *Leptosphaera* (Figure 3) [112]. Among the ascomycetes, *A. fumigatus* may well be the major GT producer and the identification of its heterocyclic structure by Bell and colleagues in 1958 builds the foundation to understand its role in invasive aspergillosis [113]. In *A. fumigatus* 13 genes form a 28 kb biosynthetic cluster of gliotoxin, of which *gliZ* (a zinc-finger transcription factor) and *gliP* (an NRPS) together with global regulator LaeA regulate its expression at the genomic level

Table 1: Overview of *Aspergillus fumigatus* secondary metabolites and their roles during virulence and in their ecological context.

Metabolite	Class	Virulence factor	Role in virulence	Ecological role/ toxicity	Reference
DHN-melanin	polyketide, phenolic polymer, pigment	yes	- prevents recognition by the immune system - prevents phagosomal acidification	- protection against UV-stress - prevents recognition by predators (e.g., amoeba) - prevents phagolysosome maturation	[45-50]
endocrocin	polyketide, pigment	–	- inhibits chemotaxis of neutrophils	- protection against UV-stress	[47,51-53]
ferricrocin	siderophore	yes	- iron homeostasis	- iron homeostasis	[54,55]
fumagillin	mero-terpenoid	–	- inhibitor of phagocyte activity - damages epithelial cells - inhibitor of methionine aminopeptidase	- cilioinhibitory - antimicrobial - antiprotozoal	[56-62]
fumigaclavine	ergot alkaloid	–	- reduces production of TNF-α – toxic to mammalian cells	- antibacterial - insecticidal - antifeedant	[63-67]
fumipyrrole	non-ribosomal peptide	–	–	- enhances growth and sporulation	[68]
fumiquinozalines	tryptophan derived peptidyl alkaloid	–	not determined	- antibacterial - antifungal	[69-72]
fumisoquin	isoquinolone alkaloid	–	not determined	- inhibits bacterial replication	[73,74]
fumitremorgin	indole diketo-piperazine alkaloid	–	- inhibitor of breast cancer resistance protein	- antifungal - antifeedant - insecticidal	[72,75]
fusarinine C/ triacetylfusarinine C	siderophore	yes	- iron acquisition	- iron acquisition	[54,55,76]
fungisporin	non-ribosomal peptide	–	not determined	- antibacterial	[41,77]
gliotoxin	epipolythiopiperazine	yes	- inhibition of immune response	- cilioinhibitory - antimicrobial - protects against amoeba predation	[78-82]
helvolic acid/ protostadienol	fusidane-type steroid	–	- cilioinhibitory	- antibacterial - antiprotozoal - antifungal	[72,83-88]
hexadehydro-astechrome	non-ribosomal peptide, tryptophan-derived iron(III) complex	yes	- iron homeostasis	- iron homeostasis	[89,90]
neosartoricin/ fumicycline	prenylated polyketide, meroterpenoid	–	- inhibition of immune response	not determined	[41,91,92]
nidulanin A	tetracyclo-peptide/ isoprene	–	not determined	not determined	[93]
pseurotin	heterocyclic γ-lactam	–	- inhibition of IgE production	- antibacterial	[94-97]
pyripyropene A	sesqui-terpenoid	–	- acetyltransferase inhibitor	- nematicide - insecticidal	[98-100]
sphingofungin A–D	sphingosine-like compound	not determined	- inhibition of serine palmitoyl transferase	- antifungal	[101-104]
trypacidin	polyketide, anthraquinone, pigment	–	- toxic to lung cells	- antiprotozoal - antiphagocytic	[53,105-107]
verruculogen	indole diketo-piperazine alkaloid	not determined	- alters electrophysical properties of human nasal epithelial cells	- antifungal	[72,108-110]

Table 1: Overview of *Aspergillus fumigatus* secondary metabolites and their roles during virulence and in their ecological context. (continued)

xanthocillin	tyrosine-derived isocyanide	–	- copper homeostasis	- copper homeostasis	[111]

[112,114-116] (Figure 3). Whereas GliT (a gliotoxin oxidoreductase) catalyses the oxidation of reactive dithiol gliotoxin (**6**) to gliotoxin and a distantly localized *S*-adenosylmethionine-dependent gliotoxin bisthiomethyltransferase (*GtmA*) is responsible for the formation of bis(methyl)gliotoxin (**7**) to maintain the GT concentration at sub-lethal levels via redox cycling and S-methylation of active disulfides in GT, respectively [117,118]. Furthermore, in terms of exogenous factors, not only GT itself but several other biotic and abiotic factors, including neutrophilic granulocytes, media composition, pH, temperature and aeration, are known to regulate gliotoxin biosynthesis [115,119,120].

The biological activity of ETP's like gliotoxin is mediated by the active disulfide bridge that targets vulnerable thiols or catalyses oxidative burst formation via redox cycling [78]. In previous studies, these cytotoxic activities of gliotoxin were shown to be immunosuppressive in humans [79-81]. Sugui and colleagues (2007) also demonstrated that a gliotoxin lacking strain of *A. fumigatus* is avirulent in mice treated with cortisone acetate [121]. Nevertheless, the fact that gliotoxin is not only produced by pathogenic *A. fumigatus* suggests a role of gliotoxin in natural microenvironments. In vitro studies have also revealed the amoebicidal activities of gliotoxin on its natural co-inhabitant *Dictyostelium discoideum* [82]. However, these pathogenic activities sometimes prove to be beneficial for other co-habitants, comparable to how *Trichoderma virens* protects cotton seedlings from its pathogen *Pythium ultimum* [122].

Trypacidin

The spore-born toxin trypacidin (**8**) is a polyketide that belongs to an anthraquinone-derived class of secondary metabolites (Figure 4) [107]. In *A. fumigatus*, the trypacidin biosynthetic cluster (*tpc*) is comprised of 13 genes that spans over a 25 kb sub-telomeric region on chromosome 4 [53,105]. It is one of the conidial secondary metabolites that are regulated by global transcriptional regulators LaeA and BrlA in *A. fumigatus* [51,123-126]. Nevertheless, trypacidin production is also regulated by cluster specific transcriptional regulators TpcD/E [53]. Though the precise mechanism of action of trypacidin remains to be elucidated, it was shown to exhibit antiprotozoal, antiphagocytic and cytotoxic activities in vitro. Gauthier and colleagues (2012) have shown that in lung cells trypacidin mediates in necrosis-mediated death [107]. In another study, absence of trypacidin was shown to be linked with increased phagocytic rates in murine alveolar macrophages and phagocytic amoeba *D. discoideum*. The authors further showed that trypacidin reduced the viability of amoebae which signifies its role in conidial protection in the environment [105].

Fumagillin

Fumagillin (**9**) belongs to the meroterpenoid class of secondary metabolites. It was discovered in 1949 from *A. fumigatus* [127].

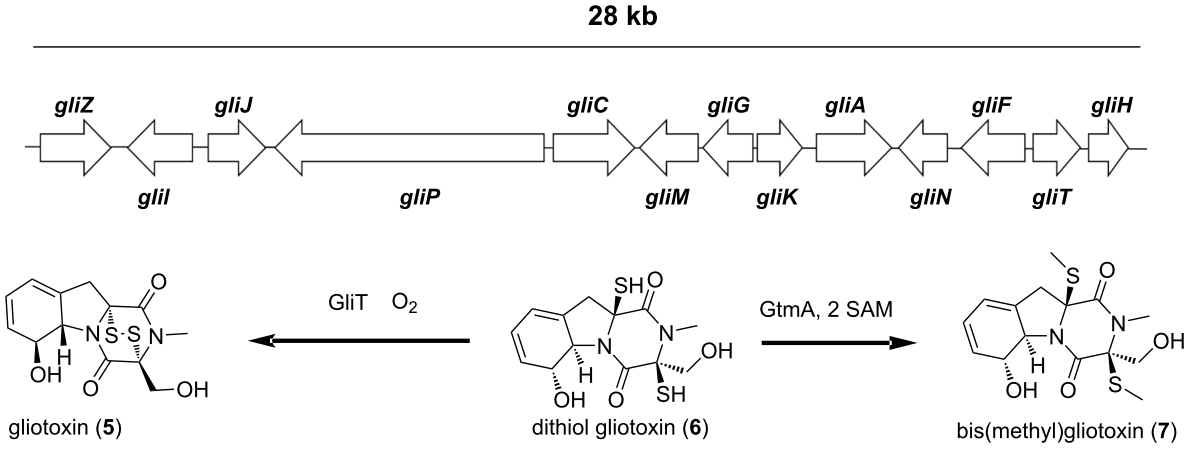

Figure 3: Gliotoxin biosynthetic gene cluster and it major biosynthetic transformations: Gliotoxin (**5**) is the oxidized form of dithiol-gliotoxin (**6**) catalysed by the gliotoxin oxidoreductase GliT. Dithiol-gliotoxin can be methylated to bis(methyl)gliotoxin (**7**) via the S-adenosyl-methionine (SAM) dependent bisthiomethyltransferase GtmA which is not part of the *gli*-cluster.

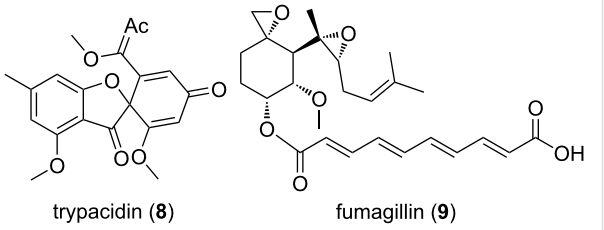

Figure 4: Amoebicidal secondary metabolites trypacidin and fumagillin of *Aspergillus fumigatus*.

Strikingly, unlike other secondary metabolite synthesizing clusters, the fumagillin biosynthetic cluster is intertwined with the pseurotin gene cluster and designated as the *fma* cluster [95,128]. Wiemann and colleagues (2013) have shown the existence of a similarly intertwined pattern in both close and distant relatives of *A. fumigatus*, and therefore suggested a role of these metabolites in survival. In *A. fumigatus*, the *fma* cluster is located on the sub-telomeric region on chromosome 8 and is comprised of 15 genes. At the cellular level fumagillin is regulated by both cluster specific regulator FumR (FapR) and global regulator LaeA [95].

Fumagillin consists of a cyclohexane ring and decatetraenedioic acid connected via an ester bond. There is also a methoxy group, an epoxide and a terpene derived aliphatic chain that contains another epoxide, linked to cyclohexane. These unstable di-epoxides are responsible for the biological activity of fumagillin, which targets the active site of the methionine aminopeptidase type-2 (MetAP-2) enzyme [129]. MetAP-2 is involved in cell proliferation, translation and post-translational modifications of nascent polypeptides and is therefore essential for cell viability [130,131]. Additionally, fumagillin is also known to be overproduced upon caspofungin treatment and damage to the cell walls while fumagillin aids in immune evasion by reducing ROS levels, degranulation and actin filamentation in neutrophils [60,132]. In nature, several fungal species are known to produce caspofungin which could trigger fumagillin production in natural environments [132,133]. *A. fumigatus* possesses an additional MetAP-2 gene in the *fma* cluster that protects itself against its own toxin [134]. Fumagillin has therapeutic potential for the treatment of intestinal microsporidiosis and nosemiasis in honey bees [58,135]. Overall, antibiotic, immunosuppressive, antitumor and antiangiogenic properties have been attributed to fumagillin [129,136-140]. Specific antibiotic activities were demonstrated against the pathogen *Entamoeba histolytica* and later against eukaryotic parasites such as *Trypanosoma* and *Plasmodium* the causative agent of malaria [141,142]. In comparison to gliotoxin, we found only minor cytotoxic activities of fumagillin against the model amoebae *D. discoideum* [82]. It could still be conceivable that other amoeba could reveal higher sensitivity, but tests against the fungivorous amoeba *P. aurantium* were not yet conducted.

DHN-melanin

Melanins are a heterogenous group of hydrophobic phenolic polymers that are found in a range of organisms including bacteria, plants, fungi and even animals. The melanin pigments are of mostly dark colours like black or brown and are associated with virulence in plant- and animal-pathogenic fungi [143-145]. Three types of melanins are known to be produced by fungi of which *A. fumigatus* is able to produce two – pyomelanin and dihydroxynaphthalene melanin (DHN-melanin). While the water-soluble pyomelanin is synthesized via the tyrosine degradation pathway, the DHN-melanin synthesis relies on its own SM-gene-cluster [146-148]. The DHN-melanin of *A. fumigatus* is a heteropolymer formed through the polymerization of 1,8-dihydroxynaphtalene (1,8-DHN) monomers (**10**) and is responsible for the unique greyish-green colour of *A. fumigatus* conidia (Figure 5).

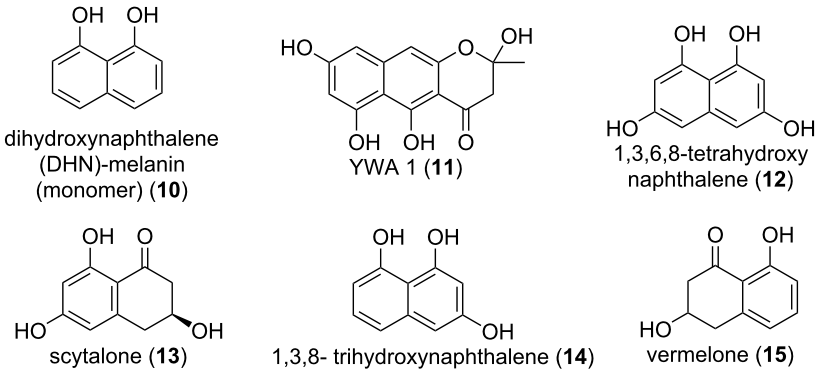

Figure 5: Intermediates of the DHN-melanin biosynthesis in *Aspergillus fumigatus*.

The genetics and biochemistry of its biosynthesis are well established: the 19 kb gene cluster contains 6 genes and lies downstream of the conidiation pathway. The polyketide synthase PksP combines the starter units acetyl-CoA and malonyl-CoA into the heptaketide naphthopyrone YWA1 (**11**). The hydrolytic activity of Ayg1 shortens the heptaketide to the pentaketide 1,3,6,8-tetrahydroxynaphthalene (1,3,6,8-THN) (**12**) and is further reduced by reductase Arp2 to scytalone (**13**), which in turn is dehydrated by Arp1 to 1,3,8-trihydroxynaphthalene (1,3,8-THN) (**14**). Again, Arp2 reduces 1,3,8-THN to vermelone (**15**) before it is dehydrated to 1,8-dihydroxynaphthalene (1,8-DHN) (**10**) by Abr1, a multi-copper reductase. In a last step polymerization of 1,8-DHN monomers is facilitated by the laccase Abr2 [45,149-152]. Knock out mutants of either *ayg1*, *arp2*, or *abr2* lead to different coloured conidia while loss of *pksP* aborts DHN-melanin synthesis completely which leads to white spores [45]. DHN-melanin is a heterogeneous polymer, as such it does not have a unique structure. Its insolubility aggravates any structural analyses of the deciphering of repetitive motives. However, there were studies doing either computational predictions or artificial oxidative polymerization studies of 1,8-DHN monomers [144,153].

Next to offering the conidia protection from UV radiation, DHN-melanin was shown to be a key factor to survival during both predation and virulence. When preyed upon by fungivorous amoeba like *P. aurantium* melanised conidia where not only internalized less than Δ*pksP* conidia but were also able to prevent maturation of phagolysosomes [50,147]. During infection DHN-melanin masks the pathogen-associated molecular patterns on the spore-surface and is thus less likely to be recognized by the immune system. The Δ*pksP* strain lacks this protection and is more easily recognized by the immune system, thus triggering a stronger immune response, including a higher pro-inflammatory response and increased recognition and ingestion by phagocytes rendering the Δ*pksP* strain less virulent. Additionally, melanised conidia are more likely to survive internalization by lung epithelial cells [147,154,155]. Although DHN-melanin is generally associated with immune evasion it was recently found to be recognized in higher animals via the C-type lectin receptor (MelLec) which interacts with the naphthalenediol domain of DHN-melanin. Additionally, the surfactant protein D (SP-D), a soluble C-type lectin receptor (CLR), is also able to recognise DHN-melanin and opsonize it to increase the immune response. However, MelLec receptors are only present on some endothelial and myeloid cells [156,157].

Fumigaclavines

Fumigaclavine C (**19**) is a tryptophan-derived indole alkaloid which was so far only shown to be produced by *A. fumigatus* while other fumigaclavines can for example also be found in *Penicillium* ssp. (fumigaclavine A (**18**) and B (**17**)) [66,158]. In all fungi, alkaloid biosynthetic pathways share a common basis, starting with the prenylation of L-tryptophan to dimethylallyltryptophan (DMAT). During several steps DMAT is converted to chanoclavine-I aldehyde, the last mutual intermediate. Branching into different pathways after this intermediate is mainly due to differences in the function of EasA, the enzyme catalysing the next biosynthetic step. In *A. fumigatus* EasA acts as a reductase and after additional steps chanoclavine-I aldehyde is converted into festuclavine (**16**) (Figure 6). Festuclavine is then oxidized to fumigaclavine B (**17**) which in turn is acetylated to fumigaclavine A (**18**). Finally a reverse prenylation of fumigaclavine A leads to fumigaclavine C (**19**), the final product of fumigaclavine biosynthesis [159]. Biosynthesis of the intermediate festuclavine as well as fumigaclavines A–C is dependent on LaeA regulation [124].

Its numerous bioactive effects hold the potential for a pharmaceutical use since it was shown to be an effective inhibitor of tumor necrosis factor-alpha (TNF-α) production by preventing the activation of TLR4 by lipopolysaccharide (LPS) and was thus proposed for potential use against atherosclerosis [67]. Furthermore fumigaclavine C has also proven effective against MCF-7 breast cancer cells by arresting the cell cycle and promoting apoptosis while showing no cytotoxicity against RAW 264.7 cells, thus demonstrating their selectivity [65,67]. Further, fumigaclavine was shown to exhibit antibacterial properties and to contribute to virulence in the model insect *Galleria mellonella* [66].

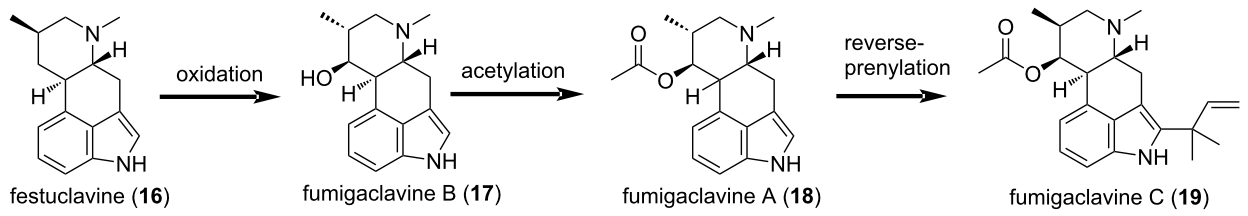

Figure 6: Intermediates and products of the fumigaclavine C biosynthesis.

Fumitremorgins

The class of fumitremorgins comprises several diketopiperazine alkaloids which are tremorgenic mycotoxins. However, there are several fumitremorgin-like indole alkaloids including tryprostatins, spiro- and cyclotryprostatins and verruculogen besides fumitremorgins themselves. They occur most often in *Aspergillus* and *Penicillium* species [160]. Fumitremorgin A (**20**), B (**21**) and C (**22**) can all be found in *A. fumigatus* (Figure 7). They are based on the precursers L-tryptophan and L-proline and are further derived from breviamide F, proposedly via tryprostatin B which is hydroxylated and methylated to tryprostatin A. Oxidative closure of the ringstructure then results in fumitremorgin C. Further modification of the structure leads to fumitremorgin B and verruculogen, which shares the same pathway [97,160-162]. Which enzyme is responsible for the conversion of verruculogen to fumitremorgin A remains to be elucidated. Like several other clusters, the biosynthesis of fumitremorgins is dependent on LaeA [124].

Fumitremorgin B was shown to have antifungal properties against phytopathogenic fungi, antifeedant properties against army-worm larvae and toxic on brine shrimp [72]. It was further shown to be cytotoxic and inhibiting cell cycle progression at G2/M phase [163]. Fumitremorgin C was shown to effect mammalian cells and inhibit the breast cancer resistance protein which imparts multidrug resistance and thus resistance to chemotherapeutics in breast cancer treatment [75,164].

Helvolic acid

Helvolic acid (HA) (**23**) is a fusidane-type antibiotic that belongs to the triterpenoid class of secondary metabolites. Originally, it was discovered from *A. fumigatus* but later several other members of the sub phylum Pezizomycotina were also found to be HA producers [165-168]. In *A. fumigatus*, the biosynthetic cluster of HA is comprised of 9 genes that spans over a 16.3 kb region on chromosome 4 (Figure 8). The cluster contains an oxidosqualine cyclase (*helA*), three Cytochrome P450 (*helB1*, *helB2*, *helB3*), a short-chain dehydrogenase/reductase (*helC*) and two acetyltransferases (*helD1*, *helD2*) and a 3-ketosteroid-Δ^1-dehydrogenase [83,169]. Helvolic acid is a tetracyclic compound containing two keto groups, two acetates and one carboxyl group which do not equally contribute to function [169]. Lv and colleagues have shown that the presence of both the C-20 carboxyl group and the 3-keto group are crucial for its antibacterial activity whereas, acetylation of the C-6 hydroxy group reduces the activity of HA [169]. Previous studies have also shown the antitrypanosomal, antifungal and cilioinhibitory properties of HA [72,83,86-88]. For these properties and little cross-resistance helvolic acid is of great pharmaceutical importance. On the other hand, these antibiotic activi-

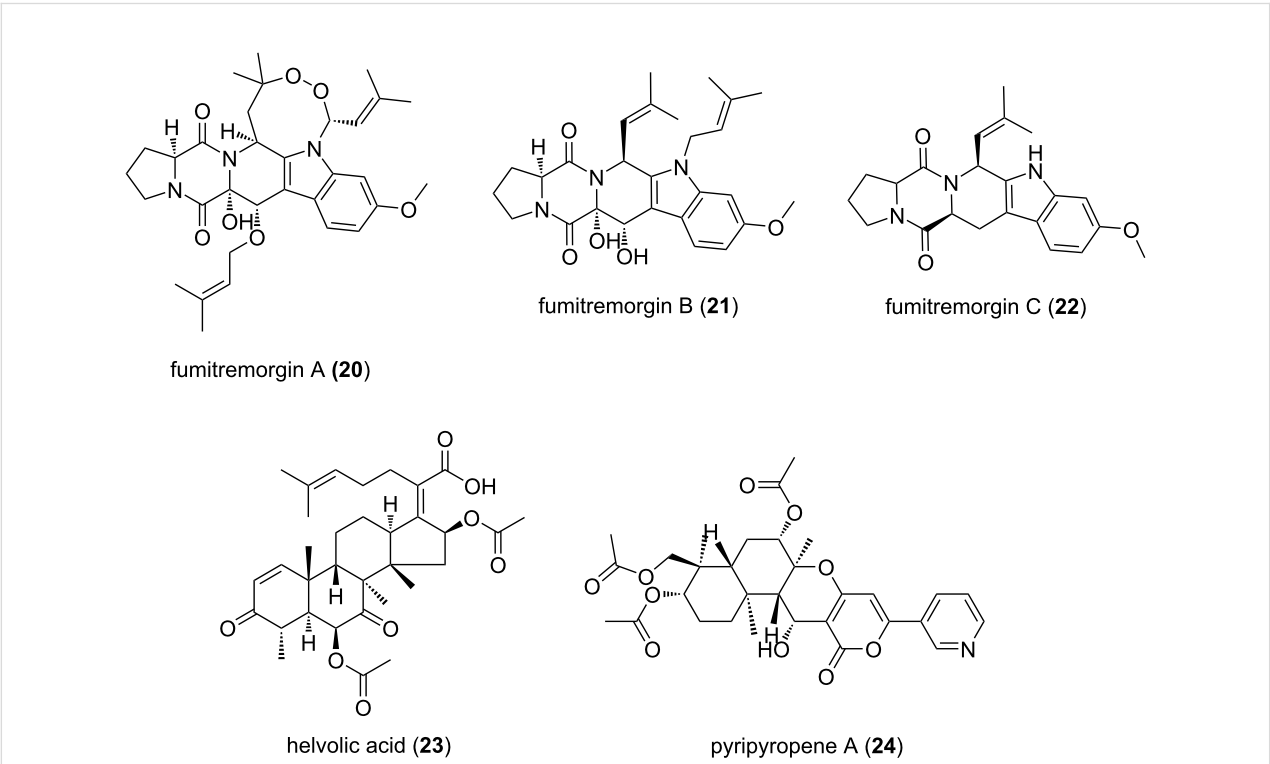

Figure 7: Bioactive secondary metabolites of *Aspergillus fumigatus*.

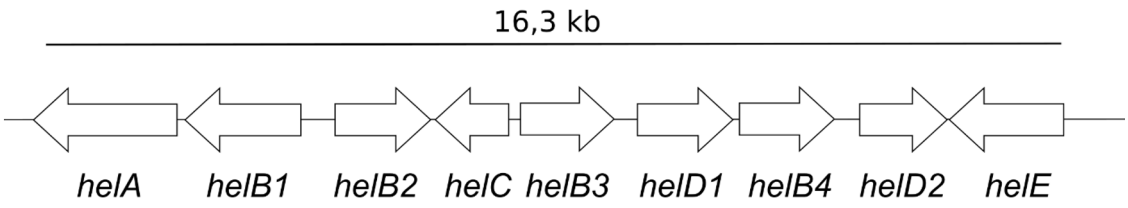

Figure 8: Helvolic acid gene cluster of *A. fumigatus*.

ties of HA could alter the soil microflora in natural habitats, an ecological role of HA that requires further investigation.

Pyripyropene A

Pyripyropene A (PPPA) (**24**) belongs to the meroterpenoid class of secondary metabolites. It was originally isolated from *A. fumigatus*, but later several other pyripyropene A producing members of *Aspergillus* and *Penicillium* ssp. were identified [98,99,170,171]. In A. fumigatus 9 genes form a pyripyropene A (pyr) biosynthetic cluster that spans a 23 kb region on chromosome 6 [172]. Chemically, pyripyropene (PP) analogs are meroterpenoids containing a fused pyridyl α-pyrone moiety and eight contiguous stereocenters [170]. Metabolically, PPPA noncovalently binds within the fifth transmembrane domain of acyl-coenzyme A (CoA):cholesterol acyltransferase ACAT2 and renders it inactive [173]. In vivo, PPPA-mediated ACAT2 inhibition was shown to protect the mice from atherosclerosis, ACAT2 enzyme mediates in lipid metabolism and is localized in the liver and intestines [174]. Furthermore, PPPA was also shown to exhibit insecticidal properties against aphids [100].

Conclusion

Increasing access to sequenced microbial genomes offers a glimpse at the untapped potential we have yet to gain access to. Fungi in particular harbor great potential to produce novel secondary metabolites with ecological and pathogenic importance. As a medically relevant fungal pathogen *A. fumigatus* is the subject of much research and since sequencing of its genome in 2005 its potential for the production of secondary metabolites was scrutinized frequently [7,43,175]. In recent years many of its BGCs could be matched with either long known or newly discovered bioactive compounds and while the bioactive potential and the ecological role of many well studied metabolites like DHN-melanin or gliotoxin is well known, newer metabolites often cannot be associated with a biological function. Due to its clinical significance, the highest interest in secondary metabolites of *A. fumigatus* was driven by its pathobiology, e.g., a role in cytotoxicity, immunosuppression or antifungal drug resistance. In natural habitats these molecules may fulfill analogous functions, such as the defense against phagocytic predators by gliotoxin [78-82]. Indeed, the need for survival is the driving force of evolution and fungi like *A. fumigatus* were able to cultivate an impressive arsenal of protective mechanism from DHN-melanin which offers mostly passive protection to more active compounds like fumigaclavines or helvolic acid with their antibacterial and antifungal activities, respectively [50,63,72,147]. Since SM activities are most often closely related to ecological conditions mimicking of more natural cultivation conditions might lead to the discovery of new compounds and their ecological role.

In the past few years, protists like *D. discoideum* and *Acanthamoeba castellani* have been widely used for the identification of virulence attributes of pathogenic fungi, including *Aspergillus* spp., for their similarity with human phagocytic cells [32]. Nevertheless, the precise identity of amoeboid, nematode and arthropod predators that target filamentous fungi in their environmental niches remained elusive and has been limited by their biological complexity. It was thus surprising to find that the environmentally abundant, fungivorous amoeba *P. aurantium* does not only graze on yeast but can specifically target filamentous fungi such as *A. fumigatus*. The mechanism of action was coined ruphocytosis and involved a locally distinct disruption of the cell wall of the fungal hyphae to feed on the fungal cytoplasm [29]. It is well conceivable that this amoeba will target a range of different filamentous fungi, and that this biotic cell wall stress can be exploited as an ecological trigger for the production and identification of new bioactive compounds in the future.

Funding

Work in the authors' lab was supported by the Deutsche Forschungsgemeinschaft (DFG, German Research Foundation) under Germany's Excellence Startegy - EXC 2051 - Project-ID 390713860 and the research grants DFG HI1574/2-1 und HI1574/4-1. The graphical abstract and Figure 1 were created with BioRender.com.

ORCID® iDs

Jana M. Boysen - https://orcid.org/0000-0001-5877-0006
Nauman Saeed - https://orcid.org/0000-0003-3627-7725
Falk Hillmann - https://orcid.org/0000-0002-5493-930X

References

1. Blackwell, M. *Am. J. Bot.* **2011,** *98,* 426–438. doi:10.3732/ajb.1000298
2. Cantrell, S. A.; Dianese, J. C.; Fell, J.; Gunde-Cimerman, N.; Zalar, P. *Mycologia* **2011,** *103,* 1161–1174. doi:10.3852/11-108
3. Sutherland, I. W. *Trends Microbiol.* **2001,** *9,* 222–227. doi:10.1016/s0966-842x(01)02012-1
4. Costa-Orlandi, C. B.; Sardi, J. C. O.; Pitangui, N. S.; de Oliveira, H. C.; Scorzoni, L.; Galeane, M. C.; Medina-Alarcón, K. P.; Melo, W.; Marcelino, M. Y.; Braz, J. D.; Fusco-Almeida, A. M.; Mendes-Giannini, M. J. S. *J. Fungi* **2017,** 3. doi:10.3390/jof3020022
5. Kowalski, C. H.; Morelli, K. A.; Schultz, D.; Nadell, C. D.; Cramer, R. A. *Proc. Natl. Acad. Sci. U. S. A.* **2020,** *117,* 22473–22483. doi:10.1073/pnas.2003700117
6. Spiteller, P. *Nat. Prod. Rep.* **2015,** *32,* 971–993. doi:10.1039/c4np00166d
7. Nierman, W. C.; Pain, A.; Anderson, M. J.; Wortman, J. R.; Kim, H. S.; Arroyo, J.; Berriman, M.; Abe, K.; Archer, D. B.; Bermejo, C.; Bennett, J.; Bowyer, P.; Chen, D.; Collins, M.; Coulsen, R.; Davies, R.; Dyer, P. S.; Farman, M.; Fedorova, N.; Fedorova, N.; Feldblyum, T. V.; Fischer, R.; Fosker, N.; Fraser, A.; García, J. L.; García, M. J.; Goble, A.; Goldman, G. H.; Gomi, K.; Griffith-Jones, S.; Gwilliam, R.; Haas, B.; Haas, H.; Harris, D.; Horiuchi, H.; Huang, J.; Humphray, S.; Jiménez, J.; Keller, N.; Khouri, H.; Kitamoto, K.; Kobayashi, T.; Konzack, S.; Kulkarni, R.; Kumagai, T.; Lafton, A.; Latgé, J.-P.; Li, W.; Lord, A.; Lu, C.; Majoros, W. H.; May, G. S.; Miller, B. L.; Mohamoud, Y.; Molina, M.; Monod, M.; Mouyna, I.; Mulligan, S.; Murphy, L.; O'Neil, S.; Paulsen, I.; Peñalva, M. A.; Pertea, M.; Price, C.; Pritchard, B. L.; Quail, M. A.; Rabbinowitsch, E.; Rawlins, N.; Rajandream, M.-A.; Reichard, U.; Renauld, H.; Robson, G. D.; de Córdoba, S. R.; Rodríguez-Peña, J. M.; Ronning, C. M.; Rutter, S.; Salzberg, S. L.; Sanchez, M.; Sánchez-Ferrero, J. C.; Saunders, D.; Seeger, K.; Squares, R.; Squares, S.; Takeuchi, M.; Tekaia, F.; Turner, G.; de Aldana, C. R. V.; Weidman, J.; White, O.; Woodward, J.; Yu, J.-H.; Fraser, C.; Galagan, J. E.; Asai, K.; Machida, M.; Hall, N.; Barrell, B.; Denning, D. W. *Nature* **2005,** *438,* 1151–1156. doi:10.1038/nature04332
8. Khaldi, N.; Seifuddin, F. T.; Turner, G.; Haft, D.; Nierman, W. C.; Wolfe, K. H.; Fedorova, N. D. *Fungal Genet. Biol.* **2010,** *47,* 736–741. doi:10.1016/j.fgb.2010.06.003
9. Brakhage, A. A.; Schroeckh, V. *Fungal Genet. Biol.* **2011,** *48,* 15–22. doi:10.1016/j.fgb.2010.04.004
10. Keller, N. P.; Turner, G.; Bennett, J. W. *Nat. Rev. Microbiol.* **2005,** *3,* 937–947. doi:10.1038/nrmicro1286
11. Gacek, A.; Strauss, J. *Appl. Microbiol. Biotechnol.* **2012,** *95,* 1389–1404. doi:10.1007/s00253-012-4208-8
12. Krause, D. J.; Kominek, J.; Opulente, D. A.; Shen, X.-X.; Zhou, X.; Langdon, Q. K.; DeVirgilio, J.; Hulfachor, A. B.; Kurtzman, C. P.; Rokas, A.; Hittinger, C. T. *Proc. Natl. Acad. Sci. U. S. A.* **2018,** *115,* 11030–11035. doi:10.1073/pnas.1806268115
13. Smith, D. J.; Burnham, M. K. R.; Edwards, J.; Earl, A. J.; Turner, G. *Bio/Technology* **1990,** *8,* 39–41. doi:10.1038/nbt0190-39
14. Keller, N. P. *Nat. Rev. Microbiol.* **2019,** *17,* 167–180. doi:10.1038/s41579-018-0121-1
15. O'Donnell, K.; Cigelnik, E.; Casper, H. H. *Fungal Genet. Biol.* **1998,** *23,* 57–67. doi:10.1006/fgbi.1997.1018
16. Martin, F.; Kohler, A.; Murat, C.; Balestrini, R.; Coutinho, P. M.; Jaillon, O.; Montanini, B.; Morin, E.; Noel, B.; Percudani, R.; Porcel, B.; Rubini, A.; Amicucci, A.; Amselem, J.; Anthouard, V.; Arcioni, S.; Artiguenave, F.; Aury, J.-M.; Ballario, P.; Bolchi, A.; Brenna, A.; Brun, A.; Buée, M.; Cantarel, B.; Chevalier, G.; Couloux, A.; Da Silva, C.; Denoeud, F.; Duplessis, S.; Ghignone, S.; Hilselberger, B.; Iotti, M.; Marçais, B.; Mello, A.; Miranda, M.; Pacioni, G.; Quesneville, H.; Riccioni, C.; Ruotolo, R.; Splivallo, R.; Stocchi, V.; Tisserant, E.; Viscomi, A. R.; Zambonelli, A.; Zampieri, E.; Henrissat, B.; Lebrun, M.-H.; Paolocci, F.; Bonfante, P.; Ottonello, S.; Wincker, P. *Nature* **2010,** *464,* 1033–1038. doi:10.1038/nature08867
17. Karwehl, S.; Stadler, M. Exploitation of Fungal Biodiversity for Discovery of Novel Antibiotics. In *How to Overcome the Antibiotic Crisis : Facts, Challenges, Technologies and Future Perspectives;* Stadler, M.; Dersch, P., Eds.; Springer International Publishing: Cham, Switzerland, 2016; pp 303–338. doi:10.1007/82_2016_496
18. Spiteller, P. *Chem. – Eur. J.* **2008,** *14,* 9100–9110. doi:10.1002/chem.200800292
19. Zeng, R. S. L.; Niu, G.; Wen, Z.; Schuler, M. A.; Berenbaum, M. R. *J. Chem. Ecol.* **2006,** *32,* 1459–1471. doi:10.1007/s10886-006-9062-7
20. González-Osnaya, L.; Soriano, J. M.; Moltó, J. C.; Mañes, J. *Food Addit. Contam.* **2007,** *24,* 1268–1274. doi:10.1080/02652030701361556
21. Reiss, J. *Chem.-Biol. Interact.* **1975,** *10,* 339–342. doi:10.1016/0009-2797(75)90055-1
22. Cary, J. W.; Harris-Coward, P. Y.; Ehrlich, K. C.; Di Mavungu, J. D.; Malysheva, S. V.; De Saeger, S.; Dowd, P. F.; Shantappa, S.; Martens, S. L.; Calvo, A. M. *Fungal Genet. Biol.* **2014,** *64,* 25–35. doi:10.1016/j.fgb.2014.01.001
23. Zhao, Y.; Ding, J.; Yuan, W.; Huang, J.; Huang, W.; Wang, Y.; Zheng, W. *Environ. Microbiol.* **2017,** *19,* 3920–3929. doi:10.1111/1462-2920.13791
24. Xu, Y.; Vinas, M.; Alsarrag, A.; Su, L.; Pfohl, K.; Rohlfs, M.; Schäfer, W.; Chen, W.; Karlovsky, P. *Nat. Commun.* **2019,** *10,* 3579. doi:10.1038/s41467-019-11377-5
25. Eadie, M. J. *Lancet Neurol.* **2003,** *2,* 429–434. doi:10.1016/s1474-4422(03)00439-3
26. Tudzynski, P.; Correia, T.; Keller, U. *Appl. Microbiol. Biotechnol.* **2001,** *57,* 593–605. doi:10.1007/s002530100801
27. Tudzynski, P.; Scheffer, J. *Mol. Plant Pathol.* **2004,** *5,* 377–388. doi:10.1111/j.1364-3703.2004.00237.x
28. Schardl, C. L.; Panaccione, D. G.; Tudzynski, P. Ergot Alkaloids – Biology and Molecular Biology. *The Alkaloids: Chemistry and Biology;* Academic Press, 2006; Vol. 63, pp 45–86. doi:10.1016/s1099-4831(06)63002-2
29. Radosa, S.; Ferling, I.; Sprague, J. L.; Westermann, M.; Hillmann, F. *Environ. Microbiol.* **2019,** *21,* 1809–1820. doi:10.1111/1462-2920.14588
30. Van Waeyenberghe, L.; Baré, J.; Pasmans, F.; Claeys, M.; Bert, W.; Haesebrouck, F.; Houf, K.; Martel, A. *Environ. Microbiol. Rep.* **2013,** *5,* 819–824. doi:10.1111/1758-2229.12082
31. Brunke, S.; Mogavero, S.; Kasper, L.; Hube, B. *Curr. Opin. Microbiol.* **2016,** *32,* 89–95. doi:10.1016/j.mib.2016.05.010
32. Tosetti, N.; Croxatto, A.; Greub, G. *Microb. Pathog.* **2014,** *77,* 125–130. doi:10.1016/j.micpath.2014.07.009
33. Sanchez, J. F.; Somoza, A. D.; Keller, N. P.; Wang, C. C. C. *Nat. Prod. Rep.* **2012,** *29,* 351–371. doi:10.1039/c2np00084a
34. Show, P. L.; Oladele, K. O.; Siew, Q. Y.; Aziz Zakry, F. A.; Lan, J. C.-W.; Ling, T. C. *Front. Life Sci.* **2015,** *8,* 271–283. doi:10.1080/21553769.2015.1033653

35. Stötefeld, L.; Scheu, S.; Rohlfs, M. *Ecol. Entomol.* **2012,** *37,* 323–329. doi:10.1111/j.1365-2311.2012.01373.x
36. Rohlfs, M. Fungal secondary metabolism in the light of animal–fungus interactions: from mechanism to ecological function. In *Biosynthesis and Molecular Genetics of Fungal Secondary Metabolites;* Zeilinger, S.; Martín, J. F.; García-Estrada, C., Eds.; Springer: New York, NY, USA, 2015; Vol. 3, pp 177–198. doi:10.1007/978-1-4939-2531-5_9
37. Künzler, M. *PLoS Pathog.* **2018,** *14,* e1007184. doi:10.1371/journal.ppat.1007184
38. Brakhage, A. A.; Langfelder, K. *Annu. Rev. Microbiol.* **2002,** *56,* 433–455. doi:10.1146/annurev.micro.56.012302.160625
39. Novohradská, S.; Ferling, I.; Hillmann, F. *Front. Cell. Infect. Microbiol.* **2017,** *7,* 497. doi:10.3389/fcimb.2017.00497
40. Latge, J.-P. *Clin. Microbiol. Rev.* **1999,** *12,* 310–350. doi:10.1128/cmr.12.2.310
41. Bignell, E.; Cairns, T. C.; Throckmorton, K.; Nierman, W. C.; Keller, N. P. *Philos. Trans. R. Soc., B* **2016,** *371,* 20160023. doi:10.1098/rstb.2016.0023
42. Frisvad, J. C.; Rank, C.; Nielsen, K. F.; Larsen, T. O. *Med. Mycol.* **2009,** *47* (Suppl. 1), S53–S71. doi:10.1080/13693780802307720
43. Inglis, D. O.; Binkley, J.; Skrzypek, M. S.; Arnaud, M. B.; Cerqueira, G. C.; Shah, P.; Wymore, F.; Wortman, J. R.; Sherlock, G. *BMC Microbiol.* **2013,** *13,* 91. doi:10.1186/1471-2180-13-91
44. Lind, A. L.; Wisecaver, J. H.; Lameiras, C.; Wiemann, P.; Palmer, J. M.; Keller, N. P.; Rodrigues, F.; Goldman, G. H.; Rokas, A. *PLoS Biol.* **2017,** *15,* e2003583. doi:10.1371/journal.pbio.2003583
45. Heinekamp, T.; Thywißen, A.; Macheleidt, J.; Keller, S.; Valiante, V.; Brakhage, A. A. *Front. Microbiol.* **2013,** *3,* 440. doi:10.3389/fmicb.2012.00440
46. Gómez, B. L.; Nosanchuk, J. D. *Curr. Opin. Infect. Dis.* **2003,** *16,* 91–96. doi:10.1097/00001432-200304000-00005
47. Nguyen, K.-H.; Chollet-Krugler, M.; Gouault, N.; Tomasi, S. *Nat. Prod. Rep.* **2013,** *30,* 1490–1508. doi:10.1039/c3np70064j
48. Brakhage, A. A.; Liebmann, B. *Med. Mycol.* **2005,** *43* (Suppl. 1), S75–S82. doi:10.1080/13693780400028967
49. Jahn, B.; Langfelder, K.; Schneider, U.; Schindel, C.; Brakhage, A. A. *Cell. Microbiol.* **2002,** *4,* 793–803. doi:10.1046/j.1462-5822.2002.00228.x
50. Ferling, I.; Dunn, J. D.; Ferling, A.; Soldati, T.; Hillmann, F. *mBio* **2020,** *11*. doi:10.1128/mbio.00862-20
51. Lim, F. Y.; Hou, Y.; Chen, Y.; Oh, J.-H.; Lee, I.; Bugni, T. S.; Keller, N. P. *Appl. Environ. Microbiol.* **2012,** *78,* 4117–4125. doi:10.1128/aem.07710-11
52. Berthier, E.; Lim, F. Y.; Deng, Q.; Guo, C.-J.; Kontoyiannis, D. P.; Wang, C. C. C.; Rindy, J.; Beebe, D. J.; Huttenlocher, A.; Keller, N. P. *PLoS Pathog.* **2013,** *9,* e1003289. doi:10.1371/journal.ppat.1003289
53. Throckmorton, K.; Lim, F. Y.; Kontoyiannis, D. P.; Zheng, W.; Keller, N. P. *Environ. Microbiol.* **2016,** *18,* 246–259. doi:10.1111/1462-2920.13007
54. Hissen, A. H. T.; Wan, A. N. C.; Warwas, M. L.; Pinto, L. J.; Moore, M. M. *Infect. Immun.* **2005,** *73,* 5493–5503. doi:10.1128/iai.73.9.5493-5503.2005
55. Schrettl, M.; Bignell, E.; Kragl, C.; Joechl, C.; Rogers, T.; Arst, H. N., Jr.; Haynes, K.; Haas, H. *J. Exp. Med.* **2004,** *200,* 1213–1219. doi:10.1084/jem.20041242
56. Kato, N.; Suzuki, H.; Okumura, H.; Takahashi, S.; Osada, H. *Biosci., Biotechnol., Biochem.* **2013,** *77,* 1061–1067. doi:10.1271/bbb.130026
57. Ehlers, T.; Furness, S.; Robinson, T. P.; Zhong, H. A.; Goldsmith, D.; Aribser, J.; Bowen, J. P. *Curr. Top. Med. Chem.* **2016,** *16,* 1478–1488. doi:10.2174/1568026615666150915121204
58. van den Heever, J. P.; Thompson, T. S.; Curtis, J. M.; Ibrahim, A.; Pernal, S. F. *J. Agric. Food Chem.* **2014,** *62,* 2728–2737. doi:10.1021/jf4055374
59. Mendoza, Y.; Diaz-Cetti, S.; Ramallo, G.; Santos, E.; Porrini, M.; Invernizzi, C. *J. Econ. Entomol.* **2017,** *110,* 1–5. doi:10.1093/jee/tow228
60. Fallon, J. P.; Reeves, E. P.; Kavanagh, K. *J. Med. Microbiol.* **2010,** *59,* 625–633. doi:10.1099/jmm.0.018192-0
61. Fallon, J. P.; Reeves, E. P.; Kavanagh, K. *Microbiology (Reading, U. K.)* **2011,** *157,* 1481–1488. doi:10.1099/mic.0.043786-0
62. Guruceaga, X.; Ezpeleta, G.; Mayayo, E.; Sueiro-Olivares, M.; Abad-Diaz-De-Cerio, A.; Aguirre Urízar, J. M.; Liu, H. G.; Wiemann, P.; Bok, J. W.; Filler, S. G.; Keller, N. P.; Hernando, F. L.; Ramirez-Garcia, A.; Rementeria, A. *Virulence* **2018,** *9,* 1548–1561. doi:10.1080/21505594.2018.1526528
63. Pinheiro, E. A. A.; Carvalho, J. M.; dos Santos, D. C. P.; Feitosa, A. d. O.; Marinho, P. S. B.; Guilhon, G. M. S. P.; de Souza, A. D. L.; da Silva, F. M. A.; Marinho, A. M. d. R. *Nat. Prod. Res.* **2013,** *27,* 1633–1638. doi:10.1080/14786419.2012.750316
64. Ma, H.-Y.; Song, Y.-C.; Mao, Y.-Y.; Jiang, J.-H.; Tan, R.-X.; Luo, L. *Planta Med.* **2006,** *72,* 387–392. doi:10.1055/s-2005-916235
65. Li, Y.-X.; Himaya, S. W. A.; Dewapriya, P.; Zhang, C.; Kim, S.-K. *Mar. Drugs* **2013,** *11,* 5063–5086. doi:10.3390/md11125063
66. Panaccione, D. G.; Arnold, S. L. *Sci. Rep.* **2017,** *7,* 8930. doi:10.1038/s41598-017-09107-2
67. Du, R. H.; Li, E. G.; Cao, Y.; Song, Y. C.; Tan, R. X. *Life Sci.* **2011,** *89,* 235–240. doi:10.1016/j.lfs.2011.06.015
68. Macheleidt, J.; Scherlach, K.; Neuwirth, T.; Schmidt-Heck, W.; Straßburger, M.; Spraker, J.; Baccile, J. A.; Schroeder, F. C.; Keller, N. P.; Hertweck, C.; Heinekamp, T.; Brakhage, A. A. *Mol. Microbiol.* **2015,** *96,* 148–162. doi:10.1111/mmi.12926
69. Lim, F. Y.; Ames, B.; Walsh, C. T.; Keller, N. P. *Cell. Microbiol.* **2014,** *16,* 1267–1283. doi:10.1111/cmi.12284
70. Garcia Silva, M.; Araçari Jacometti Cardoso Furtado, N.; Tallarico Pupo, M.; José Vieira Fonseca, M.; Said, S.; Alves da Silva Filho, A.; Kenupp Bastos, J. *Microbiol. Res.* **2004,** *159,* 317–322. doi:10.1016/j.micres.2004.06.003
71. Belofsky, G. N.; Anguera, M.; Jensen, P. R.; Fenical, W.; Köck, M. *Chem. – Eur. J.* **2000,** *6,* 1355–1360. doi:10.1002/(sici)1521-3765(20000417)6:8<1355::aid-chem1355>3.0.co;2-s
72. Li, X.-J.; Zhang, Q.; Zhang, A.-L.; Gao, J.-M. *J. Agric. Food Chem.* **2012,** *60,* 3424–3431. doi:10.1021/jf300146n
73. Baccile, J. A.; Spraker, J. E.; Le, H. H.; Brandenburger, E.; Gomez, C.; Bok, J. W.; Macheleidt, J.; Brakhage, A. A.; Hoffmeister, D.; Keller, N. P.; Schroeder, F. C. *Nat. Chem. Biol.* **2016,** *12,* 419–424. doi:10.1038/nchembio.2061
74. Khalid, S.; Baccile, J. A.; Spraker, J. E.; Tannous, J.; Imran, M.; Schroeder, F. C.; Keller, N. P. *ACS Chem. Biol.* **2018,** *13,* 171–179. doi:10.1021/acschembio.7b00731
75. González-Lobato, L.; Real, R.; Prieto, J. G.; Álvarez, A. I.; Merino, G. *Eur. J. Pharmacol.* **2010,** *644,* 41–48. doi:10.1016/j.ejphar.2010.07.016

76. Lehner, S. M.; Atanasova, L.; Neumann, N. K. N.; Krska, R.; Lemmens, M.; Druzhinina, I. S.; Schuhmacher, R. *Appl. Environ. Microbiol.* **2013,** *79,* 18–31. doi:10.1128/aem.02339-12
77. Ali, H.; Ries, M. I.; Lankhorst, P. P.; van der Hoeven, R. A. M.; Schouten, O. L.; Noga, M.; Hankemeier, T.; van Peij, N. N. M. E.; Bovenberg, R. A. L.; Vreeken, R. J.; Driessen, A. J. M. *PLoS One* **2014,** *9,* e98212. doi:10.1371/journal.pone.0098212
78. Scharf, D. H.; Brakhage, A. A.; Mukherjee, P. K. *Environ. Microbiol.* **2016,** *18,* 1096–1109. doi:10.1111/1462-2920.13080
79. Yamada, A.; Kataoka, T.; Nagai, K. *Immunol. Lett.* **2000,** *71,* 27–32. doi:10.1016/s0165-2478(99)00155-8
80. Schlam, D.; Canton, J.; Carreño, M.; Kopinski, H.; Freeman, S. A.; Grinstein, S.; Fairn, G. D. *mBio* **2016,** *7*. doi:10.1128/mbio.02242-15
81. Gardiner, D. M.; Waring, P.; Howlett, B. J. *Microbiology (Reading, U. K.)* **2005,** *151,* 1021–1032. doi:10.1099/mic.0.27847-0
82. Hillmann, F.; Novohradská, S.; Mattern, D. J.; Forberger, T.; Heinekamp, T.; Westermann, M.; Winckler, T.; Brakhage, A. A. *Environ. Microbiol.* **2015,** *17,* 2858–2869. doi:10.1111/1462-2920.12808
83. Mitsuguchi, H.; Seshime, Y.; Fujii, I.; Shibuya, M.; Ebizuka, Y.; Kushiro, T. *J. Am. Chem. Soc.* **2009,** *131,* 6402–6411. doi:10.1021/ja8095976
84. Lodeiro, S.; Xiong, Q.; Wilson, W. K.; Ivanova, Y.; Smith, M. L.; May, G. S.; Matsuda, S. P. T. *Org. Lett.* **2009,** *11,* 1241–1244. doi:10.1021/ol802696a
85. Kimura, M.; Kushiro, T.; Shibuya, M.; Ebizuka, Y.; Abe, I. *Biochem. Biophys. Res. Commun.* **2010,** *391,* 899–902. doi:10.1016/j.bbrc.2009.11.160
86. Ganaha, M.; Yoshii, K.; Ōtsuki, Y.; Iguchi, M.; Okamoto, Y.; Iseki, K.; Ban, S.; Ishiyama, A.; Hokari, R.; Iwatsuki, M.; Otoguro, K.; Ōmura, S.; Hashimoto, T.; Noji, M.; Umeyama, A. *Chem. Pharm. Bull.* **2016,** *64,* 988–990. doi:10.1248/cpb.c16-00220
87. Amitani, R.; Taylor, G.; Elezis, E.-N.; Llewellyn-Jones, C.; Mitchell, J.; Kuze, F.; Cole, P. J.; Wilson, R. *Infect. Immun.* **1995,** *63,* 3266–3271. doi:10.1128/iai.63.9.3266-3271.1995
88. Kong, F.-D.; Huang, X.-L.; Ma, Q.-Y.; Xie, Q.-Y.; Wang, P.; Chen, P.-W.; Zhou, L.-M.; Yuan, J.-Z.; Dai, H.-F.; Luo, D.-Q.; Zhao, Y.-X. *J. Nat. Prod.* **2018,** *81,* 1869–1876. doi:10.1021/acs.jnatprod.8b00382
89. Yin, W.-B.; Baccile, J. A.; Bok, J. W.; Chen, Y.; Keller, N. P.; Schroeder, F. C. *J. Am. Chem. Soc.* **2013,** *135,* 2064–2067. doi:10.1021/ja311145n
90. Wiemann, P.; Lechner, B. E.; Baccile, J. A.; Velk, T. A.; Yin, W.-B.; Bok, J. W.; Pakala, S.; Losada, L.; Nierman, W. C.; Schroeder, F. C. *Front. Microbiol.* **2014,** *5,* 530. doi:10.3389/fmicb.2014.00530
91. König, C. C.; Scherlach, K.; Schroeckh, V.; Horn, F.; Nietzsche, S.; Brakhage, A. A.; Hertweck, C. *ChemBioChem* **2013,** *14,* 938–942. doi:10.1002/cbic.201300070
92. Chooi, Y.-H.; Fang, J.; Liu, H.; Filler, S. G.; Wang, P.; Tang, Y. *Org. Lett.* **2013,** *15,* 780–783. doi:10.1021/ol303435y
93. Andersen, M. R.; Nielsen, J. B.; Klitgaard, A.; Petersen, L. M.; Zachariasen, M.; Hansen, T. J.; Blicher, L. H.; Gotfredsen, C. H.; Larsen, T. O.; Nielsen, K. F.; Mortensen, U. H. *Proc. Natl. Acad. Sci. U. S. A.* **2013,** *110,* E99–E107. doi:10.1073/pnas.1205532110
94. Mehedi, M. A. U.; Molla, A. H.; Khondkar, P.; Sultana, S.; Islam, M. A.; Rashid, M. A.; Chowdhury, R. *Asian J. Chem.* **2010,** *22,* 2611–2614.
95. Wiemann, P.; Guo, C.-J.; Palmer, J. M.; Sekonyela, R.; Wang, C. C. C.; Keller, N. P. *Proc. Natl. Acad. Sci. U. S. A.* **2013,** *110,* 17065–17070. doi:10.1073/pnas.1313258110
96. Ishikawa, M.; Ninomiya, T.; Akabane, H.; Kushida, N.; Tsujiuchi, G.; Ohyama, M.; Gomi, S.; Shito, K.; Murata, T. *Bioorg. Med. Chem. Lett.* **2009,** *19,* 1457–1460. doi:10.1016/j.bmcl.2009.01.029
97. Maiya, S.; Grundmann, A.; Li, X.; Li, S.-M.; Turner, G. *ChemBioChem* **2007,** *8,* 1736–1743. doi:10.1002/cbic.200700202
98. Omura, S.; Tomoda, H.; Kim, Y. K.; Nishida, H. *J. Antibiot.* **1993,** *46,* 1168–1169. doi:10.7164/antibiotics.46.1168
99. Hu, J.; Furutani, A.; Yamamoto, K.; Oyama, K.; Mitomi, M.; Anzai, H. *Biotechnol. Biotechnol. Equip.* **2014,** *28,* 818–826. doi:10.1080/13102818.2014.960140
100. Goto, K.; Horikoshi, R.; Mitomi, M.; Oyama, K.; Hirose, T.; Sunazuka, T.; Ōmura, S. *J. Antibiot.* **2018,** *71,* 785–797. doi:10.1038/s41429-018-0064-9
101. VanMiddlesworth, F.; Dufresne, C.; Wincott, F. E.; Mosley, R. T.; Wilson, K. E. *Tetrahedron Lett.* **1992,** *33,* 297–300. doi:10.1016/s0040-4039(00)74115-3
102. VanMiddlesworth, F.; Giacobbe, R. A.; Lopez, M.; Garrity, G.; Bland, J. A.; Bartizal, K.; Fromtling, R. A.; Polishook, J.; Zweerink, M.; Edison, A. M. *J. Antibiot.* **1992,** *45,* 861–867. doi:10.7164/antibiotics.45.861
103. Rank, C. Mapping of secondary metabolism in biotechnologically important Aspergillus species. Ph.D. Thesis, Technical University of Denmark, Lyngby, Denmark, 2010.
104. Kobayashi, S.; Furuta, T.; Hayashi, T.; Nishijima, M.; Hanada, K. *J. Am. Chem. Soc.* **1998,** *120,* 908–919. doi:10.1021/ja9730829
105. Mattern, D. J.; Schoeler, H.; Weber, J.; Novohradská, S.; Kraibooj, K.; Dahse, H.-M.; Hillmann, F.; Valiante, V.; Figge, M. T.; Brakhage, A. A. *Appl. Microbiol. Biotechnol.* **2015,** *99,* 10151–10161. doi:10.1007/s00253-015-6898-1
106. Balan, J.; Ebringer, L.; Nemec, P.; Kováč, Š.; Dobias, J. *J. Antibiot., Ser. A* **1963,** *16,* 157–160.
107. Gauthier, T.; Wang, X.; Sifuentes Dos Santos, J.; Fysikopoulos, A.; Tadrist, S.; Canlet, C.; Artigot, M. P.; Loiseau, N.; Oswald, I. P.; Puel, O. *PLoS One* **2012,** *7,* e29906. doi:10.1371/journal.pone.0029906
108. Khoufache, K.; Puel, O.; Loiseau, N.; Delaforge, M.; Rivollet, D.; Coste, A.; Cordonnier, C.; Escudier, E.; Botterel, F.; Bretagne, S. *BMC Microbiol.* **2007,** *7,* No. 1. doi:10.1186/1471-2180-7-1
109. Gallagher, R. T.; Latch, G. C. M. *Appl. Environ. Microbiol.* **1977,** *33,* 730–731. doi:10.1128/aem.33.3.730-731.1977
110. Wang, F.; Fang, Y.; Zhu, T.; Zhang, M.; Lin, A.; Gu, Q.; Zhu, W. *Tetrahedron* **2008,** *64,* 7986–7991. doi:10.1016/j.tet.2008.06.013
111. Lim, F. Y.; Won, T. H.; Raffa, N.; Baccile, J. A.; Wisecaver, J.; Rokas, A.; Schroeder, F. C.; Keller, N. P. *mBio* **2018,** *9*. doi:10.1128/mbio.00785-18
112. Bok, J. W.; Chung, D.; Balajee, S. A.; Marr, K. A.; Andes, D.; Nielsen, K. F.; Frisvad, J. C.; Kirby, K. A.; Keller, N. P. *Infect. Immun.* **2006,** *74,* 6761–6768. doi:10.1128/iai.00780-06
113. Bell, M. R.; Johnson, J. R.; Wildi, B. S.; Woodward, R. B. *J. Am. Chem. Soc.* **1958,** *80,* 1001. doi:10.1021/ja01537a065
114. Bok, J. W.; Balajee, S. A.; Marr, K. A.; Andes, D.; Nielsen, K. F.; Frisvad, J. C.; Keller, N. P. *Eukaryotic Cell* **2005,** *4,* 1574–1582. doi:10.1128/ec.4.9.1574-1582.2005
115. Cramer, R. A., Jr.; Gamcsik, M. P.; Brooking, R. M.; Najvar, L. K.; Kirkpatrick, W. R.; Patterson, T. F.; Balibar, C. J.; Graybill, J. R.; Perfect, J. R.; Abraham, S. N.; Steinbach, W. J. *Eukaryotic Cell* **2006,** *5,* 972–980. doi:10.1128/ec.00049-06

116. Kupfahl, C.; Heinekamp, T.; Geginat, G.; Ruppert, T.; Härtl, A.; Hof, H.; Brakhage, A. A. *Mol. Microbiol.* **2006,** *62,* 292–302. doi:10.1111/j.1365-2958.2006.05373.x
117. Scharf, D. H.; Remme, N.; Heinekamp, T.; Hortschansky, P.; Brakhage, A. A.; Hertweck, C. *J. Am. Chem. Soc.* **2010,** *132,* 10136–10141. doi:10.1021/ja103262m
118. Schrettl, M.; Carberry, S.; Kavanagh, K.; Haas, H.; Jones, G. W.; O'Brien, J.; Nolan, A.; Stephens, J.; Fenelon, O.; Doyle, S. *PLoS Pathog.* **2010,** *6,* e1000952. doi:10.1371/journal.ppat.1000952
119. McDonagh, A.; Fedorova, N. D.; Crabtree, J.; Yu, Y.; Kim, S.; Chen, D.; Loss, O.; Cairns, T.; Goldman, G.; Armstrong-James, D.; Haynes, K.; Haas, H.; Schrettl, M.; May, G.; Nierman, W. C.; Bignell, E. *PLoS Pathog.* **2008,** *4,* e1000154. doi:10.1371/journal.ppat.1000154
120. Sugui, J. A.; Kim, H. S.; Zarember, K. A.; Chang, Y. C.; Gallin, J. I.; Nierman, W. C.; Kwon-Chung, K. J. *PLoS One* **2008,** *3,* e2655. doi:10.1371/journal.pone.0002655
121. Sugui, J. A.; Pardo, J.; Chang, Y. C.; Zarember, K. A.; Nardone, G.; Galvez, E. M.; Müllbacher, A.; Gallin, J. I.; Simon, M. M.; Kwon-Chung, K. J. *Eukaryotic Cell* **2007,** *6,* 1562–1569. doi:10.1128/ec.00141-07
122. Vargas, W. A.; Mukherjee, P. K.; Laughlin, D.; Wiest, A.; Moran-Diez, M. E.; Kenerley, C. M. *Microbiology (Reading, U. K.)* **2014,** *160,* 2319–2330. doi:10.1099/mic.0.079210-0
123. Coyle, C. M.; Kenaley, S. C.; Rittenour, W. R.; Panaccione, D. G. *Mycologia* **2007,** *99,* 804–811. doi:10.1080/15572536.2007.11832512
124. Perrin, R. M.; Fedorova, N. D.; Bok, J. W.; Cramer, R. A.; Wortman, J. R.; Kim, H. S.; Nierman, W. C.; Keller, N. P. *PLoS Pathog.* **2007,** *3,* e50. doi:10.1371/journal.ppat.0030050
125. Twumasi-Boateng, K.; Yu, Y.; Chen, D.; Gravelat, F. N.; Nierman, W. C.; Sheppard, D. C. *Eukaryotic Cell* **2009,** *8,* 104–115. doi:10.1128/ec.00265-08
126. Upadhyay, S.; Torres, G.; Lin, X. *Eukaryotic Cell* **2013,** *12,* 1641–1652. doi:10.1128/ec.00217-13
127. Hanson, F. R.; Eble, T. E. *J. Bacteriol.* **1949,** *58,* 527–529. doi:10.1128/jb.58.4.527-529.1949
128. Lin, H.-C.; Chooi, Y.-H.; Dhingra, S.; Xu, W.; Calvo, A. M.; Tang, Y. *J. Am. Chem. Soc.* **2013,** *135,* 4616–4619. doi:10.1021/ja312503y
129. Sin, N.; Meng, L.; Wang, M. Q. W.; Wen, J. J.; Bornmann, W. G.; Crews, C. M. *Proc. Natl. Acad. Sci. U. S. A.* **1997,** *94,* 6099–6103. doi:10.1073/pnas.94.12.6099
130. Mauriz, J. L.; Martín-Renedo, J.; García-Palomo, A.; Tuñón, M. J.; González-Gallego, J. *Curr. Drug Targets* **2010,** *11,* 1439–1457. doi:10.2174/1389450111009011439
131. Vetro, J. A.; Dummitt, B.; Chang, Y.-H. Methionine Aminopeptidase. In *Aminopeptidases in Biology and Disease;* Hooper, N. M.; Lendeckel, U., Eds.; Proteases in Biology and Disease, Vol. 2; Springer: Boston, MA, USA, 2004; pp 17–44. doi:10.1007/978-1-4419-8869-0_2
132. Conrad, T.; Kniemeyer, O.; Henkel, S. G.; Krüger, T.; Mattern, D. J.; Valiante, V.; Guthke, R.; Jacobsen, I. D.; Brakhage, A. A.; Vlaic, S.; Linde, J. *BMC Syst. Biol.* **2018,** *12,* 88. doi:10.1186/s12918-018-0620-8
133. Netzker, T.; Fischer, J.; Weber, J.; Mattern, D. J.; König, C. C.; Valiante, V.; Schroeckh, V.; Brakhage, A. A. *Front. Microbiol.* **2015,** *6,* 299. doi:10.3389/fmicb.2015.00299
134. Guruceaga, X.; Perez-Cuesta, U.; Abad-Diaz de Cerio, A.; Gonzalez, O.; Alonso, R. M.; Hernando, F. L.; Ramirez-Garcia, A.; Rementeria, A. *Toxins* **2019,** *12,* 7. doi:10.3390/toxins12010007
135. Molina, J.-M.; Tourneur, M.; Sarfati, C.; Chevret, S.; de Gouvello, A.; Gobert, J.-G.; Balkan, S.; Derouin, F. *N. Engl. J. Med.* **2002,** *346,* 1963–1969. doi:10.1056/nejmoa012924
136. Keller, N.; Bok, J.; Chung, D.; Perrin, R. M.; Keats Shwab, E. *Med. Mycol.* **2006,** *44* (Suppl. 1), S83–S85. doi:10.1080/13693780600835773
137. Romsdahl, J.; Wang, C. C. C. *Med. Chem. Commun.* **2019,** *10,* 840–866. doi:10.1039/c9md00054b
138. Wang, J.; Sheppard, G. S.; Lou, P.; Kawai, M.; BaMaung, N.; Erickson, S. A.; Tucker-Garcia, L.; Park, C.; Bouska, J.; Wang, Y.-C. *Cancer Res.* **2003,** *63,* 7861–7869.
139. Yamaoka, M.; Yamamoto, T.; Ikeyama, S.; Sudo, K.; Fujita, T. *Cancer Res.* **1993,** *53,* 5233–5236.
140. Tucker, L. A.; Zhang, Q.; Sheppard, G. S.; Lou, P.; Jiang, F.; McKeegan, E.; Lesniewski, R.; Davidsen, S. K.; Bell, R. L.; Wang, J. *Oncogene* **2008,** *27,* 3967–3976. doi:10.1038/onc.2008.14
141. McCowen, M. C.; Callender, M. E.; Lawlis, J. F., Jr. *Science* **1951,** *113,* 202–203. doi:10.1126/science.113.2930.202
142. Arico-Muendel, C.; Centrella, P. A.; Contonio, B. D.; Morgan, B. A.; O'Donovan, G.; Paradise, C. L.; Skinner, S. R.; Sluboski, B.; Svendsen, J. L.; White, K. F.; Debnath, A.; Gut, J.; Wilson, N.; McKerrow, J. H.; DeRisi, J. L.; Rosenthal, P. J.; Chiang, P. K. *Bioorg. Med. Chem. Lett.* **2009,** *19,* 5128–5131. doi:10.1016/j.bmcl.2009.07.029
143. Eisenman, H. C.; Casadevall, A. *Appl. Microbiol. Biotechnol.* **2012,** *93,* 931–940. doi:10.1007/s00253-011-3777-2
144. Cecchini, M. M.; Reale, S.; Manini, P.; d'Ischia, M.; De Angelis, F. *Chem. – Eur. J.* **2017,** *23,* 8092–8098. doi:10.1002/chem.201701951
145. Tsai, H.-F.; Washburn, R. G.; Chang, Y. C.; Kwon-Chung, K. J. *Mol. Microbiol.* **1997,** *26,* 175–183. doi:10.1046/j.1365-2958.1997.5681921.x
146. Schmaler-Ripcke, J.; Sugareva, V.; Gebhardt, P.; Winkler, R.; Kniemeyer, O.; Heinekamp, T.; Brakhage, A. A. *Appl. Environ. Microbiol.* **2009,** *75,* 493–503. doi:10.1128/aem.02077-08
147. Perez-Cuesta, U.; Aparicio-Fernandez, L.; Guruceaga, X.; Martin-Souto, L.; Abad-Diaz-de-Cerio, A.; Antoran, A.; Buldain, I.; Hernando, F. L.; Ramirez-Garcia, A.; Rementeria, A. *Int. Microbiol.* **2020,** *23,* 55–63. doi:10.1007/s10123-019-00078-0
148. Tsai, H.-F.; Wheeler, M. H.; Chang, Y. C.; Kwon-Chung, K. J. *J. Bacteriol.* **1999,** *181,* 6469–6477. doi:10.1128/jb.181.20.6469-6477.1999
149. Fujii, I.; Yasuoka, Y.; Tsai, H.-F.; Chang, Y. C.; Kwon-Chung, K. J.; Ebizuka, Y. *J. Biol. Chem.* **2004,** *279,* 44613–44620. doi:10.1074/jbc.m406758200
150. Langfelder, K.; Jahn, B.; Gehringer, H.; Schmidt, A.; Wanner, G.; Brakhage, A. A. *Med. Microbiol. Immunol.* **1998,** *187,* 79–89. doi:10.1007/s004300050077
151. Tsai, H.-F.; Fujii, I.; Watanabe, A.; Wheeler, M. H.; Chang, Y. C.; Yasuoka, Y.; Ebizuka, Y.; Kwon-Chung, K. J. *J. Biol. Chem.* **2001,** *276,* 29292–29298. doi:10.1074/jbc.m101998200
152. Sugareva, V.; Härtl, A.; Brock, M.; Hübner, K.; Rohde, M.; Heinekamp, T.; Brakhage, A. A. *Arch. Microbiol.* **2006,** *186,* 345–355. doi:10.1007/s00203-006-0144-2
153. Manini, P.; Bietti, M.; Galeotti, M.; Salamone, M.; Lanzalunga, O.; Cecchini, M. M.; Reale, S.; Crescenzi, O.; Napolitano, A.; De Angelis, F.; Barone, V.; d'Ischia, M. *ACS Omega* **2018,** *3,* 3918–3927. doi:10.1021/acsomega.8b00155

154. Chai, L. Y. A.; Netea, M. G.; Sugui, J.; Vonk, A. G.; van de Sande, W. W. J.; Warris, A.; Kwon-Chung, K. J.; Kullberg, B. J. *Immunobiology* **2010,** *215,* 915–920. doi:10.1016/j.imbio.2009.10.002
155. Thywißen, A.; Heinekamp, T.; Dahse, H.-M.; Schmaler-Ripcke, J.; Nietsche, S.; Zipfel, P. F.; Brakhage, A. A. *Front. Microbiol.* **2011,** *2,* 96. doi:10.3389/fmicb.2011.00096
156. Stappers, M. H. T.; Clark, A. E.; Aimanianda, V.; Bidula, S.; Reid, D. M.; Asamaphan, P.; Hardison, S. E.; Dambuza, I. M.; Valsecchi, I.; Kerscher, B.; Plato, A.; Wallace, C. A.; Yuecel, R.; Hebecker, B.; da Glória Teixeira Sousa, M.; Cunha, C.; Liu, Y.; Feizi, T.; Brakhage, A. A.; Kwon-Chung, K. J.; Gow, N. A. R.; Zanda, M.; Piras, M.; Zanato, C.; Jaeger, M.; Netea, M. G.; van de Veerdonk, F. L.; Lacerda, J. F.; Campos, A.; Carvalho, A.; Willment, J. A.; Latgé, J.-P.; Brown, G. D. *Nature* **2018,** *555,* 382–386. doi:10.1038/nature25974
157. Wong, S. S. W.; Rani, M.; Dodagatta-Marri, E.; Ibrahim-Granet, O.; Kishore, U.; Bayry, J.; Latgé, J.-P.; Sahu, A.; Madan, T.; Aimanianda, V. *J. Biol. Chem.* **2018,** *293,* 4901–4912. doi:10.1074/jbc.m117.815852
158. Kozlovskii, A. G.; Zhelifonova, V. P.; Antipova, T. V. *Appl. Biochem. Microbiol.* **2013,** *49,* 1–10. doi:10.1134/s0003683813010092
159. Robinson, S. L.; Panaccione, D. G. *Toxins* **2015,** *7,* 201–218. doi:10.3390/toxins7010201
160. Li, S.-M. *J. Antibiot.* **2011,** *64,* 45–49. doi:10.1038/ja.2010.128
161. Grundmann, A.; Li, S.-M. *Microbiology (Reading, U. K.)* **2005,** *151,* 2199–2207. doi:10.1099/mic.0.27962-0
162. Yamazaki, M.; Fujimoto, H.; Kawasaki, T. *Chem. Pharm. Bull.* **1980,** *28,* 245–254. doi:10.1248/cpb.28.245
163. Cui, C.-B.; Kakeya, H.; Osada, H. *Tetrahedron* **1997,** *53,* 59–72. doi:10.1016/s0040-4020(96)00978-7
164. Rabindran, S. K.; Ross, D. D.; Doyle, L. A.; Yang, W.; Greenberger, L. M. *Cancer Res.* **2000,** *60,* 47–50.
165. Chain, E.; Florey, H.; Jennings, M.; Williams, T. *Br. J. Exp. Pathol.* **1943,** *24,* 108.
166. Rank, C.; Larsen, T. O.; Frisvad, J. C. Functional systems biology of Aspergillus. In *Aspergillus: molecular biology and genomics;* Machida, M.; Gomi, K., Eds.; Caister Academic Press: Norfolk, UK, 2010; pp 173–198.
167. Tamiya, H.; Ochiai, E.; Kikuchi, K.; Yahiro, M.; Toyotome, T.; Watanabe, A.; Yaguchi, T.; Kamei, K. *J. Infect. Chemother.* **2015,** *21,* 385–391. doi:10.1016/j.jiac.2015.01.005
168. Cole, R. J.; Jarvis, B. B.; Schweikert, M. A. *Handbook of secondary fungal metabolites;* Elsevier, 2003.
169. Lv, J.-M.; Hu, D.; Gao, H.; Kushiro, T.; Awakawa, T.; Chen, G.-D.; Wang, C.-X.; Abe, I.; Yao, X.-S. *Nat. Commun.* **2017,** *8,* 1644. doi:10.1038/s41467-017-01813-9
170. Tomoda, H.; Nishida, H.; Kim, Y. K.; Obata, R.; Sunazuka, T.; Omura, S.; Bordner, J.; Guadliana, M.; Dormer, P. G.; Smith, A. B., III. *J. Am. Chem. Soc.* **1994,** *116,* 12097–12098. doi:10.1021/ja00105a078
171. Kim, Y. K.; Tomoda, H.; Nishida, H.; Sunazuka, T.; Obata, R.; Omura, S. *J. Antibiot.* **1994,** *47,* 154–162. doi:10.7164/antibiotics.47.154
172. Itoh, T.; Tokunaga, K.; Matsuda, Y.; Fujii, I.; Abe, I.; Ebizuka, Y.; Kushiro, T. *Nat. Chem.* **2010,** *2,* 858–864. doi:10.1038/nchem.764
173. Das, A.; Davis, M. A.; Tomoda, H.; Ômura, S.; Rudel, L. L. *J. Biol. Chem.* **2008,** *283,* 10453–10460. doi:10.1074/jbc.m709460200
174. Ohshiro, T.; Matsuda, D.; Sakai, K.; Degirolamo, C.; Yagyu, H.; Rudel, L. L.; Ōmura, S.; Ishibashi, S.; Tomoda, H. *Arterioscler., Thromb., Vasc. Biol.* **2011,** *31,* 1108–1115. doi:10.1161/atvbaha.111.223552
175. Raffa, N.; Keller, N. P. *PLoS Pathog.* **2019,** *15,* e1007606. doi:10.1371/journal.ppat.1007606

License and Terms